UNIVERSITEIT VAN PRETORIA
UNIVERSITY OF PRETORIA
YUNIBESITHI YA PRETORIA

INVESTIGATION INTO STABILITY AND THERMAL-FLUID BEHAVIOUR OF HYBRID NANOFLUIDS AS HEAT TRANSFER FLUIDS

by

Nwaokocha, Collins Chukwuneku

Submitted in partial fulfilment of the requirements for the degree

Doctor of Philosophy (PhD) in Mechanics

Department of Mechanical and Aeronautical Engineering

University of Pretoria

Pretoria

August 2021

Supervisors: Professor Mohsen Sharifpur and Professor Josua P. Meyer

Abstract

Title: Investigation into stability and thermal-fluid behaviour of hybrid nanofluids as heat transfer fluids.

Supervisor: Professor M. Sharifpur and Professor J.P. Meyer

Department: Mechanical and Aeronautical Engineering

Degree: Doctor of Philosophy (PhD) in Mechanics

The need to improve the poor thermal conductivity of conventional fluids to produce adequate heat transfer fluid cannot be over-emphasized, knowing fully well that heat transfer is key in any engineering process line. Hence, the birth of nanofluids, which is the formulation of a composite of suspended nanoparticles in a basefluid. Nanofluids have found wide applications ranging from heat exchangers, electronic cooling, automotive industry, medical, military, solar energy, manufacturing industry, to mention but a few. But the limitations of nanofluids led to the entrance of a new working fluid named binary nanofluid and ternary nanofluid.

This study experimented with the trio influence of temperature (*T*), percent weight ratios (PWRs), nanoparticles size (NS) on the thermophysical behaviour of MgO–ZnO/Deionised water binary nanofluids (BNFs). 20 nm nano-size of ZnO nanoparticles were hybridised with MgO nanoparticles of nano-sizes 20 nm and 100 nm, and dispersed in deionised water to prepare 0.1 vol% binary nanofluids for percent weight ratios of MgO:ZnO (20:80, 40:60, 60:40 and 80:20). The viscosity (μ), electrical conductivity (σ), pH, and thermal conductivity (κ) of the binary nanofluids were experimentally evaluated for temperature 20 to 50 °C. Morphology was checked, and stability was monitored. The impact of temperature, PWRs, and nano-size on the pH, μ, σ, and κ of the binary nanofluid were ordered as PWR >NS >*T*, NS> PWR>*T*, *T*>NS >PWR, and *T* >NS >PWR, respectively. Using the obtained experimental dataset,

correlations were proposed for the thermal property of each binary nanofluid as a function of temperature.

Also, investigating the trio impact of PWR, temperature and φ on the thermophysical characteristics of MgO-ZnO/DIW BNFs, to help close up the scarce literature gap. 20 nm nanoparticle sizes of MgO and ZnO were hybridized together and dissolved in deionized water to formulate 0.1 vol% and 0.05 vol.% binary nanofluids (NFs) for PWR of 20:80, 40:60, 60:40, 80:20 (MgO:ZnO). The κ for all BNFs was enhanced under the impact of rising temperature, with maximum κ enhancement of 5.60% and 22.07% relative to the deionised water (DIW) achieved for 0.05 vol% and 0.10 vol%, separately. The σ was enhanced slightly under the influence of increasing temperature, with maximum enhancement of 21.82% and 30.91% achieved for 0.050 vol% and 0.10 vol%, respectively. In addition, viscosity under temperature increase exhibited a decreasing pattern for all nanohybrids and basefluid. Furthermore, to better harness the benefit of the BNFs for thermal application, thermoelectrical conductivity (TEC) was evaluated with BNFs of 0.05 vol% observed to have higher TEC values than 0.10 vol% BNFs. The BNFs were found suitable as thermal fluids.

A novel manner of furthering thermo-convection behaviour of thermal applications is the use of BNFs as heat transfer fluids. This study experimented the natural convection behaviour of MgO-ZnO NPs suspended in basefluid for φ = 0.050 vol.% and 0.10 vol% at percent weight ratios of 20:80, 40:60, 60:40, 80:20 (MgO:ZnO) inside a square enclosure. Factors like Rayleigh number, Nusselt number (Nu_{av}), coefficient of convective heat transfer (h_{av}), and heat transfer rate (Q_{av}) for various temperatures (20°C to 50°C) were examined. PWRs and temperature gradient of BNPs inside the binary nanofluids was observed to augment Nu_{av}, h_{av}, and Q_{av}. Also, highest improvement of 72.60% (Nu_{av}), 76.01% (h_{av}), and 72.20% (Q_{av}) was achieved. Employing BNFs in square enclosure yielded fine improvement for natural convection behaviour.

Artificial intelligence (AI) methods, like artificial neural network (ANN) and surface fitting method were deployed to model the thermal conductivity of BNFs. For the ANN model, a learning algorithm was developed to determine the optimum neuron number. The ANN having 19 neurons in the inner layer got the optimized performance. A surface fitting method was also used on the experimental data, and the generated surface shows the behaviour of the BNFs. The outcome affirmed that the designed ANN model is best for predicting the thermal conductivity of MgO-ZnO/DIW binary nanofluids for different temperatures, nanoparticle sizes, PWRs and volume concentration over the surface fitting method.

Keywords: *Artificial intelligence; ANN; binary nanofluids; concentration; electrical conductivity; experimental data; DIW; heat transfer; heat transfer co-efficient; heat transfer improvement; pH; percent weight ratio; MgO; modelling; nano-size; Nusselt number; square cavity; sonication energy; temperature; ternary nanofluids; thermal conductivity; thermo-convection; thermophysical properties; viscosity; volume concentration; ZnO.*

Publications

The underlisted publications have been prepared as this study progressed. Some have been submitted for publications. One is accepted for publication while two is published.

Published

1. S. O. Giwa, M. Momin, C. N. Nwaokocha, M. Sharifpur, J. P. Meyer (2021). Influence of nanoparticles size, percent weight ratio, and temperature on the thermal properties of water-based MgO-ZnO nanofluid: an experimental approach. *Journal of Thermal Analysis and Calorimetry*, Volume 143: 1063-1079. https://doi.org/10.1007/s10973-020-09870-x.

2. C. Nwaokocha, M. Momin, S. Giwa, M. Sharifpur, S. Murshed, J. Meyer (2022). Experimental investigation of thermo-convection behaviour of aqueous binary nanofluids of MgO-ZnO in a square cavity. *Thermal Sciences and Engineering Progress*, 2022, Volume 28, 101057. https://doi.org/10.1016/j.tsep.2021.101057

Submitted

3. C. N. Nwaokocha, M. Sharifpur, S. O. Giwa, M. Momin, Mahyar Ghazvini, Hikmet S. Aybar, J. P. Meyer (2021). Experimental formulation and GMDH modelling of thermal conductivity of MgO-ZnO/deionized water hybrid nanofluid.

4. C. Nwaokocha, M. Momin, M. Sharifpur, J. P. Meyer (2021). Influence of concentration, mixing ratios, and working temperature on the thermal behaviour of binary nanofluids of MgO-ZnO: an experimental investigation.

5. C. Nwaokocha, M. Momin, M. Sharifpur, J. P. Meyer (2021). Artificial neural network development to predict thermal conductivity of MgO-ZnO/Deionised Water binary nanofluids.

6. C. Nwaokocha, M. Sharifpur, J. P. Meyer (2021). Applications of binary nanofluids – emerging issues.

Dedication

This thesis is dedicated to:

The Good Lord for the privilege of life and His unlimited mercies,

My dear wife, Funmilayo Amarachi, for her prayers, great support, and sacrifices,

My parents, Mr. Nelson and Mrs. Augustina Nwaokocha for the prayers and mentoring.

Acknowledgements

For the success of this study, I cannot fully thank the people who made it possible

- My Promoter, Professor Mohsen Sharifpur and Co-promoter, Professor Josua P. Meyer for support, mentoring and discussions throughout this study.
- Olabisi Onabanjo University, Ago-Iwoye, Nigeria, for having granted me study leave.
- Tertiary Education Trust Fund (TETFund), Abuja, Nigeria, for benefiting in the Academic Staff Training and Development (AST&D) intervention program.
- University of Pretoria Postgraduate Bursary for Doctoral Students.
- The foundational guidance of Dr. Solomon Giwa, my Laboratory partner Modaser Momin and technical support of Mr. Chris Govender and Mr. Donald Keetse at the Nanofluids Laboratory is acknowledged.
- Ms. Terisa Evans and Ms. Karabo Kunene for administrative assistance in the Department.
- The National Overseer, Pastor John Amoni, his family and members of the Deeper Christian Life Ministry, South Africa for affording us good fellowship.

Above all, I bless the Good Lord God, Creator of heaven and earth for His mercies and ever-faithfulness. Shalom!

Table of Contents

List of Figures

List of Tables

Nomenclature

A	Area of cavity	m^2
Ag	Silver	
AIN	Aluminium nitride	
Al	Aluminium	
Al_2O_3	Aluminium oxide	
AR	Aspect ratio	
Au	Gold	
BF	Basefluid	
CNT	Carbon nanotube	
C_p	Specific heat capacity at constant pressure	J/kg K
CTAB	Cetyl trimethyl ammonium bromide	
Cu	Copper	
CuO	Copper oxide	
DIW	Deionised water	
DW	Distilled water	
DWCNT	Double-walled carbon nanotube	
EDL	Electrical double layer	
EG	Ethylene glycol	
EG-DIW	Ethylene deionised water	
EO	Engine oil	
Fe	Iron	
Fe_2O_3	Iron (III) oxide	
Fe_3O_4	Iron (II) oxide	
G	Graphene	
GA	Gum Arabic	
GL	Glycerol	
GNF	Green nanofluid	
GO	Graphene oxide	
GON	Graphene oxide nanosheet	
h	Coefficient of convective heat transfer	W/m^2K
H	Height	m
HNF	Hybrid nanofluid	
HNP	Hybrid nanoparticle	
m	Gradient	
MgO	Magnesium oxide	
MNF	Magnetic nanofluid	
MO	Mineral oil	
MOD	Margin of deviation	
MWCNT	Multi-walled carbon nanotube	
ND	Nano-diamond	
NF	Nanofluid	
Ni	Nickel	

NP	Nanoparticles	
Nu	Nusselt number	
PG	Propylene glycol	
PVP	Poly vinyl pyrolidone	
Q	Heat transfer rate	W
Ra	Rayleigh number	
Re	Reynolds number	
SDBS	Sodium dodecyl benzene sulfonate	
SDS	Sodium dodecyl sulphate	
SiC	Silicon carbide	
SiO_2	Silicon oxide	
SiO_x	Silicon oxides	
SWCNT	Single-walled carbon nanotube	
T	Temperature	°C
TEC	Thermoelectrical conductivity	
TiO_2	Titanium oxide	
TO	Transformer oil	
V	Volume	m^3
W	Water	
X	Ratio of hybrid nanoparticles	wt.%
Zn	Zinc	
ZnO	Zinc oxide	
ΔT	Temperature difference	°C

Greek letters

Δ	Difference	
ρ	Density	m^3/kg
β	Thermal coefficient of expansion	1/K
μ	Dynamic viscosity	mPa.s
σ	Electrical conductivity	μS/cm
κ	Thermal conductivity	W/m K
φ	Volume concentration of nanoparticles	vol.%
δ	Uncertainty	

Subscripts

eff	Effective
av	Average
S	Side
h	Hot
c	Cold
Exp	Experiment
Pred	Predicted

CHAPTER 1

INTRODUCTION

1.1 BACKGROUND

Energy use and its impact on the environment has called for global concern, hence the need for a sustainable approach that will attenuate the increasing trend of global warming and its attendant environmental problem. Really, energy use remains the thermometer for growth and development. As the search for a sustainable, economical and alternative energy resource is increasing and gaining global attention, so should the concept of energy and environmental balance gain momentum globally [1-3]. Beyond the issue of balance for energy demand and supply, which has led to search for cheap and sustainable energy resource; energy sustainability and efficiency is greatly needed to enable good energy and environmental balance as advocated by the 17-point Sustainable Development Goals (SDGs) agenda of the United Nations (UN). The UN policy was initiated in 2016, to run till 2030 with the global aim of addressing energy and environmental issues [4, 5].

Recent technological innovations keep advancing the need for improvement in energy efficiency and sustainability. Effective thermal energy management is key to numerous process engineering applications. The concept of miniaturization, fins and surface modification for thermal equipment are reaching their limits as regards heat transfer improvement [6-8]. The use of common working fluids (acetone, ethylene glycol (EG), propylene glycol, organic liquid, polymer solution (PS), oils and water) as cooling media in heat transfer applications is no longer sustainable due to the low thermal conductivity of these working fluids. These limitations necessitated a century-long search by Maxwell [9-11] in 1873, who first conceived the idea of developing an energy-efficient fluid with improved thermophysical properties. The formulated suspension-mix (solid particles + basefluid) gave an improved thermal conductivity, with noticeable drawbacks like pressure drop, channel clogging and sedimentation. Later, a similar investigation was conducted by Ahuja [12, 13] in 1975 by suspending micrometre-sized polystyrene particles in aqueous sodium chloride and glycerin solution (as basefluid). An improved thermal conductivity was observed, three times higher than the basefluid, yet the drawback of rapid sedimentation was noticed. Further investigation was carried out by Liu et al. [14] in 1988 and same like-minded researchers too in 1992 at the Argonne National Laboratory (ANL) [15-17], all on the premise of Maxwell's work. Similar drawbacks were reported, as observed by Maxwell and Ahuja [18]. Sometimes in 1993, Masuda et al. [19] came to the rescue with a concept of using ultrafine particles of alumina, silica and titanium dioxide suspended in water, which yielded an enhanced thermal conductivity, without the drawbacks earlier reported by Maxwell and Ahuja. In 1995, after extensive investigation at the ANL, Choi and Eastman [20] named the innovative fluid as 'Nanofluid', considering the improved results.

The need keeps rising in the thermal energy field for improved thermo-convection performance, requiring the advancement of compact devices with lightweight and miniaturized design, finely stable performance, and augmented thermal efficiency. For better heat transfer performance using working fluids, binary nanofluids and ternary nanofluids have found optimized use over the use of single nanofluids because of blended characteristics of nanoparticles [21-30]. The progress in the study of nanofluids advanced the dispersion of various nanoparticles of various volumes/masses, thermal behaviour and geometries to prepare BNFs and TNFs [21, 31-38]. The newly formulated thermal fluids (BNF and TNF) help to improve thermo-convection characteristics as related to mono-nanofluids and conventional basefluids [39-42]. This progressing investigation which continued over a decade ago was pioneered by Jana et al. [43] and Chopkar et al. [44] who birthed the idea of hybridizing various nano-materials for an optimal thermal fluid.

1.2 PROBLEM STATEMENT

The need to augment the poor thermal conductivity of traditional fluids to make them efficient cannot be over-emphasized, knowing that heat transfer fluid is key in the process line of many industrial production concerns. Hence, the birth of nanofluids is the formulation of the composite of suspended nanoparticles in a basefluid [16]. Nanofluids have found applications ranging from heat exchangers, electronic cooling, automotive, medical, military, solar energy, manufacturing, to mention but a few [18, 45-51]. However, nanofluids have limitations premised on certain specific benefits due to the characteristics of the dispersed nanoparticle [31, 52-55], thus, the entrance of a new generation heat transfer fluid called binary nanofluids (BNFs) and ternary nanofluids (TNFs) [21, 34, 36-38, 56-58].

Binary nanofluids (HNFs) and ternary nanofluids (TNFs) is an emerging area of nanofluids research where different nanomaterial's physical and chemical properties are blended together to form a new nano-product possessing an improved homogeneous phase [21, 59-63]. This is prepared by suspending two or more different nanoparticles in composite or mixture form in basefluids. The limitation of individual conventional nanofluids necessitates this great enhancement. Literature is limited on the stability of hybrid nanofluids. Thus a comprehensive investigation into the stability of hybrid nanofluids is necessary because it is a key issue that influences the thermal-fluid behaviour of hybrid nanofluids applications. The issue of sample preparation parameters will also be investigated to see how it relates to stability. A research gap apparently exists on the trio influence of percent weight ratios (PWRs), temperature, volume concentration (φ) on the thermal properties of nanohybrids, which was experimentally examined. Furthermore, the dual effect of volume concentrations and mixing ratios on the thermo-convection performance of binary nanofluids in a squared enclosure of different temperature ranges were experimentally examined, as gaps exist here in literature as regards thermo-convection performance of binary nanofluids in various cavity geometries. Also, the growth in industrial processes has necessitated commensurate growth in heat transfer systems' efficiency by optimizing thermal processes and properties [21, 64]. Really, experimental set-ups to determine thermophysical and thermo-convection properties is quite expensive and takes time [64, 65]. So, in handling the occurrence of repeated experiments and encourage optimised big data handling, the application of Artificial Intelligence (AI) techniques [34, 66-72] (like Artificial Neural Network (ANN), Fitting Method and Group Method of Data Handling (GMDH) models, etc) were used to predict the thermophysical properties of BNFs. Considering the future of works in relation to current realities posed by Covid-19, which has led to working remotely, the application of AI option cannot but be adopted in this area of research. The study's novelty led to the development of appropriate correlations for the thermal properties.

1.3 AIM OF STUDY

This investigation aimed to experimentally formulate stable and homogenized binary nanofluids (MgO-ZnO/deionized water (DIW) and MWCNT-Al_2O_3/DIW) and ternary nanofluids (MgO-ZnO-MWCNT/DIW) using an optimized approach, performed experimental investigations by measuring the viscosity (μ), pH, thermal conductivity (κ) and electrical conductivity (σ) of the stable nanofluids, investigate the thermo-convection heat transfer performance of the stable nanofluids in a square enclosure, as well as proposed accurate models through artificial intelligence methods to predict some thermophysical properties.

1.4 OBJECTIVES

The specific objectives of this investigation were:

1. To formulate stable MgO-ZnO/deionized water, MWCNT-Al_2O_3//deionised water binary nanofluids (BNFs), and MgO-ZnO-MWCNT/deionised water ternary nanofluids (TNFs), by optimising sample preparation parameters like amplitude, sonication time, and dispersion fraction of surfactants;

2. To characterise nanoparticles and formulated BNFs and TNFs using techniques like transmission electron microscope (TEM) and ultra-violet visible spectrophotometer, respectively;

3. To measure the thermal properties of BNFs and TNFs at various volume concentrations, nanoparticles sizes (NS), temperatures, and percent weight ratio (PWR);

4. To investigate the thermo-convective behaviour of BNFs in a square cavity;

5. To develop correlations for the prediction of the thermal properties and Nusselt number of BNFs.

6. To propose accurate models to predict some thermophysical properties through artificial intelligence methods.

1.5 SCOPE OF STUDY

In this study, the impact of percent weight ratios (PWRs), nanoparticles sizes (NS), working temperatures, volume concentration (φ) was examined on the thermal properties of the formulated nanohybrids.

Experiments on thermo-convection behaviour were conducted in a square cavity at diverse temperature range (20 °C to 50 °C) under atmospheric conditions. Data of temperatures and flow rates were automatically measured by a datalogger and fed into the personal computer.

Artificial intelligence models were used to predict thermal properties based on the results of the experimental study. Artificial Neural Network (ANN) and surface fitting models were used to predict some thermophysical properties of the formulated nanohybrids.

1.6 ORGANISATION OF THE THESIS

A run-through of the structure of the chapters of this thesis is detailed in this sub-section. For proper structuring, chapters are classified as sections and subsections. The thesis comprises eight chapters in total.

Chapter 1 introduces nanofluid as an innovative working fluid for thermal management in heat transfer applications. First, the background of the study was presented, explaining the advent of nanofluids to the recent ternary nanofluids. The rest of the sub-divisions are problem statement, aim, objectives and scope of the study.

Chapter 2 presents a literature search on the formulation and measurement of thermal properties of nanohybrids. The morphology and thermo-convection performance of nanohybrids were also reviewed. The use of artificial intelligence models to predict thermal properties was reviewed as well.

Chapter 3 details the methods and materials necessary for the formulation and measurement of thermal properties of nanohybrids. The experimental setup for thermo-convection behaviour of nanohybrids in a square enclosure was stated. The chapter also explained the validation of the cavity, data reduction, uncertainty estimation, and model development.

Chapter 4 presents the experimental results for the production and morphology of the stable nanohybrids.

Chapter 5 presents the experimental results and discussion for the measurement of thermal properties of stable nanohybrids. Proposed correlations for the thermal properties of the nanohybrids were presented and discussed.

Chapter 6 details the experimental investigation, results, and discussion for the thermo-convection performance of nanohybrids in a square cavity.

Chapter 7 presents the use of artificial intelligence (AI) models to predict thermal properties based on the results of the experimental study. AI methods, like ANN and surface fitting method are employed to model some thermophysical properties of the formulated nanohybrids.

Chapter 8 details the general summary of the thesis and presents recommendations for further study.

CHAPTER 2

LITERATURE REVIEW[1,2,3,4,5,6]

2.1 INTRODUCTION

The concept of nanosuspension has gained prominence in the research field of thermal applications and applicable working fluids over the century. It kicked off with Maxwell's [9-11] formulated suspension-mix in 1873 to improve fluid properties. The colloidal suspension improved thermal conductivity, with noticeable drawbacks like pressure drop, channel clogging and sedimentation, which were limitations to achieving a meaningful engineering solution. Similar results and challenges emanated from Ahuja's [12, 13] investigation in 1975.

Choi's [73, 74] work in 1995 which was premised on Maxwell's study came with hope, thus pioneering the nanosuspension concept which has helped produced various nanofluids. Nanofluids (NFs) are better working fluids with better thermophysical properties over conventional basefluids (BFs). Nanofluids are nanosuspensions containing various nanoparticles like:

This chapter is reflected in parts in the following papers:

[1]Giwa, S., Momin, M., Nwaokocha, C., Sharifpur, M., and Meyer, J. *Influence of nanoparticles size, per cent mass ratio, and temperature on the thermal properties of water-based MgO–ZnO nanofluid: an experimental approach.* Journal of Thermal Analysis and Calorimetry, 2021. **143**(2): p. 1063-1079.

[2]Nwaokocha, C., Momin, M., Giwa S., Sharifpur, M., Murshed S.M.S., Meyer, J.P., *Experimental investigation of thermo-convection behaviour of aqueous binary nanofluids of MgO–ZnO in a square cavity.* Thermal Science and Engineering Progress, 2021. **28**: 101057.

[3]Nwaokocha, C., Giwa S., Ghorbani B., Momin, M., Sharifpur, M., Gharzvini M., Chamkha, A.J., Meyer, J.P., *Experimental formulation and GMDH modelling of thermal conductivity of MgO–ZnO/deionised water hybrid nanofluids.* Ready for submission.

[4]Nwaokocha, C., Momin, M., Sharifpur, M. and Meyer, J., *Influence of concentration, mixing ratios, and working temperature on the thermal behaviour of binary nanofluids of MgO–ZnO: an experimental investigation.* Ready for submission.

[5]Nwaokocha, C., Momin, M., Sharifpur, M. and Meyer, J., *Artificial neural network development to predict thermal conductivity of MgO–ZnO/Deionised Water binary nanofluids.* Ready for submission.

[6]Nwaokocha, C., Sharifpur, M. and Meyer, J., *Application of binary nanofluids – Emerging issues.* Ready for submission.

- Metals: copper (Cu) [75-78], silver (Ag) [56, 79-82], iron (Fe) [60, 78, 83], gold (Au) [49, 75, 84-86], zinc (Zn) [85, 87], nickel (Ni) [78, 88-91], alumina (Al) [26, 92-96];
- Metal carbides/carbides ceramics – silicon carbide (SiC) [40, 97-99], titanium carbide (TiC) [99-101];
- Nitride ceramics/metal nitrides – aluminum nitride (AlN) [47, 102, 103], silicon nitride (SiN) [104, 105], boron nitride (BN) [106-109];
- Metal oxides/oxide ceramics – aluminium oxide (Al_2O_3) [58, 96, 110-115], Tungsten-oxide (WO_3) [116-119], copper oxide (CuO) [115, 120-124], Cerium-oxide (CeO_2) [114, 125-127], titanium dioxide (TiO_2) [56, 113, 128-131], iron (III) oxide (Fe_2O_3) [31, 45, 96, 132, 133], iron (II) oxide (Fe_3O_4) [124, 134-136], silicon dioxide (SiO_2) [61, 99, 110, 137, 138], zirconium oxide (ZrO_2) [139-141], zinc oxide (ZnO) [21, 142-144];
- Carbon materials – carbon nanotube (single wall - SWCNT, double walls - DWCNT, multi wall – MWCNT, or shell composites), graphite, and nano-diamond [61, 115, 128, 130, 134, 135, 137, 145-153].

Nanoparticles (NPs) are dispersed into conventional basefluids (BF) (acetone, bio-glycol, coconut oil, engine oil, ethylene glycol (EG), glycerol, ionic fluid, organic liquid, palm oil, polymer solution (PS), propylene glycol (PG), transformer oil and water) to formulate nanofluids (NFs). This concept was first advanced by Jana et al. [43], and Chopkar et al. [44]. The drawbacks in the efficiency of NFs led to the birth of binary nanofluids (BNFs) and ternary nanofluids (TNFs), which possess improved thermal transport characteristics better than NFs and BFs. BNFs are formulated by hybridizing dissimilar nanoparticles (NPs) of varying sizes, shapes and thermal properties and thereafter dispersed into BFs. Literature abounds with several works investigating the thermophysical properties (electrical conductivity, density, viscosity, specific heat capacity, and thermal conductivity) of NFs, BNFs and THFs. They reported good augmentation at various volume concentrations for different temperatures [33, 42, 154-162]. As a result, this innovative working fluid has found wider application potentials due to its improved thermal conductivity, homogeneity, and fine stability. In recent time as well, basefluids are also mixed together before suspending nanoparticles in it, examples are: water-ethylene glycol [115, 131, 134, 163, 164], water-propylene glycol [164-167], acetone-water [168, 169], ethanol-water [168-170], etc.

The attendant issues with mono-nanofluids (single-nanoparticle based nanofluid) are assessed using the following parameters - chemical inertness, energy saving level, higher production cost, thermal behaviour, rheological properties, usefulness in diverse fields, increased pumping power defects, heat transfer behaviour, stability, etc – since they do not solely possess suitable ability for specific use. Hence, a trade-off is needed, allowing for dispersing various nanoparticles in basefluid (BF) or binary base-fluid (BBF). This is called binary nanofluid (BNF). An extension by further investigation is the development of ternary-nanofluids (TNF), which contain three different types of nanoparticles. Figure 2.1 presents the graphical summary of commonly used nanoparticles and basefluids to formulate mono-nanofluids, binary nanofluids, binary base-fluids, ternary-nanofluids [21, 31, 39, 119, 131, 149, 152, 153, 163, 171-174].

2.2 CONCEPT OF MONO, BINARY AND TERNARY NANOFLUIDS

After the preliminary works of Maxwell [9, 10] and Ahuja [12, 13], the suspension of nanoparticles was found better than the suspension of micro- sized or millimeter-sized particles. Nanofluids are engineered nanosuspension with good thermophysical properties over conventional basefluids (BFs). NFs are engineered nanosuspension having NPs of nanosizes less than 100 nm. The ground-breaking work of Masuda et al. [19] affirmed that engineered nanosuspension had found good use in heat transfer applications. They investigated the use of ultrafine particles of alumina, silica and titanium dioxide dispersed in water, which yielded an enhanced thermal conductivity than the basefluid. This ground-breaking result in thermal conductivity enhancement led to further investigation of suspending different types of NPs into conventional fluids. NPs of metals, metal carbides/carbides ceramics, metal oxides/oxide ceramics, nitride ceramics/metal nitrides, carbon materials (nanotubes/shell composites, graphite, and nano-diamond) and biomass are dispersed in different BFs like water, acetone, EG, PS, PG, etc., or mixture of both to form binary base-fluids [21, 110, 115, 119, 134, 135, 144, 164, 166, 168, 169]. The measurements of thermal conductivity gain primacy in the preceding studies, thereafter the measurements of other thermophysical properties, like viscosity, electrical conductivity, density, specific heat capacity.

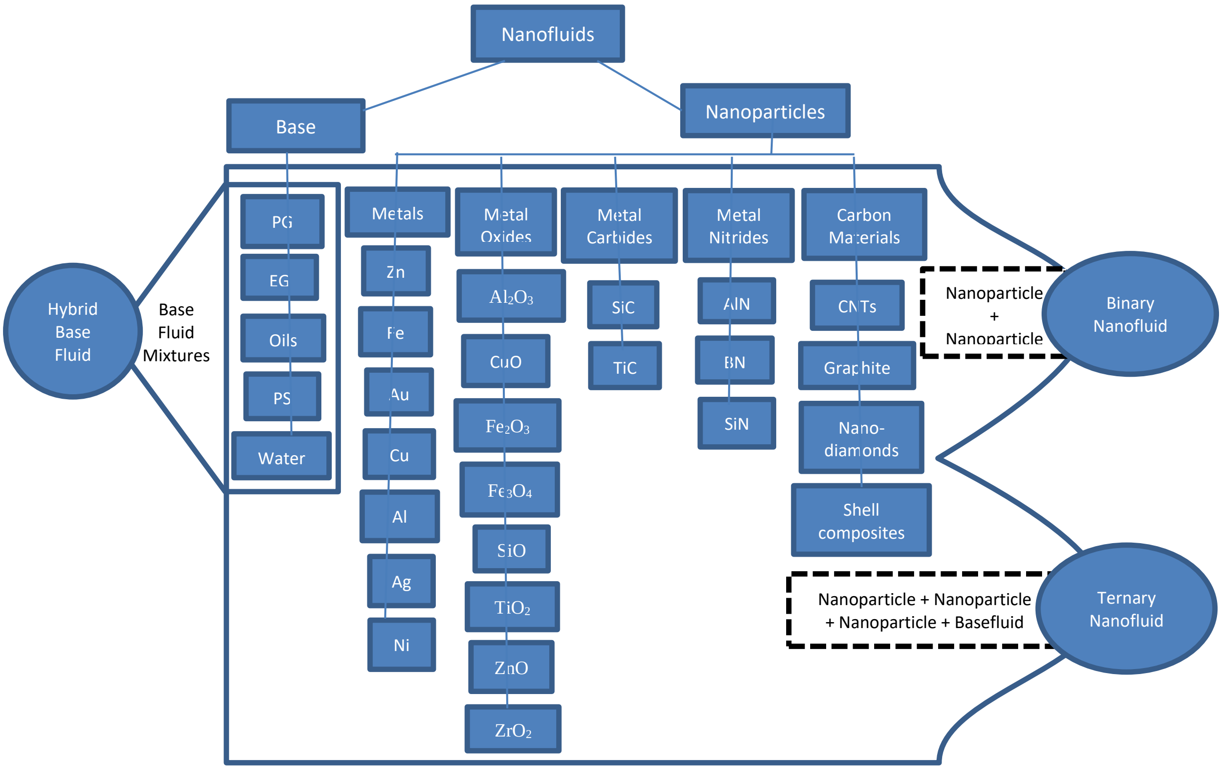

Figure 2.1: Graphical presentation showing the relationship between mono-particle nanofluids, binary nanofluids, binary basefluid, and ternary nanofluids.

The concept of thermal conductivity (κ) values of solid materials, with reference to metals having higher thermal conductivity than conventional fluids, led to the birth of nanofluids via the process of material size reduction to nano-sizes and subsequent nanosuspension into basefluids. In a similar sense, BNFs and TNFs were conceived because NPs with various thermal properties can be combined together at different weight ratios to produce better heat transfer fluids [21, 28, 31, 36, 39, 57, 96, 144]. Over a decade ago, it was first advanced by Jana et al. [43] and Chopkar et al. [44], who pioneered the idea of hybridizing diverse nano-materials for optimal thermal management. Their works reported improved thermal conductivity. Chopkar et al. [44] published a thermal conductivity improvement of 50-150% when they synthesized Ag_2Al and Al_2Cu HNPs in EG and water to formulate BNFs for volume concentration (φ) range of 0.20 to 1.50 vol.%. Contrarywise, Jana *et al.* [43] formulated and measured κ for water-based single-NFs (Au, CNT and Cu) and water-based BNFs (CNT-Au and CNT-Cu). They reported that the single-NFs had an higher κ than the BNFs. Jha et al. [34] published κ of Cu-MWCNT dispersed in DIW and EG has had higher value than that of NFs of MWCNT/EG and MWCNT/DIW, which supported the finding of Chopkar et al. [38] and was consistent with the work of Chen et al. [175], who reported an improved κ of Ag–MWCNT/Water BNF over the MWCNT/water NF.

2.3 PREPARATION OF NANOFLUIDS

The formulation of NFs is done by suspending NPs into conventional fluids, known as basefluid [157, 158, 173]. As well, the formulation of BNFs is done by dispersing two NPs into basefluid or basefluids [21, 31, 96, 172]. Also, the formulation of TNFs is done by suspending three NPs into basefluid or basefluids [36, 38, 39]. In all, the durability, stability, and chemical inertness of nanofluids is very key to real time applications, starting with the measurement of thermophysical properties and thermo-convection studies. It is established that the hybridisation of dual or more nanoparticles for the preparation of binary or ternary nanofluids reveals that an optimized blend (percent weight) ratio will be attained for which enhanced thermal properties are achieved, birthing an engineered nanosuspension with better thermal property.

The formulation of nanofluids uses either a one-step or two-step process. The one-step approach entails the simultaneous synthesis and suspension of nanoparticles in basefluids, the production of nanoparticles and preparation of nanofluids concurrently [176, 177]. This method allows for high stability and uniform dispersion. It also eliminates the burden of drying, storage and dispersals. The limitation with this method is the problem associated with commercial production and capital intensive [176]. The two-step process first entails the synthesis of nanoparticles, nanotubes and nanocomposites in powdery form by using chemical or mechanical processes like grinding, vapor phase, milling and sol-gel method, and subsequent suspension in basefluids. The two-step process is commonly reported in the literature [21, 31, 96, 176, 178], because of its ease of large-scale production for industrial application and cost-effectiveness. The drawback related to the two-step process is sedimentation and agglomeration due to the Van der Waal force of attraction among the particles.

2.4 CHARACTERISATION OF NANOFLUIDS

Different methods abound in literature for the characterisation of NFs, BNFs and TNFs for the nano-properties of their NPs, BNPs and TNPs like crystalline structure, dispersion, distribution, elemental composition, functional groups, nano-shapes/structure, nano-sizes, surface morphology, etc. These methods range from Energy Dispersive X-ray Spectroscopy (EDX or EDS), Field Emission Scanning Electron Microscopy (FESEM), Fourier Transform Infrared Spectroscopy, High-resolution transmission electron microscopy, Light scattering, Raman Spectroscopy, Scanning Electron Microscopy (SEM), Transmission Electron Microscopy (TEM), Vibrating Sample Magnetometer (VSM), X-Ray Diffractometer (XRD) [179-184]. The commonly used technique for characterising NFs, BNFs and TNFs is TEM, SEM and XRD. These methods are adopted on a stand-alone basis or combined for characterisation. TEM helps to ascertain the sizes, shapes and dispersion of NPs, BNPs and TNFs in NFs, BNFs and TNFs, respectively, as SEM is used to identify elemental mapping and surface morphology. XRD presents the crystalline structure and grain size of NPs, BNPs and TNFs in NFs, BNFs and TNFs respectively [39, 185-190].

2.5 STABILITY OF NANOFLUIDS

The process of suspending NPs, BNPs and TNPs into different BFs establishes charges in the BFs, leading to the generation of an electrical double layer (EDL) on the surface of the suspended nanoparticles. The EDL contributes actively to improving both electrical conductivity and convective heat transfer, which is a result of the active electrophoretic mobility emanating from the charged nano-suspended particles. Furthermore, the formation of EDL strongly correlates with nanosize, volume fraction, and surface charge of the nanoparticles, along with the ionic concentration of the BFs [191-193].

The even or stable distribution of NPs, BNPs and TNPs in BFs is key to using NFs, BNFs, and TNFs for engineering applications. The efficiency, optical property and thermophysical charateristics (mainly thermal conductivity and viscosity) of NFs, BNFs and TNFs has a significant relationship with the concentration of NPs, BNPs or TNPs in the nanosuspension [40, 194-197]. The use of two-step method to improve the stability of NFs, BNFs and TNFs to help remove sedimentation and agglomeration, is achieved using four techniques, viz - surfactant addition, mechanical (sonication), surface modification, and pH control techniques.

2.5.1 Methods For Enhancing The Stability of Nanofluids

2.5.1.1 Use of Dispersant

Dispersants, also known as surfactants, are chemical compositions used to stabilize nanofluids by diminishing the surface energy of host fluids, thus increasing the dispersibility of nanoparticles [198, 199]. The stability of NFs, BNFs, and TNFs is enhanced as surfactants or dispersants help reduce the interfacial tension within NPs, BNPs and TNPs. Commonly used surfactants or dispersants are Dodecyltrimethylammonium bromide (DTAB) [200], Gum

Arabic (GA) [171], Hexadecyltrimethylammonium Bromide (HCTAB) [201], NanoSperse AQ [202, 203], Oleic acid [204], Polyvinyl pyrrolidone (PVP) [171, 204], Salt [204], sodium dodecyl benzene sulfonate (SDBS) [171, 203], Sodium dodecyl Sulfate (SDS) [21, 96]. This procedure is poorly effective at a working temperature greater than 60 °C because of possible weakening of the bonds between nanoparticles and surfactants. Note, the amount of surfactant substantially influences the uniformity of suspension [204].

2.5.1.2 Mechanical (Sonication)

Sonication is a method used to achieve a uniform mixture of NPs or BNPs or TNPs when dispersed in BFs to formulate stable NFs, BNFs and TNFs. Literature affirmed that sonication impacts cluster size, absorbance wavelength, particle size, diameter of CNTs, dispersants/surfactants, thermal conductivity and viscosity [21, 31, 96, 171, 205, 206]. The time lag for sonication has been published to span minutes to hours, thus requiring an optimum sonication time to help achieve enhanced stability. Sonication time may depend on basefluid, concentration, mixing ratio of nanoparticles, shape, size, type, and preparation method, etc. [171, 204]. The ultra-sonification technique reduces the sedimentation and clustering issues in nanosuspension. After a certain time, the increase in sonication time reduces stability, thus resulting in the damage and/or heavy nanoparticle breakdown when the suspension has a low % of volume concentration range. Hence, the concept of optimum sonication time to prevent this, else further increase in sonication results in deterioration of stability and thermal conductivity of NFs, BNFs and TNFs [171, 206].

2.5.1.3 Surface Modification

The functionalisation or surface modification of NPs or BNPs or TNPs is another method used to stabilize NFs, BNFs and TNFs, without dispersants. This technique allows the dispersal of nanoparticles in BFs after functionalizing the surfaces of NPs or BNPs or TNPs using various methods. For the treated NPs or BNPs or TNPs, the sedimentation layer is not found at boiling temperature. The following methods are employed to functionalize: grafting, plasma treatment, wet mechanochemical reaction, etc. [204, 207, 208].

2.5.1.4 pH Modification

The modification of pH value can also achieve the stability of NFs, BNFs and TNFs. The dispersion of NPs or BNPs or TNPs into BFs generates surface electric charges, representing the isoelectric point (IEP) of nanohybrids (NFs, BNFs and TNFs), with zeta potential having zero value. As pH value is farther from the IEP, nanohybrids (NFs, BNFs and TNFs) gain stability and durability due to strengthened repulsive forces within the NPs or BNPs or TNPs, thus improving zeta potential [204, 207, 208]. Choudhary [209] posited that adding NaOH or HCl to NFs or BNFs or TNFs to make it a bit basic or acidic returns a durable result with enhanced zeta potential. Note that optimized pH value differs from sample to sample, thus the need to maintain a safe work environment.

In conclusion, Table 2.1 presents various methods of improving the stability of NFs, BNFs and TNFs.

2.5.2 Methods For Analysing Stability of Nanofluids

2.5.2.1 Visual Observation

Visual observation of sediments of particles (NPs or BNPs or TNPs) remains the simplest and mostly used method to examine the stability of NFs, BNFs and TNFs. Though it takes a lot of time to inspect sediments, it remains a cheap medium for stability analysis. Though not a scientific method, but with the process NFs or BNFs or TNFs can be called stable for a certain period that the nanosuspension remains consistent with time. Literature abounds with the use of this method to capture sediment's image as a guide to viewing stability [21, 31, 96, 204-206, 210, 211]. Visual inspection is used along with scientific monitoring techniques.

Table 2.1: Methods of improving the stability of NFs, BNFs and TNFs

Authors	NFs or BNFs	Size	Synthesis method	Temp.	Concen-tration	Stability technique	Stability time
Elias et al. [212]	Al_2O_3/Water-EG	13 nm	Two-step	10-50 °C	0-1%	30 min. sonication	3 days
Nikkam et al. [213]	Cu/diethylene glycol	5–100 nm	One-step	20 °C		Sonication	Several weeks
Senthilrala et al. [214]	CuO/distilled water	27 nm	Two-step	50 °C		4 hour ultrasonication	Several hours
Sundar et al. [215]	CuO/EG-water	27 nm	Two-step	15-50 °C	0.2-0.8%	2 hour ultrasonication	Stable; ZPV = -20 mV
Amiri et al. [216]	SiO_2/EG, SiO_2/Water, SiO_2-Cu/EG, SiO_2-Cu/Water	SiO_2 – 50–80nm, Cu–10nm		20-40 °C	0.002-0.01%	Surface modification by Cu and 2 hr ultrasonication	Two weeks
Sundar et al. [217]	Nanodiamond/distilled water	11.4 nm	Two-step	59.85 °C	1%	Surface modification and 2 hr bath sonication	30 days
Sundar et al. [217]	Nanodiamond/EG-Water	19 nm	Two-step	60 °C		Surface modification and 2 hr bath sonication	ZPV = -30 mV
Choudhary et al [209]	Al_2O_3/Distilled Water	20 nm			0.01-0.1%	Addition of 0.1% HCl or NaOH; 60, 120 and 180 min of sonication	16 days
Kakati et al. [218]	Al_2O_3/Deionized Water			10-50 °C	0.1-0.8%	Addition of 0.03% (wt) SDS	4-5 days
Sundar et al. [219]	Fe_3O_4/Distilled Water	13 nm	Two-step			2 hr sonication with CTAB (CTAB to NPs mass ratio – 1:10)	60 days

2.5.2.2 Zeta Potential Test

Zeta potential test is a technique for assessing the stability of nanosuspensions. The electrostatic repulsion existing amidst the particle's surface and the static layer of fluid is called zeta potential [204, 209, 210]. Thus, the correlation between zeta potential value and the stability of NFs or BNFs or TNFs. Higher zeta potential values (positive or negative) indicate a stable condition, while a lower value suggests an unstable condition. Table 2.2 presents the relationship between zeta potential value and stability of nanofluids. Literature reports the use of zeta potential test in measuring the stability of NFs and BNFs [209-211, 220, 221].

Table 2.2: Zeta potential value and stability of nanofluids [204, 220]

Zeta potential value (mV)	Stability of nanofluids
0	Instability
15	Little stability with fast particle settlement
30	Moderate stability
45	Fine stability, slight settlement
60	Excellent stability

2.5.2.3 Ultra-Violet Visible (UV-vis) Spectroscopy

The ratio of absorbency of NPs or BNPs or TNPs has a proportional relationship with the concentration of NFs or BNFs or TNFs, respectively. Spectral absorbency technique via UV-vis spectrophotometer is one of the most used and authentic techniques used to evaluate the stability of NFs, BNFs and TNFs. This method is able to constantly monitor stability at specific time intervals for a time period running to weeks and months, thus returning quantitative results equal to the concentration of NFs, BNFs and TNFs; which is an advantage over other methods [21, 206, 221, 222]. Like other methods, it is also used along with visual observation and zeta potential.

2.5.2.4 Thermophysical Properties Check

The stability of NFs, BNFs and TNFs is also defined by assessing their thermophysical properties. Giwa et al. [223] used viscosity to assess the stability of formulated MWCNT-Fe_2O_3/DIW binary nanofluid (0.5 vol%) for an experimental run time of 2580 min (43 h). Garbadeen et al. [27] used effective viscosity to monitor the stability of MWCNT/DIW for an experimental run time of 250 minutes. Joubert et al. [224] also monitored the stability of Fe_2O_3/DIW NFs for 20 hr by measuring effective viscosity.

2.5.2.5 Other Techniques

There are further techniques used to monitor the stability of nanofluids (NFs), binary nanofluids (BNFs) and ternary nanofluids (TNFs), such as centrifugation, etc. [225, 226].

2.6 THERMOPHYSICAL PROPERTIES OF NFs, BNFs and TNFs

2.6.1 Stability of Nanofluids

The thermal conductivity of NFs is widely published in the literature. Since binary nanofluids (BNFs) and ternary nanofluids (TNFs) are emerging nanohybrids, published works are also emerging fast on thermal conductivity measurement. Literature has widely reported dramatic enhancement in thermal conductivity with the additions of NPs, BNPs, and TNPs into various BFs at very low concentrations [21, 39, 42, 62, 96, 114, 128, 140, 151, 152, 156, 160, 171, 181, 188, 210, 220, 227-232]. However, with the growing volume of literature with time, some key inconsistencies were observed in the research findings. Such discrepancies in thermal properties' enhancement can result from the following factors, like applied stability methods, measurement techniques, mixing ratio, nanoparticle's purity, nanoparticle's size, particle shape, pH of the suspension, scale of agglomeration, temperature, to mention some.

Aybar et al. [233] widely reviewed the system (static and dynamics) suggested to be accountable for the atypical improvement of effective thermal conductivity as a result of the dispersion of NPs or BNPs or TNPs into different BFs. The static system presumed that NPs are stationary in NFs and this entails - aggregation, fractal geometry, interface thermal resistance, nanolayering, and percolation, while the dynamic components assumed chaotic movement of NPs in NFs, like Brownian motion and nanoscale convection. Masuda et al. [19] first measured effective thermal conductivity of NFs and published a κ enhancement of 30%, when alumina NPs (13 nm) was suspended into the water at φ = 4.3 vol.%. Studies on the formulation and measurement of thermal conductivity (κ) of NFs seems to be on the increase. Jana *et al.* [43] formulated and measured κ for aqueous-based single-NFs (Au, CNT and Cu) and observed a lower value than the BF. Choi and Eastman [20] reported a 3.5-fold κ improvement for aa aqueous-based Cu NF at φ = 20 vol.%. Again, Choi et al. [234] studied the κ of water-based NF using SWCNTs. They reported a 19.40% improvement of 0.89 wt% at SWCNT. Also, Agarwal et al. reported an enhancement of 31% and 30% for κ_{eff} for EG- and DW-based Al_2O_3 NFs at temperature of 70 °C and φ = 2.0 vol.%. Next, Pastoriza-Gallego et al. formulated Fe_2O_3/EG and Fe_3O_4/EG NFs at φ = 0.011 – 0.069 vol.% and temperature 10 – 50 °C and reported a κ_{eff} enhancements of 2% – 15% and 1% – 11%, respectively. Wang et al.

[235] published the κ_{eff} of Cu/DIW and Al_2O_3/DIW NFs with an enhancement of 18% and 15% for weight fraction of 0.8% at room temperature.

Recent works were also published on the formulation and measurement of thermal conductivity (κ) of BNFs and TNFs, majorly on the factor of temperature and φ. Chopkar et al. [44] reported an improved κ of 50-150% when Ag_2Al and Al_2Cu HNPs were synthesized in water and EG to prepare BNFs for φ range of 0.20 to 1.50 vol.%. Amiri et al. [216] examined the κ of single-NFs (SiO_2/EG and SiO_2/water) and compared with κ results of BNFs of SiO_2-Cu/EG and SiO_2-Cu/water. The authors reported that the steady addition of SiO_2 NP leads to 2% enhanced κ and increasing deposition of Cu NPs produces about 11% and 11.5% augmentation of κ of EG and water, respectively. They investigated the effect of temperature (25 to 50 °C) and φ range 0.10 - 3.50 vol.%, Toghraie et al. [236] formulated ZnO-TiO_2/EG BNF and reported an enhanced κ under increasing φ and temperature. The highest κ enhancement of 32% was observed at 3.5 vol.% for temperature 50 °C. Investigating using MWCNT (0.05 vol%)–Fe_2O_3 (0.020 vol.%) aqueous-based BNF at room temperature, Chen et al. [237] reported augmentation of 27.75% over the BF. Again, Chen et al. [175] published an enhanced κ of Ag–MWCNT/Water BNF over the MWCNT/water NF for a 1.0% volume fraction and temperature range 5–65 °C. Next, Askari et al. [238] studied the κ for Fe_3O_4–Graphene (20:80)/DIW nanohybrid at a mass percentage of 0.1–1.0 mass% under the influence of increasing temperature 20–40 °C, which reported an improvement of 14–32%. Furthermore, Esfahani et al. [239] investigated the κ of aqueous-based ZnO-Ag (50%:50%) BNF at temperature 25–50 °C and φ of 0.125–2.0% and reported the highest κ at 50 °C and 2.0 vol%. Recently, Rostami et al. [240] studied the κ for CuO–GO(50:50)/EG-W(50:50 vol%) nanohybrid at increasing φ of 0.10 to 1.60 vol.% for temperatures 25 to 50 °C. They obtained the highest enhancement of 43.4% when φ was 1.6 vol% at 50 °C. In addition, Harandi et al. [241] published 30% improvement for thermal conductivity ratio (TCR) of FMWCNTs-Fe_3O_4/EG HNF for the particle concentration 2.30

vol.% at 50 °C. They further discovered that temperature visibly influenced TCR at higher concentrations. Lately, the influence of variation in φ (0.005–0.1 vol%), temperatures (25–40 °C), and PMRs (30:70, 50:50, 70:30) on the κ of Al_2O_3-Ag/DW BNF was examined by Aparna et al. [227]. The authors published the highest κ with the 50:50 ratio. The BNF had a maximum κ than the NFs of Ag/DW and Al_2O_3/DW. Rostami et al. [123] also published a 30.8% augmentation in κ at 0.60 vol.% for CNT-CuO/Water nanohybrid. Also, Du *et al.* [156] studied TCE of water-based Fe_3O_4 NF and Fe_3O_4-MWCNT BNF for temperature ranges 25–50 °C for φ = 0.2–1.0 vol%. The NF and BNF achieved κ enhancement of 32.76% and 33.23% at 50 °C and 1.0 vol%, respectively. The nanohybrid of Fe_3O_4-MWCNT obtained κ of 0.47%. Again, Soltani et al. [242] determined κ for MWCNT-Tungsten oxide/engine oil BNF, and reported a highest improvement of 19.85% at 60 °C and 0.6 vol% of the HNPs. More recently, Wole–sho et al [179] also examined the influence of changing temperatures 25 to 40 °C at φ of 0.33–1.67 vol% and NMRs (1:2, 1:1, 2:1) of distilled water-based Al_2O_3-Zn nanohybrid. The κ enhancements values are 35%, 36%, and 40% for PMRs of 1:1, 1:2, and 2:1 respectively, at φ = 1.67 vol% and 40 °C. Gangadevi and Vinayagam [243] compared the κ performance for water-based NFs of CuO and Al_2O_3 and BNF of CuO-Al_2O_3 (50:50) for changing φ (0.05–0.20 vol%) and temperature (20–60 °C). κ improved at 21%, 12.16%, and 11.2%, for CuO- Al_2O_3/W BNF, CuO/W NF and Al_2O_3/W NF respectively, at 0.20 vol% and 60 °C in comparison with BF. The nanohybrid effectively reduced the temperature of a hybrid solar collector, thus improving overall system efficiency. Considering changes in temperatures (30–60 °C), PMRs (25:50, 50:50, and 75:25) and φ (0.1–0.5 vol%), Mechiri et al. [244] evaluated experimentally for κ of Cu–Zn (50:50)/groundnut HNF. They observed that φ and temperature had impact on κ more than PMR.

In addition, the formulation of green NFs (GNFs) was also noticed to enhance thermal conductivity (κ), with great potential for the future considering environmental factors. Khdher et al. [48] examined the κ_{eff} of Al_2O_3 NPs suspended in different BFs - green BF (bio-glycol), EG, and PG and reported κ_{eff} augmentation of 17%, 9%, and 3.6% (1.0 vol.% and 30 °C), respectively. Yarmand et al. [102] also studied the κ_{eff} of BNF (0.02 – 0.6 wt.% and 20 – 40 °C) formulated using synthesised NPs of fruit bunch and GO NPs dispersed in EG, and published a maximum augmentation of 6.47% at 0.06 wt.% and 40 °C.

Considering TNFs, Ahmed et al. [189] examined κ_{eff} of ZnO-Al_2O_3-TiO_2/DW TNF for temperatures 20 to 45 °C for wt.% concentrations of 0.025, 0.05, 0.075, and 0.1. The authors reported an increasing trend in κ_{eff} as temperature values increases. The suspension of all metal oxide NPs in distilled water resulted in an enhancement in κ_{eff} steadily by the variations in nanofluids temperature, which makes it good for heat transfer applications. Also, Mousavi et al [24] elucidated the effects of NPs volume concentration (0.1–0.5%) and temperature (15–60 °C) on the κ of aqueous-based CuO–MgO–TiO_2 TNF. The authors published an increased κ at increasing temperature and solid particles volume concentration. Next, Xuan et al. [39] reported that mixing ratio 40:40:20 (Al_2O_3:TiO_2:Cu) had the optimum thermal conductivity for a water-based Al_2O_3:TiO_2:Cu TNF, measured at 0.005-1 vol.% over temperature 20 – 60 °C. Again, Cakmak et al. [245] formulated a rGO-Fe_3O_4-TiO_2 TNPs dispersed in EG for 0.01–0.25 mass.% and over temperature 25 – 60 °C. They reported a significant κ increase with increase in mass concentration and temperature, with maximum enhancement achieved at 13.3% at 60 °C for 0.25 wt.%, making it useful for both cooling and heating applications with long term stability.

2.6.2 Viscosity

Viscosity (μ) is a thermal property that defines the resistance to flow of fluid under shear stress. The dispersion of NPs, BNPs and TNPs into BFs produced an increased effective viscosity (μ_{eff}). The enhancement in μ_{eff} associated a related increase in κ_{eff} (with an increase in φ) through improved heat transfer of NFs, BNFs and TNFs for thermal applications, at the cost of high pump power. Hence, the challenge of using nanofluids for thermal transport applications. It is of note that at high φ, high μ_{eff} overrules the advantage of high κ_{eff} and thus deteriorates heat transfer rather than enhancement when nanofluids is adopted as coolants for thermal systems. But, at lower φ, which denotes lower μ_{eff}, nanofluids works well as heat transfer fluid. Viscosity is reported to be dependent on parameters like temperature, pH, nano-shape, nano-size, sonication time and intensity, and volume concentration [246]. The entrance of BNFs and TNFs for thermal applications also calls for μ_{eff} measurements [21, 30, 32, 68, 83, 96, 119, 148, 151, 160, 172, 185, 188, 205, 210, 223, 228, 247-255]. It is well observed for the trio of NFs, BNFs and TNFs that temperature increase leads to a reduction in μ_{eff}, while a rise in φ produced an increment in μ_{eff}. Soltani and Akbari [256] examined the effect of temperature 30 to 60 °C and particle concentration 0 to 1.0% on μ of MgO-MWCNT/EG BNF and reported a Newtonian behavior with μ in a reducing trend at temperature increase and enriched μ at increased particle concentration. Also, Esfe et al. [257] evaluated the μ of an aqueous-based nanohybrid of Ag–MgO (50:50) for φ = 0–2%, and achieved enhancement with increasing φ. Suresh et al. [258] achieved an enhancement of 8–115% for μ for an aqueous-based Cu-Al_2O_3 (10%:90%) BNF at φ = 0.1–2%. Next, Asadi and Asadi [252] examined the μ of MWCNT-ZnO/Engine Oil (10W40) BNF and reported temperature having a higher impact on μ than particle concentration, thus achieving a maximum deterioration in dynamic viscosity of 85% for temperature 55 °C. Also, Afrand et al. [250] computed a recent model to predict μ of hybrid nanolubricant of MWCNT–SiO_2/AE40 using experimental values. They further developed an optimized ANN model to predict μ, making a comparison. They reported the ANN model having better performance than the empirical model. Next, Gangadevi and Vinayagam [243] compared μ performance for water-based NFs of CuO and Al_2O_3 and BNF of CuO-Al_2O_3 (50:50) for increasing φ (0.05–0.20 vol%) and temperature (20–60 °C). μ improved at 2–11% as compared with aqueous-based CuO NF, Al_2O_3/W NF had the minimum. The nanohybrid effectively reduced the temperature of a hybrid solar collector, thus improving overall system efficiency. In addition, Alirezaie et al. [259] examined the rheological behaviour of *f*MWCNT-MgO/Engine oil BNF and reported an abrupt reduction in μ with temperature. Further observation was a non-Newtonian behaviour at reduced temperature and Newtonian at higher temperatures. Recently, Motahari et al. [260] experimentally studied the μ of MWCNT-SiO_2/SAE20W50 nanohybrid at φ = 0.05–1.0 vol% and temperature range 40 to 100°C. The nanohybrid exhibited Newtonian behaviour for all concentrations and temperatures, with an enhanced μ of 171% at peak particle concentration and temperature.

Considering changes in temperatures (30–60 °C), PMRs (25:50, 50:50, and 75:25) and φ (0.1–0.5 vol%), Mechiri et al. [244] evaluated experimentally for μ of Cu–Zn (50:50)/groundnut HNF. They observed that φ and temperature affect μ more than PMR. Both BF and nanohybrid exhibited Newtonian behaviour. Also, Hamid et al. [261] studied μ for TiO_2–SiO_2 (40–60)/W-EG (60:40) BNF for varying PMRs (20:80–80:20) for temperatures 30–80 °C at φ = 1.0 vol%. They reported a maximum improvement for μ for PMR 40:60, which makes it good for thermal cooling purposes. PMR of 50:50 has the poorest cooling properties. Also, Giwa et al. [172] investigated the impact of PMRs (20:80, 40:60, 60:40, 80:20, and 90:10) and different temperatures 15–55 °C on the μ of Al_2O_3–MWCNT/DIW BNF. They obtained a peak augmentation of 288.0% and 442.9% for μ of Al_2O_3–MWCNT/DIW BNF at PMRs of 20:80 and 90:10, respectively, compared to DIW. Also observed is that with increasing temperatures, μ deteriorates significantly, making it viable for engineering systems. Again, Giwa et al. [96] first investigated the trio effects of temperatures 20–50 °C, φ (0.05–0.75 vol.%), and BFs (EG-DIW and DIW) on the performance of μ of nanohybrid of Al_2O_3– Fe_3O_4 (25:75). They reported that μ was improved by 3.23–43.64% and 2.79–49.38% for the DIW-based and EG–DIW-based nanohybrid compared to the individual BF. They further discovered that enhancing φ improves μ for the two BNFs, while an augmented temperature deteriorated μ. The DIW-based

BNF possessed minimal μ over the EG–DIW-based nanohybrid. Furthermore, Giwa et al. [154], for the first time, experimented with the trio influence of PWRs (20:80, 40:60, 60:40, 80:20), NS and temperature (20–50 °C) on the thermal behaviour of MgO (20 and 100 nm)-ZnO/DIW BNF at 0.1 vol%. Authors reported that BNF with 100 nm MgO NP had higher values of μ than that of BNF with 20 nm MgO NP. Also, it observed that temperature increase deteriorates μ. The highest augmentation for μ was 8.29–17.46% (60:40). More recently, Wanatasanapan et al. [262] studied the impact of Al_2O_3-TiO_2 NPs mixing composition on the thermal-fluid behaviour of the water-based BNFs. The water-based BNFs were formulated with five various ratios of Al_2O_3 and TiO_2 NPs at a constant 1.0 vol% for temperatures 30–70 °C. The BNFs exhibited a Newtonian fluid pattern for all NPs temperature and mixing ratios, with ratio 80:20 having the maximum μ of 1.98 mPas.

In addition, the formulation of green NFs (GNFs) for the measurement of viscosity was reported. Adewumi et al. [247], Kallamu et al. [254], and Sharifpur et al. [158] published the μ_{eff} of GNFs formulated by dispersing synthesised NPs of coconut fibre carbon, banana fibre, and mango bark into EG-DIW (60:40), DIW, DIW, respectively. They reported a similar pattern for μ_{eff} of GNFs compared with NFs under increasing temperature and φ. Adewumi et al. [247] and Kallamu et al. [254] reported μ_{eff} enhancement of 50% (1 wt.% and 60 °C) and 22% (60 °C and 1.5 vol.%) for the coconut fibre carbon and banana fibre NFs in comparison to EG-DIW and DIW, respectively. In addition, Yarmand et al. [263] [102] first formulated and measured the μ_{eff} of binary green-metallic nanofluid, prepared by despersing synthesised NPs of fruit bunch and GO NPs into EG. They published a maximum μ_{eff} improvement of 4.16% (0.06 wt.% and 40 °C) compared to EG.

For TNFs, Zayan et al. [38] reported that the deionised water dispersed graphene-based TNFs (GO-TiO2-Ag and rGO-TiO2-Ag) exhibited a Newtonian behaviour at higher concentrations. Also, Ahmed et al. [189] reported higher viscosity values at 0.1 wt.% concentrations of ZnO-

Al_2O_3-TiO_2/DW TNF, compared to the other three concentrations (0.025, 0.05 and 0.075 wt.%) at similar experimental conditions. Furthermore, Mousavi et al. [24] elucidated the effects of NPs volume concentration (0.1–0.5%) and temperature (15–60 °C) on the dynamic viscosity of aqueous-based CuO–MgO–TiO_2 TNF. The authors published an increased dynamic viscosity at increasing temperature and solid particles volume concentration. All TNF samples displayed Newtonian behaviour. Next, Xuan et al. [39] reported that mixing ratio 40:40:20 (Al_2O_3:TiO_2:Cu) had the lowest viscosity for a water-based Al_2O_3:TiO_2:Cu TNF, measured at 0.005-1 vol.% over temperature 20 – 60 °C.

2.6.3 Electrical Conductivity

The electrical conductivity (σ) of nanohybrids is the ability to enhance the mobility of electrical charges due to ionized nanoparticles activated during nanodispersion, thus making it conduct electricity upon applying an electric potential across it. This property aids the monitoring of stability and the extent of suspension of NPs in the basefluids [21, 31, 96, 172, 204, 255, 264, 265]. Unlike viscosity and thermal conductivity, literature are emerging on the σ of NFs, BNFs and TNFs, compared to viscosity and thermal conductivity. This thermal property σ has direct and strong relation with electrostatic characteristics (IEP, EDL, and zeta potential), φ, nanosheets φ, NPs size, and nanosheets charge and stability of NFs/BNFs/TNFs [21, 30, 172, 223, 266-269].

The formulation of various NFs, BNFs and TNFs from different NPs and basefluids, literature reports that the electrical conductivity of NFs, BNFs or TNFs either augmented with temperature increase and mass/volume fraction or concentration [21, 30, 103, 172, 223, 238, 267, 269-271] or independent of temperature [30, 272, 273], or distracted with a rise in volume/mass concentration or fraction [274, 275]. Considering the impact of φ (0.5 – 3.0 vol.%), temperature (20 – 70 °C) and nano-sizes (20 nm and 100 nm), Adio et al. [271] published a highest enhancement of 6000% for σ_{eff} of MgO/EG NF, which increases as temperature, φ, nano-size increases too. For temperature 25 – 45 °C and φ (0 – 100 vol.%), Guo et al. [276] formulated SiO_2/EG-W nanofluids for 0.3 wt.% and measured an augmented σ_{eff} at increased temperature and reduced EG content of basefluid. Next, Shoghl et al. [277] investigated the σ_{eff} of aqueous-based nanofluids of Al_2O_3, CNT, CuO, MgO and ZnO, at 27 °C and noticed that the augmentation of σ_{eff} is dependent on an increase in φ and types of nanoparticles. ZnO/W nanofluid produced the highest σ_{eff} for lower φ and CNT/W nanofluid yielded the maximum σ_{eff} at high φ.

Also engaging BNFs, Yarmand et al. [263] investigated the σ_{eff} of green-metallic BNF and observed augmentation as temperature and φ increases, with maximum enhancement of 787.5% at 0.06 wt.% for 45 °C. Similar results align with the works of Adio et al. [269, 271], Awua et al. [32], Giwa et al. [21, 96, 223], Heyhat et al. [278], Naddaf et al. [279]. For TNFs, Manjunatha et al. [280] mathematically defined the σ of aqueous based TiO_2-SiO_2-Al_2O_3 TNF.

2.6.4 Specific Heat Capacity

Specific Heat Capacity (C_p) is another significant thermal property of NFs, BNFs and TNFs. It is described as a measure of the heat retentive property or heat storage capacity of NFs, BNFs and TNFs [281, 282]. Thus, defining the thermal behaviour of the NFs/BNFs/TNFs. It is a key parameter for assessing energy and exergy performance [282, 283]. Also useful for computing thermal conductivity [282, 284], thermal diffusivity [285, 286], spatial temperature within a flow [287] and for assessing the convective flow positions [288] of NFs/BNFs/TNFs. A huge research gap exists on the latter. The limited literature on the measurement of C_p posits that two sets of BFs (high and low temperature) are needed for suspending various NPs, BNPs and TNFs in it at different temperatures and mass/weight/volume fractions or concentrations [30, 283]. For the type with high temperature, molten nanosalts is used as BFs, while conventional BFs (DW, DIW, EG-DIW, EG, EO, ionic liquids, PG, thermal oil, W, etc.) is used for the low-temperature category. Note, measured values of $C_{p\text{-}eff}$ will differ in line with the BFs type, all a function of temperature, φ, and nano-size.

A lot of disparity is reported in the literature on the impact of temperature and φ on the $C_{p\text{-}eff}$ property of NFs/BNFs/TNFs. Reviewing NFs, Robertis et al. [289] examined the $C_{p\text{-}eff}$ of Cu–EG NF and observed a C_p enhancement with rise in temperature, while a rise in φ led to reduction in $C_{p\text{-}eff}$ (values lower than C_p BF). A similar pattern was noticed by Vajjha and Das [290], who investigated the $C_{p\text{-}eff}$ of EG-DW(60:40)-based Al_2O_3, ZnO, and SiO_2 NFs for increasing temperature (42 – 90 °C) and φ (2 – 10 vol.%). Similar temperature rise improved $C_{p\text{-}eff}$, but reduced with an increased φ, and $C_{p\text{-}eff}$ of NFs found lower than that of the BF. A slight shift was published by Ijam et al. [272], who reported a $C_{p\text{-}eff}$ enhancement for $\varphi < 0.05$ wt.% by 3.59% – 5.28% as temperature rises when GO/DW-EG NF was examined for temperature (25 – 60 °C) and φ (0.01 – 0.1 wt.%).

A contrasting pattern was advanced by Oster et al. [291], who reported a $C_{p\text{-}eff}$ enhancement for ionanofluids at both temperatures (25 – 90 °C) and φ (0.5 – 3.0 wt%) increases. Similar trend was published by Yarmand et al. [263], who reported a $C_{p\text{-}eff}$ enhancement as both temperature and φ increases for an EG-based green-metallic BNF. At 50°C, $C_{p\text{-}eff}$ was enhanced by 2.25% for φ of 0.060 wt.%. For TNFs, Mousavi et al [24] elucidated the effects of NPs volume concentration (0.1–0.5%) and temperature (15–60 °C) on the specific heat capacity of aqueous-based CuO–MgO–TiO_2 TNF. The authors published an initial decrease of up to 35 °C and thereafter enhanced with increasing temperature. These values will be due to the individual C_p of NPs and the nanolayer effect.

2.6.5 Density

Density (ρ_{eff}) has a direct relationship with Nusselt number (*Nu*), Rayleigh number (*Ra*), friction factor, Reynolds number (*Re*), and pressure drop of NF for convective heat transfer.

As a thermal property of NFs/BNFs/TNFs, it is scarce in the literature but reported along with other thermal properties [24, 56, 105, 155, 189, 238, 263, 277]. Literature report an augmentation in ρ_{eff} as NPs, BNPs and TNPs is dispersed in various basefluids and detracts as temperature rises, because NPs, BNPs and TNPs possess higher density than basefluids [24, 30, 155, 189, 238]. For NFs, Sharifpur et al. [155] reported a ρ_{eff} augmentation for NFs (CuO-GL, MgO-GL, SiO_x-EG/Water (60:40), and SiO_2-W) as φ raised from 1.0 – 6.0 vol.% and detracted as temperature progressed 10 – 40 °C. Shoghl et al. [277] published a similar pattern of enhanced ρ_{eff} as φ rises from 0.01 – 2 wt% and detracts with temperature rises 30 – 40 °C for water-based Al_2O_3, CuO, MgO, MWCNT, TiO_2, and ZnO NFs.

For BNFs and TNFs, literature reporting the measurement of ρ_{eff} is quite limited. Yarmand et al. [263] published a highest augmentation of 0.090% for 20°C at φ of 0.060 wt.% for EG-based green-metallic BNF. Askari et al. [238] reported similar trend for ρ_{eff} enhancement for Fe_3O_4-G/DIW BNF. For TNFs, Mousavi et al. [24] elucidated the effects of NPs volume concentration (0.1–0.5%) and temperature (15–60 °C) on the density of aqueous-based CuO–MgO–TiO_2 TNF. The authors reported a light enhancement in a linear pattern concerning NPs loading. Note, density is linearly deteriorated as the temperature of the TNFs increases. Also, Ahmed et al. [189] reported a reduction in density as temperature increases for all wt.% (0.025, 0.05 and 0.075 wt.%) for ZnO-Al_2O_3-TiO_2/DW TNF.

2.6.6 Other Properties

Other measured thermal properties of NFs in open literature are breakdown voltage [292-294], contact angle [295-297], extinction coefficient [153, 196, 298], flash point [299, 300], shear stress [301, 302], surface tension [142, 297], transmittance [153, 196, 303], volumetric heat capacity [153, 304]. Also, for BNFs, the following are reported - breakdown voltage [305, 306], contact angle [143, 307], extinction coefficient [308, 309], flash point [310], shear stress [39, 311], surface tension [143, 312], transmittance [308, 309]. Using TNFs, the following were measured - contact angle [313], extinction coefficient [314, 315], shear stress [24, 188], surface tension [24, 316], transmittance [314].

2.7 THERMO-CONVECTION OF NFs, BNFs and TNFs IN CAVITIES

Thermo-convection or natural convection persists in finding increasing use [78, 161, 317-325] in thermal-based systems, with the growing application of BNFs and TNFs as optimum thermal fluids due to their improved thermal properties when compared to NFs and traditional fluids. Thermo-convection or natural convection is a heat transfer method in which thermal transport is basically dependent on the density gradients of applied working (thermal) fluid. Thermo-convection applications span agriculture, aviation, desalination, electronic cooling system, geophysical systems, heat exchangers, industrial processes, nano-lubrication, nuclear energy, photovoltaic modules, power generation, solar energy transport, telecommunication, to thermal energy storage systems.

Khanafer *et al.* [326] analytically pioneered the natural convective properties of nanofluids (Cu/Water) inside a squared enclosure. Thus, more investigation with the use of nanofluids, BNFs and TNFs for free convection in different enclosure shapes (more prominent is squared enclosure, others are cylinder, porous, rectangular, and triangular) continue to accumulate momentum, either by numerical method or experiment-based [25-27, 29, 70, 102, 253, 317, 321, 327-332]. The parameters that impact thermo-convection performance are cavity design, the concentration of NPs, nanofluids types, PWRs, and particle density. Putra et al. [333] first experimentally studied the thermo-convection behaviour of nanofluids inside a cavity. The laboratory set-up employed distilled water-based Al_2O_3, and CuO NFs at φ of 1-4 vol%, charged inside a differentially-heated cylindrical shaped (positioned horizontal-wise) with aspect ratio (AR) equals to 0.5 - 1.5. The experimental set-up yielded a detracted their-convection performance, as estimated by aspect ratio, φ and ρ of nanoparticle sample.

2.7.1 Square Cavities

Using NFs, Kouloulias et al. [159] investigated the thermo-convection heat transfer of Al_2O_3/W (0.01 – 0.12 vol%) NF within a square enclosure. The authors observed a heat transfer deterioration compared to the BF. Next, Hu et al. [334] investigated the impact of various weight concentrations (3.85 – 10.71 wt.%) of TiO2/DIW nanofluid inside a square enclosure experimentally and observed a heat transport depletion as related to basefluid. Li et al. [335] studied the impact of ZnO nanoparticles dispersed in EG/DIW (25/75; 15/85; 5/95 vol%) basefluid with φ of 5.25 wt.% inside a square enclosure. Authors published a heat transfer detraction compared to EG-DIW, but augments as EG rises in the mixture ratio of basefluid. Also, studying the impact of volume concentrations, Garbadeen *et al*. [27] examined the thermo-convection behaviour of MWCNT/Water nanofluid experimentally inside a squared enclosure for φ of 0 to 1.0 vol.%, and $Ra = 10^8$. An optimal heat transfer enhancement of 45% was recorded at 0.1 vol.%.

The free convective heat transfer of DW-based Al_2O_3 (0.1 – 4 vol.%) NF charged into three separate square cavities was examined by Ho et al. [336], with a heat transfer enhancement at lower φ (0.1 vol.%) for all cavities and augmented with cavity size. Heat transfer enhancement was maximum with the largest cavity at 18% when compared to DW. In addition, Joshi and Pattamatta [337] examined by experiment the thermo-convection behaviour of Al_2O_3/Water and MWCNT/Water nanofluids inside a square enclosure, at φ of 0.1-2 vol.% for Al_2O_3/Water nanofluids and 0.10-0.50% for MWCNT/Water nanofluids. An improved Nusselt number was recorded for the two nanofluids at enhanced *Ra*, and maximum *Nu* enhancement at 0.10 vol.%, while MWCNT/Water nanofluids possessing maximum *Nu* improvement. Solomon et al. [338] experimented with the impact of aspect ratios (1, 2, 4) on enclosures on the natural convection of water-based Al_2O_3 NFs. They observed that the aspect ratios of the enclosure had a major impact on the heat transfer coefficient and *Nu*. They reported an optimal heat transfer for each aspect ratio of the enclosures to correlate with NF concentration. For an aspect ratio of 1, the convective heat transfer coefficient and highest heat transfer were achieved for 0.10 vol%. It was also observed that *Ra* had a big influence on buoyancy and the *Nu*.

Open literature is just gaining numbers as regards BNFs. Thus an excellent thermo-convective performance is observed when compared to nanofluids. Giwa et al. [329] pioneered the laboratory study of natural convection behaviour of Al_2O_3-MWCNT (95:5 and 90:10)/DIW BNF inside a squared enclosure at φ of 0.10 vol%, that produced an enhanced heat transfer over that of Al_2O_3/DIW NF and BF. Further study by Giwa et al. [317] investigated the effect of percent weight ratios (80:20, 60:40, 40:60, 20:80 for MWCNT/Al_2O_3) for 0.10 vol.% at *Ra* of 1.65×10^8–3.80×10^8 on natural convection behaviour in a squared cavity. The BNF sample with 40:60 PWR got the maximum values for *Ra*, Nu_{av}, h_{av}, and Q_{av} at various temperatures. When compared with basefluid, the highest enhancement of 16.20%, 20.50% and 19.40% were achieved for Nu_{av}, h_{av}, and Q_{av}, respectively, at $\Delta T = 50$ ^oC. Results demonstrate an increase of heat transfer coefficient with increasing temperature difference. However, nanoparticles concentrations reveal interesting trends, such that the lowest concentration (0.05 vol.%) produced maximum heat transfer coefficient, which detracts with growing concentration.

2.7.2 Triangular Cavities

Literature is limited on the experimental investigation of thermo-convection performance using triangular enclosures. Umar et al. [339] conducted a thermo-convection experiment for ZrO_2/W nanofluid in triangular and rectangular channel geometry and recorded HTC improvement of 5–10% for volume concentration (φ) of 0.05 vol.% in comparison to BF. Next, the influence of two empirical models with an experimental-based model on the *Nu* and *h* ratio of water-based SiO_2 (0.5 – 2.0 vol.%) nanofluid inside a triangular enclosure was examined by Mahian et al. [340]. The authors recorded a detraction in Nusselt number (*Nu*) with increased volume concentration (φ), an independent parameter of *Ra*. For any *Ra*, *h* of nanofluid was noticed to be more than BF. Maximum heat transfer was achieved at volume concentration (φ) of 0.5 vol.%.

2.7.3 Rectangular Cavities

Open literature is replete with the use of rectangular cavities for thermo-convection heat transfer. Sharifpur et al. [330] studied the thermo-convection performance of TiO_2-DIW (0.05 – 0.8 vol.%) NF inside a rectangular cavity and noticed enhanced heat transfer between 0.05 – 0.2 vol.% and detracted thereafter. The highest augmentation of 8.2% was reported at 50 °C and 0.05%. Ghodsinezhad et al. [25] published a 15% increase for convective heat transfer coefficient (HTC) for Al_2O_3 (0.05 – 0.6 vol.%)/DIW nanofluid in a rectangular cavity at φ = 0.1 vol.%. For weight concentration of 0-1.0 wt% for MWCNT/thermal oil nanofluids, charged in a rectangular cavity (vertical), Ilyas *et al.* [341] observed a detraction for *Nu* and *h*, while φ rises. In addition, Nnanna et al. examined the free convection behaviour of Al_2O_3 (0.2–8 vol.%)/DIW NF within a rectangular cavity and noticed a heat transfer augmentation for 0.2–2.0 vol.% thereafter deteriorated at over 2%. Maximum enhancement was observed at 0.2 vol.%. Next, Solomon et al. [331] investigated the thermo-convection heat transfer behaviour of green (Mango bark/DIW) nanofluid in a rectangular enclosure for φ of 0.01–0.50 vol%. They recorded a detracted heat transfer coefficient in relation to basefluid. A rectangular cavity having MWCNT-hexylamine/TO (0.001 – 0.005 wt.%) NFs was studied by Amiri et al. [292] for thermo-convection performance [143] and recorded an enhanced *Nu* and *h* of NFs over the BF, which increased with φ. Choudhary [342] tested the impact of φ (0.01% & 0.1%) for DIW-based Al_2O_3 NFs with ARs (0.3-2.5) for a rectangular enclosure for heat transfer behaviour. They recorded that natural convection behaviour is dependent on AR, φ, and *Ra*, for the highest enhancement of 29.50% for 0.010 vol.% (for AR of 0.5 and $Ra = 7.89 \times 10^8$). Lately, Sharifpur et al. [173], for the first time, investigated the free convective heat transfer of ZnO/DIW nanofluid inside a rectangular enclosure for diverse φ (0.100, 0.180, 0.360, 0.50, and 1.0 vol.%). They published an improved heat transfer coefficient of 9.14% when related to DIW, for 0.1 vol.% and change in temperature 32 °C. So, the free convection performance of the nanofluid detracted when volume concentration (φ) increased over 0.10 vol%. Then, *Nu* and heat transfer rate enhanced by 8.42% and 6.75% for 0.10 vol%, respectively.

2.7.4 Cylinder Cavities

Putra et al. [333] tested the natural-convection within a cylinder (horizontal) geometry of aspect ratio (0.5–1.5) having DW-based Al_2O_3 and CuO (φ = 1–4 vol.%) nanofluid. The authors recorded a detraction in heat transfer due to AR, φ and nanoparticle density. Next, Ali et al. [343] experimented with free convection inside a cylinder geometry of aspect ratio (0.0635 and 0.127) and φ (0.21–0.75 vol.%) for Al_2O_3/DW nanofluid. A diminishing heat transfer performance was observed due to aspect ratio and φ when compared to basefluid. Also, Mahrood et al. [344] examined the thermo-convection behaviour within a cylinder (vertical) geometry of AR (0.5 – 1.5) with carboxymethyl cellulose-based TiO_2 and Al_2O_3 nanofluid. They published maximum enhancement of 23.5% and 19.5% for φ = 0.1 vol.% and 0.2 vol.% for TiO_2 and Al_2O_3 nanofluid, respectively. Also, AR improvement augments *Nu* for both nanofluids. In addition, Suganthi and Rajan examined the convective heat transfer performance for PG-based ZnO (0.25 – 2.0 vol.%) nanofluids inside a cylindrical cavity under fixed heat flux and temperature factors. An enhanced heat transfer at increased volume concentration (φ) was observed for both factors. For fixed heat flux, the highest improvement of 4.24% was achieved, while 25.6% enhancement for a fixed temperature, both at volume concentration of 2.0 vol.%. Note, enhanced viscosity (μ_{eff}) detraction and enhanced thermal conductivity (κ_{eff}) aided augmentation.

2.7.5 Porous Cavities

Solomon et al. [345] experimented with a porous media for the thermo-convection heat transfer performance of Al_2O_3/EG-DIW(60:40) nanofluid. The nanofluid was charged into a rectangular enclosure with porous media under ΔT = 20 – 50 °C for φ of 0.05 – 0.4 vol.%. Authors reported an enhanced Nusselt number (*Nu*) for the clear cavity than the porous cavity, where an increase in *Ra* enhanced *Nu*. At φ of 0.05 vol.% and temperature 50 °C, *Nu* was maximum and reduced with increased volume concentration (φ).

2.8 ARTIFICIAL INTELLIGENCE MODELS TO PREDICT THERMAL PROPERTIES OF NANOFLUIDS

Progress in industrial concern has afforded commensurate growth in heat transfer systems' efficiency by optimizing thermal processes and properties [21, 64]. Binary nanofluids (BNFs) have found a good use for enhancing heat transfer applications, since BNFs have very good thermal behaviour than BFs [176, 346]. The improvement of thermal properties of BNFs has caught the attention of global research. Really, the experimental design for determining the thermal characteristics is costly and time-consuming [65]. Thermophysical properties like thermal conductivity and viscosity has to be defined experimentally, as numerical method is scanty or inadequate, while convective heat transfer rate can be calculated numerically [64, 347]. So, to handle the event of repeated experiments and encourage optimum data handling for big data, research is gradually shifting towards using artificial intelligence methods (like machine learning models, etc.) to industrial, engineering and scientific systems. Artificial Neural Network (ANN) is an iterative algorithm used to learn processes and has found good use in predicting the thermophysical properties of binary nanofluids [34, 35, 64, 66, 82, 96, 179, 181, 348-351]. Comparing with the classical approach, artificial neural network (ANN) is simple in design, of wide capacity and high process speed [72, 352-355]. Using generated experimental data, developed ANN models have great potential in accurately predicting thermal conductivity.

Literature abounds with artificial neural network application used for predicting the thermal conductivity of nanofluids. Papari et al. [356] proposed an artificial neural network model to predict the thermal conductivity of MWCNTs dispersed in ethylene glycol (EG), oil, and water, which gave a very good value than theoretical methods. Next, Esfe et al. [352] also developed a model for the thermal conductivity (k) of Al_2O_3/Water NF using an artificial neural network, which presented a consistent value with experimental data. Also, Longo et al. [357] used the ANN model to predict the thermal conductivity of oxide-water NFs, with good values. In addition, Tahani et al. [358] used an artificial neural network to model the prediction of TC of GO/W nanofluid, which resulted in brilliant precision with the experimental dataset. Aghayari et al. [359] also used an artificial neural network approach for predicting the thermal conductivity of Fe_3O_4/W nanofluid, which gave a good thermal conductivity prediction. Also, Hosseinian Naeini et al. [360] employed artificial neural network modelling to predict the thermal conductivity of Fe_2O_3/water NF, the model had an effective result. Verma et al. [361] equally deployed an artificial neural network model to predict the TC of TiO_2 with different basefluids (EG, EO and W), a brilliant consistency with Laboratory data sets was noticed. The deployment of the artificial neural network model gave an excellent consistency with the generated datasets from experiments.

A lot of literature addressed the use of artificial neural network (ANN) for predicting thermal conductivity (k) of binary nanofluids. Esfe et al. [362] deployed a MLP-ANN of two input parameters (temperature and volume concentration (φ)) to predict the thermal conductivity of Cu-TiO_2/W-EG BNF. Results showed good performance. Amani et al. [363] deployed artificial neural network to predict viscosity and thermal conductivity (k) of $MnFe_2O_4$/Water nanofluid, using various experimental values of nanoparticles concentration, temperature, and magnetic field as inputs to the model. Esfe et al. [364] employed a MLP-ANN to predict the thermal conductivity of SWCNT–Al_2O_3/EG BNFs with a higher deviation of 1.94% when predicted values were compared to experimental values. Adun et al. [66] applied seven input parameters: thermal conductivity, nanosize, volume concentration, NMR, temperature, nanoparticle bulk density, and basefluid, to predict the thermal conductivity of binary nanofluids. A multilayer perceptron artificial neural network and support vector regression (SVR) models were developed with the accurate capacity to predict the thermal conductivity of binary nanofluids for ranges of binary nanoparticles combinations. He et al. [348] also used an artificial neural network to effectively predict the thermal conductivity of Ag-ZnO(0.5:0.5)/Water binary nanofluid depending on volume fraction and temperatures of nanoparticles.

Esfe et al. [65, 365] predicted the thermal conductivity of ZnO–DWCNT/EG hybrid nanofluids and ferromagnetic nanofluids respectively with good accuracy and minimal error. Rostamian et al. [366] used artificial neural networks (ANN) to predict the thermal conductivity of CuO–SWCNTs hybrid nanofluids and proved that ANN predicted a good thermal conductivity. Moghaddari et al. [367] also used artificial neural networks (ANN) for prediction of thermal conductivity of MWCNT-OH-(Au, Ag, Pd) composites. Sharifpur et al. [368] employed the group method of data handling (GMDH-NN) to model the effective viscosity of Al_2O_3–glycerol nanofluid. The obtained correlations gave better accuracy in predicting the experimental dataset compared with cited models in open literature. Maleki et al. [369] applied the group method of data handling (GMDH) to determine the thermal conductivity of nanofluids and achieved good R^2 value. Mohamadian [370] confirmed that GMDH artificial neural network is a reliable model to predict the dynamic viscosity of Ag/water nanofluid when concentration, temperature, and size of particles were used as input data. The achieved results for R^2 was equal to 0.9996, indicative of perfect precision. Ahmadi et al. [371] also used the group method of data handling (GMDH) artificial neural networks to model the dependency of thermal conductivity on nanosize, temperature and concentration considered as input parameters. Results obtained were precise and accurate for prediction.. For a solar working fluid, Loni et al. [372] used the group method of data handling (GMDH) artificial neural networks to propose a model for thermal efficiency and the cavity heat gain of the Hemispherical Cavity Receiver. Ambient temperature, solar irradiation, outlet temperature were used as input variables for the model. Achieved R^2 values based on a 3-variable model, were 0.9567 and 0.9709 for thermal efficiency and the cavity heat gain of the Hemispherical Cavity Receiver, respectively. Results proved a precise and applicable model. A whole lot of artificial intelligence model is predicted for nanofluids than binary nanofluids, hence a good research gap

2.9 APPLICATIONS OF BINARY NANOFLUIDS

2.9.1 Automobile and Manufacturing Applications

2.9.1.1 Nanofluid Coolant

Over a long time, the crises of inadequate energy led automobile manufacturers to think of improved aerodynamic designs of new and smart vehicles and later fuel economy. This competition led to manufacturers reducing the quantity of energy used to overcome drag force. An optimum design of radiator shape, size and repositioning aided an improved cooling effect of incoming air. Binary nanofluids serves as a viable substitute to augment engine cooling rate and thereby reduce the complexity of the thermal management system design. Enhancement in the heat transfer rates leads to the design of lighter and compact radiators, particularly for the heavy-duty engines and machinery [40, 45, 47, 110, 147, 302, 373-382]. Machining procedures entails high friction and high-temperature environments. Thus the need for a fast cooling system is essential [383-388].

2.9.1.2 Brake Nanofluid

Lately, smart vehicle design aims at advanced aerodynamics and detraction in drag forces, hence the need for a sophisticated braking system with efficient heat dissipation capability with the use of brake nanofluids. In the process of applying brakes, kinetic energy is dispersed through the heat produced and transmitted throughout the brake fluid in the hydraulic braking system. This affects the brake oil, so a binary nanofluid with improved properties will optimize performance and handle safety issues. Copper-oxide brake nanofluid (CBN) is a good example [50, 57, 126, 374, 389-392]

2.9.1.3 Transmission Nanofluid

The application of binary nanofluids can also be employed in cooling automatic transmission systems in engines. When nanoparticles are suspended into engine transmission oil for the engine, this augments its thermal performance by possessing the least transmission temperatures at low and high speeds [163, 374, 392-395].

2.9.1.4 Nanofluid in Fuels

The addition of water-based aluminium and alumina nanoparticles in a diesel engine fuel augments the combustion property. At combustion, pure aluminium particles serve as an oxidizing agent, and alumina nanofluid serves as a catalyst. The wide contact surface area of aluminium nanoparticles increases the decomposition of water; thus, it enhances hydrogen yield and detracts the concentration of exhaust emissions [101, 121, 126, 147, 374-377, 396, 397].

2.9.1.5 Nano-Lubricant

Deploying binary nanofluids for lubrication taps from it’s optimal and rheological properties. Literature reports that stable dispersal of nanoparticles with surface-modification in mineral oils produces enhanced tribological properties, thereby reducing wear, friction and improving load-carrying capacity [89, 100, 130, 374, 390, 398-404].

2.9.1.6 Corrosion Control

Aside nano-cooling, binary nanofluids also works as corrosion inhibitors to metals. Literature is emerging on the corrosion behaviour of binary nanofluids [405-410].

2.9.2 Heat Transfer Applications

2.9.2.1 Heat Pipes

This is heat-transfer devices that possess fine thermal conductivity and phase transition for effective transfer of heat between two solid interfaces. They are a compact system used in electronic device cooling, heat exchangers and renewable energy systems. The natural attributes of higher thermal conductivity possessed by binary nanofluids are used to augment heat pipes' thermal performance [54, 411-416].

2.9.2.2 Heat Exchanger

Heats exchangers are devices employed to transport heat between two fluids without been mixed. It has wide industrial applications. The demand for smart design of heat exchangers to handle maximum possible load led to the deployment of binary nanofluids for heat extraction. Research study in this area is receiving a remarkable increase, since energy conservation is of significant challenge [47, 88, 92, 101, 121, 124, 327, 417-429].

2.9.2.3 Nuclear Reactor

The removal of heat from the reactor core is of great concern for the operation of the nuclear power plant. Binary nanofluids (BNFs) is employed to improve the cooling capacity, thus enhancing the efficiency of nuclear reactor, while detracting thermal-hydraulics problems [81, 379, 430-434].

2.9.2.4 Geothermal Power

The global geothermal power resource can provide the world's energy need with technological improvement. Nanofluids can be used to cool equipment that works in a high temperature and friction environment during drilling operations. Like a "fluid superconductor," nanofluids is a working fluid used for energy extraction from the earth's core, and thus produces large amounts of energy because the heat transfer capability of geothermal systems is enhanced. The use of BNFs helps to augment the efficiency of a power generation cycle using geothermal energy [48, 435-441]

2.9.2.5 Boiling

Boiling is a major industrial process useful in various engineering thermal processes like metallurgy, power generation, desalination, chemical, etc. Boiling as a heat transfer process is a key phase phenomenon in many thermal systems, thus the use of binary nanofluid to improve heat transfer properties. Binary nanofluids catalyze the boiling process by enhancing the critical heat flux (CHF). Studies are increasing in using binary nanofluids for boiling [136, 442-447].

2.9.2.6 Cooling Applications

As the quest for better living standards continues, the need arises for thermal comfort in vehicles and buildings, thus resulting in improved energy consumption. The integration of nanohybrid based phase change materials (PCMs) helps to decrease energy use and thus enhances the thermal comfort in buildings. Building parts like concrete, floors, wallboards, etc. are integrated with PCMs to help enhance their performance. Furthermore, the constraint of space, energy and weight allows for an effective cooling system for aircraft, space and defence application, which BNFs handle better than conventional fluids [33, 37, 51, 448-452].

2.9.3 Biomedical Applications

2.9.3.1 Nanomedicine

Binary nanofluids has also found commercial applications in the medical and pharmaceutical field. The methods entail biosensors, microfluidics, drug delivery, tissue engineering, nanobiotechnology, etc. Their properties allow for their use as a drug delivery system. Hence, the use of nanogels to produce nanodrugs, for both *in vitro* and *in vivo* assay. For example, a nanohybrid called Graphene quantum dots (GQDs) has found numerous applications, especially in biomedical research, as a result of its unique physico-chemical characteristics and excellent biocompatibility. Emerging research and developments are on, especially in synthesis methods, in vivo imaging, and in vitro biosensing applications [86, 453-458].

2.9.3.2 Cancer Therapeutics

Magnetic nanohybrids have found usefulness for cancer imaging and drug delivery. The idea is that magnetic-based nanohybrids are employed to guide the particles along the bloodstream to locate a tumour using magnets to supply the drug to the tissue without damage to surrounding healthy tissue. This happens to be a key side effect of using the traditional cancer treatment approach [456, 457, 459-464].

2.9.3.3 Nanocryosurgery

Nanocryosurgery is a medical procedure that uses a lower temperature to destroy unwanted tissues. This ground-breaking approach is finding popularity due to its relevant clinical advantages, like cancer and tumour treatment. Aside from being less invasive when compared to traditional surgical resection, it reduces bleeding, pain, and attendant complications of surgery. It is also cheaper than other treatment methods and needs a more reduced recovery time and hospital stay [457, 465-471].

2.9.3.4 Cryopreservation

Nanofluids has also found usefulness in preserving organ against damage during surgical operations. For vaccines, PCMs are used to maintain them at recommended temperature during transport [457, 460, 465, 472-476].

2.9.4 Electronic Applications

2.9.4.1 Microchip Cooling

Fast heat dissipation is a key challenge in developing miniature microchips and nanochips. However, due to their high thermal conductivity, BNFs are used for the liquid cooling of computer processors. New generation computer chips or microprocessors incorporate nanofluids for super-high-heat flux electronic systems. Nguyen et al. [477] studied the heat transfer improvement and behaviour of Al_2O_3-water nanofluid for application in a closed-cooling system meant for a microprocessor or similar electronic devices. The result was remarkable [477-484].

2.9.4.2 Microfluidic Applications

Binary nanofluids have also found usefulness for fluidic digital display devices, optical devices and majorly in microelectromechanical systems (MEMS). Also, it finds practical applications in the pharmaceuticals industry [457, 476, 477, 485-488].

2.9.5 Renewable Energy Applications

2.9.5.1 Photovoltaic-Thermal System

Photovoltaic (PV) modules are applied to direct solar energy conversion to domestic electricity. The PV modules absorb about 81% of the radiations striking the module surface. Still, a small quantity is converted to electric power, and the rest is transformed to heat, hence reducing the efficiency of the cell and the overall lifespan of the module. This operational constraint can be solved by cooling the surface of the module using a binary nanofluid, thus yielding improved electrical efficiency [489-494].

2.9.5.2 Solar Collectors

Binary nanofluids augment the performance of photothermal conversion, unlike traditional fluids. In addition, the improved thermal properties and optical characteristics of binary nanofluids as working fluids make room for an excellent absorption range [120, 124, 135, 150, 162, 449, 495-498].

2.9.5.3 Micropower Generation

The optical and thermal properties of binary nanofluids were used to absorb and transform light to heat for electrical generation purposes. An open-circuit voltage of 1.6 mV was achieved at 900 µL nanofluid. Emerging research is opening room for improvement [55, 489, 490, 493, 499-502].

2.9.6 Other Applications

Binary nanofluids has numerous use in other areas like detergency [46, 503-505], soil remediation [46, 506-509], oily soil removal [508-510], enhanced oil recovery [55, 71, 139, 511-514], military application [51, 147, 515-517], etc. Figure 2.2 details the applications of applications of binary nanofluids.

2.10 CHALLENGES WITH BINARY NANOFLUIDS AND FUTURE DIRECTIONS

Running through numerous applications and utilization of binary nanofluids, a few challenges need to be addressed to enable the extensive use of binary nanofluids. The major issues are:

2.10.1 Stability

Generally, instability remains the key issue with nanofluids. Parameters that affect nanofluid's stability are stirring time, type of surfactant, nanoparticle combinations, nanoparticle concentration, fluid temperature, pH value, ultrasonication and base fluid. Nanosuspension of nanoparticles in basefluid faces challenges due to surface charge (negative or positive), which varies amidst particles, thus leading to abatement in heat transfer. For proper suspension of nanoparticles, the aforementioned factors are gaps for future studies [55, 63, 120, 328, 518-523]. Open literature is gaining momentum with nanofluids' meaningful stability time span, especially binary nanofluids and ternary nanofluids. A sixty (60) days stability time span was published by Sundar et al. [524] for MWCNT- Fe_3O_4/water; Ali et al. [120] for CNTs-Fe_3O_4/water; Hussein [525] for AlN/EG; Yarmand et al. [526] for GNP-Ag/water; while Farbod et al. [527] recorded a stability time span of eighty (80) days for MWCNTs/water; Tiwari et al. [171, 528] published for ninety (90) days for CeO_2+MWCNT binary nanoparticles for various basefluids (ethyl glycol, water, silicone oil and therminol VP-I). Frequently used methods for estimating stability of binary nanofluids are centrifugation, spectroscopy, sedimentation analysis and zeta-potential [36, 39, 41, 120, 176, 346, 529].

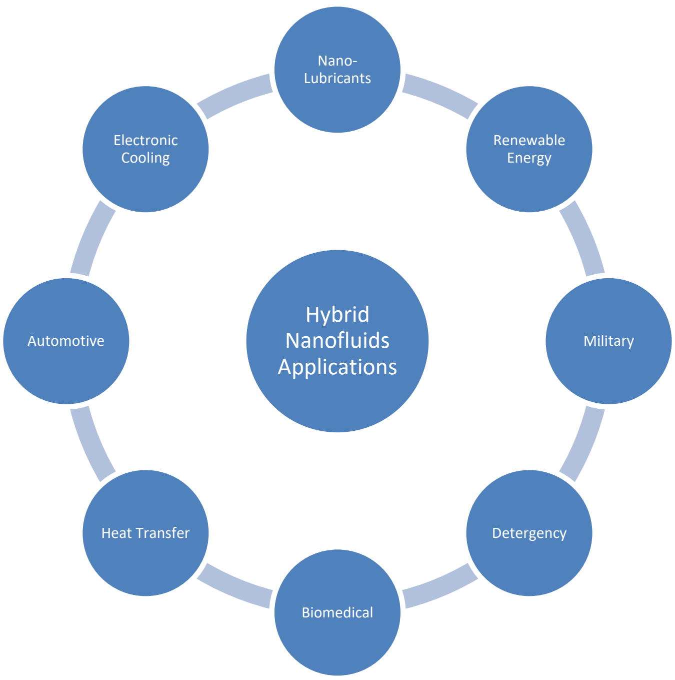

Figure 2.2: Practical application of binary nanofluids.

2.10.2 Selection of Nanohybrid Materials

Binary nanofluids exhibit individual behaviour. To select optimum nanomaterial, a comprehensive comparison is essential. This selection has an impact on the thermal conductivity and stability performance. Suresh et al. [258] affirmed that ceramic substances possess chemical inertness and good stability, but lower thermal conductivity when related to metallic nanoparticles. Metallic nanoparticles possess maximum thermal conductivity compared with ceramic nanoparticles, so when hybridized, binary nanofluids with augmented thermal conductivity and stability are produced [31, 40, 45, 160, 171, 204, 258. The basefluid choice relates to the primary area of application [53]. The methods for formulating binary nanofluids or ternary nanofluids should also be examined - aerosol method, chemical reduction method, polymerization, wet chemical [530-533].

2.10.3 Production Cost

The production cost of binary nanofluids depends on the production approach used and suspension in basefluids. The choice of basefluid also affects cost. The methods for producing binary nanofluids are named one step and two-step methods. The equipment used is expensive and sophisticated [53, 55, 388, 534, 535].

2.10.4 Pumping Power

The viscosity of binary nanofluids is a function of temperatures, as it varies with it. The dispersed nanoparticles aid the viscosity, enhancing friction factor and enabling pumping power [53, 120, 526, 536].

2.10.5 Model For Thermal Conductivity

Progress in industrial processes has necessitated commensurate growth in heat transfer systems' efficiency by optimizing thermal processes and properties with the use of binary nanofluids. Really, experimental set-up to determine the thermophysical properties of binary nanofluids is expensive and time-consuming, thus using modelling techniques. So, in handling repeated experiments and encouraging optimised big data handling, researchers are gradually shifting to applying artificial intelligence techniques (like machine learning models, etc) to engineering, industrial and scientific applications. Literature abounds with a prediction model for binary nanofluids. Predicted values agrees with experimental results [61, 64, 67, 92, 96, 141, 148, 160, 174, 181, 350, 362, 433, 537].

2.11 CONCLUSION

The need to augment the poor thermal conductivity of conventional fluids to produce efficient heat transfer fluid cannot be over-emphasized, knowing fully well that heat transfer is a key component in the process line of many industrial production concerns. Hence, the birth of nanofluids is the formulation of a composite of suspended nanoparticles in a basefluid. Nanofluids have found wide applications ranging from heat exchangers, electronic cooling, automotive industry, medical, military, solar energy, manufacturing industry, to mention but a few. But nanofluids has limitations premised on certain specific benefits due to the characteristics of the dissolved nanoparticle. Thus, the entrance of a new class heat transfer fluid named binary nanofluid and ternary nanofluid. This Chapter presented a wide range of recent and future applications of nanofluids with a focus on related issues that allow for suitability for industrial applications. Note, the few noticed gaps must be addressed to allow for effective industrial applications.

The review focused on the preparation and application of binary nanofluids. Binary nanofluids and ternary nanofluids are advanced mixture of heat transfer fluids with optimized thermal properties. Thus, the need to develop an optimized model for the formulation of binary nanofluids for improved industrial applications. Artificial neural network (ANN) possesses a strong possibility in modelling the thermal properties of binary nanofluids. Emerging issues of optimized concern are stability and instability, nanomaterials selection, enhanced formulation methods, use of binary basefluids, temperature, bias in experimental outcomes and simulated predictions, thermal network mechanism, environmental impact, to mention a few.

CHAPTER 3

METHODOLOGY[1,2,3,4]

3.1 INTRODUCTION

This chapter explains the method and material for the experimental study and the artificial intelligence model applied to nanofluids properties. It details the information about materials, equipment, stability, sample preparation, measurement of thermophysical properties, nanofluid characterisation, and natural convection properties of BNFs engaged in the experimental study. The details will be discussed in the following sub-sections.

3.2 MATERIALS AND EQUIPMENT

3.2.1 Materials

For the study, nanoparticles of MgO (20 nm, 40 nm and 100 nm, ≥99% purity), ZnO (20 nm, ≥99.5% purity), and γ-Al_2O_3 (7nm diameter and ~98% purity) were purchased at Nanostructured and Amorphous Materials Inc., Houston, Texas, USA, while. Functionalised MWCNT (inner diameter of 3-5 nm, outer 10-20 nm and length of 10-30 μm) obtained from MKnano Company, Ontario, Canada. To enhance the stability of the formulated NFs, BNFs and TNFs, a surface activator Sodium-dodecyl sulphate (SDS) with purity ≥ 98.50% was purchased from Sigma-Aldrich, Germany. Deionised water (DIW) was the basefluid and obtained in the laboratory.

This chapter is reflected in parts in the following papers:

[1]Giwa, S., Momin, M., Nwaokocha, C., Sharifpur, M., and Meyer, J. *Influence of nanoparticles size, per cent mass ratio, and temperature on the thermal properties of water-based MgO–ZnO nanofluid: an experimental approach.* Journal of Thermal Analysis and Calorimetry, 2021. **143**(2): p. 1063-1079.
[2]Nwaokocha, C., Momin, M., Giwa S., Sharifpur, M., Murshed S.M.S., Meyer, J.P., *Experimental investigation of thermo-convection behaviour of aqueous binary nanofluids of MgO–ZnO in a square cavity.* Thermal Science and Engineering Progress, 2021. **28**:101057.
[3]Nwaokocha, C., Momin, M., Sharifpur, M. and Meyer, J., *Influence of concentration, mixing ratios, and working temperature on the thermal behaviour of binary nanofluids of MgO–ZnO: an experimental investigation.* Ready for submission.
[4]Nwaokocha, C., Momin, M., Sharifpur, M. and Meyer, J., *Artificial neural network development to predict thermal conductivity of MgO–ZnO/Deionised Water binary nanofluids.* Ready for submission.

The free convection experiment of MgO-ZnO/deionised water BNF was done inside a squared enclosure (breadth 96.0 mm × length 96.0 mm × height 105.0 mm). Polyurethane material was used for insulation during the thermo-convection investigation. The opposite walls of the cavity were differentially heated, while insulation (20 mm with k = 0.033) was done for other walls, along with the pipe networks. The temperature in the enclosure was measured employing the T-type thermocouple manufactured by Omega Engineering Inc., USA, (accuracy 0.1 °C), set at particular points within (spaces (11) and walls (6)) and without (2 inlet and 4 outlet pipes) the enclosure. Thermocouples are calibrated before performing the experiment with temperature 10 – 50 °C, for the uncertainty of 0.16 °C. Glass wares like beakers, conical flasks and volumetric flasks were also used for the experiment.

3.2.2 Equipment

A meter rule and vernier calliper were used to measure the dimensions (within and without) of the cavity. The quantity of the nanoparticles and dispersants/surfactants used for the study were measured with a digital weigh balance (Radwag AS220.R2; 10 mg – 220 g and ± 0.01 g precision). The mixtures of SDS, BNPs and DIW were stirred at a controlled temperature employing a magnetic stirrer (Lasec hotplate stirrer - H4000-HSB, 500 W, 50Hz) to attain an even suspension before sonicating. Homogenizing was achieved employing an Ultrasonicator (QSonica Q-700; 20 kHz and 700 W). Water baths were employed to retain a constant temperature for the test samples (LAUDA ECO RE1225 and PolyScience, USA: PR 20R-30-A12E, −30 °C and 200 °C, precision 0.0050 °C). Employing an electrical conductivity meter (EUTECH Instrument (CON700, precision ± 1%)), the electrical conductivity (σ) of the prepared nanofluids (mono, binary and ternary) were measured and applied to indicate the optimization of amplitude, dispersion fraction, and sonication time. The pH is measured using a pH meter (Jenway 3510; range of − 2 to 19.999; accuracy ± 0.3%). The stability of formulated nanofluids is measured using an Ultraviolet (UV) visible Spectrophotometer (Jenway Model

7315). TEMPOS thermal properties analyzer (METER Group) measures thermal conductivity. Volumetric flow rates were valued by employing a flow meter (Burkert Type 8081). A Vibro-viscometer (SV-10, A&D, Japan) measures viscosity. Transmission electron microscope (JEOL JEM-2100F) measures morphology. Experimental values for flow rate and temperature were logged with a National Instrument Data logger (Type SCXI-1303; 32 channels) into the computer with a LABVIEW® software (2014 version) interface. A summary of the equipment and the accuracies are presented in Table 3.1.

Table 3.1: Accuracy of equipment.

Instrument	Range	Accuracy
Electrical conductivity meter	0 µS - 200 mS	± 1%
Flow meter	0.0666 – 0.3333 l/s	±0.01% of full-scale flow rate + 2% (measured value)
Graduated cylinder	250 ml	± 2.0 ml
Thermal bath	-200 – 150 °C	± 0.005 °C
Thermal conductivity meter	0.2 – 2.0 W/m K	±10%
Thermocouple	< 150 °C	±0.1 °C
Vernier calipers	0.02 mm	0.02 mm
Viscometer	0.3 – 10,000 mPa.s	±3%
Weighing balance	10 mg – 220 g	0.01

3.3 FORMULATION OF BINARY NANOFLUIDS

As published in [21], a two-step method was used in formulating a MgO-ZnO/DIW BNFs with four percent weight ratios (PWR) of 20:80, 40:60, 60:40, and 80:20 (MgO: ZnO). MgO nanoparticles with nano-sizes of 20 nm, 40 nm and 100 nm were employed. A SDS surfactant was used to help the dispersion of the binary nanoparticles in deionised water. To enhance the stability of the binary nanofluids, amplitude (70 – 80%), dispersion fraction (0.60 – 1.20), and sonication time (30 – 120 min) were optimised. The remaining parameters are constant to optimize a particular variable while one is varied. Sonication time was optimised first for a fixed dispersion fraction and amplitude. Thereafter, the dispersion fraction was optimized and last, the amplitude.

A certain percent weight ratio (80:20 (MgO: ZnO)) for the binary nanofluid for volume concentration of 0.05 vol% was formulated and employed in the optimisation study. The specified nanoparticles and dispersant were weighed using the digital weight balance (Radwag AS 220.R2; 10 mg – 220 g and accuracy ± 0.01 g) by the estimate derived from Equation 3.1 [239] based on the volume of deionised water (70 ml) and concentration (0.05 vol%). With an electrical conductivity instrument (EUTECH Meter (CON700); ±1% accuracy), the electrical conductivity of the synthesised binary nanofluids was evaluated and employed to indicate the optimised amplitude, dispersion fraction, and sonication time. The pH (Jenway 3510; –2 to 19.999 range; precision ±0.30%) was also valued to estimate the optimized results of the variables. The blend of basefluid, surfactant, and binary nano-particles were first stirred for 30 minutes at 40 °C with a magnetic stirrer prior to sonicating. An Ultra-sonicator (QSonica; Q-700; 700 W and 20 kHz) was employed to homogenise the blend to afford good suspension of the binary nano-particles in basefluid. A beaker containing the mixture was immersed in a water bath (LAUDA ECO RE1225) and sustained at 20 °C while sonicating.

$$\varphi = \left(\frac{x_{MgO}\left(\frac{M}{\rho}\right)_{MgO} + x_{ZnO}\left(\frac{M}{\rho}\right)_{ZnO}}{x_{MgO}\left(\frac{M}{\rho}\right)_{MgO} + x_{ZnO}\left(\frac{M}{\rho}\right)_{ZnO} + \left(\frac{M}{\rho}\right)_{DIW}} \right) \qquad \textbf{3.1}$$

Where;

X_{MgO} = ratio of MgO nanoparticles with 20 nm or 100 nm;

X_{ZnO} = ratio of ZnO nanoparticles with 20 nm;

M = nanoparticle mass;

ρ = nanoparticle density;

DIW = basefluid.

As the optimised variables were achieved, the binary nanofluids at the preset percent weights and at 0.1 vol.% were prepared for 200 mL of basefluid. To achieve optimized stability for the formulated binary nanofluids and allow for repeatability of this experiment (which is scarce in literature), optimization of sonication parameters (time: 30–120 minutes, amplitude frequency: 70–80%, and a 7 seconds PULSE ON and 2 seconds PULSE OFF) and surfactant's dispersion fraction (0.6 – 1.2) was done ab initio. Dispersion fraction is expressed as Equation 3.2. For the formulation of BNF, φ, percent weights of BNPs, and volume of BF type were employed in Equation 3.1 to estimate the weights of the BNPs that would be used to formulate the BNF. Volumes of 70 ml, 100 ml and 1400 ml of different basefluids (DIW) were used for the optimisation process, thermal properties measurement and thermo-convection experiment, respectively. The weights of surfactants and BNPs used for formulating the MHNFs are estimated and provided in Appendix A.

$$Dispersion\ fraction = \frac{weight\ of\ surfactant}{weight\ of\ binanoparticles} \qquad \textbf{3.2}$$

A parameter was varied and others fixed until optimum results were achieved. Also, the margin of deviation (MOD) of measured properties of the BNFs were estimated using Equation 3.3 [538].

$$\text{MOD (\%)} = \left(\frac{M_{Exp.} - M_{Pred.}}{M_{Exp.}}\right) \times 100 \qquad \textbf{3.3}$$

Where $M_{\text{Exp.}}$ and $M_{\text{Pred.}}$ are the experimental and predicted readings for a specific property, respectively.

Note, three sets of MgO (20 nm)-ZnO/DIW BNFs, MgO (40 nm)-ZnO/DIW BNFs and MgO (100 nm)-ZnO/DIW BNFs were produced to allow for the investigation of nanosize effects on thermal characteristics. Single-particled nanofluids of MgO(20 nm)/DIW nanofluids, MgO

(100 nm)/DIW nanofluids, and ZnO (20 nm)/DIW nanofluids were prepared to allow for comparison in the enhancement of thermal characteristics compared to binary nanofluids.

3.4 STABILITY AND MORPHOLOGY OF BINARY NANOFLUID

A transmission electron microscope (TEM) (JEOL JEM-2100F) was used to check the morphology of the hybrid and mono-particle nanofluids. To keep an eye on the stability of mono-particle nanofluids and binary nanofluids, both visual inspection and absorbance test using UV-visible spectrophotometer (Jenway Model 7315) were employed. An Ultra-Violet (UV) visible spectrophotometer (Jenway Model 7315) was employed to measure the absorbance of the formulated binary nanofluids, which is indicative of stability [338]. Absorbance test was conducted for 20 hours for samples of MgO (20 nm)-ZnO/DIW BNF and MgO (100 nm)-ZnO/DIW BNF at a percent weights of 20:80 and 80:20 and for all single-particled nanofluids. Also of note, as each property was measured for each volume concentration, 6 hours was used, while the absorbance test covered 20 hours to allow for good observation of stability. Visual inspection was done on the BNF samples for a week and on a daily basis.

3.5 MEASURED THERMAL PROPERTIES OF BINARY NANOFLUID

3.5.1 Measurement of Thermal Conductivity

Thermal conductivity (κ) was measured using TEMPOS thermal property analyser (METER Group; 0.2 – 2.0 W/m K range; ± 10% accuracy). The meter was calibrated for temperature ranging 20–50 °C in intervals of 5 °C for this experimental investigation. To get an accurate value, readings were measured for twelve rounds. As a self-calibrating device, readings were taken after switching it on and allowed to stabilize. Measured κ readings of BF was compared with standard measurements [539] for the studied temperature range to confirm the reliability of the measurement meter. A good agreement existed at an error 0.4890%. The associated uncertainty of κ readings was ± 02.00%. Thermal conductivity ratio (TCR) or effective thermal conductivity (κ_{eff}) and thermal conductivity enhancement (TCE) were estimated by Equations 3.4 and 3.5, respectively.

$$TCR = \kappa_{eff} = \frac{\kappa_{bnf}}{\kappa_{bf}} \quad (3.4)$$

$$TCE\ (\%) = \left(\frac{\kappa_{bnf} - \kappa_{bf}}{\kappa_{bf}}\right) \times 100 \quad (3.5)$$

where κ_{bnf} and κ_{bf} are the thermal conductivity (TC) of the binary nanofluids (BNFs) and DIW, respectively.

3.5.2 Measurement of pH

After calibrating the meter using standard fluids, the pH of binary nanofluids (BNFs) samples and DIW were estimated for the studied temperatures 20–50 °C, after calibrating the meter using standard fluids. The uncertainty related to the pH readings was ± 2.49%.

3.5.3 Measurement of Electrical Conductivity

Electrical conductivity was measured using a Eutech meter (CON700 model, ± 10% accuracy). The device was calibrated using the manufacturer's standard calibration fluid (glycerine). Glycerine was measured at 25 °C thrice, and an average reading of 1414 $\mu S.cm^{-1}$ was achieved, which is near to the manufacturer's reading of 1413 $\mu S.cm^{-1}$. Thereafter, the σ for DIW and formulated BNFs were valued for temperatures 20 to 50 °C. The uncertainty related to the σ measurement was ±2.99%. Figure 3.1 presents the experimental set-up for the investigation. The relative σ (σ_{rel}) and the σ improvement (σ_{enhan}) of the nanohybrids was estimated with Equations 3.6 and 3.7, respectively [540, 541].

$$\sigma_{rel} = \frac{\sigma_{bnf}}{\sigma_{bf}} \quad (3.6)$$

$$\sigma_{enh}\ (\%) = \left(\frac{\sigma_{bnf} - \sigma_{bf}}{\sigma_{bf}}\right) \times 100 \quad (3.7)$$

where σ_{bnf} and σ_{bf} are the viscosity of the BNFs and DIW, respectively.

3.5.4 Measurement of Viscosity

Viscosity (μ) of BNFs and BF were measured using a Vibro-viscometer (SV-10, A&D Japan, accuracy ± 3%) at temperatures 20–50 °C, after calibrating using basefluid (DIW). The accuracy of the device was determined by comparing the μ of DIW with standard values of water published in the literature [539, 541], with an error of 2.78% and uncertainty of ± 2.85%.

Figure 3.1 presents the experimental set-up for the investigation. The μ_{rel} and μ_{enh} of the nanohybrids as related to basefluid (DIW) were estimated using Equations 3.8 and 3.9, respectively [540, 541].

$$\mu_{rel} = \frac{\mu_{bnf}}{\mu_{bf}} \quad (3.8)$$

$$\mu_{enh}\,(\%) = \left(\frac{\mu_{bnf} - \mu_{bf}}{\mu_{bf}}\right) \times 100 \quad (3.9)$$

where μ_{bnf} and μ_{bf} are the viscosity of the BNFs and DIW, respectively.

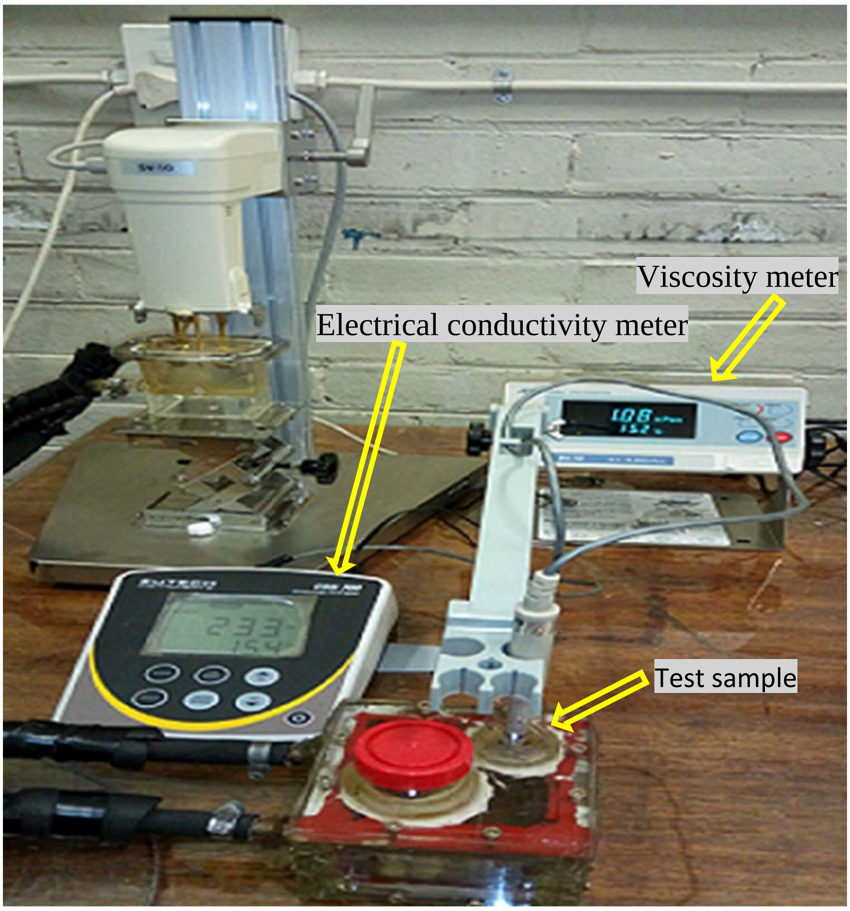

Figure 3.1: Experimental set-up for electrical conductivity and viscosity.

3.5.5 Other Properties

The density (ρ), specific heat capacity (C_p), and thermal coefficient of expansion (β) of BNFs were necessary for data reduction (detailed in Sub-Section 3.7). They are estimated from empirical models modified for BNFs, as they are not experimentally measured. Equation 3.10 and Equations 3.11 – 3.13 presents the theoretical and empirical correlations [542] for determining density, specific heat, and coefficient of thermal expansion of BNFs, respectively.

$$\frac{k_{nf}}{k_{bf}} = \left(\left(k_{MgO}X_{MgO} + k_{ZnO}X_{ZnO}\right) + 2k_{DIW} + 2\left(\varphi_{MgO}k_{MgO}X_{MgO} + \varphi_{ZnO}k_{ZnO}X_{ZnO}\right) - 2\varphi_{bnp}k_{DIW}\right) \times \left(\left(k_{MgO}X_{MgO} + k_{ZnO}X_{ZnO}\right) + 2k_{DIW} - \left(\varphi_{MgO}k_{MgO}X_{MgO} + \varphi_{ZnO}k_{ZnO}X_{ZnO}\right) + \varphi_{bnp}k_{DIW}\right)^{-1} \quad 3.10$$

$$\rho_{bnf} = \varphi_{MgO}\rho_{\mathrm{MgO}} + \varphi_{ZnO}\rho_{ZnO} + (1 - \varphi_{bnf})\rho_{DIW} \quad 3.11$$

$$(\rho\beta)_{bnf} = \varphi_{MgO}(\rho\beta)_{MgO} + \varphi_{ZnO}(\rho\beta)_{ZnO} + \left(1 - \varphi_{bnf}\right)(\rho\beta)_{DIW} \quad 3.12$$

$$(\rho C_p)_{bnf} = \varphi_{\mathrm{MgO}}(\rho C_p)_{\mathrm{MgO}} + \varphi_{\mathrm{ZnO}}(\rho C_p)_{\mathrm{ZnO}} + \left(1 - \varphi_{bnf}\right)(\rho C_p)_{DIW} \quad 3.13$$

3.6 THERMO-CONVECTION OF BINARY NANOFLUIDS IN CAVITY

The natural convection behaviour of MgO-ZnO/DIW BNF inside a squared enclosure of 96 mm length by 96 mm breadth by 105 mm height) was studied by experiment. A squared enclosure was employed due to its wide application compared to other cavity types. The opposite walls of the enclosure were heated differentially, and other walls were insulated (20 mm with *k* = 0.033), alongside the pipe connection. A T-type thermocouple was employed to measure temperature within the cavity, arranged at certain points within (6 walls and 11 spaces) and without (2 inlet and 4 outlet pipes) the enclosure, as featured in Figures 3.2 and 3.3. Thermocouples were calibrated before conducting the experiments, with temperature 10-50°C, and uncertainty of 0.16°C. Details regarding calibration procedure and estimating uncertainty associated with the thermocouples are briefed in Appendices B and C.

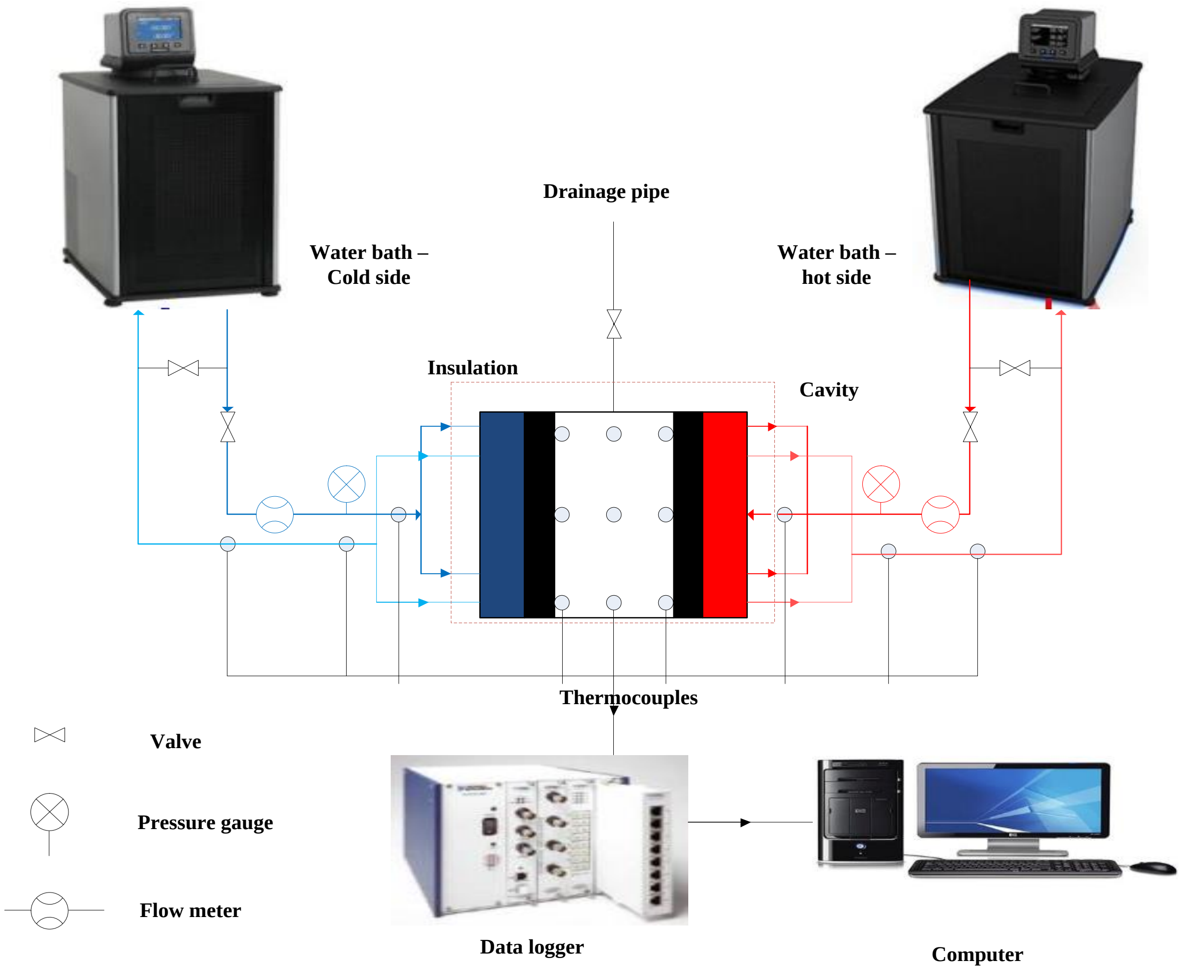

Figure 3.2: Arrangement of thermo-convection experiment [58].

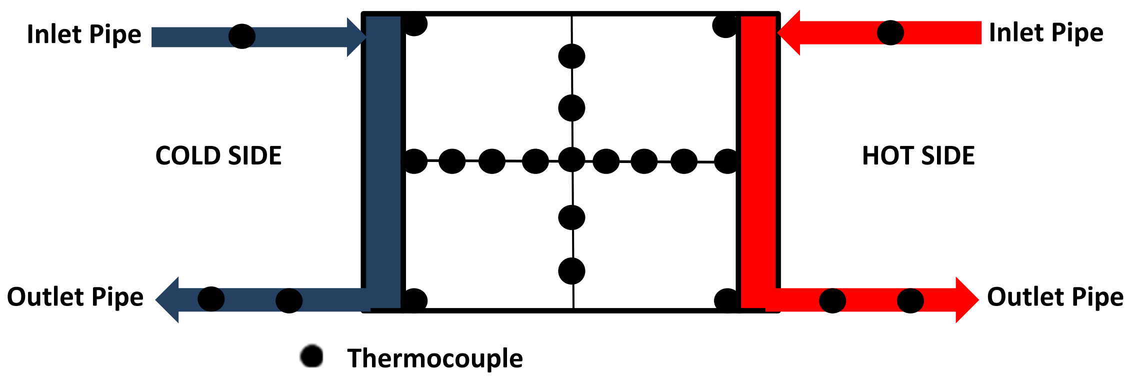

Figure 3.3: Position of thermocouples in the square enclosure.

For thermocouples arranged outside of the enclosure, it was observed that 5% heat loss happened due to temperature difference between cavity and the environ. Shell heat exchanger (counter-flow) and isothermal tube were employed to sustain the constant temperature of the two differentially heated walls. So, water maintained at a constant temperature (20 °C and 50 °C) was transported within the heat exchangers employing two Programmable water baths (PolyScience, USA: PR 20R-30-A12E, −30 °C and 200 °C, precision 0.0050 °C), one for hot side and the other cold side. Flow meters were positioned at the inlet of heat exchangers to measure flow rates between water baths and heat exchangers. Measure values for flow rate and temperature were logged using a National Instrument Data logger (Type SCXI-1303; 32 channels) linked to the Desktop computer interfaced with a LABVIEW® software (2014 version). BNFs samples and DIW were charged inside the squared enclosure and permitted thermal equilibrium. The experiments were done for a uniform temperature change of 30 °C, amidst 20 to 50°C for all samples.

3.7 DATA REDUCTION

Main variables like Ra, Nu_{av}, h_{av} Q_{av}, etc., were determined by employing the valued flow rates, temperatures, and thermal properties of basefluid and BNF in the data reduction process. Heat transfer rate within an enclosure as a function of differential heating on the vertical walls is presented employing Equation 3.14,

$$Q = \dot{m}C_p\Delta T \qquad 3.14$$

Where;

$$\Delta T = \left(T_i - \left(\frac{T_{o,1}+T_{o,2}}{2}\right)\right)_h = \left(\left(\frac{T_{o,1}+T_{o,2}}{2}\right) + T_i\right)_c \qquad 3.15$$

The h_{av}, Ra and Nu_{av} related with the thermo-convection of the BNF sample within the square enclosure was estimated using Equations 3.16 - 3.18,

$$h_{av} = \frac{Q_{av}}{A(T_h - T_c)} \quad 3.16$$

$$Ra = \frac{g\beta(T_h - T_c)(\rho)^2(C_p)(L)^3}{\mu \, \kappa} \quad 3.17$$

$$Nu_{av} = \frac{h_{av}L}{\kappa_{eff}} \quad 3.18$$

3.8 MODEL DEVELOPMENT

3.8.1 Thermophysical Properties

The entrance of BNFs and increasing investigation into their thermal characteristics have advanced the need to develop models to help predict these properties. Note, MgO-ZnO/DIW BNF was studied for the first time, hence no existing models in the literature to predict their κ_{eff} and μ_{eff}. Thus, the need to develop new models for the thermal properties of the BNF.

3.8.2 Nusselt Number

As a result of scarce literature on the experimental studies of thermo-convection characteristics of binary nanofluids in cavities and few existing models derived from experimental data for the prediction of *Nu*, this present study was conducted to develop a model in that regard for the BNF sample. Experimental datasets of Nu_{av} for the binary nanofluid was used for model development to predict Nu_{av}. The margin of deviation (MOD) for the developed models was expressed using Equation 3.3.

3.9 CAVITY VALIDATION

Cavity validation were achieved by employing the experimental dataset of Nu_{av} for basefluid measured while conducting the experiment, related with *Nu* values of published numerical models. The developed models of Berkovsky & Polevikov [543], Cioni *et al*. [544], and Leong *et al*. [545] to predict Nusselt Number of water within an enclosure were described in

Equations 3.18 [543], 3.19 [544] and 3.20 [545], respectively. The Pr and Ra results of DIW were included in Equations 3.18 to 3.20 to get *Nu*.

$$Nu = 0.18\left(\frac{Pr}{0.2 + Pr}\ Ra\right)^{0.29} \quad (Pr \leq 10^5;\ Ra \leq 10^{10};\ 1 \leq H/L \leq 10) \tag{3.18}$$

Where $Pr = \frac{\mu C_P}{k}$

$$Nu = 0.145 \times Ra^{0.292} \quad (3.70\times10^8 \leq Ra \leq 7\times10^9) \tag{3.19}$$

$$Nu = 0.08461 \times Ra^{0.3125} \quad (10^4 < Ra < 10^8) \tag{3.20}$$

3.10 ESTIMATION OF UNCERTAINTY

3.10.1 Thermophysical Properties

The estimation of uncertainty related with the measurements of μ_{eff} and κ_{eff} for BNF was premised on the method employed by Adio et al. [205]. To estimate μ uncertainty, errors from the formulation (weights of BNPs and volumes of BFs) of BNFs, temperature, and μ readings were considered, whereas weights of BNPs, volumes of BFs, and κ measurement were error sources for the κ uncertainty (as expressed in Equations 3.21 and 3.22). Total uncertainty for κ and μ measurements were determined employing Equations 3.24 and 3.25 with the bias components expressed in Equations 3.21 and 3.22, and the precision components described in Equation 3.23. The accuracy of the equipment is provided in Table 3.1. The accuracy of the applicable instruments and the obtained data for the viscosity and thermal conductivity of BNF were substituted in Equation 3.21 – 3.25. Details of the uncertainty estimation are provided in Appendices C.

$$U_{b_\mu} = \sqrt{\frac{\Delta m}{m} + \frac{\Delta V}{V} + \frac{\Delta T}{T} + \frac{\Delta \mu}{\mu}} \tag{3.21}$$

$$U_{b_\kappa} = \sqrt{\frac{\Delta m}{m} + \frac{\Delta V}{V} + \frac{\Delta \kappa}{\kappa}} \tag{3.22}$$

$$U_{p_{\mu/\kappa}} = \pm(t_{v,p} \times SD_{\mu/\kappa}) \quad 3.23$$

$$\delta\mu = U_{\mu} = \pm\sqrt{\left(U_{b_{\mu}}\right)^2 + \left(U_{p_{\mu}}\right)^2} \quad 3.24$$

$$\delta\kappa = U_{\kappa} = \pm\sqrt{\left(U_{b_{\kappa}}\right)^2 + \left(U_{p_{\kappa}}\right)^2} \quad 3.25$$

3.10.2 Thermo-convection

The derivation of uncertainty related to the study was done to ascertain the degree of reliability of the experimental dataset. Datasets of temperature and flow rate were observed as the foundational error sources and disseminated using Equations 3.26 – 3.28 to determine the uncertainty related with *Nu*, *Q* and *h*, respectively. Table 3.2 features the determination of uncertainties.

$$\delta Q = \left(\left(\frac{\partial Q}{\partial \dot{m}}\delta\dot{m}\right)^2 + \left(\frac{\partial Q}{\partial C_{P_{DIW}}}\delta C_{P_{DIW}}\right)^2 + \left(\frac{\partial Q}{\partial T_H}\delta T_H\right)^2 + \left(\frac{\partial Q}{\partial T_C}\delta T_C\right)^2\right)^{\frac{1}{2}} \quad 3.26$$

$$\delta Nu = \left(\left(\frac{\partial Nu}{\partial h}\delta h\right)^2 + \left(\frac{\partial Nu}{\partial L_C}\delta L_C\right)^2 + \left(\frac{\partial Nu}{\partial \kappa_{eff}}\delta\kappa_{eff}\right)^2 + \left(\frac{\partial Nu}{\partial T_C}\delta T_C\right)^2\right)^{\frac{1}{2}} \quad 3.27$$

$$\delta h = \left(\left(\frac{\partial h}{\partial Q}\delta Q\right)^2 + \left(\frac{\partial h}{\partial A}\delta A\right)^2 + \left(\frac{\partial h}{\partial T_H}\delta T_H\right)^2 + \left(\frac{\partial h}{\partial T_C}\delta T_C\right)^2\right)^{\frac{1}{2}} \quad 3.28$$

Table 3.2: The estimation of uncertainties.

Heat Transfer Rate	$\frac{\partial Q}{\partial \dot{m}} = C_{p-bf}\Delta T$	Substitute into Equations 3.26
	$\frac{\partial Q}{\partial C_{p-bf}} = \dot{m}\Delta T$	
	$\frac{\partial Q}{\partial \Delta T} = \dot{m}C_{p-bf}$	
Nusselt Number	$\frac{\partial Nu}{\partial h} = \frac{L_c}{\kappa}$	Substitute into Equations 3.27
	$\frac{\partial Nu}{\partial L_c} = \frac{h}{\kappa}$	
	$\frac{\partial Nu}{\partial h} = \frac{-hL_c}{\kappa}$	

Convective Heat Transfer Coefficient	$\frac{\partial h}{\partial Q} = \frac{1}{(T_h - T_c)A}$ $\frac{\partial h}{\partial A} = \frac{-Q}{(T_h - T_c)A^2}$ $\frac{\partial h}{\partial T_h} = \frac{-Q}{(T_h - T_c)^2 A}$ $\frac{\partial h}{\partial T_c} = \frac{Q}{(T_h - T_c)^2 A}$	Substitute into Equations 3.28

3.11 ARTIFICIAL INTELLIGENCE

In recent times, the concept of future work has necessitated applying artificial technique (AI) techniques to simulate real-life engineering problems. However, the experimental estimation of the thermal properties of nanofluids (mono, binary and ternary nanofluids) is quite expensive and at times complex. So, to limit the cost and time of experiments, researchers and scientists adopted the idea of developing models and correlations, such as using machine learning models to predict the accurate thermal conductivity of binary nanofluids. Artificial neural network (ANN) is a commonly used machine learning model and mathematical model that are good tools for regression analysis. Literature abound with developed ANN models deployed to predict the thermal conductivity of nanofluids and binary nanofluids for use as heat transfer fluids (HTFs). To achieve a robust and reliable result, these techniques are hybridised with other techniques, as individual method may be deficient in handling high non-linear complex systems.

3.11.1 ANN Architecture

Works on MgO-ZnO/DIW hybrid nanofluids using data-driven techniques like artificial neural network are scarce in the literature. Literature [64, 123, 156, 181, 348, 351, 365, 546-548] affirm that data-driven techniques are good to predict fast, simple and reliable results compared to conventional mathematical approaches under-estimate or over-estimate predicted outputs. The common mathematical approach is either complex or takes a long time to compute predicted output.

The artificial neural network is a combination of components called neurons. The individual layer has many neurons with an activation function to process input data. The mathematical detail for data processing is presented in Equation (3.29).

$$T_i = f_i\left(\sum_{j=1}^{n} w_{ij}x_j + b_i\right) \quad \textbf{3.29}$$

In Equation 3.29, *T* stands for the ANN output, while *n* is the amount of data sets, *f* is for activation function, x_j is the *j*th input parameter, and b_i is the bias of the ith neuron and w_{ij} is the mass. For this work, the activation parameter for every layer is presented as tan *sig (x)* aside output layer. The activation function for the output layer is called Purelin. The Tan *sig* parameter is Tangent Sigmoid and presented in Equation 3.30, and the linear (Purelin) transfer functions presented as Equation 3.31.

$$Tan\ sig\ (x) = \frac{2}{2 + e^{-2x}} - 1 \quad \textbf{3.30}$$

$$Purelin\ (x) = x \quad \textbf{3.31}$$

Purelin represents a linear transfer parameter used to determine the outcome of the model. The Levenberg–Marquardt back-propagation algorithm was used as the learning algorithm for less training time. The algorithm was proposed first in 1944 by Kenneth Levenberg and in 1963 retooled by Donald Marquardt.

Using ANN method in a MATLAB (R2021a) software, experimental data sets were classified as training, validation, and testing randomly. The training data generates biases and masses for the testing, the validation data was used to modify the masses during training session, while the test data sets were used to determine the performance of the neural network. For this work, an optimized ANN to predict k_{bnf} was determined by comparing the performances of the varied neuron numbers within the inner layers, then finally using the best neuron number. This was done by modifying the ANN architecture to determine the optimized neuron number. The suggested learning algorithm is presented as Figure 3.4.

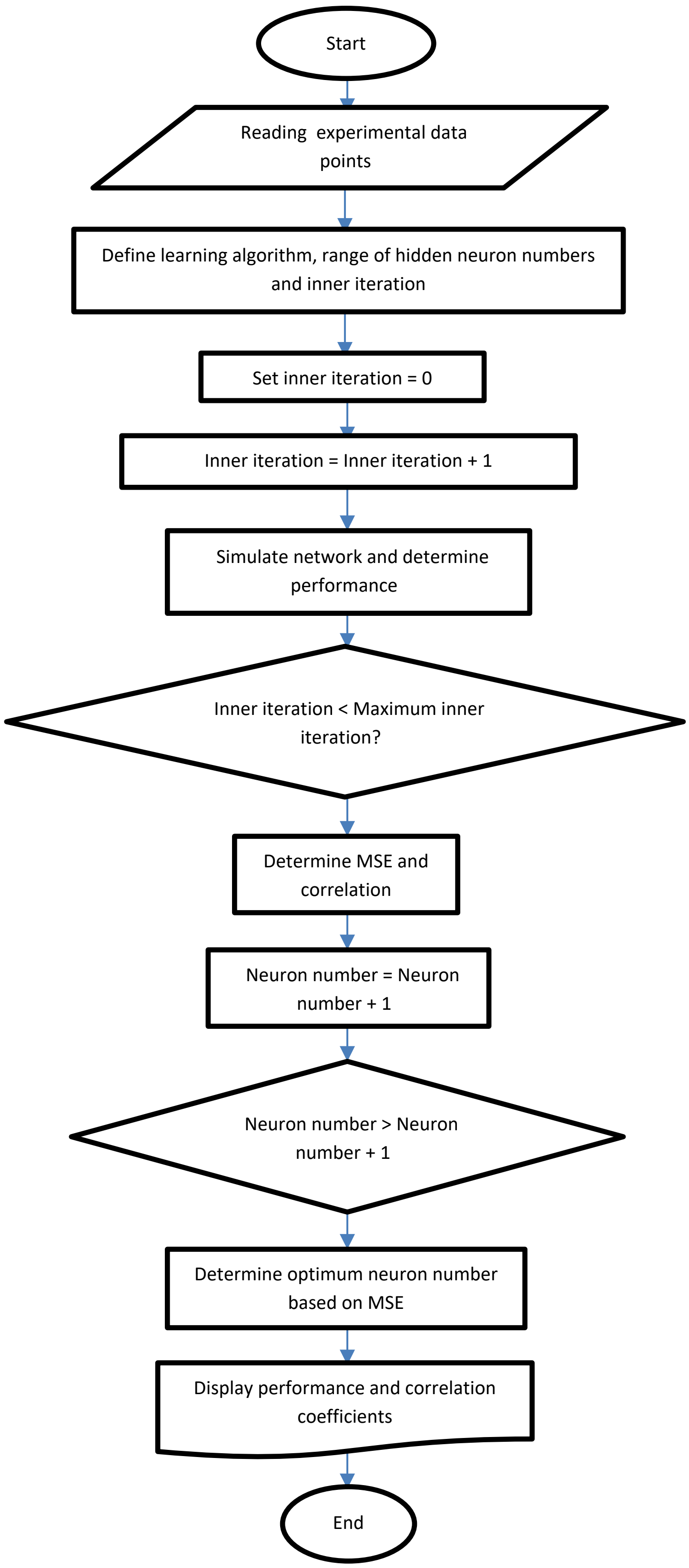

Figure 3.4: Proposed learning algorithm to determine optimized ANN.

3.12 CONCLUSION

The details of equipment, materials, measurements, characterisation, and experiments entailed in this study was given in this chapter. The process for formulating BNFs, the measurements of thermal properties of BNFs, and the thermo-convection performance of BNFs in a squared enclosure were presented. Also, model development for thermophysical properties and *Nu*, and the estimation of uncertainty for thermophysical properties and thermo-convection experiments were detailed in this chapter. ANN as an artificial intelligence method was discussed.

CHAPTER 4

PREPARATION, MORPHOLOGY, AND STABILITY OF BINARY NANOFLUIDS[1,2,3]

4.1 INTRODUCTION

This chapter presents the start of the result presentation obtained in this experimental work. The optimisation of parameters needed for the formulation of BNFs were presented. Then, the morphology of the formulated BNF are identified using TEM analysis and reported. Also, the stability of BNF was monitored and reported.

4.2 PREPARATION OF BINARY NANOFLUIDS

In formulating MgO–ZnO/DIW binary nanofluids (BNF), a two-step approach was used by suspending required volumes of nanoparticles (NPs) samples of MgO (20 nm, 40 nm and 100 nm, ≥99% purity) and ZnO (20 nm, ≥99.5% purity) in basefluid (DIW), for percent weight ratio (PWR) of 20:80, 40:60, 60:40, and 80:20 (MgO/ZnO). A dispersant/surfactant (SDS) was applied to help the nanosuspension process in the basefluid. To augment the stability of the binary nanofluids, three operating parameters of amplitude (70–80%), dispersion fraction (0.6 – 1.2), and sonication time (30 – 120 min) were optimised by measuring electrical conductivity (σ). With this, the Critical micelle concentration (CMC) was obtained via measuring electrical conductivity (σ). The optimisation of the dispersion fraction of BNF is shown in Figure 4.1. The weights of MgO nanoparticles, ZnO nanoparticles, SDS, and basefluid employed in the formulation of BNF are detailed in Appendix A.

This chapter is reflected in parts in the following papers:

[1]Giwa, S., Momin, M., Nwaokocha, C., Sharifpur, M., and Meyer, J. *Influence of nanoparticles size, per cent mass ratio, and temperature on the thermal properties of water-based MgO–ZnO nanofluid: an experimental approach.* Journal of Thermal Analysis and Calorimetry, 2021. **143**(2): p. 1063-1079.

[2]Nwaokocha, C., Giwa S., Ghorbani B., Momin, M., Sharifpur, M., Gharzvini M., Chamkha, A.J., Meyer, J.P., *Experimental formulation and GMDH modelling of thermal conductivity of MgO–ZnO/deionised water hybrid nanofluids.* Ready for submission.

[3]Nwaokocha, C., Momin, M., Sharifpur, M. and Meyer, J., *Influence of concentration, mixing ratios, and working temperature on the thermal behaviour of binary nanofluids of MgO–ZnO: an experimental investigation.* Ready for submission.

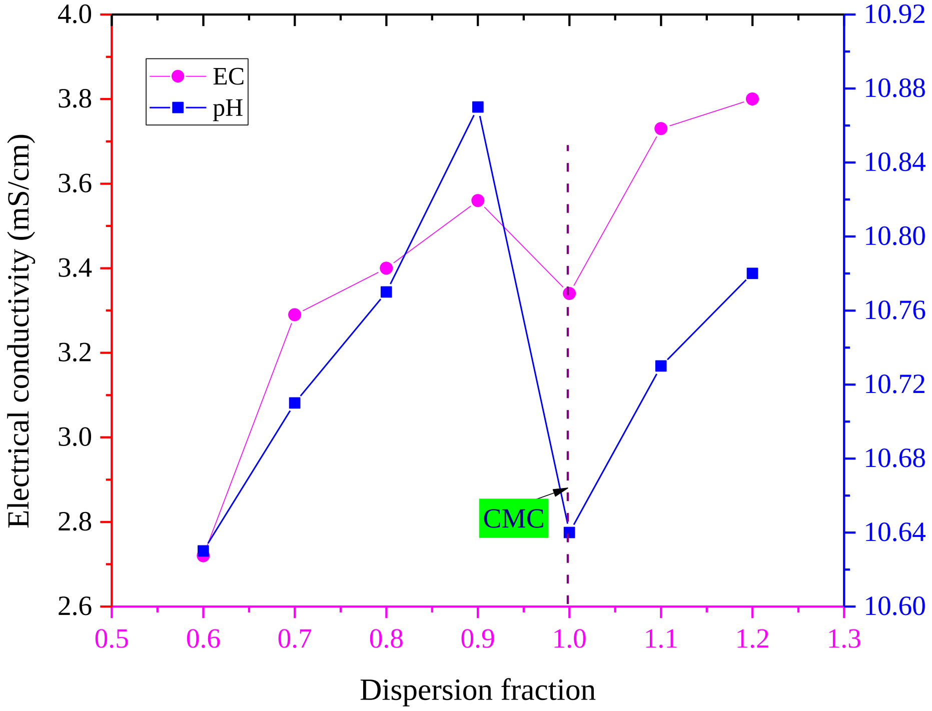

Figure 4.1: Optimization of dispersion fraction using pH and electrical conductivity.

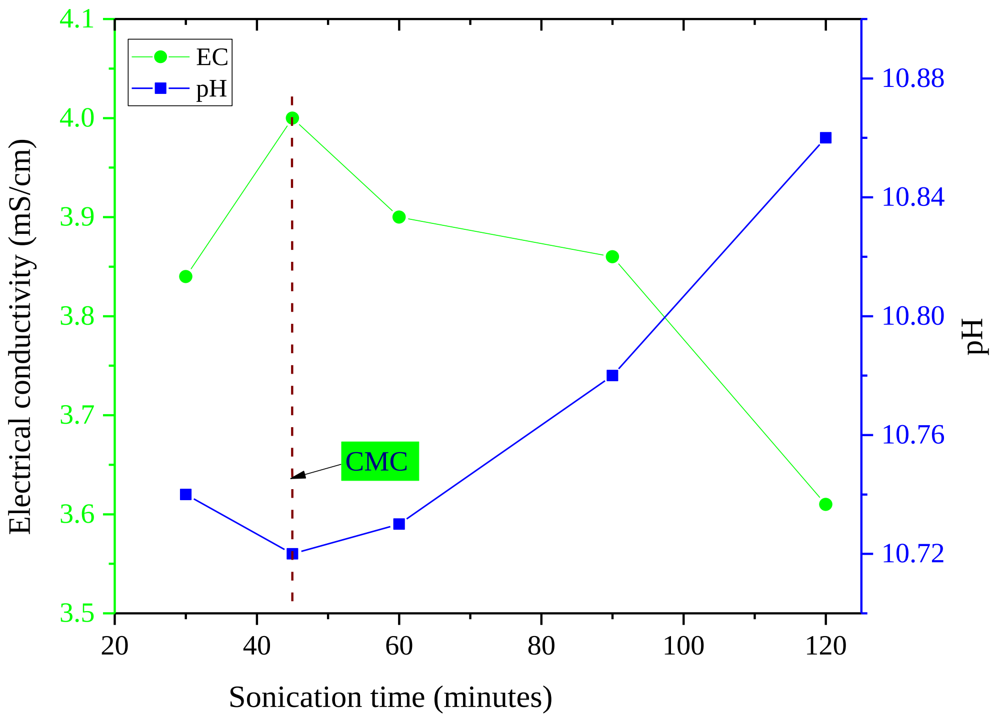

Figure 4.2: Optimization of sonication time employing pH and electrical conductivity.

To achieve the optimized values of three operating parameters (amplitude, dispersion fraction and sonication time), the electrical conductivity (σ) of the binary nanofluid for a percent weight ratio 80:20 (MgO/ZnO) was estimated to derive the Critical micelle concentration. The point for which a deflection was noticed in the σ values trend indicated the CMC which is the optimized result of the variable parameter. Thus, Figures 4.1 and 4.2 depicts the sonication time and optimized dispersion fraction for the prepared DIW-based binary NF. For a dispersion fraction of 1 and a 45 minutes sonication time, CMC (optimal values) was achieved as shown in Figures 4.1 and 4.2. A detraction in the pH and σ values was noticed after improving the two parameters, which later enhanced as the dispersion fraction increased. The dropping point in value is referred to as the point of inflection: the CMC and finally, the optimal dispersion fraction [549, 550]. Also, Figure 4.3 presents the optimized amplitude of the formulated binary nanofluid as 75%. The electrical conductivity (σ) was noticed to detract as the amplitude rises from 70% to 75%, and σ augments as amplitude keeps rising to 80%. The obtained optimized values were used in the formulation of BNF for φ = 0.05 vol.% and 0.1vol.% using Equation 3.1 for the measurement of thermal properties and thermo-convection experiment. Three class of binary nanofluids of MgO(20 nm)–ZnO/DIW, MgO (40 nm)–ZnO/DIW and MgO (100 nm)–ZnO/DIW was prepared to examine the influence of nano-size on thermal properties. Single-particled nanofluids of MgO (100 nm)/DIW, MgO (20 nm)/DIW, and ZnO (20 nm)/DIW were also prepared for comparison.

Giwa et al. [96] dispersed binary nanoparticles of 75% (Fe_2O_3):25% (Al_2O_3) into DW and EG/DW(50:50) basefluids using a two-step method for an optimized dispersion fraction of 1.1, sonication time of 120 minutes and amplitude of 70%. Also, Giwa et al. [31] formulated MWCNT-Fe_2O_3/DIW binary nanofluids (0.1 vol%) using SDS as dispersant for an optimized dispersion fraction of 0.5, sonication time of 120 minutes and amplitude of 70%. Sundar et al. [551] used a surfactant to formulate CNT-Fe_3O_4/DIW nanofluid at an optimized dispersion fraction of 0.5. The optimized sonication time (120 minutes) and amplitude (70%) were within the published range when compared with previous works. Garbadeen et al. [27] formulated MWCNT/DIW nanofluid using Gum Arabic as dispersant for a dispersion fraction of 4, sonication time of 40 minutes and amplitude of 75%. Joubert et al. [224] also formulated Fe_2O_3/DIW nanofluid using SDS surfactant for a 1.0 dispersion fraction, a 42 minutes sonication time and amplitude of 65%.

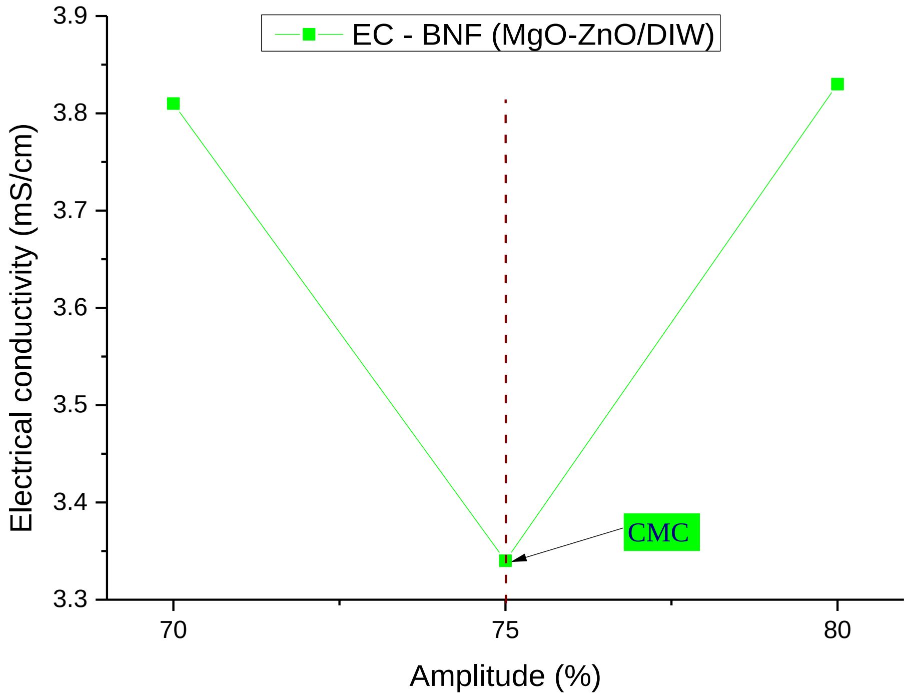

Figure 4.3. Determination of optimized amplitude for BNF.

4.3 MORPHOLOGY AND STABILITY OF MONO-NANOFLUIDS

In monitoring the stability of single-particled nanofluid (DIW-based MgO-100 nm, MgO-20 nm and DIW-based ZnO nanofluid), absorbance was monitored for 20 hours duration using a UV-visible spectrophotometer. Figure 4.4 shows that the absorbance of individual samples was stable with time along a nearly straight-line in the horizontal axis. It observed that the absorbance of DIW-based ZnO nanofluid was higher when compared to DIW-based MgO-100 nm and MgO-20 nm nanofluids. In like manner, the wavelength of ZnO/DIW NF (369 nm) was observed to be more than that of DIW-based MgO (100 nm and 20 nm) NFs (291 nm), as shown as in Table 4.1. In addition, visual checks of mono-nanofluids samples showed nil or little sedimentation for the duration considered.

4.4 MORPHOLOGY AND STABILITY OF BINARY NANOFLUIDS

In monitoring the stability of MgO-ZnO/DIW binary nanofluids, absorbance was also monitored for a 20-hour duration using a UV-visible spectrophotometer. Figure 4.5 shows that MgO/ZnO (20:80) binary nanofluids have more absorbance than MgO/ZnO (80:20) binary nanofluids. In a similar pattern, MgO/ZnO (20:80) binary nanofluids had more wavelengths (330 nm and 362 nm) over that of MgO/ZnO (80:20) binary nanofluids (293 nm and 298 nm). The feedback (for wavelength and absorbance) can be ascribed to hybridizing MgO and ZnO nanoparticles. So, Table 4.1 presents the absorbances and wavelengths of the selected BNFs.

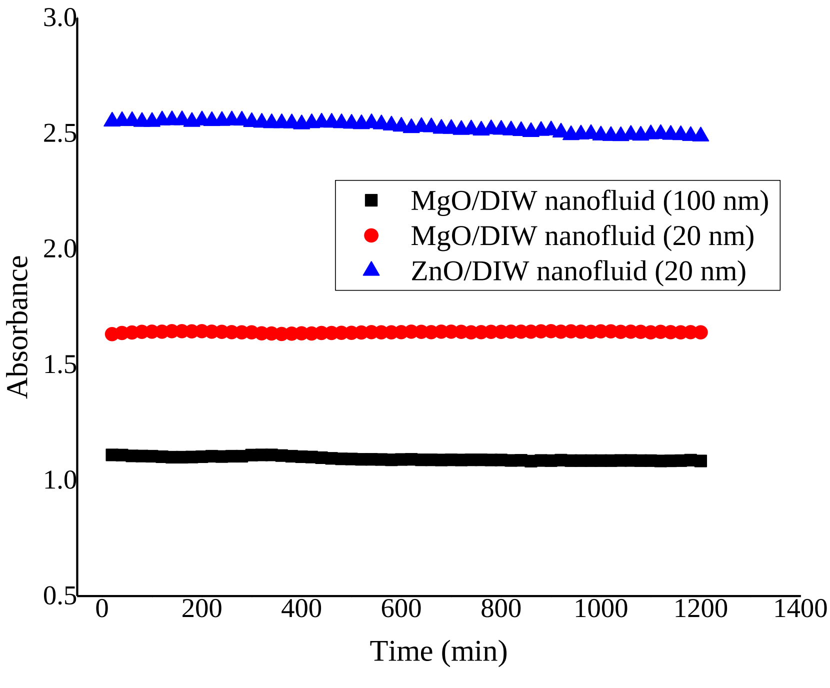

Figure 4.4. Monitoring of stability of single-particle nanofluids

Open literature affirms that the absorbances of 1.631, 2.125, 2.341, 2.602, and 3.138 at a wavelength range of 289 nm – 292 nm was published for 0.05 vol%, 0.10 vol.%, 0.30 vol.%, and 0.40 vol.%, respectively. The wavelengths of 225, 252, 264 and 410 nm were reported for nanofluids of Al_2O_3/DIW, CNT/DW, MWCNT-Ag/W and Ag/DW nanofluids, respectively [552, 553]. The absorbance for the BNF was observed to be slightly higher than that of single-particle nanofluids of MgO and ZnO, which makes for a reasonable degree of hybridisation of ZnO and MgO nanoparticles in the BNF. Visual inspection of single-particle nanofluids and binary nanofluids showed nil or little sediments for the duration considered, further supporting these samples' stability.

Table 4.1: Wavelength and absorbance of mono- and binary nanofluids

Variable	MgO (20 nm)	MgO (100 nm)	ZnO (20 nm)	MgO-ZnO (20:80)-20 nm	MgO-ZnO (20:80)-100 nm	MgO-ZnO (80:20)-20 nm	MgO-ZnO (80:20)-100 nm
Absorbance	1.650	1.773	2.565	4.364	4.468	2.869	1.839
Wavelength	291	291	368	362	330	298	292

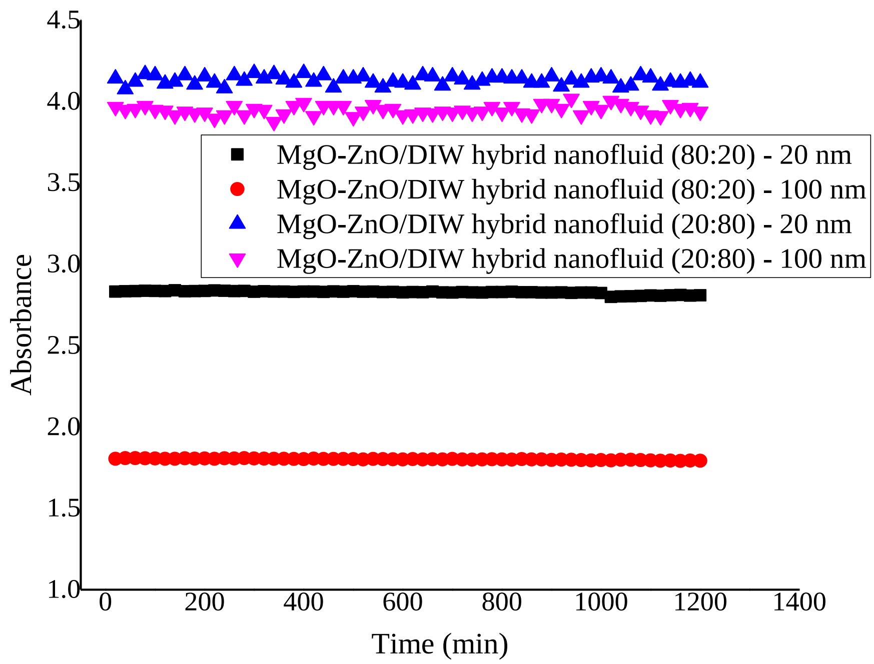

Figure 4.5. Monitoring of stability of selected binary nanofluids

In addition, the binary nanofluids samples were observed to be stable as visual checks showed nil or little sediments for the duration considered. The TEM image as presented in Figure 4.6 showed that the nanoparticles of MgO and ZnO were observed to be well dispersed in DIW. Figures 4.6 showed light spots representing ZnO nanoparticles, while Dark spots represented MgO nanoparticles. The examined samples revealed more light spots than dark spots, which means the TEM discovered more ZnO nanoparticles over MgO nanoparticles. This outcome agrees with the binary nanofluids samples employed for the TEM analysis. In Figure 4.6a, TEM images discovered almost 20 nm for ZnO nanoparticle, and 100 nm for MgO nanoparticles, while Figure 4.6b shows 20 nm was detected for ZnO nanoparticles and 20 nm for MgO nanoparticles, and Figure 4.6c shows 20 nm was detected for ZnO nanoparticles and 40 nm for MgO nanoparticles. That is, results were close to that specified by the manufacturers of the BNPs. In summary, Figure 4.6 reveals a good degree of nanoparticles dispersion was achieved for all percent weights ratio.

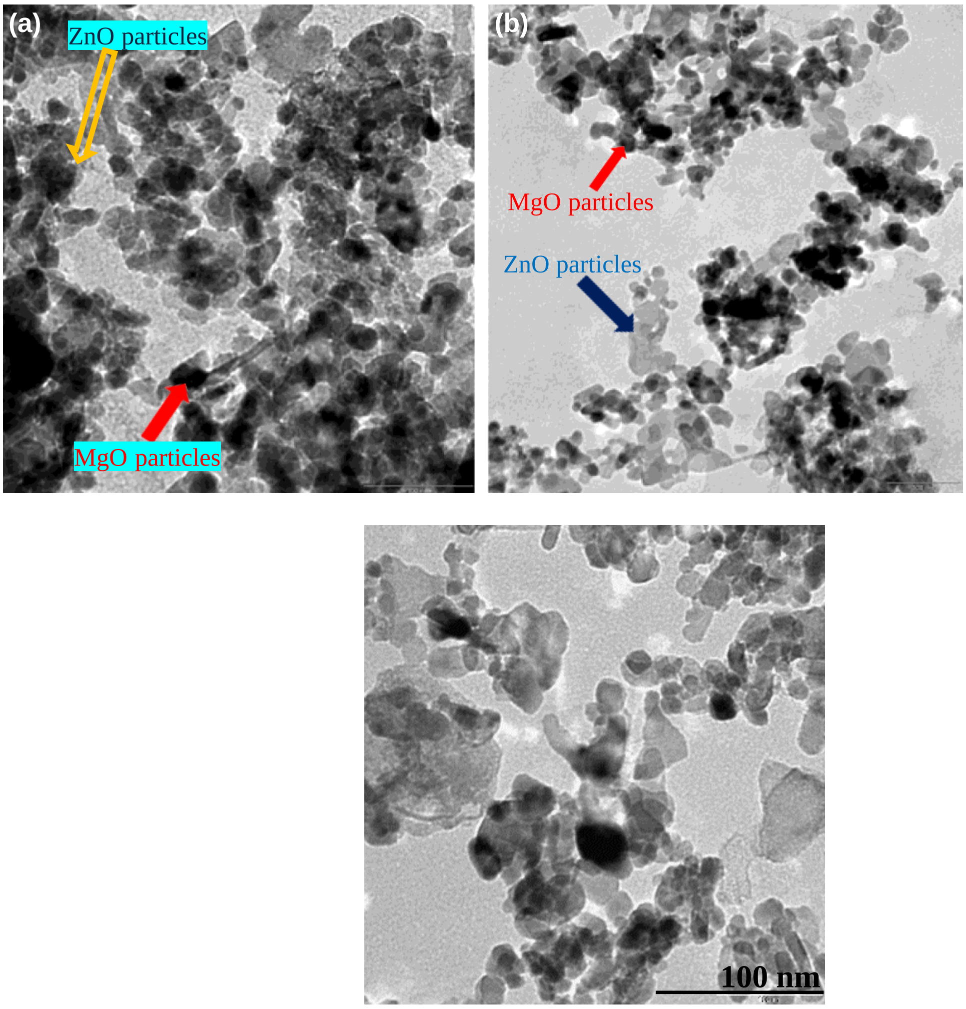

Figure 4.6. The TEM image for: **(a)** MgO(100 nm)–ZnO(20:80)/DIW binary nanofluids, **(b)** MgO(20 nm)–ZnO(20:80)/DIW binary nanofluids, and **(c)** MgO(40 nm)–ZnO (20:80)/DIW binary nanofluid.

4.5 CONCLUSION

Open literature has affirmed scarcity in the values for optimum parameters (amplitude, dispersion fraction, pulse used, and sonication time) for formulating mono-particle nanofluids and binary nanofluids. This affects the repeatability of such experiments. This investigation formulated mono-particle nanofluids of MgO and ZnO, for comparison with binary nanofluids of MgO-ZnO/DIW for φ of 0.10 vol.% and 0.05 vol.% via optimized operating parameters leading to a stable BNFs. TEM images detected nanoparticle sizes close to the manufacturers and a good degree of nanosuspension stability. In addition, the stability of BNFs as observed by the absorbance was found stable. Thus stability and morphology is confirmed satisfactory. Hence, further investigation on thermal properties and thermo-convection was done, and the results were presented and discussed in subsequent chapters.

CHAPTER 5

MEASUREMENT OF THERMAL PROPERTIES OF BINARY NANOFLUIDS[1,2,3]

5.1 INTRODUCTION

The estimation of thermal properties of binary nanofluids is of great interest as it serves as indicators for its potential use in engineering applications, especially for thermo-convection investigation as done in this study. This Chapter presents the thermal properties of stable BNF as measured under study temperatures and volume concentration, using applicable equipment. Measured thermophysical characteristics of MgO–ZnO/DIW binary nanofluids are pH, viscosity (μ), thermal conductivity (κ), and electrical conductivity (σ), under temperatures of 20-50 °C. In addition, models were developed for the BNF samples using measured datasets, as models are scarce in the open literature for BNFs.

5.2 THERMAL CONDUCTIVITY OF BINARY NANOFLUIDS

To affirm the degree of correctness for the measuring instrument for the thermal conductivity (κ) of binary nanofluids (BNFs), a validation check was necessary to examine temperatures 20 ^{O}C to 50 ^{O}C. This was ascertained by relating the experimental dataset with documented standards in the ASHRAE standard handbook. Figure 5.1 depicts the compared dataset, which shows a deviation from experimental values compared to the data in the ASHRAE standard handbook [555] as 1.3%, which has been the measurement accuracy.

This chapter is reflected in parts in the following papers:

[1]Giwa, S., Momin, M., Nwaokocha, C., Sharifpur, M., and Meyer, J. *Influence of nanoparticles size, per cent mass ratio, and temperature on the thermal properties of water-based MgO–ZnO nanofluid: an experimental approach.* Journal of Thermal Analysis and Calorimetry, 2021. **143**(2): p. 1063-1079.
[2]Nwaokocha, C., Giwa S., Ghorbani B., Momin, M., Sharifpur, M., Gharzvini M., Chamkha, A.J., Meyer, J.P., *Experimental formulation and GMDH modelling of thermal conductivity of MgO–ZnO/deionised water hybrid nanofluids.* Ready for submission.
[3]Nwaokocha, C., Momin, M., Sharifpur, M. and Meyer, J., *Influence of concentration, mixing ratios, and working temperature on the thermal behaviour of binary nanofluids of MgO–ZnO: an experimental investigation.* Ready for submission.

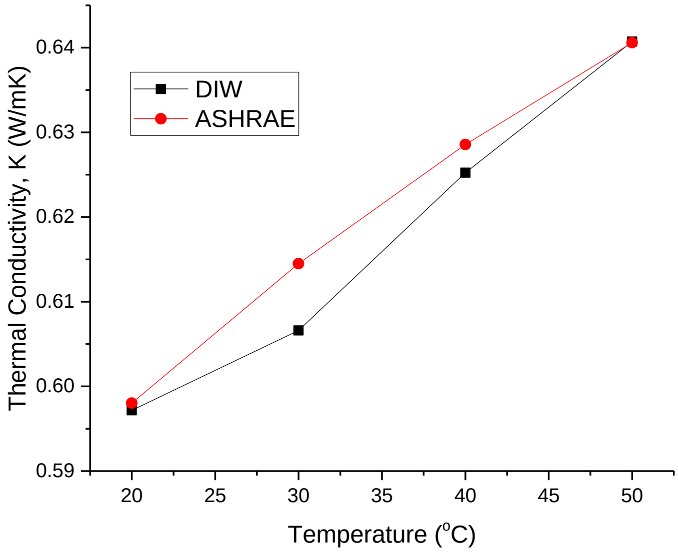

Figure 5.1. Comparison of DIW with reference values.

The thermal conductivity (κ) of DIW-based mono-particles nanofluids (100 nm-MgO, 20 nm-MgO and 20 nm ZnO) is shown in Figure 5.2. It was noticed that by dispersing nanoparticles into basefluid, its κ enhanced notably with an increase in temperature, which agrees with the literature [132, 215, 217, 554, 555]. Figure 5.2 shows a higher κ for MgO/DIW NFs over ZnO/DIW nanofluids. Also, MgO(20 nm)/DIW NF was observed to have a more effective κ over MgO(100 nm)/DIW NF.

5.2.1 Influence of Nanosize, Percent Weight Ratios and Temperature on Thermal Conductivity

The trio influence of nanoparticle size (NS), various percent weight ratios (PWRs) under rising temperature on the thermal conductivity of MgO-ZnO/DIW binary nanofluid for 0.1 vol.% is presented in Figures 5.2 to 5.4. From Figures 5.2 to 5.4, it can be deduced that dispersing nanoparticles into DIW, its κ enhanced significantly with steady increase in temperature, which agrees with open literature [42, 132, 152, 171, 215, 217, 554, 555]. As presented in Figure 5.3 for 20 nm-MgO, the 40:60 BNF sample had the maximum effective thermal conductivity (κ), then other BNF samples follow in order of 60:40, 80:20, and 20:80. A similar trend was noticed for MgO(100 nm)-ZnO/DIW binary nanofluid, as seen in Figures 5.4. The synergy between the thermal conductivity of MgO (54.9 W/mK) and ZnO (29 W/mK) nanoparticles [556] could be responsible for the obtained results. Also, the 20 nm-MgO based binary nanofluids had more effective thermal conductivity over 100 nm-MgO BNFs, for the studied PWRs. Figures 5.3 and 5.4 deduced that MgO nano-size had a great influence on κ, then PWR and finally temperature.

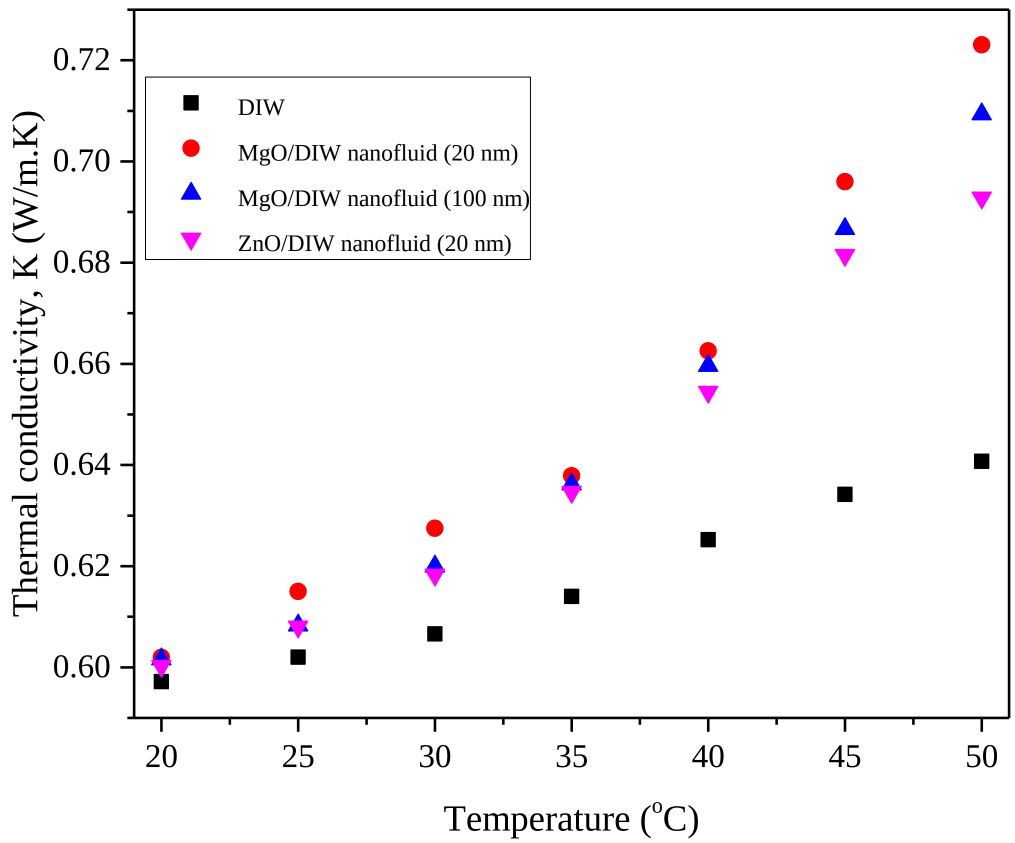

Figure 5.2. Effective thermal conductivity of single-particled nanofluids as temperature rises.

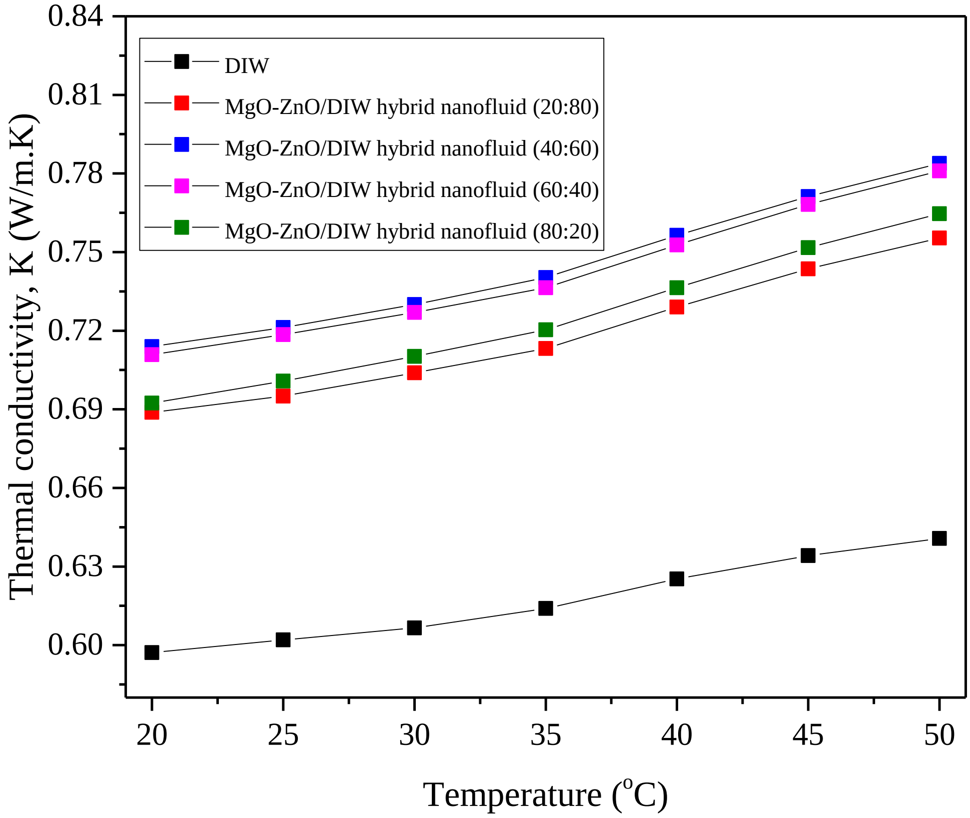

Figure 5.3. Effective thermal conductivity for MgO(20 nm) based binary nanofluids as temperature rises.

From Figure 5.3, the effective κ of 20 nm-based binary nanofluids was enhanced by 15.35% – 22.33% under rising temperature, while it improved by 9.52% – 17.91% for 100 nm-based binary nanofluids as presented in Figure 5.4 when compared to DIW. Maximum augmentation of 19.56% – 22.33% and 14.95% – 17.91% was observed for 40:60 BNF sample of 20 nm-MgO and 100 nm-MgO nanoparticle's sizes, respectively. In the same vein, the lowest detraction in effective κ was observed for 15.35%–17.89% and 9.52%–12.97% for 20 nm-MgO and MgO (100 nm) based 20:80 BNFs, respectively. Siddiqui et al. [557], and Hamid et al. [261] published a maximum κ augmentation for 50:50 (Cu-Al_2O_3/DIW) and 20:80 (TiO_2-SiO_2/W-EG). An enhancement of 14.17% was reported by Giwa et al. [132] for κ for Fe_2O_3-Al_2O_3 (75:25)/DIW BNF for 0.3 vol% and 40 °C. Aparna et al. [227] published a maximum κ augmentation of 23.82% for Al_2O_3-Ag (50:50)/DIW binary nanofluids at 0.1 vol% for 52 °C. Also, Zadkhast et al. [349] published an effective κ enhancement of 30.38% [45] for CuO-

MWCNT (50:50)/DIW binary nanofluids for 0.60 vol.% at 50 °C. Next, Sundar et al. [551] reported an effective *κ* improvement of 24.46% for CNT-Fe_3O_4 (26:74)/DIW binary nanofluids at 0.30 vol.% for 60 °C. In addition, Sundar et al. [90] attained the highest *κ* enhancement of 29.39% for ND-Ni/DIW BNF at 0.3 vol% and 60 °C. Taherialekouhi et al. [558] also achieved a maximum *κ* augmentation of 33.9% for GO-Al_2O_3/DIW BNF. The obtained results from this current investigation were noticed to be within published range in the open literature.

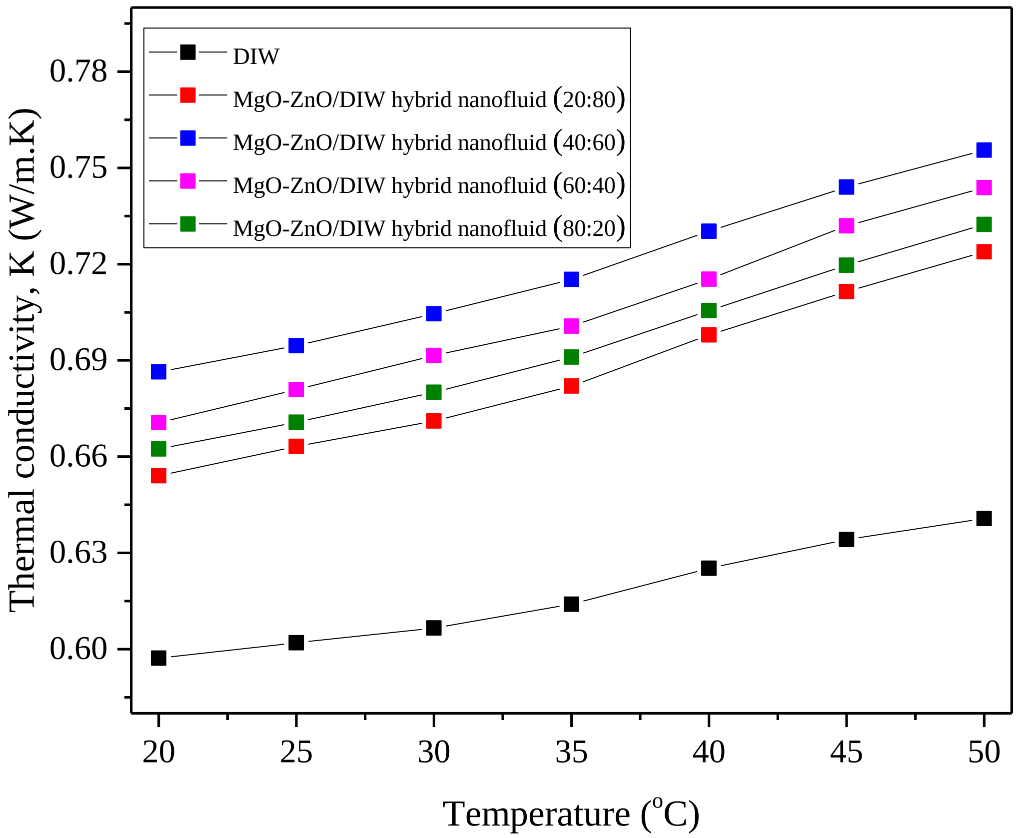

Figure 5.4. Effective thermal conductivity for MgO(100 nm) based binary nanofluids as temperature rises.

5.2.2 Influence of Concentration, Mixing Ratios and Temperature on Thermal Conductivity

The thermal conductivity (κ) of BNFs as a function of *φ* (0.05 and 0.1 vol.%) for different PWRs and temperatures 20–50 °C is presented in Figures 5.5 and 5.6. The nanosuspension of

BNPs into DIW clearly enhanced κ. The κ of BNFs was observed to show good improvement for all PWRs at rising temperature. This supports published works [33, 96, 154, 156, 262, 278, 362, 559-561]. As presented in Figure 5.5 for 0.05 vol% BNFs, the 60:40 nanohybrid samples were observed to possess a maximum *κ,* next 40:60, 80:20 and 20:80 BNFs samples. For 0.10 vol% BNFs illustrated in Figure 5.6, it was observed that 40:60 BNF sample was observed to possess maximum *κ* and then trailed by 60:40, 80:20, and 20:80 samples.

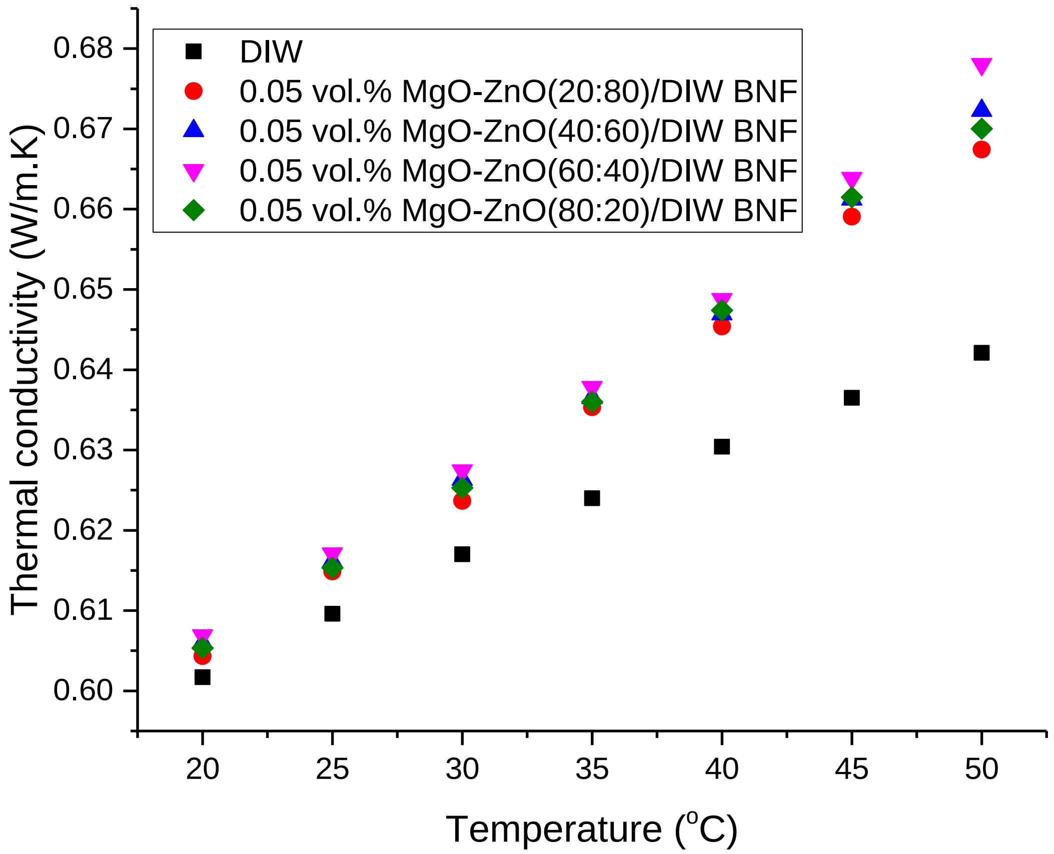

Figure 5.5. Thermal conductivity of MgO-ZnO/DIW binary nanofluids (0.05 vol%) with temperature increase for different percent weight ratios.

The synergy between *κ* of NPs, PWR and volume concentration may be responsible for the results. Maximum *κ* of 0.67803 W/mK was observed for BNF (60:40) for φ = 0.05 vol% at temperature 50 °C, while lowest *κ* value of 0.60433 W/mK was obtained for BNF (20:80) at temperature 20 °C. For BNFs of φ = 0.10 vol%, highest *κ* result was 0.78381 W/m.K for BNF (40:60) at temperature 50 °C, while lowest *κ* value of 0.68883 W/m.K was observed for BNF

(20:80) at temperature 20 °C. Increase in temperature augmented κ for the BNFs as compared to the BF, due to the impact of Brownian motion on NPs at higher temperatures. The influence of Brownian motion on κ of NFs is published in the literature [69, 145, 261, 561-565].

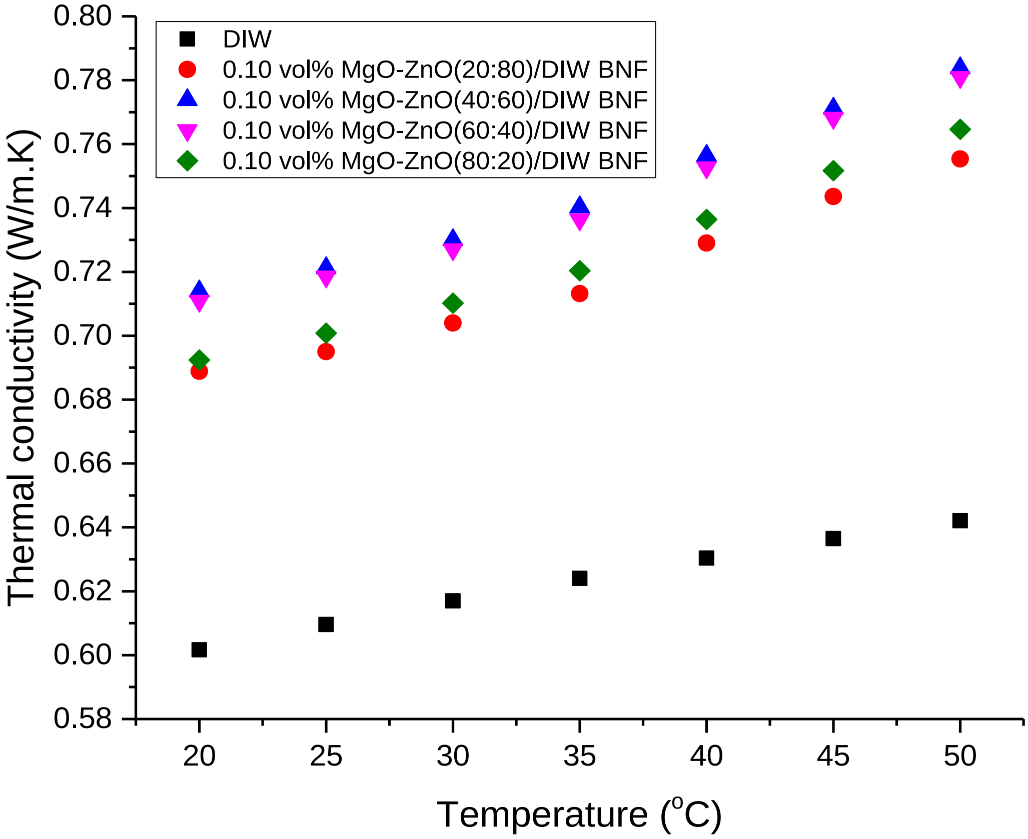

Figure 5.6. Thermal conductivity of MgO-ZnO/DIW binary nanofluids (0.1 vol%) with temperature increase for different percent weight ratios.

Thermal conductivity enhancement (TCE, %) of BNFs under the influence of temperature (20 °C to 50 °C) is presented as Figures 5.7 and 5.8 for two-volume concentrations (0.05 vol% and 0.1 vol%) and four PWRs. Figure 5.7 presents maximum TCE enhancement of 5.60% for 60:40 nanohybrid sample of 0.05 vol% BNFs, while for 0.1 vol.% BNFs, highest improvement of 22.07% for 40:60 BNF sample was achieved as shown in Figure 5.8. Figures 5.7 and 5.8 shows that the dispersion of MgO-ZnO NPs augments κ greatly, especially at higher temperatures. Open literatures reported κ improvement of 66.5% for TiO_2-Al_2O_3(50:50)/W at 1.0 vol.% and 70°C [262], 17.7% for ND- Fe_3O_4(72:28)/W at 0.2 vol.% and 60°C [566], 14.17% for

MWCNT-Fe_2O_3/DIW at 0.4 vol.% and 40°C [28], 22.1% for TiO_2-SiO_2(60:40)/W-EG at 3.0 vol.% and 70°C [229].

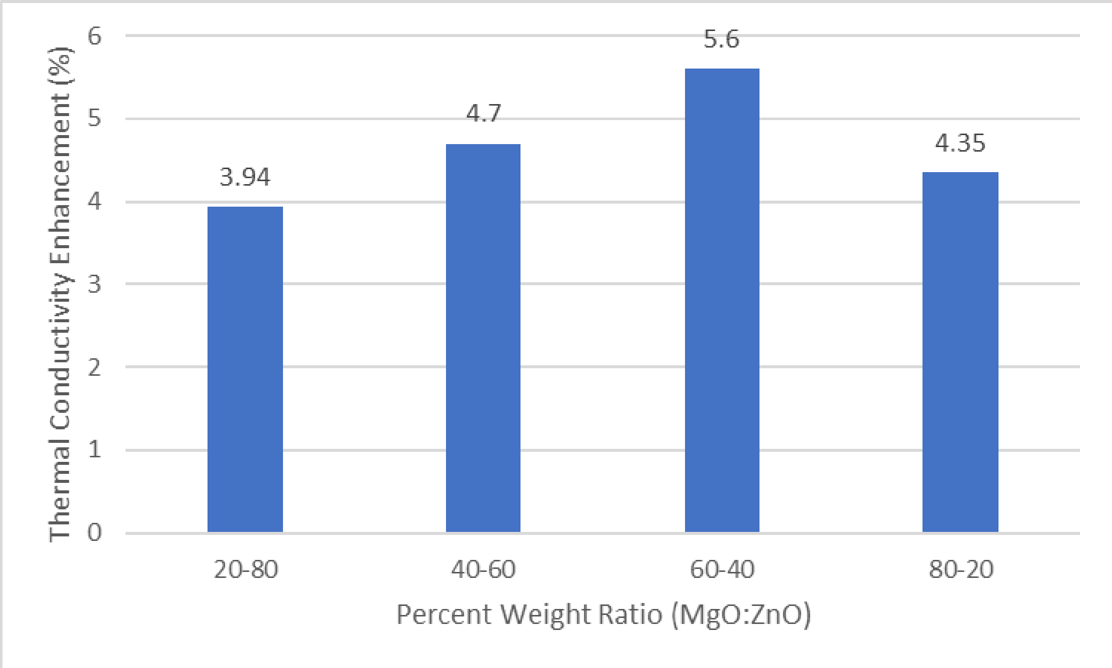

Figure 5.7. Thermal conductivity enhancement (%) for 0.05 vol% BNF.

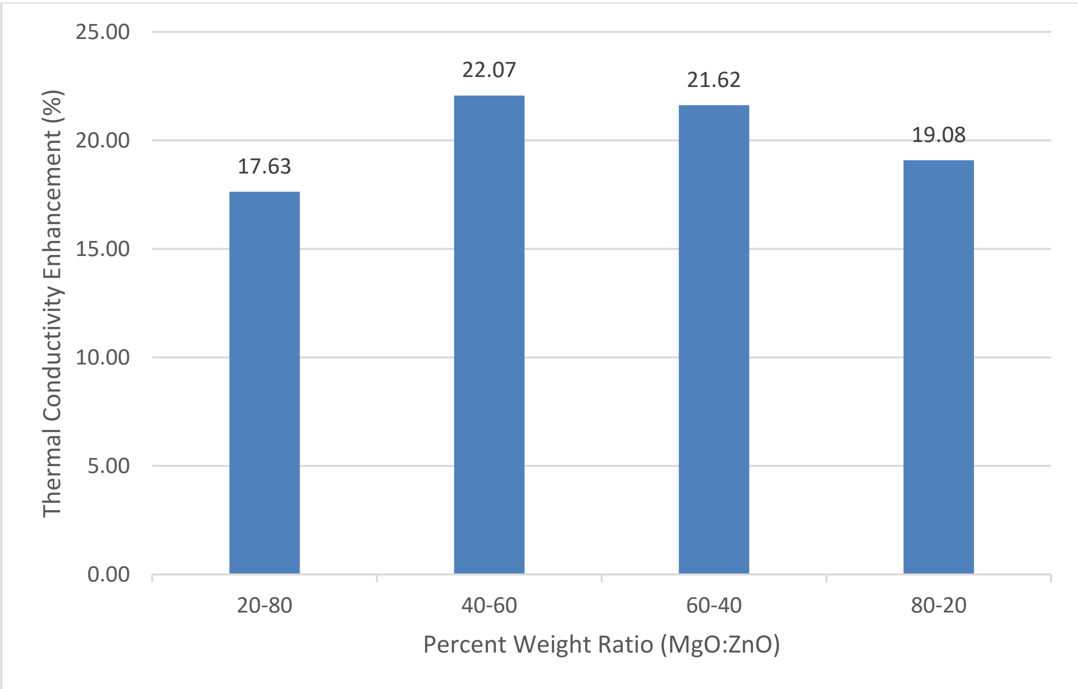

Figure 5.8. Thermal conductivity enhancement (%) for 0.10 vol% BNF.

Figures 5.9 and 5.10 also presents the influence of PWRs on κ of MgO-ZnO/DIW BNFs (0.05 and 0.10 vol%) for the studied temperatures. It is observed in Figure 5.9 that κ increases as PWR of MgO increase steadily to a higher value for 60:40 sample and then detracts. Also, the lowest κ was observed for the 20:80 BNF nanohybrid sample has had the least composition of MgO NP between the temperature range 20°C to 50°C. It is observed in Figure 5.10 that κ increases as PWR of MgO increase steadily to a higher value for 40:60 sample. In addition, a further rise in MgO NP detracted thermal conductivity, with the least κ for the lowest composition of MgO NP (20:80) for the studied temperature. The detraction in κ could be attributed to the deterioration in dispersion stability as observed visually.

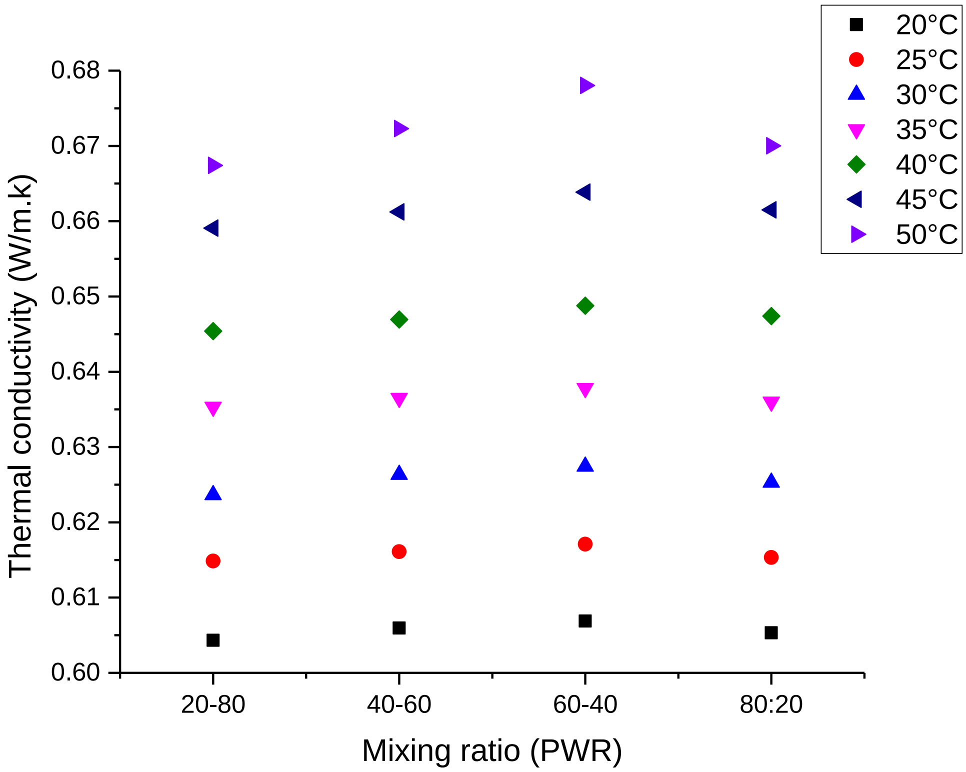

Figure 5.9. Influence of PWRs on the thermal conductivity of 0.05 vol% BNF.

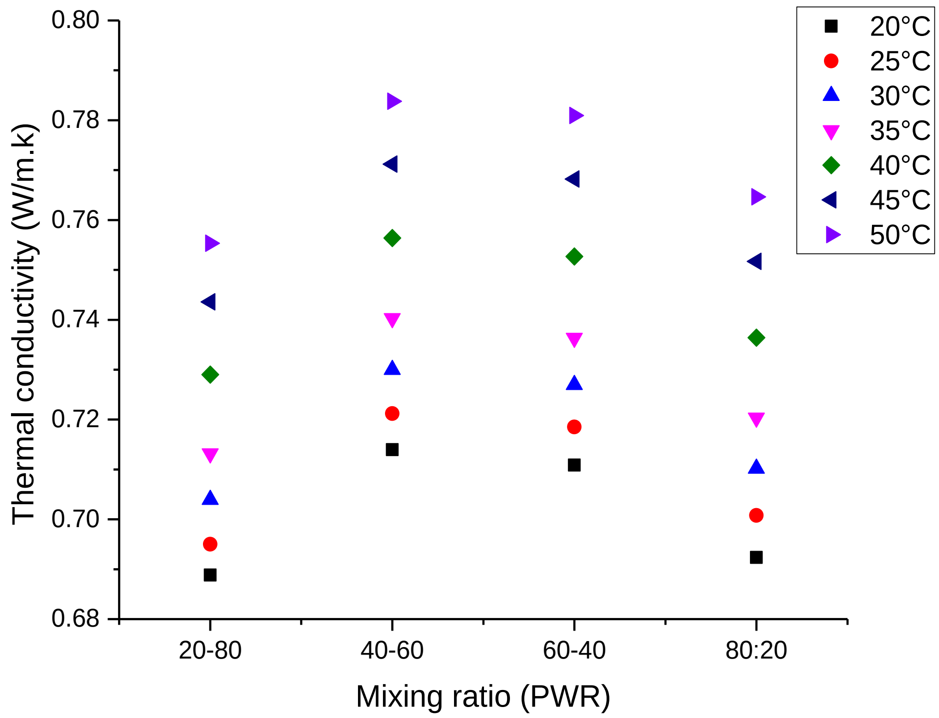

Figure 5.10. Influence of PWRs on the thermal conductivity of 0.10 vol% BNF.

5.3 VISCOSITY OF BINARY NANOFLUIDS

Viscosity (μ) explains the resistance to the flow of fluid under shear stress. In investigations that involves the estimation of the thermal properties of nanofluid, viscosity follows thermal conductivity measurement.

5.3.1 Influence of Nanosize, Percent Weight Ratio and Temperature on Viscosity

MgO and ZnO possess nano--densities of 3.56 g/m^3 and 5.606 g/m^3 [556], respectively, with the viscosity of ZnO NPs higher than MgO NPs. Hence, the viscosity of the binary nanofluids is the offshoot of the blend between the density of MgO and ZnO nanoparticles and DIW, as naratted in Figure 5.11. So in Figure 5.11, it was noticed that ZnO/DIW nanofluid had a more effective viscosity over MgO/DIW nanofluids for both nano-sizes of 20 nm and 100 nm. This observation is in agreement with the investigation of Assdi et al. [556], who published a more viscosity for ZnO/EO nanofluid than MgO/EO nanofluid. Also, MgO(20 nm)/DIW nanofluid had the least viscosity over 100 nm MgO/DIW nanofluid. This negates the result of Adio et al.

[32] for MgO/EG nanofluids with nano sizes of 15, 21, and 125 nm. This discrepancy may be accounted for by density and basefluid type.

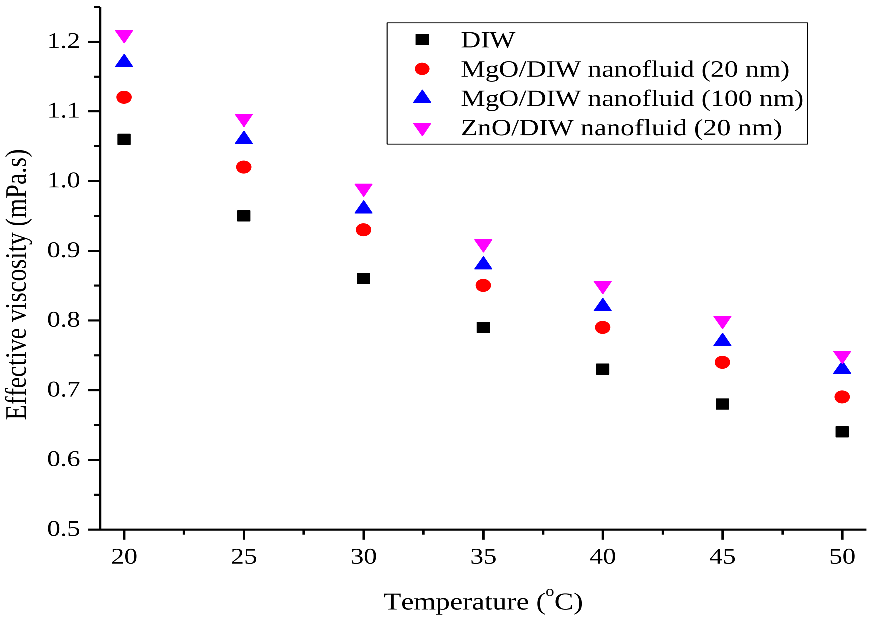

Figure 5.11. Effective viscosity of single-particle nanofluids with temperature rise.

In Figures 5.12 and 5.13, the impact of temperature and PWRs on the viscosity of binary nanofluid samples was depicted for MgO nanoparticles (20 nm and 100 nm). From Figures 5.12 and 5.13, as temperature increases from 20 to 50 °C, it gradually detracts the relative viscosity of binary nanofluids. This outcome agrees with published results on the effect of temperature on the effective viscosity of nanofluids [21,32–35]. As observed in Figure 5.12, the PWR 60:40 had the maximum effective viscosity, while 20:80 sample BNF sample had the least effective viscosity for 20 nm-MgO based BNFs. A similar trend was noticed in Figure 5.13 for the 100 nm-MgO based binary nanofluids with the 60:40 and 20:80 binary nanofluids possessing the highest and lowest effective viscosity, respectively. Open literature posits a different result for highest effective viscosity compared with Giwa et al. [36] (80:20; Al_2O_3-MWCNT) and Hamid et al. [21] (50:50; TiO_2-SiO_2), who published the viscosity of DIW and W/EG based binary nanofluids with Al_2O_3 and TiO_2 nano-particles being denser than MWCNT and SiO_2 nanoparticles, respectively.

When comparing Figures 5.12 and 5.13, a minor discrepancy was observed for the effective viscosity results of the experimental formulation of MgO-ZnO/DIW binary nanofluid with various nano-sizes of MgO nanoparticles and different PWRs. Also, using the MgO nano-size of 20 nm to formulate the BNF, a detraction in μ was observed. A rise in the nano-size of MgO NPs from 20 nm to 100 nm enhanced the μ for all BNF samples. Adio et al. [32] reported a different result, such that a rise in NPs' size (21 nm to 125 nm) led to a μ detraction for MgO/EG nanofluids. However, a different outcome was reported for μ based on the nano-size of nanofluids [246]. In summary, MgO nano-size greatly influenced the μ of BNFs, trailed by the impact of temperature and, finally, PWR of binary nano-particles.

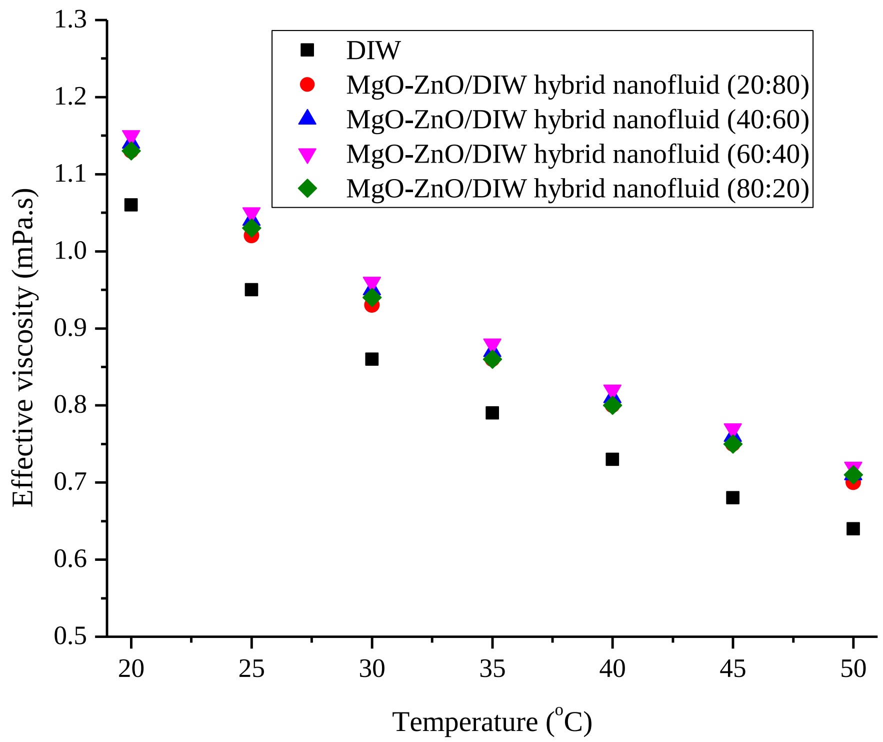

Figure 5.12. Effective viscosity of MgO (20 nm) based binary nanofluids as temperature rises.

Upon comparison to the basefluid (DIW), an enhanced μ for single-particle nanofluid was observed as 5.46% – 9.52% for 20 nm-MgO/DIW nanofluids, 10.17% – 15.87% for 100 nm-MgO/DIW nanofluids, and 13.94% – 19.05% for DIW-based ZnO (20 nm), for the temperature range studied. This supports the works of Asadi and Pourfattah [37] who reported a 75% and 124% enhancements for EO-based MgO and ZnO nanofluid for 1.5 vol% at 55 °C. For 20 nm-MgO based binary nanofluids, μ improvements of 6.40% – 11.1% and 8.29% – 14.29% were observed for PWRs of 60:40 and 20:80, respectively compared to DIW. For 100 nm-MgO based binary nanofluids, μ improvements of 11.11% – 15.87% and 12.99% – 17.46% was also observed for PWRs of 60:40 and 20:80, respectively when related to DIW for the examined temperatures. Sundar et al. [90] published the highest viscosity enhancement of 23.24% for ND-Ni/DIW BNF at 0.30 vol% and 60 °C. Giwa et al. [36] reported the highest μ enhancements of 24.56% for 0.1 vol% at 55 °C for a DIW-based Al_2O_3-MWCNT (80:20). Sundar et al. [11] achieved the highest 1.5-fold viscosity enhancement at 0.3 vol% and 60 °C for DIW-based CNT-Fe_3O_4 (26:74). Giwa et al. [39] achieved μ enhancements of 4.55 – 20.43% for at 0.05 – 0.30 vol% and 20 – 60 °C) for DIW-based Al_2O_3-Fe_2O_3 (25:75) nanofluids.

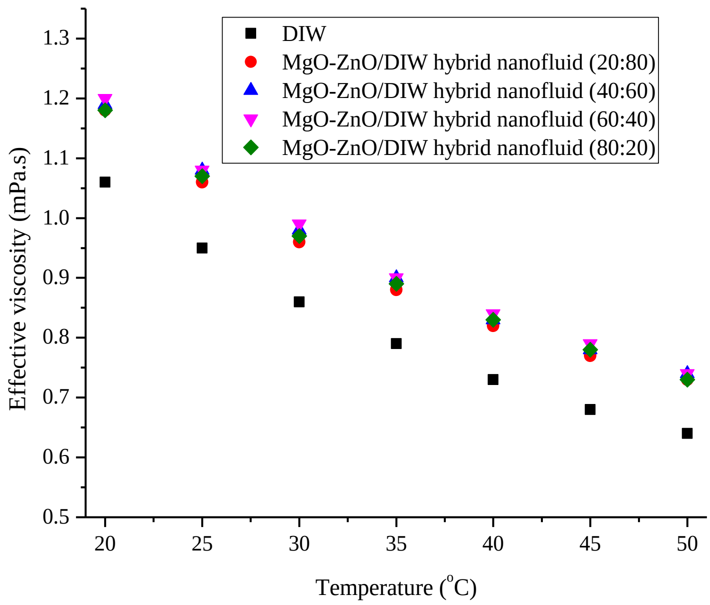

Figure 5.13. Effective viscosity of MgO (100 nm) based binary nanofluids as temperature increases.

5.3.2 Influence of Concentration, Mixing Ratio and Temperature on Viscosity

As viscosity (μ) plays major role in defining the pumping power requirements of heat exchangers, hence nanofluid's viscosity behaviour is key. Figures 5.14 and 5.15 presents the μ of BNFs for φ of 0.05 and 0.1 vol.% for four separate nanoparticle mixing ratios for each φ under the influence of rising temperatures from 20–50 °C. From Figures 5.14 and 5.15, it was observed that at rising temperature, μ of the BNFs and DIW detracted steadily, which agrees with the literature [21, 31, 39, 96, 248, 261, 262, 368, 567, 568]. This observation is premised on the improvement of the kinetic energy of nanoparticles at higher temperatures, leading to a faster rate of movement of molecules. Figures 5.16 and 5.17 presents the impact of PWRs on μ of MgO-ZnO/DIW BNFs (0.05 and 0.10 vol%) for the considered temperatures. It is observed in Figures 5.16 that μ rises gradually to a peak for PWR of MgO-ZnO at 40:60 and detracts thereafter. But for Figures 5.17, μ rises steadily to a peak value when PWR of MgO-ZnO is 60:40 and reduces after that.

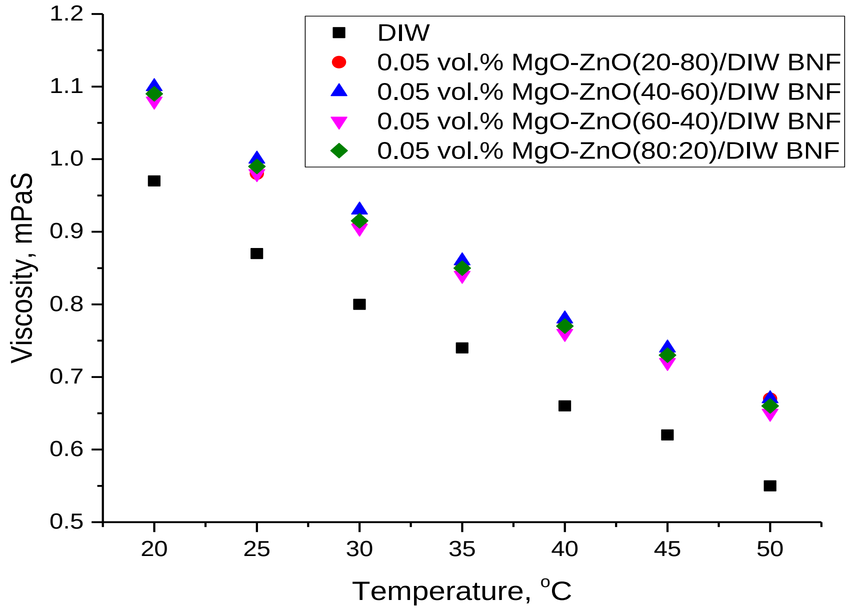

Figure 5.14. Viscosity of MgO-ZnO/DIW BNFs(0.05 vol%) under temperature increase for different percent weight ratios.

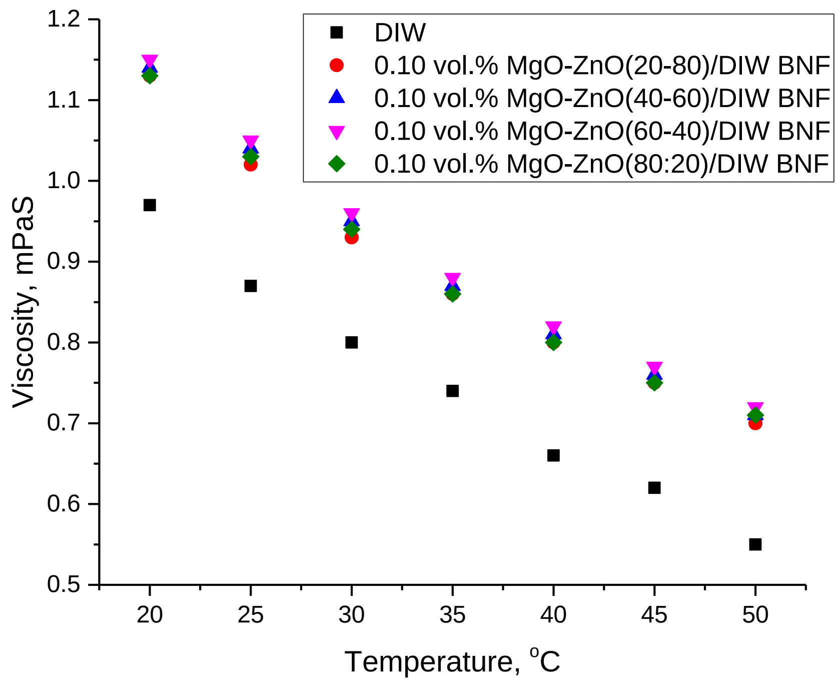

Figure 5.15. Viscosity of MgO-ZnO/DIW BNFs (0.1 vol%) under temperature increase for different percent weight ratios.

For the 0.05 vol.% BNFs in Figure 5.14 and 5.16, it was observed that maximum μ of 1.1 mPaS was achieved for BNF sample of PWR 40:60 for temperature 20 °C, while the 60:40 sample had the least μ. However, with a steady rise in temperature, the μ of all the BNF samples and DIW exhibited a decreasing trend, which agrees with the literature. For the 0.10 vol.% BNFs in Figures 5.15 and 5.17, the 60:40 BNF sample had the highest μ, while the least is 20:80. The mixing ratio influenced the variation in μ for the BNFs.

Figures 5.18 and 5.19 present BNFs' viscosity enhancement (%) over DIW under rising temperature for the two-volume concentrations (0.05 vol% and 0.1 vol%) and four separate mixing ratios. The BNFs of 0.05 vol.% as depicted in Figure 5.18, presents 20:80 and 40:60 BNF samples with the highest enhancement of 21.82%, while for 0.1 vol.% BNF samples, the highest enhancement was 30.91% for 60:40 BNF sample as presented in Figure 5.19. This outcome agrees with literature [21, 58, 90, 91, 132, 144, 162, 568-570]. To compare Figures 5.18 and 5.19, a discrepancy was noticed for the μ results for the two different volume concentrations used to formulate the BNFs. It can be deduced that using 0.05 vol% to formulate the BNFs led to reduced μ values, while an increase to 0.1 vol% produced enhanced μ values for its BNFs.

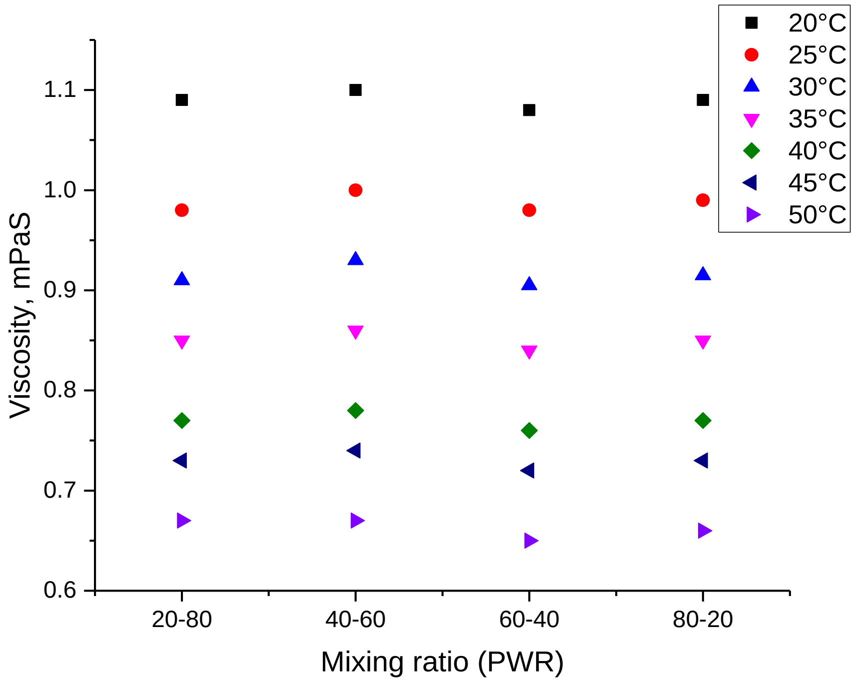

Figure 5.16. Influence of mixing ratio on the viscosity of 0.05 vol% BNFs.

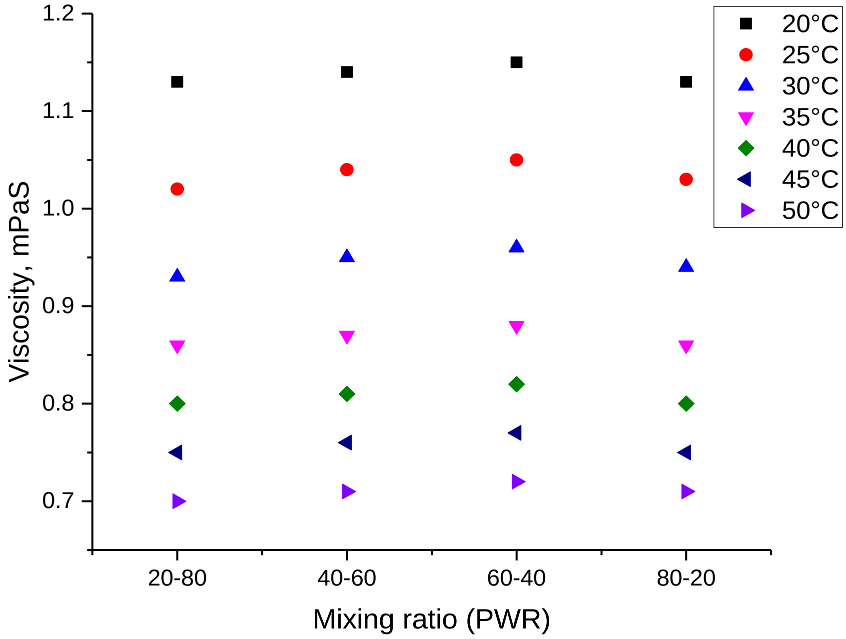

Figure 5.17. Influence of mixing ratio on the viscosity of 0.10 vol% BNFs.

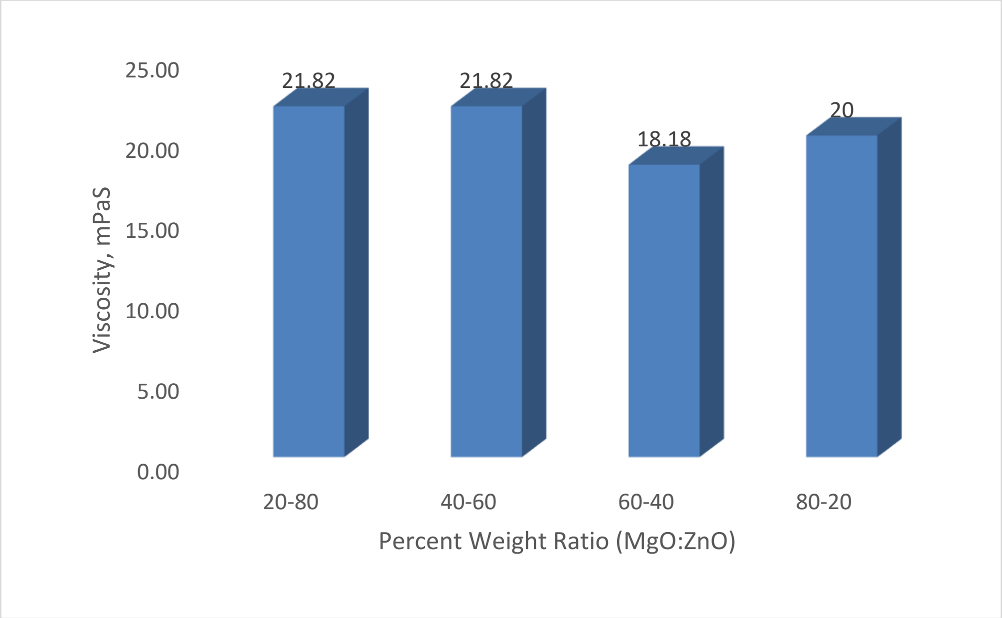

Figure 5.18. Viscosity enhancement (%) for 0.05 vol% BNFs.

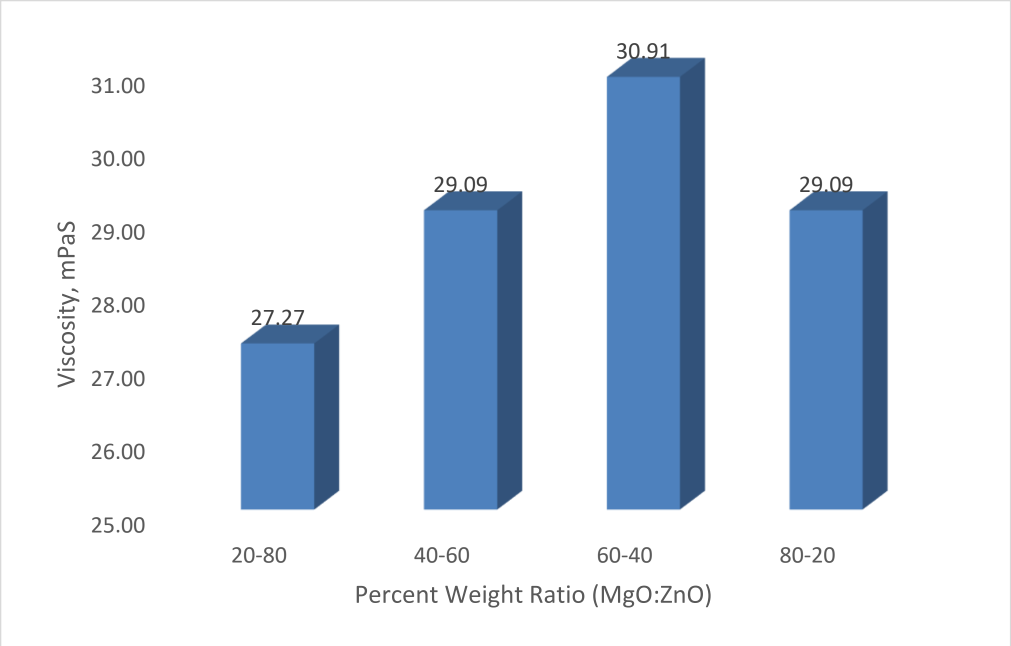

Figure 5.19. Viscosity enhancement (%) for 0.10 vol% BNFs.

5.4 pH OF BINARY NANOFLUIDS

The pH of an aqueous medium indicates its level of basicity or acidity, so the pH of mono-particle and binary nanofluids were valued in this investigation. An optimized pH value defines a good nanosuspension due to improved electrostatic repulsive forces, which detracts the agglomeration impact of particles and improves the stable limit of nanofluids.

5.4.1 Influence of Nanosize, Percent Weight Ratio and Temperature on pH

Figure 5.20 depicts that the pH of single-particle nanofluid was more than basefluid, because of the nanosuspension influencing the pH of the basefluid. Also, a rise in temperature detracted the pH of DIW and nanofluids. This agrees with Adio et al. [271] for 0.1 – 3.0 vol.% MgO/EG NFs at 20–70 °C but contrasted with Adio et al. [269], who recorded Al_2O_3/glycerol at volume concentration ≤ 0.5 vol% and 20–70 °C. The dispersion of 100 nm-MgO NPs into basefluid produced the maximum pH improvement (38.23%), while ZnO nano-particles led to pH improvement (least) by 22.652%. Figure 5.20 showed a variation in pH of 20 nm- and 100 nm-based MgO/DIW NFs were reducing for an increased temperature with a huge change amidst them and the pH of ZnO/DIW nanofluid closed slightly with increase in temperature. Adio et al. [271] published a more pH for MgO (20 nm)/EG nanofluid than 100 nm-MgO/EG nanofluid, which differs from the results in the current study.

Figures 5.21 and 5.22 presents the pH of 20 nm- and 100 nm-MgO based BNFs for different percent weight ratios at varying temperatures. It is observed in Figure 5.21 that the least pH enhancement (30.20% – 39.59%) was measured when compared with Figure 5.22, which had a higher enhancement (31.99% – 40.68%). In Figures 5.21 and 5.22, 40:60 BNF had the highest pH while 20:80 sample had the least. A rise in temperature was observed to detract pH for both BNFs and nanofluids. For the single-particle and binary nanofluids with over pH of 7, basic-natured aqueous fluid was prepared as the nanoparticles were dispersed in DIW. This is consonant with the dispersion of ZnO nanoparticles in water [571] and with MgO nanoparticles in EG [271], with individual nanofluid having a basic pH (above 7). Figures 5.21 and 5.22 posits that temperature possessed a higher influence on the pH of binary nanofluids, trailed by nano-size of MgO, and then percent weight ratios.

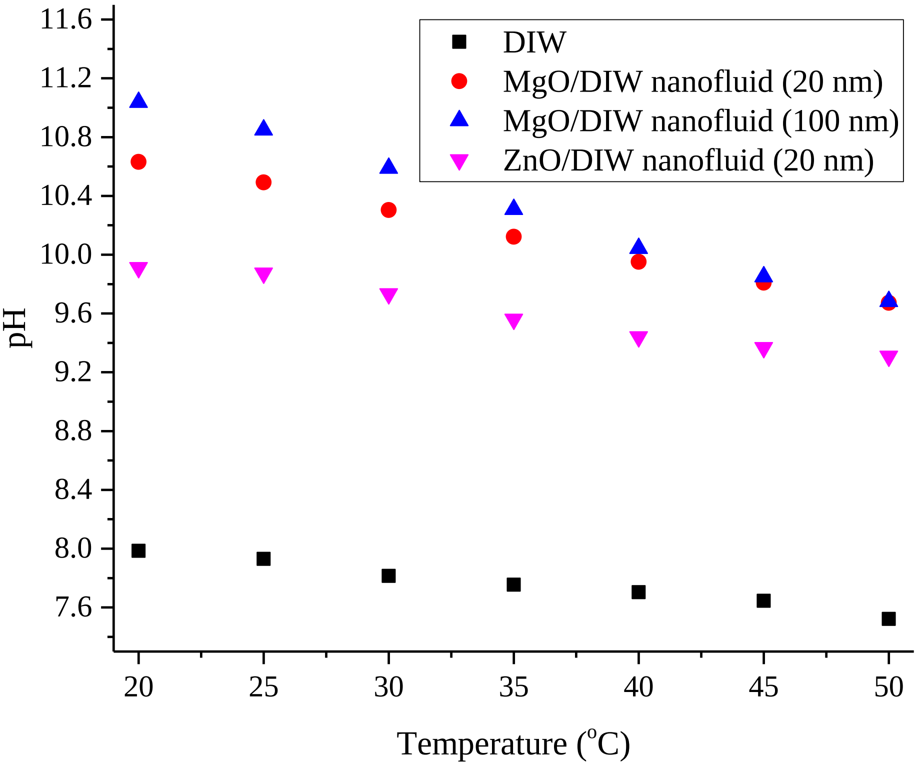

Figure 5.20. pH of single-particle nanofluid as temperature rises.

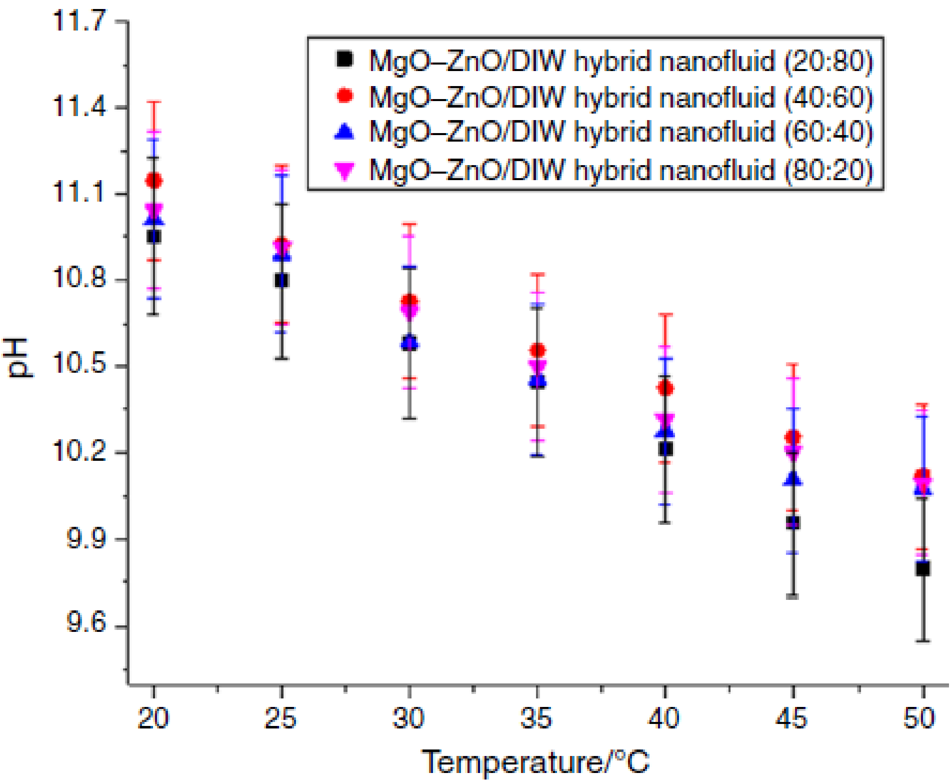

Figure 5.21. pH of MgO (20 nm) based binary nanofluids as temperature increase.

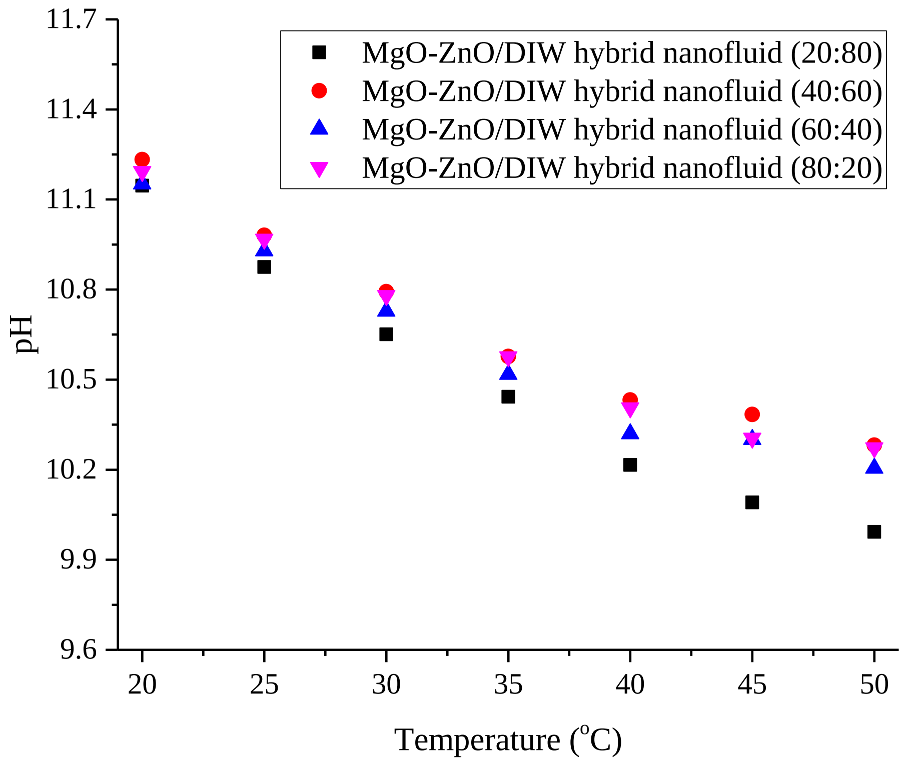

Figure 5.22. pH of MgO (100 nm) based binary nanofluids with temperature increase.

5.4.2 Influence of Concentration, Mixing Ratio and Temperature on pH

Figures 5.23 and 5.24 provides the pH values for the BNFs (at φ = 0.05 and 0.1 vol%), respectively, for different PWRs for the studied temperatures (20–50 °C). The suspension of BNPs into DIW clearly improved the pH. The pH for all PWRs of the BNFs reflects a gradual decline with increasing temperature, which is consonant with published works [21, 32, 171, 265, 271, 572]. Since the BNFs has a pH over 7, an alkaline nanosuspension was formulated. Hence, Figures 5.23 and 5.24 depict temperature's influence on the pH, followed by volume concentration and finally PWRs.

Figures 5.25 and 5.26 illustrates the influence of φ (0.05 and 0.1 vol%), different PWRs and temperature (20–50 °CS) on pH enhancement (pHE). Figure 5.25 had a pHE of 27.04% to 40.74% for 0.05 vol% BNFs, with 60:40 nanohybrid sample having the maximum enhancement. While Figure 5.26 had pHE ranging 30.20% to 39.59% for 0.10 vol% BNFs, with the highest improvement for 40:60. Figures 5.27 and 5.28 illustrates the impacts of PWRs on pH of MgO-ZnO/DIW BNFs (0.05 and 0.10 vol%) for the studied temperatures. Figure 5.27 depicts that pH rises gradually as MgO's PWRs also increase and get to the highest value for PWR 60:40. But, a least pH for PWR 80:20 at a temperature range of 20°C to 50°C. Also, Figure 5.28 provides pH increasing gradually and peaked PWR 40:60.

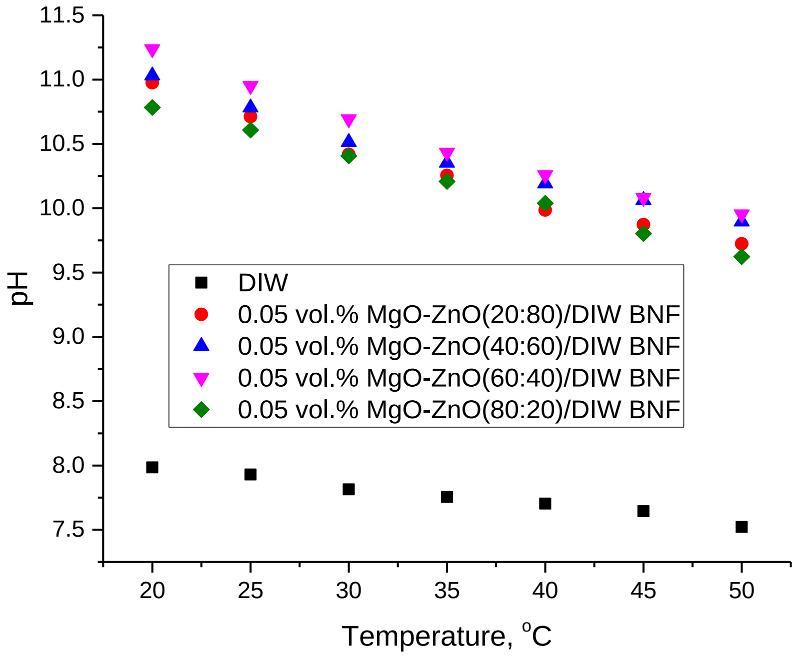

Figure 5.23. pH of MgO-ZnO/DIW BNFs (0.05 vol%) with temperature increase for different percent weight ratios.

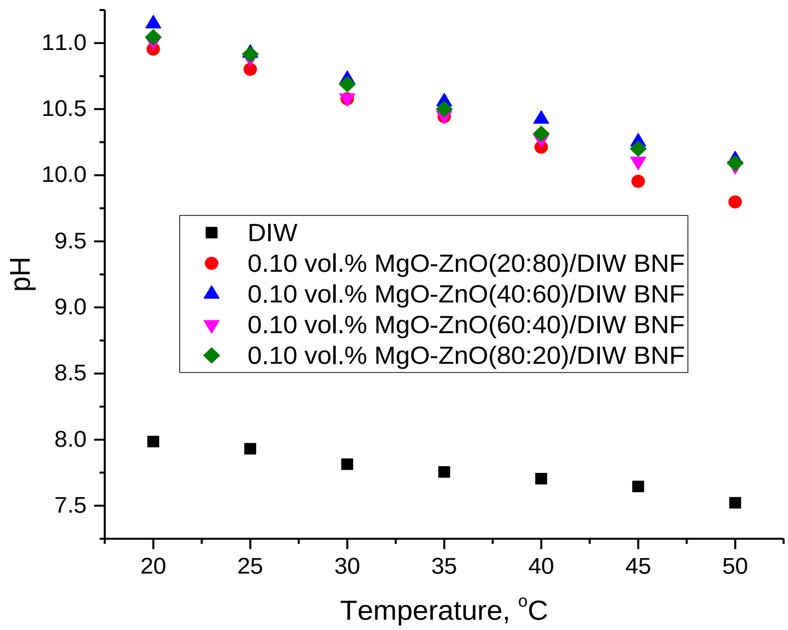

Figure 5.24. pH of MgO-ZnO/DIW BNFs (0.1 vol%) with temperature increase for different percent weight ratios.

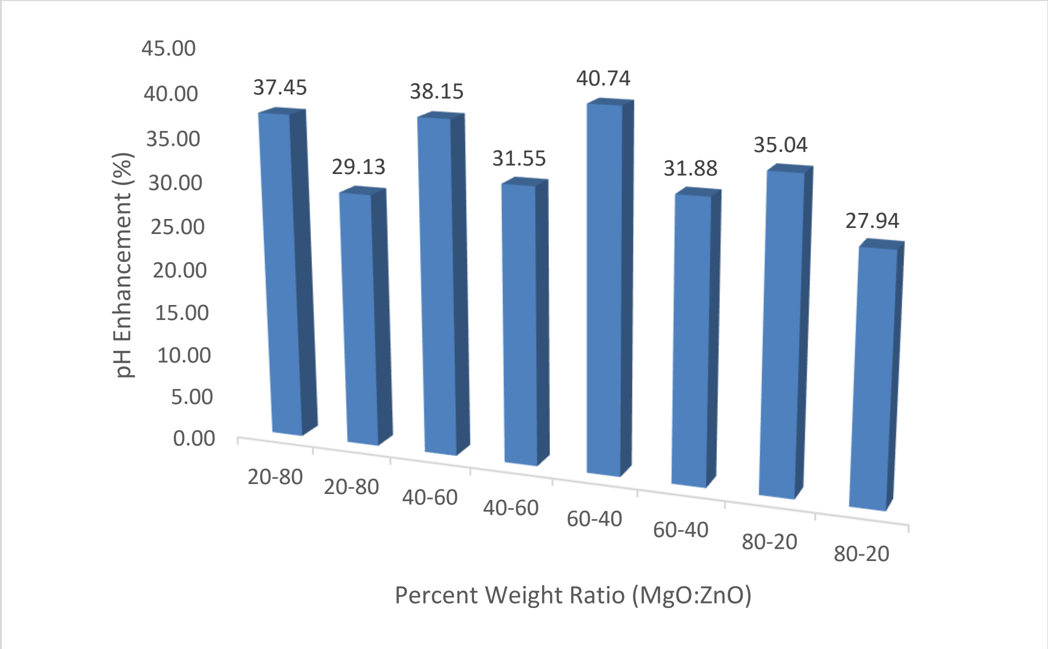

Figure 5.25. pH enhancement (%) for 0.05 vol% BNF.

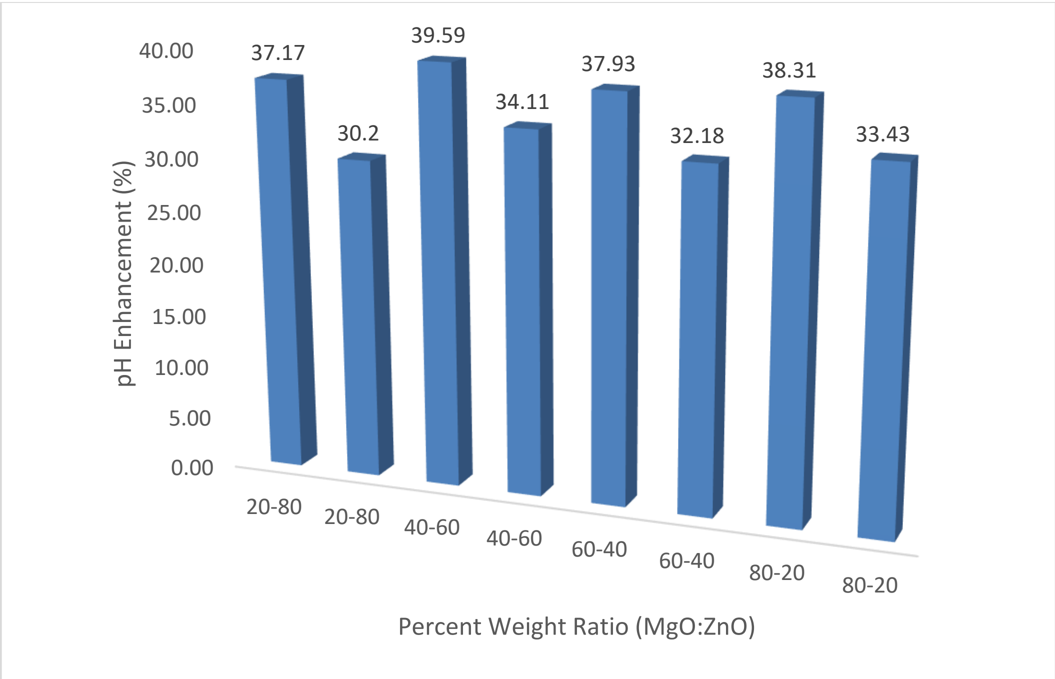

Figure 5.26. pH enhancement (%) for 0.10 vol% BNF.

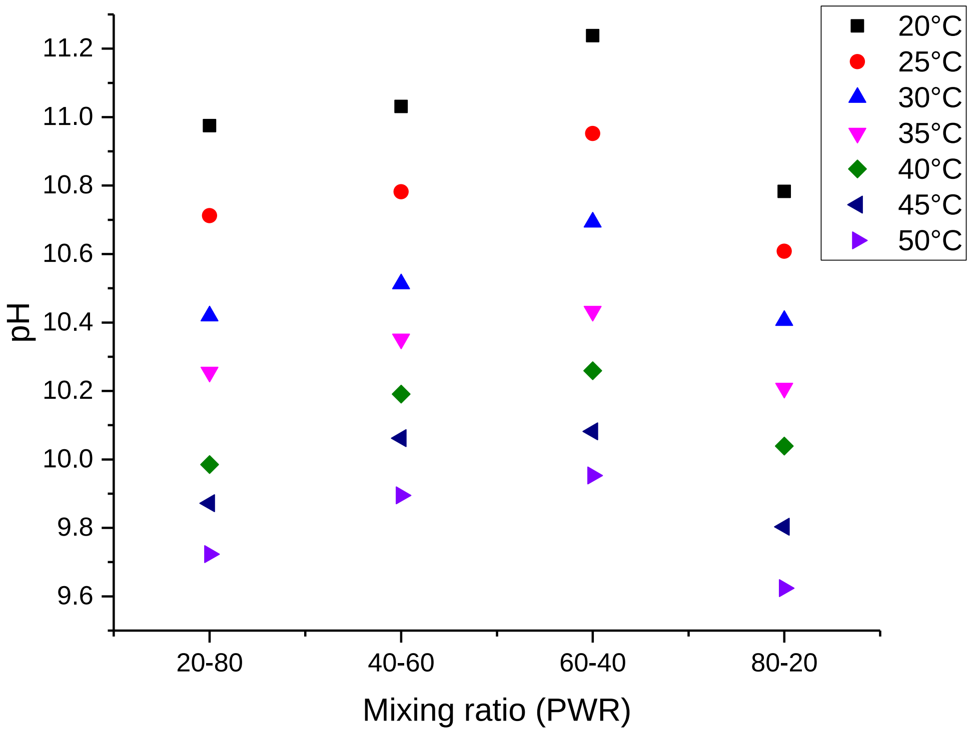

Figure 5.27. Influence of mixing ratio on the pH of 0.05 vol% BNF.

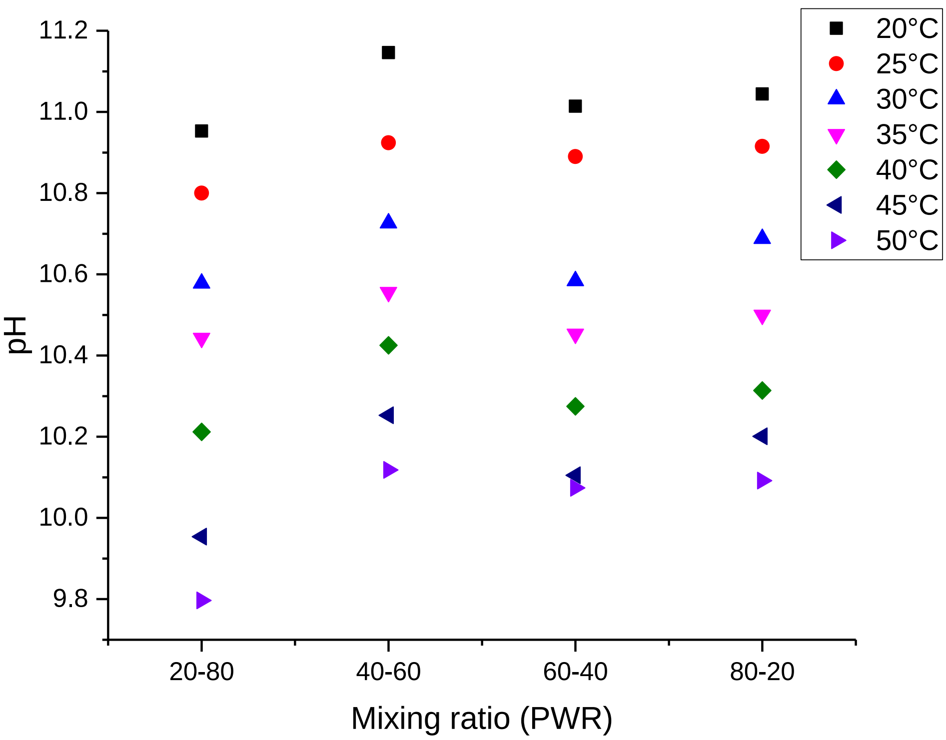

Figure 5.28. Influence of mixing ratio on the pH of 0.10 vol% BNF.

5.5 ELECTRICAL CONDUCTIVITY OF BINARY NANOFLUIDS

The electrical conductivity (σ) of nanohybrids is the ability to enhance the movement of electrical charges, due to ionized nanoparticles activation during dispersion, thus making it conduct electricity upon applying an electric potential across it. This property aids the keen observation of stability and the extent of suspension of nanoparticles in the basefluids [21, 31, 96, 172, 204, 264, 265]. However, unlike the measurement of viscosity and thermal conductivity, literature is scarce on the measurement of σ of binary nanofluids.

5.5.1 Influence of Nanosize, Percent Weight Ratio and Temperature on EC

Figure 5.29 presents the impact of percent weight ratios, rise in temperature and nanosize on the effective σ for MgO (20 nm)-based BNFs. The dispersion of binary nanoparticles into DIW significantly enhanced electrical conductivity over DIW. The PWR of 40:60 yielded the maximum effective electrical conductivity (2.99 – 3.19 mS/cm), while sample 80:20 had the least σ. An increase in temperature (20 – 50 °C) led to a gradual improvement in electrical conductivity for all binary nanofluids (Figures 5.29 – 5.30) and DIW (Figures 5.31), as reported in the literature [96, 269, 270, 278, 573]. Figure 5.30 illustrates the influence of percent weight ratios, rise in temperature and nanosize on the effective electrical conductivity (σ) for 100 nm-MgO based BNFs. Also, an increase in temperature (20 – 50 °C) slightly improved effective electrical conductivity for all PWRs of binary nanofluids. Highest effective electrical conductivity of 3.31 – 3.65 mS/cm was observed for PWR 40:60, and the lowest effective electrical conductivity (2.38–2.50 mS/cm) was noticed for PWR 80:20 for a temperature rise of 20 – 50 °C.

In comparing Figures 5.29 and 5.30, effective σ for 100 nm-MgO based BNFs was noticed to possess more effective σ of 20 nm-MgO based BNFs. This agrees with Adio et al. [271], who examined the effective σ of EG-based MgO (20 nm) and MgO (100 nm). For PWR 40:60, maximum effective σ was observed for both 20 nm-MgO and 100 nm-MgO based BNFs. Also, Figures 5.29 and 5.30 showed that temperature had a significant impact than MgO nano-size and PWRs in augmenting effective σ for the BNFs. PWRs had the least influence.

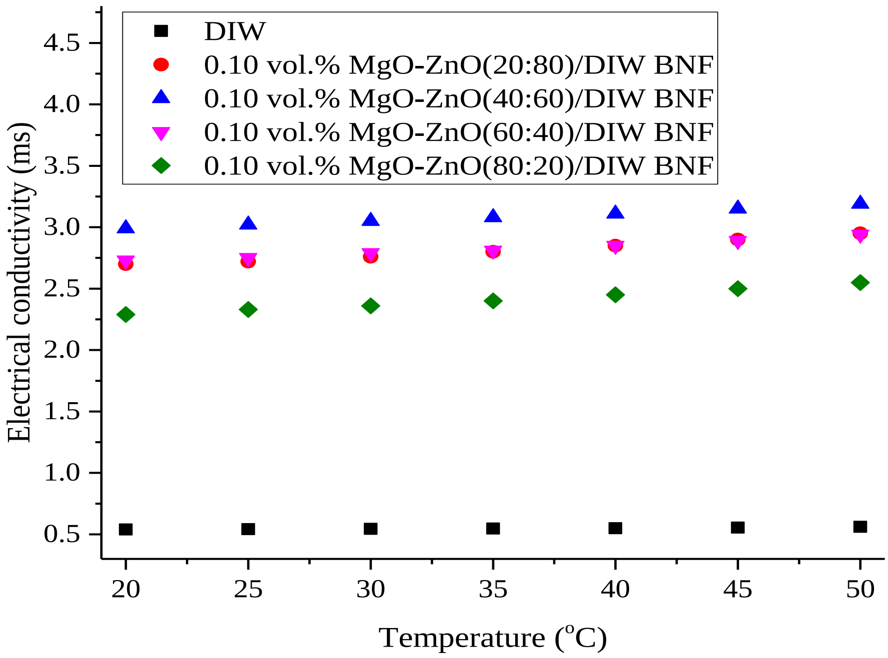

Figure 5.29. Electrical conductivity of MgO (20 nm) based binary nanofluids with temperature increase.

From Figure 5.31, it was observed that for a rise in temperature, effective σ of MgO/DIW NFs (2.05 – 2.16 mS/cm) was higher than the effective electrical conductivity of ZnO/DIW NF (1.95 – 2.13 mS/cm). Using MgO(100 nm)/DIW nanofluids, a lightly more effective electrical conductivity (2.08–2.20 mS/cm) was observed in comparison to MgO(20 nm)/DIW nanofluids (2.05 – 2.16 mS/cm). Adio et al. [271] reported a relatively more effective σ for MgO(20 nm)/EG nanofluid over that of MgO(100 nm)/EG nanofluid at 0.1 – 3 vol% and 20 – 70 °C.

For Figures 5.29 and 5.30, an effective σ for 40:60 sample of 20 nm-MgO based BNFs was augmented by 453.70% – 468.63%, whereas 100 nm-MgO enhanced by 512.96% – 550.62%. Also, the PWR 80:20 of 20 nm-MgO based BNFs was improved by 324.07% – 354.55% while 100 nm-MgO augmented by 340.74% – 345.63%. They were compared to DIW for studied temperature (20 – 50 °C). The result obtained agrees with the following literature - Giwa et al.

[34] reported enhancements of 163.37 – 1692.16% for Fe_2O_3-Al_2O_3 (75:25)/DIW nanofluids at 0.05 – 0.75 vol% and temperature 20 – 50 °C. Sundar et al. [18] reported improvements of 1339.81% – 853.15%, for Ni-ND (15:85)/DW nanofluids at 0.10 vol.% and temperature 24 – 65 °C. Qing et al. [19] reported 97% – 557% improvements for SiO_2-G/naphthenic mineral oil nanofluids for 0.01 – 0.08 wt% at room temperature.

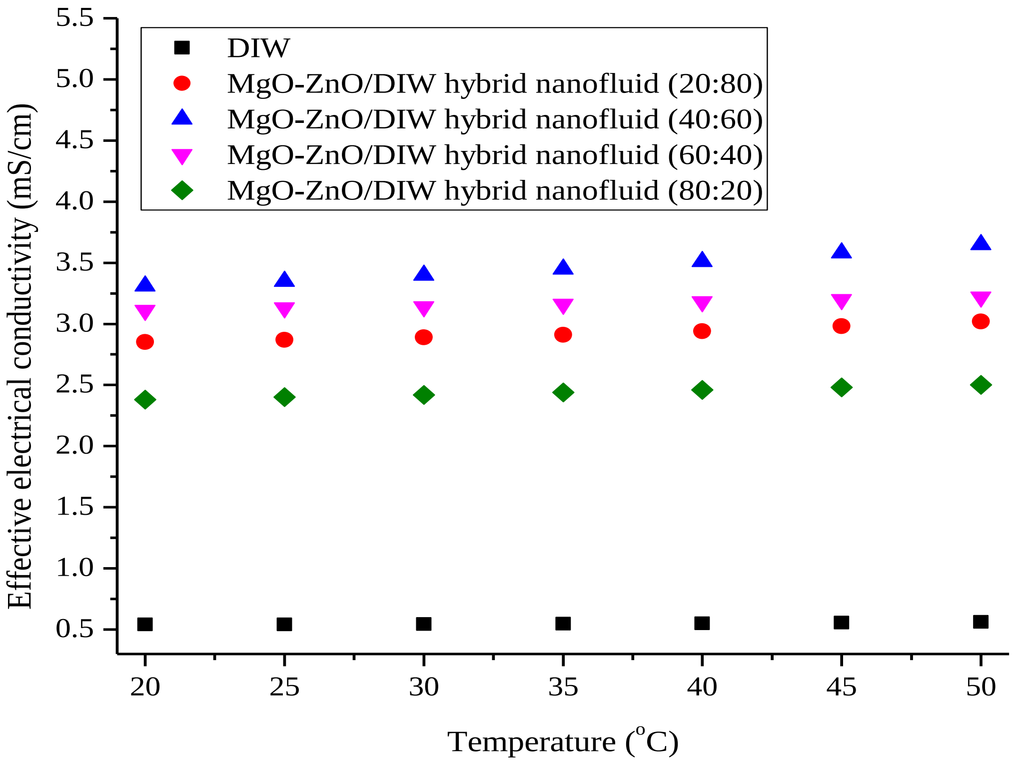

Figure 5.30. Electrical conductivity of MgO (100 nm) based BNFs as temperature rises.

However, improvements of 262.04% – 279.68%, 279.63% – 285.03%, and 285.19% – 292.16% were determined for ZnO/DIW nanofluids, MgO (20 nm)/DIW nanofluids, and MgO (100 nm)/DIW nanofluids, respectively when related with DIW. Adio et al. [271] published a 6000% augmentation for MgO/EG NF at 25 °C and 0.5 vol%. Also, literature confirmed improvements of 2370% for Al_2O_3/water nanofluid at 2 vol% and 25.9 °C [264], enhancements of 833% for Al_2O_3/water nanofluid at 0.5 vol% and 24 °C [273], enhancements of 360% for Fe_3O_4/water nanofluid at 0.50 vol.% and 60 °C [268]. The outcomes above show that the effective electrical conductivity of binary nanofluids had good augmentation compared to mono-particle nanofluids. Nanosuspension was observed to possess a positive influence on the σ of BNFs.

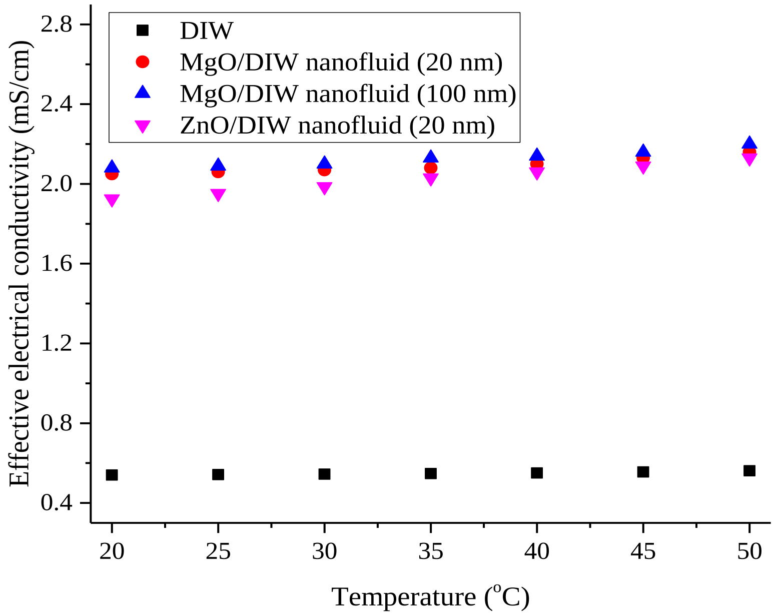

Figure 5.31. Effective electrical conductivity of single-particle nanofluid as temperature rises.

5.5.2 Influence of Concentration, Mixing Ratio and Temperature on EC

Figures 5.32 and 5.33 explains the impact of volume concentration (0.05 and 0.10 vol%), PWRs and increasing temperatures on the electrical conductivity (σ) of BNFs. In Figure 5.32, PWR 40:60 had maximum σ (2.26-2.59 ms), whereas PWR 20:80 had the least σ values (1.93-1.97 ms). Also, in Figure 5.33, PWR 40:60 had maximum σ (2.99-3.19 ms), whereas PWR 80:20 had the least σ values (2.29-2.55). Figures 5.32 and 5.33 illustrate that at rising temperature of 20 to 50 °C, a gradual σ enhancement of DIW and the BNFs were observed, in agreement with literature [21, 31, 32, 96, 143, 270, 271, 278, 574-576]. Comparing Figures 5.32 and 5.33, σ of MgO-ZnO/DIW BNFs (0.10 vol%) was observed to be higher than that of MgO-ZnO/DIW BNFs (0.05 vol%), with 40:60 PWR BNF recording the maximum σ for both volume concentrations. Also, the effect of temperature was more notable in improving σ for the BNFs, than φ and PWR.

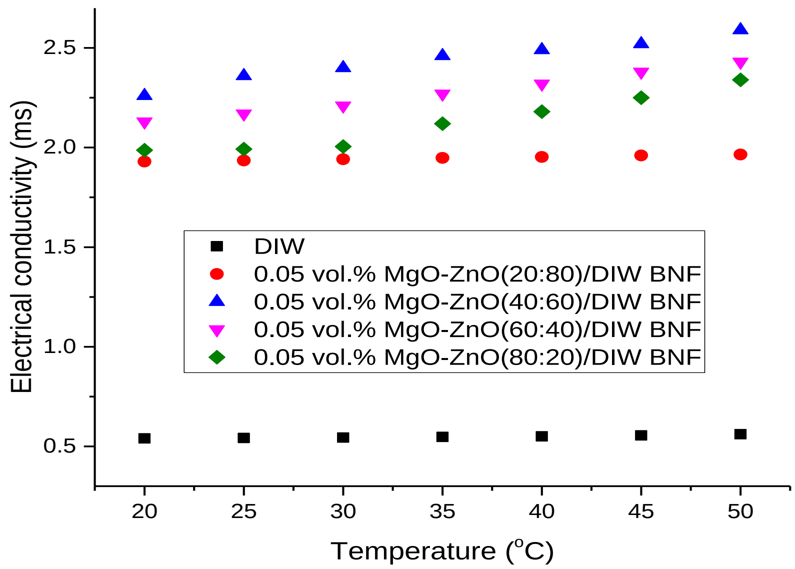

Figure 5.32. Electrical conductivity of MgO-ZnO/DIW BNFs (0.05 vol%) under temperature increase for various PWRs.

In addition, Figures 5.34 and 5.35 illustrates that σ of MgO-ZnO/DIW BNFs (0.05 and 0.10 vol%) had a maximum improvement for 40:60 BNF samples for the two volume concentrations. Upon comparing with DIW, PWR 40:60 (0.05 vol%) was augmented by 318.52-361.68%, whereas PWR 40:60 BNF (0.10 vol%) had an enhancement of 453.70-468.63%, which agrees with published results [21, 31, 32, 41, 96, 172, 264, 270, 271, 569].

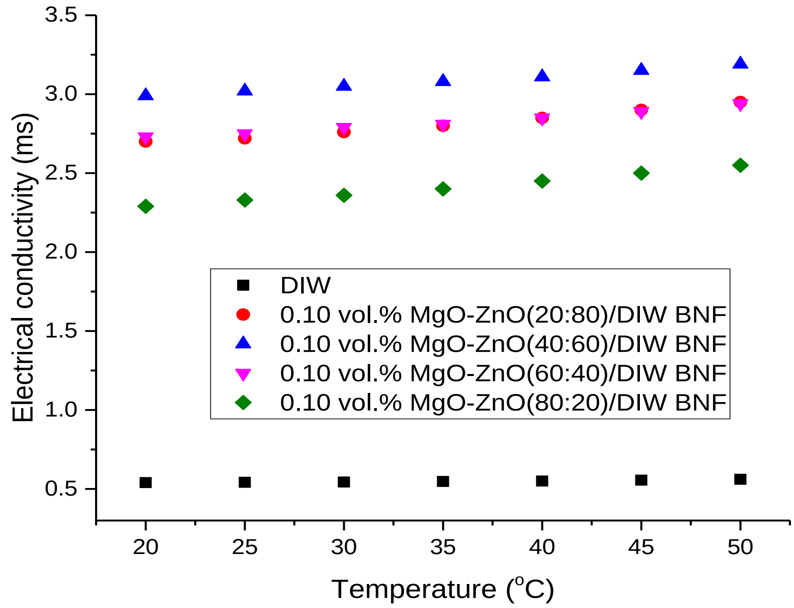

Figure 5.33. Electrical conductivity of MgO-ZnO/DIW BNFs (0.10 vol%) under temperature increase for various PWRs.

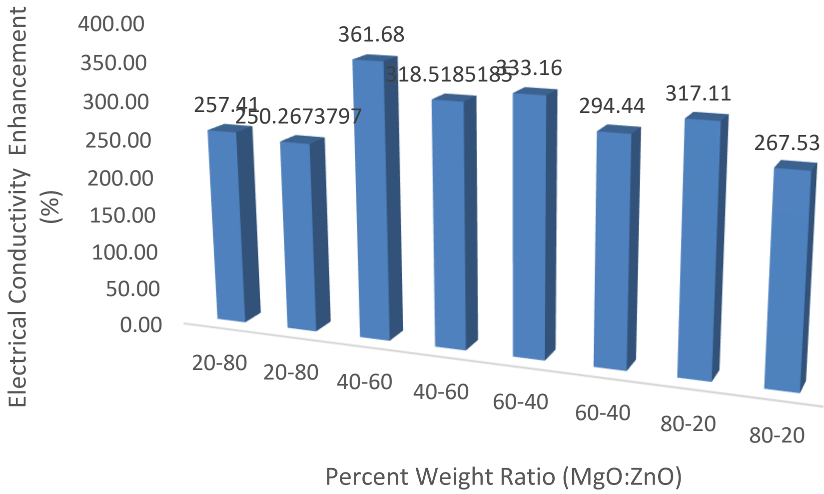

Figure 5.34. Electrical conductivity enhancement (%) for 0.05 vol% BNF.

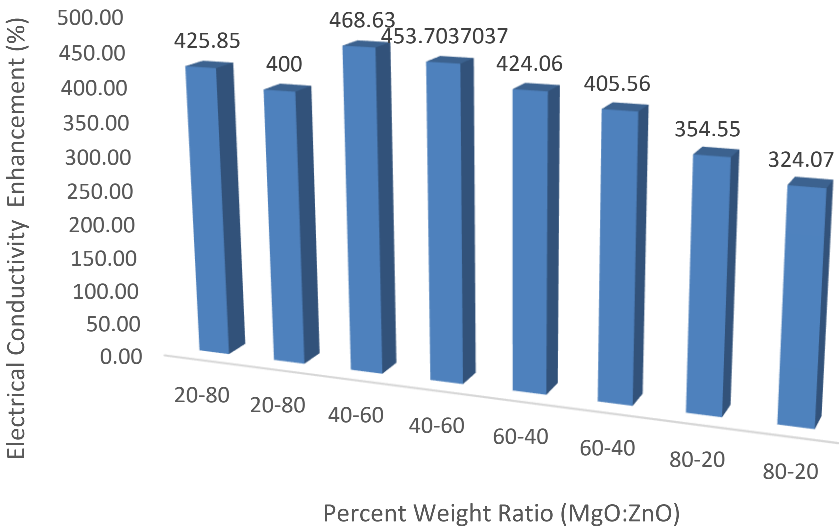

Figure 5.35. Electrical conductivity enhancement (%) for 0.10 vol% BNF.

Figures 5.36 and 5.37 illustrates the impact of PWRs on σ of MgO-ZnO/DIW BNFs (0.05 and 0.10 vol%) for rising temperatures. Figure 5.36 reveals that σ rises slightly as MgO's PWRs gradually increase to a maximum value PWR of 40:60 for MgO-ZnO. But the least σ was observed for PWR 20:80, which has the lowest composition of MgO NP for rising temperatures of 20°C to 50°C. Also, Figure 5.37 illustrates σ rising gradually as mixing rates of MgO is enhanced and attained the highest value when PWR of MgO-ZnO is 40:60. But, further increase of MgO NP detracted electrical conductivity, but least σ was observed for the BNF sample with the maximum composition of MgO NP (80:20) under rising temperature. The nanoparticles' hybridisation was noticed to have a good impact on the BNFs' σ. The difference in σ is enhanced by the differences in φ, temperature, and particle ratios of binary nanoparticles employed to formulate the BNFs.

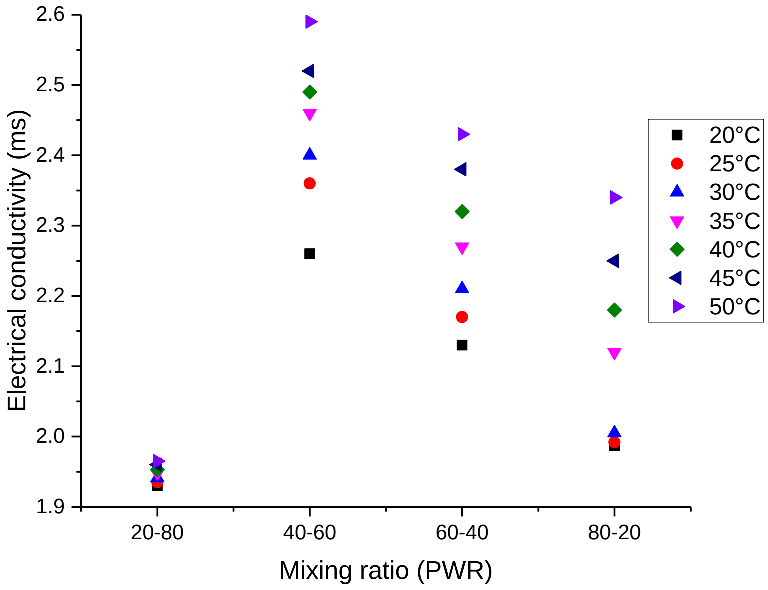

Figure 5.36. Influence of mixing ratio on the electrical conductivity of 0.05 vol% BNF.

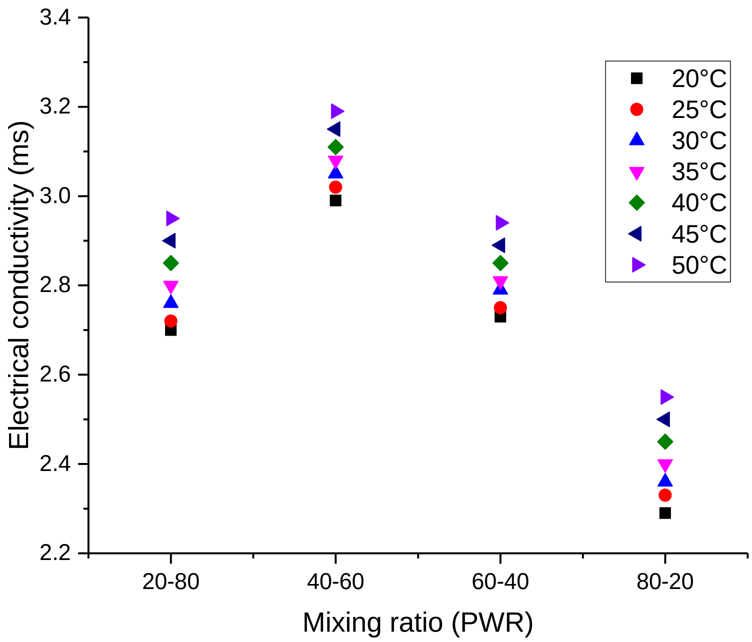

Figure 5.37. Influence of mixing ratio on the electrical conductivity of 0.10 vol% BNF.

5.6 DEVELOPMENT OF CORRELATIONS

The originality of this work handles the inadequacy of documentation of thermal behaviour of MgO-ZnO/DIW binary nanofluids and the use of correlations for engineering design of thermal applications. Advancement in nanofluids research has led to an increased need for model development that will accurately predict thermophysical properties of new nanofluids [35, 39, 64, 66, 96, 181, 232, 577-579]. This work employed the experimental datasets of the studied BNFs' thermal properties (thermal conductivity, electrical conductivity, and viscosity) to develop prediction models. Table 5.1 shows the developed correlations for the three thermal properties as a function of temperature.

Table 5.1. Developed correlations for 0.10 vol% BNFs

Variable	MgO-ZnO (20:80)	MgO-ZnO (40:60)-100	MgO-ZnO (60:40)-	MgO-ZnO (80:20)
		Viscosity (MgO – 20 nm)		
$\frac{\mu_{BNF}}{\mu_{DIW}}$	$= 1.053 + 4.22 \times 10^{-3}T$	$= 1.070 + 4.23 \times 10^{-3}T$	$= 1.075 + 4.50 \times 10^{-3}T$	$= 1.054 + 4.36 \times 10^{-3}T$
		Viscosity (MgO – 100 nm)		
$\frac{\mu_{BNF}}{\mu_{DIW}}$	$= 1.098 + 4.07 \times 10^{-3}T$	$= 1.117 + 4.08 \times 10^{-3}T$	$= 1.123 + 4.12 \times 10^{-3}T$	$= 1.105 + 4.16 \times 10^{-3}T$
		Electrical conductivity (MgO – 20 nm)		
$\frac{\sigma_{BNF}}{\sigma_{DIW}}$	$= 5.159 - 8.86 \times 10^{-3}T$	$= 5.832 - 1.66 \times 10^{-2}T$	$= 5.43 - 1.03 \times 10^{-3}T$	$= 4.346 - 5.37 \times 10^{-3}T$
		Electrical conductivity (MgO – 100 nm)		
$\frac{\sigma_{BNF}}{\sigma_{DIW}}$	$= 5.568 - 1.5 \times 10^{-2}T$	$= 6.309 - 9.55 \times 10^{-3}T$	$= 6.168 - 2.02 \times 10^{-2}T$	$= 4.686 - 1.35 \times 10^{-2}T$
		Thermal conductivity (MgO – 20 nm)		
$\frac{\kappa_{BNF}}{\kappa_{DIW}}$	$= 1.038 + 7.26 \times 10^{-4}T$	$= 1.093 + 5.78 \times 10^{-4}T$	$= 1.065 + 7.90 \times 10^{-4}T$	$= 1.052 + 6.97 \times 10^{-4}T$
		Thermal conductivity (MgO – 40 nm)		
$\frac{\kappa_{BNF}}{\kappa_{DIW}}$	$= 1.118 + 1.50 \times 10^{-3}T$	$= 1.079 + 9.93 \times 10^{-3}T$	$= 1.058 + 1.09 \times 10^{-2}T$	$= 1.053 + 9.76 \times 10^{-3}T$
		Thermal conductivity (MgO – 100 nm)		
$\frac{\kappa_{BNF}}{\kappa_{DIW}}$	$= 1.097 + 4.65 \times 10^{-4}T$	$= 1.137 + 5.07 \times 10^{-4}T$	$= 1.132 + 5.13 \times 10^{-4}T$	$= 1.099 + 6.91 \times 10^{-4}T$

For the developed relative viscosity correlations, R^2 and average absolute deviation (AAD) results of 94.93%–98.80% and 0.1558% –0.4682% (20 nm-MgO based binary NFs) and 91.10%–98.54% and 0.1836%–1.0582% (100 nm-MgO based binary nanofluids), respectively, were achieved. For developed correlations for electrical conductivity, predicted performance and AAD of 98.77% –99.83% and 0.0903% – 0.1763% (20 nm-MgO based binary nanofluids) and 98.17% –99.91% and 0.0565%–0.5281% (100 nm-MgO based binary nanofluids) respectively, were achieved. Finally, the prediction accuracy and AAD of 97.85% - 99.00% and 0.1084% –0.1387% for 20 nm-MgO based binary nanofluids, and 98.29% - 99.66% and 0.0681% –0.1534% for 100 nm-MgO based BNFs, respectively, were obtained for correlations related to thermal conductivity.

Figures 5.38 – 5.40 compare fitted correlations of the studied thermal conductivity, viscosity, and electrical conductivity with existing published correlations. Figure 5.38 presents the proposed correlations of Sundar et al. [270] and Giwa et al. [96] for predicting the electrical conductivity of BNFs, which was found inadequate to define the electrical conductivity of MgO-ZnO/DIW BNFs (as the highest (40:60 (20 nm and 100 nm)) and least (80:20 (20 nm and 100 nm)) values upon comparison. As presented in Figure 5.39, Zadkhast et al. [349] proposed correlations for thermal conductivity, which was noticed to predict 20:80 finely (20 nm-MgO) BNF with absolute errors of 3.78% and 4.64%, 20:80 (100 nm-MgO) with absolute errors of 0.41 – 0.66%, and 40:60 (100 nm-MgO) for absolute errors of 3.91 – 4.37%. Else, the proposed correlations of Taherialekouli et al. [558] and Esfahani et al. [239] for effective thermal conductivity underpredicted the MgO-ZnO/DIW BNFs (40:60 and 20:80 of 20 nm- and 100 nm MgO based NPs) when compared. Also, the developed correlations of Hamid et al. [261], as presented in Figure 5.40, underpredicted the relative viscosity of 60:40 (20 nm-MgO) and 20:80 (100 nm-MgO) binary nanofluids while the correlations of Sundar et al. [580] overestimated them. Then, the proposed correlations of Giwa et al. [96] estimated the 20:80 (20 nm-MgO), 60:40 (20 nm-MgO) and 20:80 (100 nm-MgO) binary nanofluids for absolute errors of 0.15% – 1.40%, 1.19% – 4.10%, and 3.00% – 4.56%, respectively. From Figure 5.41, the fitted correlations for the optimum thermal conductivity (with binary nanofluids with particle weight ratio of 40:60 and MgO nano-sizes of 20, 40, and 100 nm) were compared with those of previous studies, and the latter was observed to underpredict the former.

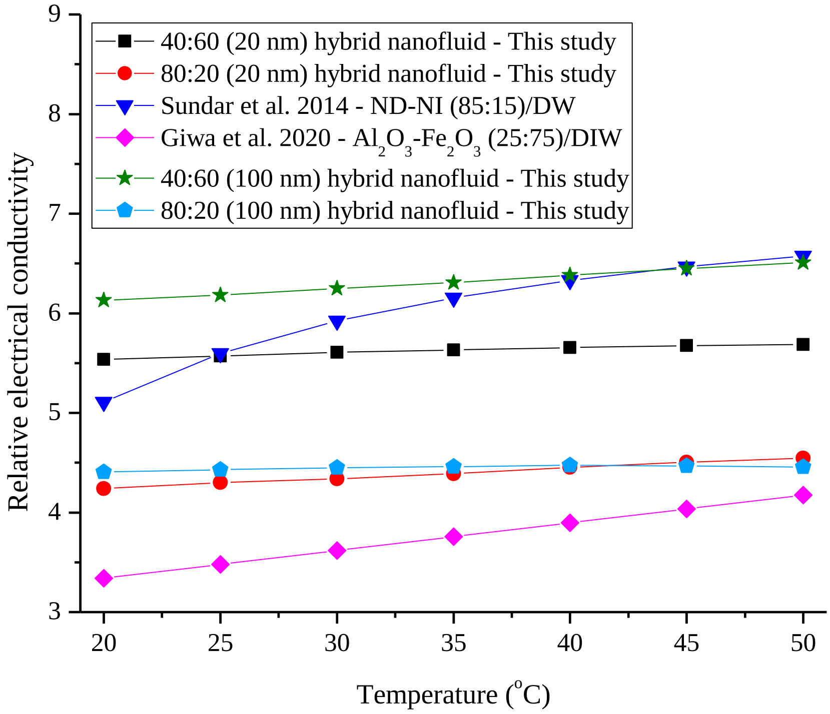

Figure 5.38. Comparing proposed correlations of electrical conductivity of MgO-ZnO/DIW BNFs with existing correlations as a function of temperature.

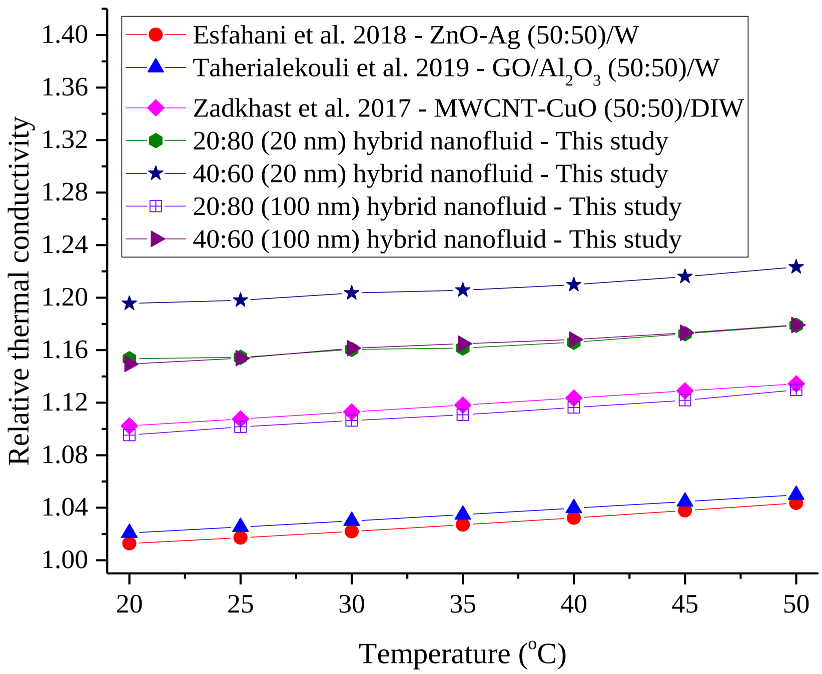

Figure 5.39. Comparing proposed correlations of relative thermal conductivity of MgO-ZnO/DIW binary nanofluids with existing correlations as a function of temperature.

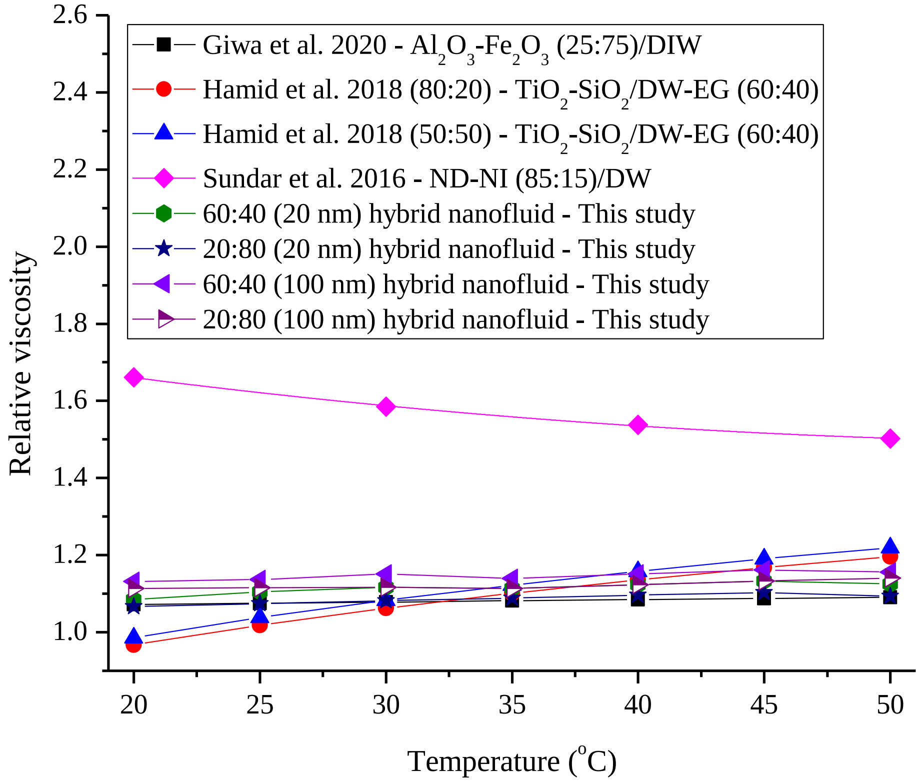

Figure 5.40. Comparison of proposed correlations for relative viscosity of MgO-ZnO/DIW binary nanofluids with existing correlations as a function of temperature.

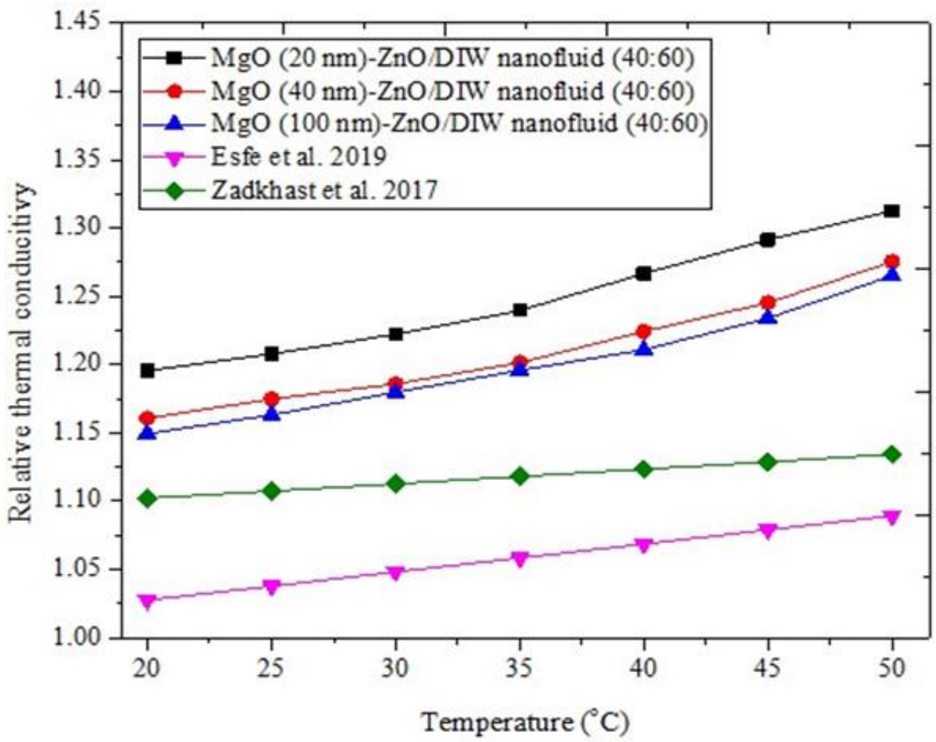

Figure 5.41. Comparison of obtained thermal conductivity correlations in this present study with proposed correlations in literature.

The facts above developed correlations with good prediction ability and of essence. Since different types of nanoparticles, particle ratio of nanoparticles, size of nanoparticles, temperature, basefluid, etc., influence the thermal conductivity of binary nanofluids, the need to propose unique correlations of experimental data of thermal properties related to different nanofluids is very crucial [145, 227, 366, 554, 581-583].

5.7 THERMOELECTRICAL CONDUCTIVITY RELATIONS

The thermoelectrical conductivity (TEC) relation between the σ and κ is essentially useful in selecting an optimized BNFs to be used in an electrically active system for thermal applications. Figures 5.42 and 5.43 illustrate BNFs' TEC with different volume concentrations and PWRs under increasing temperatures. The effective decision for selecting BNFs as thermal fluids is a function of the TEC value. BNFs of 0.05 vol% were observed to have higher TEC values than that of 0.10 vol% BNFs (Figures 5.42 and 5.43). Also noticed is that an increment in temperature reduced the TEC values for both volume concentrations, which falls in agreement with the literature [21, 84, 274, 278, 584]. Therefore, the BNFs samples investigated in this work under studied temperature were suitable for thermal application considering the calculated TEC results.

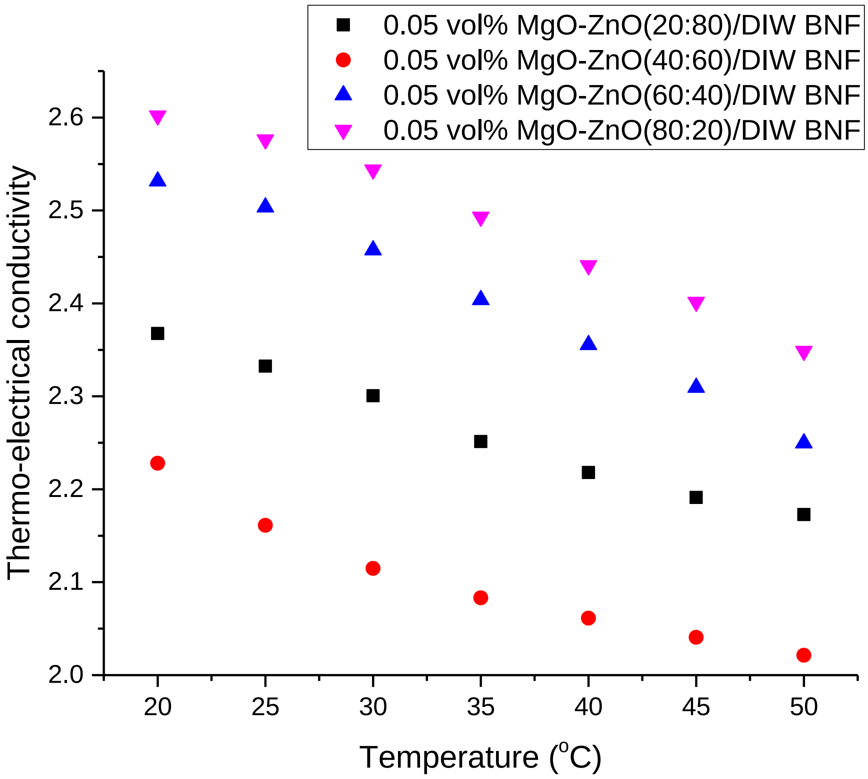

Figure 5.42. Thermoelectrical conductivity values for 0.05 vol% BNFs.

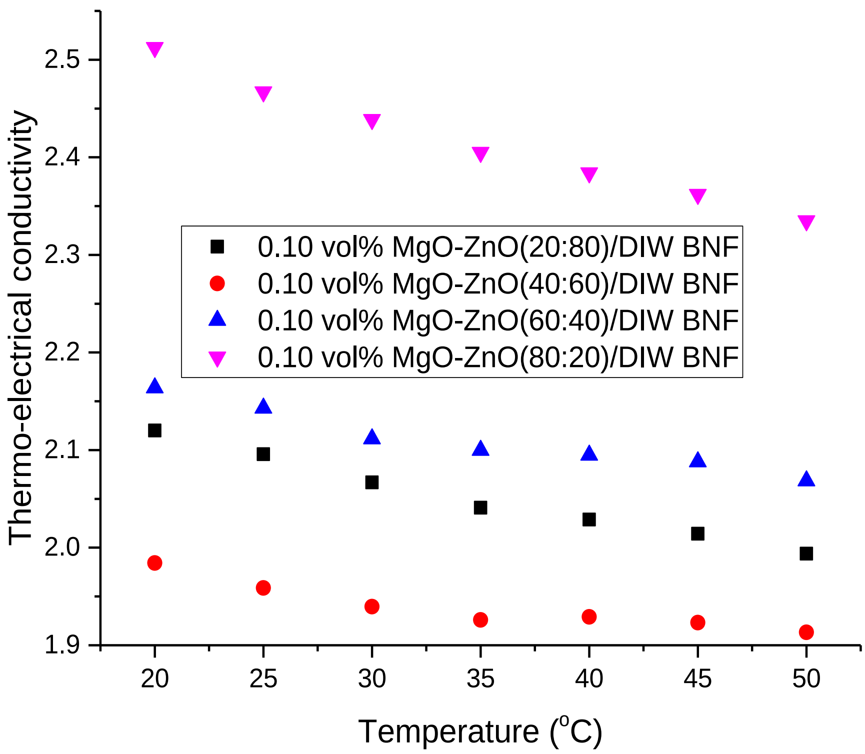

Figure 5.43. Thermoelectrical conductivity values for 0.10 vol% BNFs.

5.8 PROPERTIES ENHANCEMENT RATIO

Property enhancement ratio (PER) is a factor employed to determine the convective heat transfer behaviour of nanofluids for laminar flow within thermal applications [540]. This is based on nanofluids' augmentation capability of thermal conductivity and viscosity. So, PER is the relationship existing between the enhancement of thermal conductivity and viscosity enhancement as presented in Equation 5.1.

$$PER = \frac{C_\mu}{C_\kappa} = \frac{\mu_r - 1}{\kappa_r - 1} \leq 4 \qquad 5.1$$

Where: C_μ, C_κ, κ_r, and μ_r were effective viscosity enhancement, effective thermal conductivity enhancement, relative thermal conductivity, and relative viscosity, respectively.

Figures 5.44 and 5.45 give the PER of 20 nm- and 100 nm-MgO based binary nanofluids (0.1 vol.%), which reduced with enhancement in temperature. It can be observed in the Figures that as the temperature rises, PER is enhanced. For 20 nm-MgO based BNFs, lowest and highest PER values are 0.38 – 0.57 (for 40:60) and 0.44 – 0.65 (for 60:40), while 0.81 – 0.97 (40:60) and 1.17 – 1.22 (for 20:80) were reported for the 100 nm-MgO based BNFs, respectively. Prasher et al. [540] posited that binary nanofluids are considered useful as thermal fluids when the thermal conductivity improvement is 4-fold more or equal to the enhancement of viscosity. Figures 5.44 and 5.45 further posits that all BNFs samples were below PER of 4 and thus beneficial as thermal fluids (up to 50 °C) for thermal applications subject to further investigation on the convective heat transfer performance. Related results were reported by Akilu et al. [98] for EG-based SiC-CuO/C (4:1) binary nanofluids and Hamid et al. [261] for TiO_2-SiO_2 (20:80 – 80:20)/DW-EG binary nanofluids.

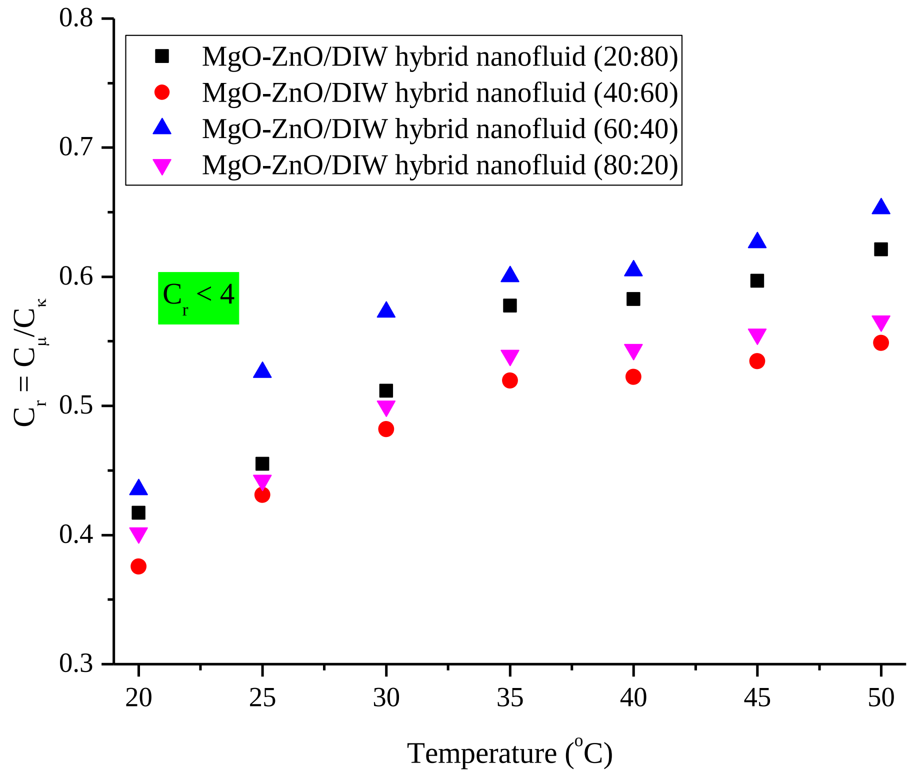

Figure 5.44. PER of MgO (20 nm) based binary nanofluids (0.1 vol.%) with temperature increase.

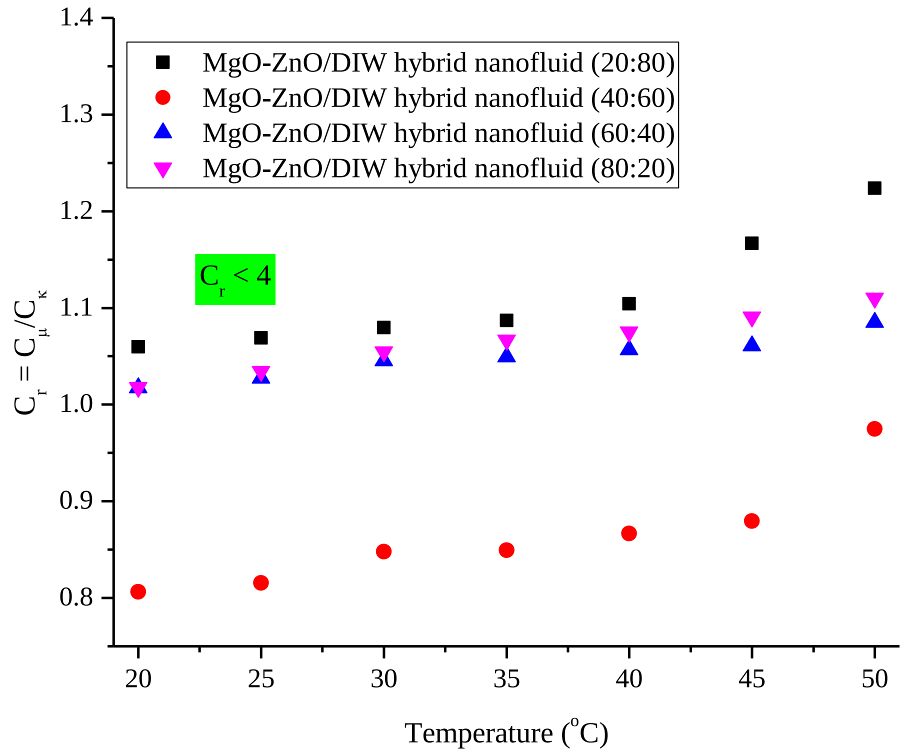

Figure 5.45. PER of MgO (100 nm) based binary nanofluids (0.1 vol.%) with temperature increase.

5.9 CONCLUSION

In this experimental investigation, the thermal conductivity (κ), pH, viscosity (μ) and electrical conductivity (σ) of MgO-ZnO/DIW BNFs (0.05 and 0.10 vol%) were successfully studied for PWR of 20:80, 40:60, 60:40, 80:20 (MgO:ZnO) at temperatures gradients of 20 to 50°C. The κ of the BNFs for all PWR was augmented under the influence of increasing temperature as compared to DIW. The highest κ enhancement of 5.60% and 22.07% relative to the basefluid was obtained at 0.05 and 0.10 vol.%, respectively, which shows that the dispersion of MgO-ZnO NPs enhances κ greatly, especially at higher temperatures. Also, the pH of MgO-ZnO/DIW BNFs (0.05 and 0.10 vol%) for all mixing ratios reflects a steady decline as temperature increases. The BNFs possessed pH values more than 7, thus formulating an alkaline fluid. It was observed that temperature greatly influenced the pH of the BNFs, then volume concentration and finally PWR. pH enhancements of 27.04% to 40.74% and 30.20% to 39.59% were achieved for BNFs (at φ of 0.05 and 0.1 vol%, respectively) at different PWRs for temperature ranges of 20–50 °C. Then, the BNFs' electrical conductivity (σ) for all the PWR was slightly enhanced under the influence of increasing temperature. Dispersing hybrid NPs into DIW significantly improved the σ of DIW. Maximum enhancement of 21.82% and 30.91% were observed for 0.05 and 0.1 vol%, respectively. In addition, the viscosity (μ) of MgO-ZnO/DIW BNFs (0.05 and 0.10 vol%) as temperature improves gradually exhibited a detracting trend for all nanohybrids and basefluid. Thus, it was deduced that using 0.05 vol% to formulate the BNFs led to reduced μ values, while an increase to 0.1 vol% produced enhanced μ values for its BNFs. The difference in MgO-ZnO NPs mixing ratio led to variation in μ for the BNFs for temperatures examined. The effective criteria in selecting BNFs for thermal applications is a function of the TEC value. It was observed that BNFs of 0.05 vol% were observed to have higher TEC values than that of 0.10 vol% BNFs. Also noticed is that an increment in temperature reduced the TEC values for both volume concentrations. The BNFs samples investigated in this work under the studied temperature range are suitable for thermal application. The PER revealed that at 0.10 vol.% and temperature of 20 – 50 °C, all binary nanofluids are applicable for thermal cooling purposes. The 40:60 binary nanofluids happens to be suitable sample with minimum viscosity and maximum thermal conductivity which was beneficial to engineering use. Using the experimental results, correlations were proposed to estimate the studied BNFs' thermophysical properties.

CHAPTER 6

THERMO-CONVECTION PERFORMANCE OF BINARY NANOFLUIDS[1]

6.1 INTRODUCTION

This chapter experimentally examined the natural convection performance of MgO-ZnO nano-particles suspended in DIW for volume concentrations of 0.05 and 0.10 vol% for PWRs of 20:80, 40:60, 60:40, 80:20 (MgO:ZnO) charged inside a square enclosure. The temperature profile of the cavity when filled with samples of DIW under varying ΔT was presented. This involved the temperatures at the centre and heated walls of the cavity. The thermo-convection behaviour of the binary nanofluid samples for parameters such as Ra, Nu_{av}, h_{av}, and Q_{av} at various temperature range (20°C to 50°C) were studied and duly reported. A new model linked to volume concentration (φ) and percent weight ratios were introduced to predict Nu_{av}.

6.2 CAVITY VALIDATION

For the validation of the performance of the square cavity employed in the thermo-convection experiment, the measured Nusselt number (Nu) dataset for basefluid (DIW) were compared with published numerical models for thermo-convection [25, 161, 325, 543-545, 585]. Figure 6.1 shows the validation of the squared cavity using basefluid (DIW), by way of illustrating Nu plotted with Rayleigh number (Ra) for basefluid, with experimental values and published models. At Ra of 8.05×10^8, it is observed that the experimental Nusselt number dataset was minimum in comparison to the forecasted dataset by the correlations. This is indicative that the correlation predicts the experimental dataset accurately.

This chapter has been published in part as:

[1]Nwaokocha, C., Momin, M., Giwa S., Sharifpur, M., Murshed S.M.S., Meyer, J.P., *Experimental investigation of thermo-convection behaviour of aqueous binary nanofluids of MgO–ZnO in a square cavity.* Thermal Science and Engineering Progress, 2022, **28**: 101057.

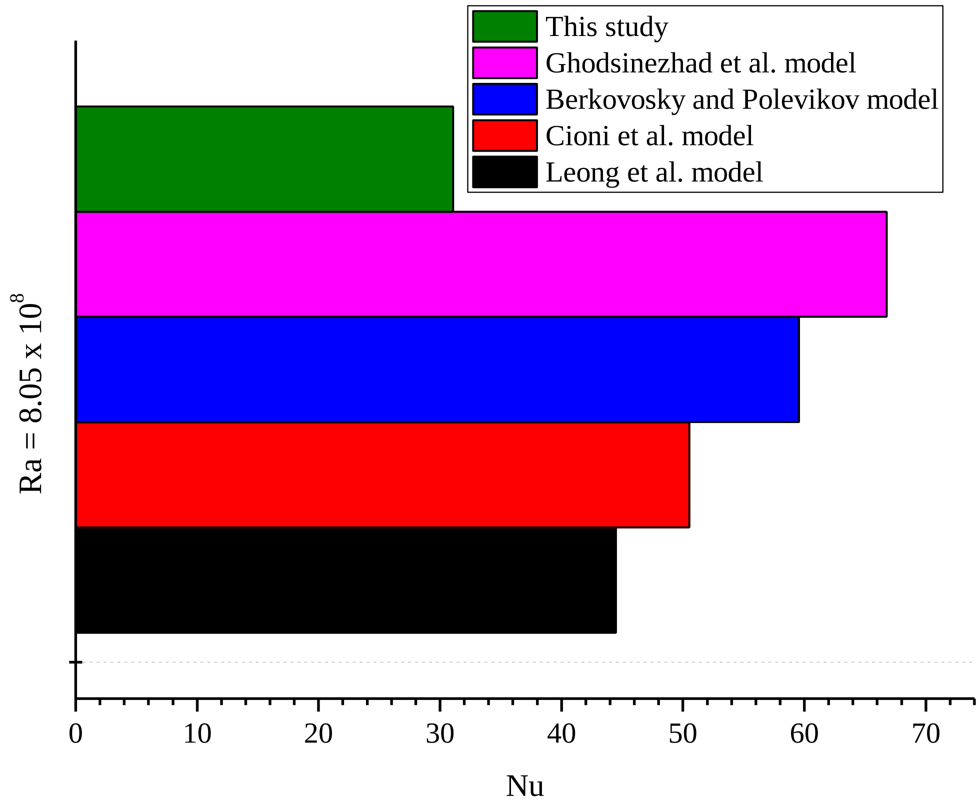

Figure 6.1: Comparison of measured *Nu* of MgO-ZnO/DIW BNFs with the proposed correlations of Leong et al. [545], Cioni et al. [544], Berkovosky and Polovikoy [543] and Ghodsinezhad et al. [25].

6.3 THERMAL TRANSPORT PERFROMANCE

The performance of the thermal transport for various PWRs of MgO–ZnO/DIW binary nanofluids for 0.05 vol% and 0.10 vol.% charged in a squared cavity under the influence of temperature change was examined. Temperatures were measured using thermocouples at various locations within and without the square enclosure. Figure 6.2 presents the influence of *Ra* on Nu_{av} for various φ and different ΔT for the DIW and BNF. As *Ra* augments, Nu_{av} rises for all BNF samples, with basefluid possessing the highest *Ra* value over BNF, which agrees with Giwa et al. [28] and Sharifpur et al. [173]. The detraction in the values of *Ra* for all BNFs was due to the suspension of BNPs (MgO and ZnO) in DIW, which improved *Nu* for BNF samples under different ΔT than for DIW. As φ increases from 0.05 to 0.1 vol.%, a reduction in *Nu* was observed, as published by Sharifpur et al. [173]. An augmented Ra was observed at rising temperature, with DIW possessing maximum *Ra*. Thus, *Ra*, *Nu*, and ΔT were observed to be closely linked, and in agreement with the literature [25, 330, 586, 587], this explains the changes in the thermal property of basefluid as influenced by the dispersion of BNPs in it. Figure 6.2 also presents 0.05 vol% BNF samples that has had the maximum *Nu* values when related with 0.10 vol.% BNF samples, with sample (80:20) attaining the highest Nu_{av} (53.62) for $Ra = 4.32 \times 10^8$ at ΔT = 18.09°C. This is seconded by 0.05 vol.% BNFs 40:60 (49.03), 20:80 (48.95), 60:40 (48.57) and trailed by 0.10 vol.% BNF samples 60:40 (40.41), 20:80 (37.77), 80:20 (37.48), 40:60 (37.47), in that order and finally, the basefluid (DIW). The *Nu* values differ from the result of Sharifpur et al. [173], which difference could be attributed to the various *Ra* ranges for all PWRs and both experiments.

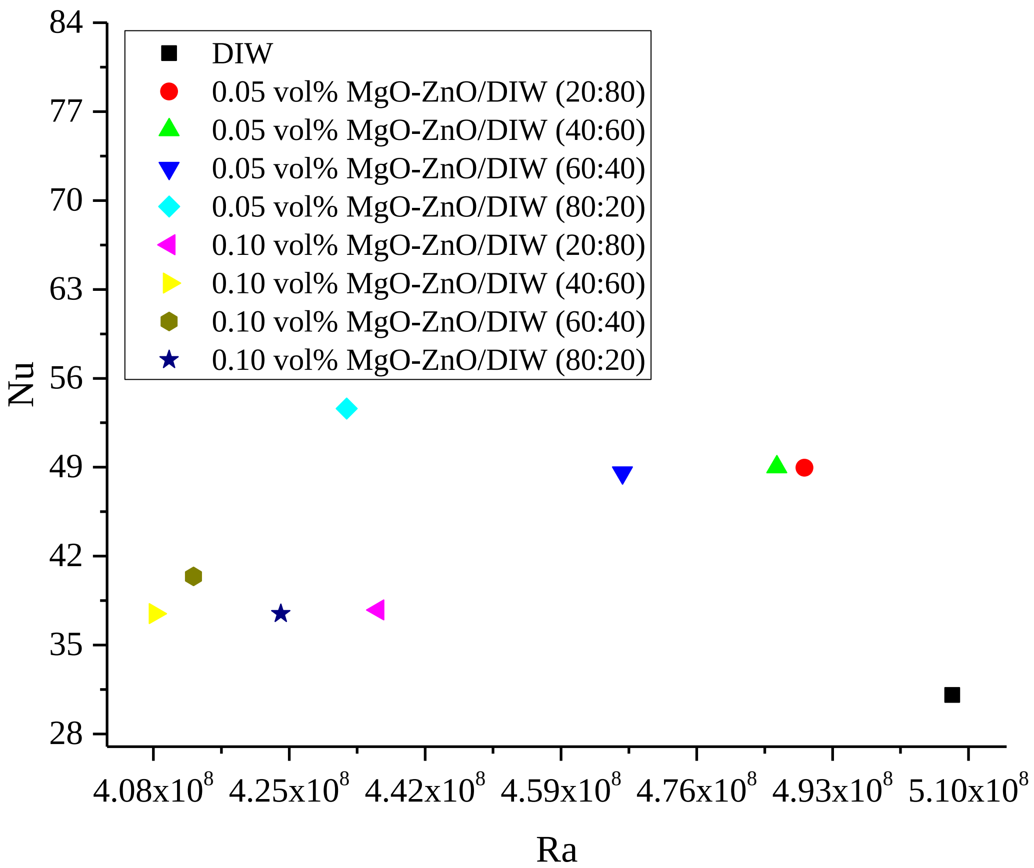

Figure 6.2: The impact of *Ra* on Nu_{av} at various φ.

Figure 6.3 presents the impact of ΔT and φ on the Nu_{av} for studied samples. For rising ΔT, an undeviating influence was observed for Nu_{av} by way of enhancement, but otherwise, as φ enhances, it improves for 0.05 vol.% and detracts for 0.10 vol.%. When related to DIW, an augmented Nu_{av} of 56.33% - 72.60% for 0.05 vol.% BNFs was observed detracted by 20.61% - 30.08% for 0.10 vol.% BNFs. The highest augmentation (72.60%) of Nu_{av} was attained in the investigation, which was over 8.42% highest enhancement published by Sharifpur et al. [173] when compared to basefluid, supports thermo-convection enhancement when binary nanofluids are employed for thermo-convection studies. Table 6.1 illustrates the contents of the tested samples. It is reported that effective viscosity of BNF was enhanced with increase in φ, giving room for buoyant forces in the square enclosure to be reduced at the highest concentration of the BNPs due to enhanced viscosity. An increase in φ results in improved thermal conductivity and enhanced viscosity of binary nanofluids at maximum φ resulting in the convective flow of binary nanofluids inside the enclosure decreasing. Thus, a detracting Nu_{av} as φ rises will continue to enhance the viscosity of binary nanofluids.

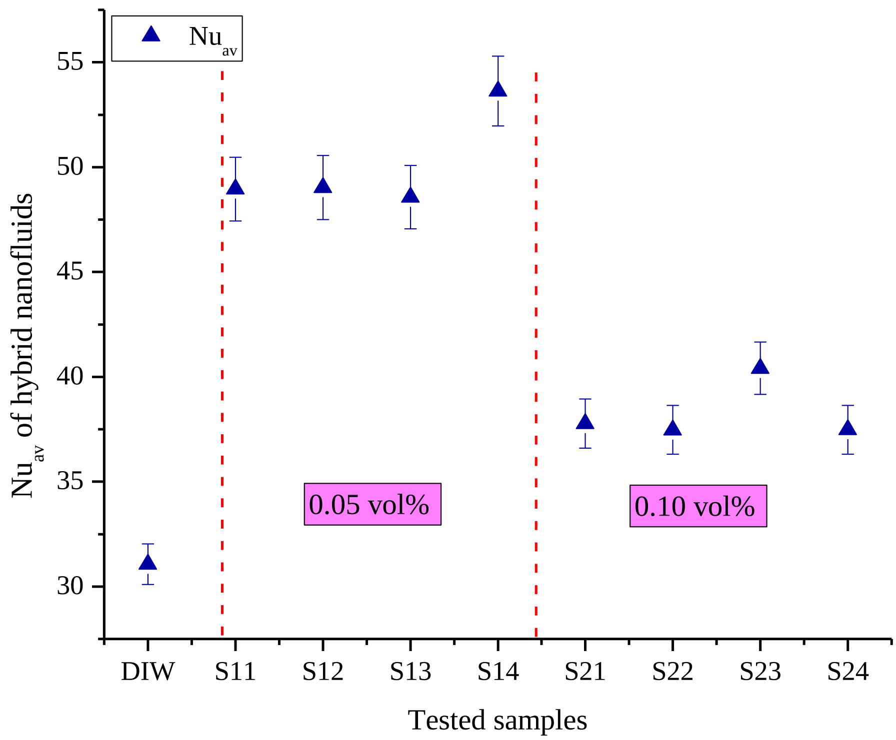

Figure 6.3: Impact of φ on Nu_{av} for the tested BNF samples.

Table 6.1. Tested BNF samples

Tested samples	0.05 vol.%	0.10 vol.%
MgO-ZnO (20:80)	S11	S21
MgO-ZnO (40:60)	S12	S22
MgO-ZnO (60:40)	S13	S23
MgO-ZnO (80:20)	S14	S24

The experimental dataset of *Ra*, Nu_{av} and PWR (*R*) was employed to propose a model as presented in Equation 6.1, such that Nu_{av} was estimated from φ and *R* with good precision. Published models for predicting Nu_{av} of nanofluid's performance in different enclosures mainly depends on φ and *R*. This is not applicable in the current study [25, 341, 588-593]. A fit of the proposed model is depicted by Figure 6.4.

$$Nu = 0.6184R - 235.24\varphi + 60.81 \quad (6.1)$$

The proposed model could predict the experimental dataset with a margin of deviation (MOD) of −5.74% to 5.75%. So, Figure 6.4 illustrates the relationship amidst the experimental and predicted Nu_{av} results.

Figure 6.5 illustrates the results of the impact of ΔT and φ on h_{av} for the studied BNFs in the investigation. h_{av} was enhanced with rising temperature difference and the use of binary nanofluids. Still, the situation changed when φ was enhanced as 0.05 vol.% rises to 0.10 vol%. Figure 6.5 further explains that the h_{av} of the binary nanofluids peaked for 0.05 vol.% BNF samples S11 to S14 and detracted for 0.10 vol.% samples S21 to S24, this is a clear indication of the effect of PWR and φ of the BNPs playing key roles in each h_{av} values [562, 585, 593]. For 0.05 vol.% BNFs, h_{av} of basefluid was enhanced by 61.28%, 61.79%, 60.33% and 76.01% for samples S11 (20:80), S12 (40:60), S13 (60:40), and S14 (80:20), while 0.10 vol.% samples had least outcomes of enhancement by 29.33%, 34.33%, 42.19% and 29.71% for samples S21 (20:80), S22 (40:60), S23 (60:40), and S24 (80:20). The detraction in the augmentation of h_{av}

for 0.10 vol.% binary nanofluids can be related to improved viscosity for this concentration, which reduced the convective heat transfer within the enclosure and eventually detracted h_{av} values. The highest h_{av} improvement attained in the experiment was over 25.6% enhancement reported by Suganthi and Rajan [594], who examined free convection of ZnO/PG nanofluid at 2.0 vol.% in a cylinder enclosure. The big difference can be related to the use of BNPs, basefluid, φ and cavity type. In some rectangular enclosures, Ho *et al.* [336] reported an improvement of 18% for h_{av} for Al_2O_3/DIW nanofluid at 0.10 vol.%; Ghodsinezhad et al. [25] published the highest enhancement of 15% for h_{av} for Al_2O_3/DIW NF; and Giwa et al. [329] achieved 19.4% as a maximum enhancement for h_{av} for Al_2O_3-MWCNT/DIW BNF (90:10 weight ratio) at 0.10 vol.%.

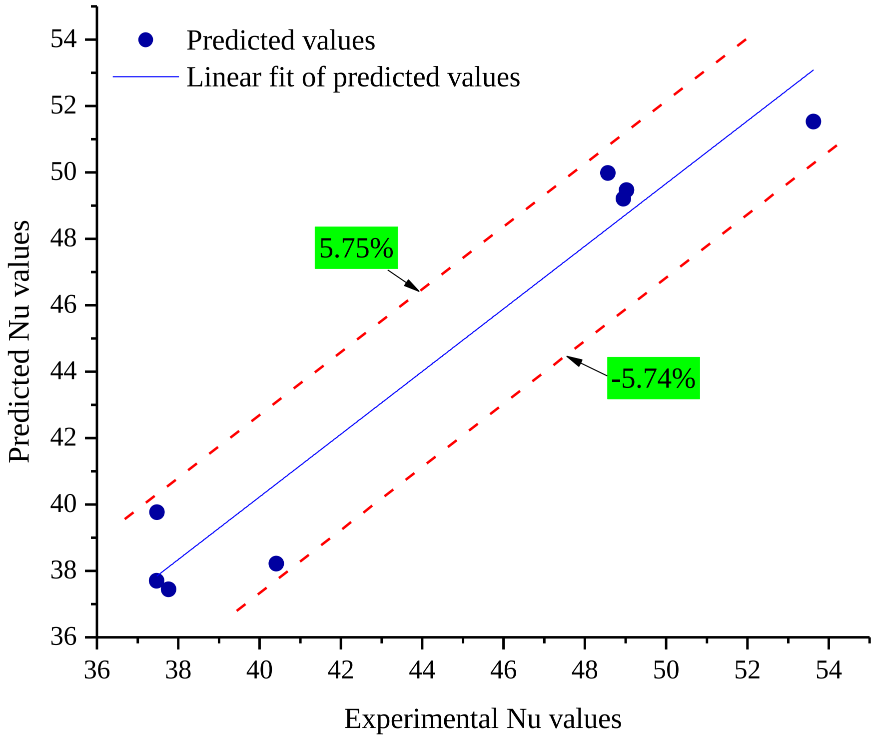

Figure 6.4: Fit of the developed model to predict *Nu*.

Analyzing the free convection thermal transfer capability of binary nanofluids within the enclosure, the Q_{av} as a relation of φ at different PWR and ΔT were investigated and illustrated as Figure 6.6. Figure 6.7 presents the quantity of heat transferred by the studied samples across the enclosure as a factor of various φ, PWR and ΔT. As the same pattern recorded for *Ra*, Nu_{av} and h_{av} was replicated for Q_{av}, obvious that an enhanced Q_{av} is a function of PWRs of BNPs in the binary nanofluid and ΔT. So, an augmentation of φ for binary nanofluids was observed to both augment and decrease Q_{av} for all BNF samples [562, 585, 593]. Figure 6.8 also presents a steady maximum improvement for 0.05 vol% binary nanofluid samples more than 0.10 vol.% binary nanofluid samples. The highest augmentation achieved was for 0.05 vol% binary nanofluid sample S12 (40:60) by 72.20% in relation to the basefluid. Sharifpur et al. [173] reported a Q_{av} enhancement of 6.75% at 0.10 vol% for ZnO/DIW nanofluid square enclosure. Also, Suganthi and Rajan [594] published Q_{av} augmentation of 4.24% at 2.0 vol% inside a cylindrical enclosure. Using a rectangular enclosure, Garbadeen et al. [27] recorded a 45% enhancement for Q_{av} for MWCNT/DIW nanofluid for 0.10 vol%, while Giwa et al. [329] published 9.80% for Al_2O_3-MWCNT/DIW BNF for 0.10 vol.%.

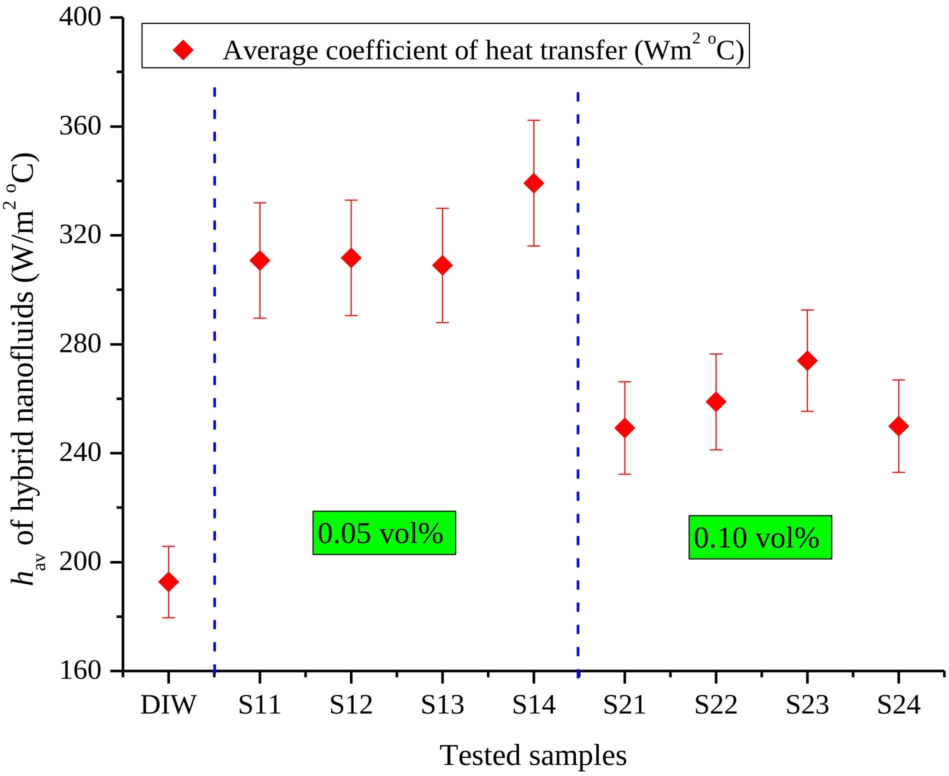

Figure 6.5: Effect of φ on h_{av} for the tested samples.

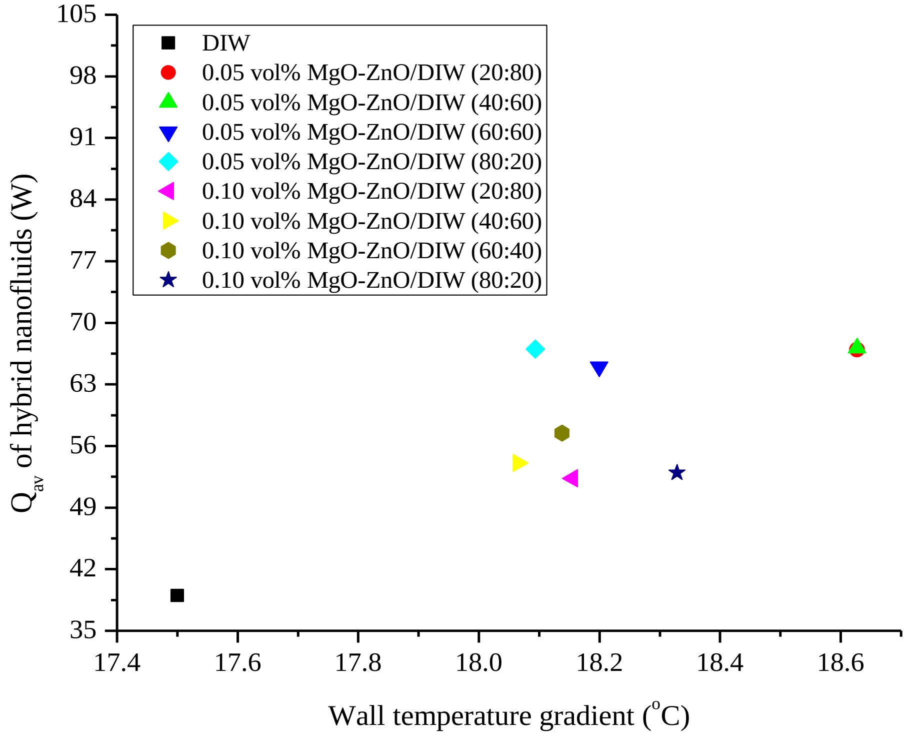

Figure 6.6: Q_{av} versus φ at different wall temperature ranges.

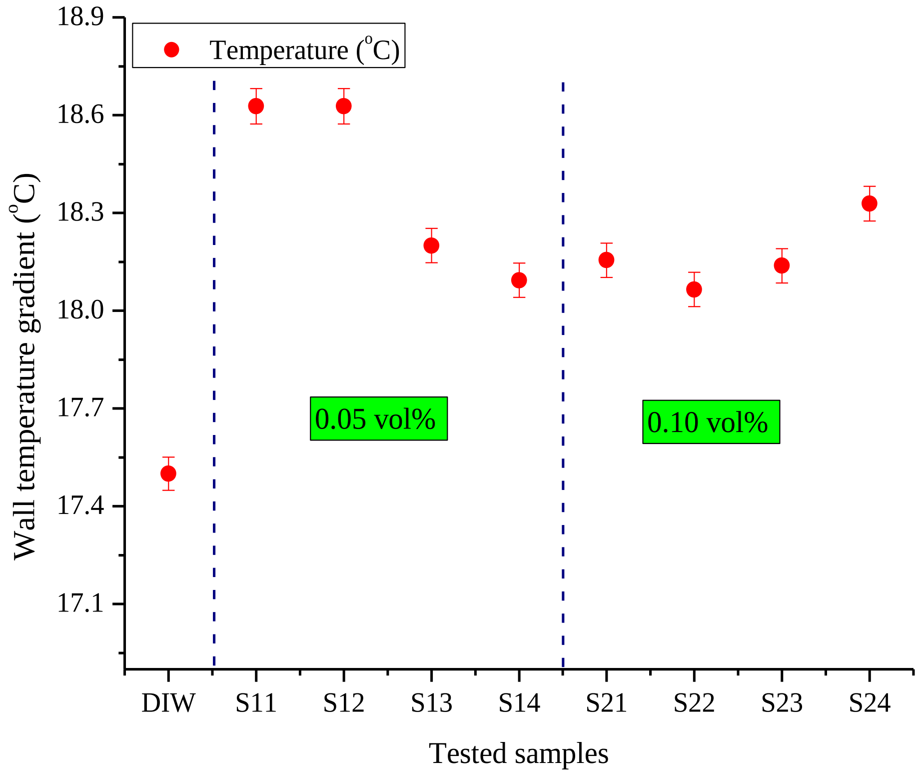

Figure 6.7: Effect of φ on wall temperature gradients on the tested samples.

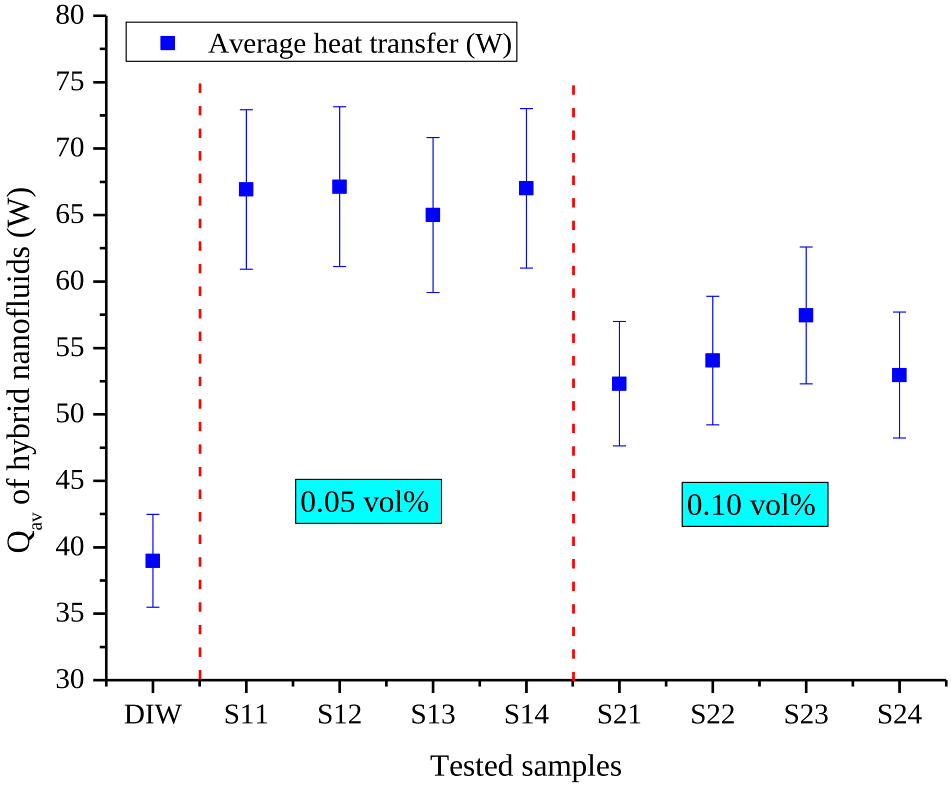

Figure 6.8: Effect of φ on Q_{av} on the tested BNF samples.

6.4 CAVITY TEMPERATURE DISTRIBUTION

The heat transfer investigation was done within uniform thermal conditions and measured temperatures with thermocouples at specific locations inside and outer side of the enclosure, as explained before now. The mean temperature of the basefluid and tested BNF samples under the effect of φ is illustrated in Figure 6.9. Figures 6.10 and 6.11 presents the temperature distribution profile across the hot side, cold side and the inner section of the cavity for all tested samples (basefluid and BNFs) under various temperature change and volume concentrations [562, 585, 592, 593, 595].

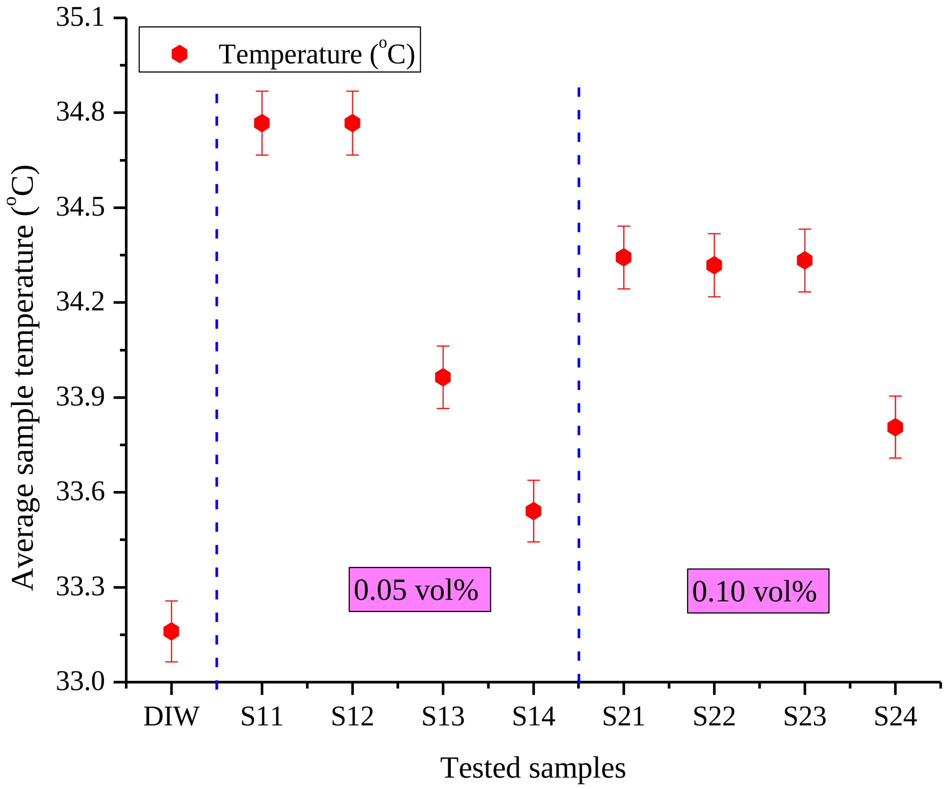

Figure 6.9: Effect of φ on temperatures of the tested BNF samples.

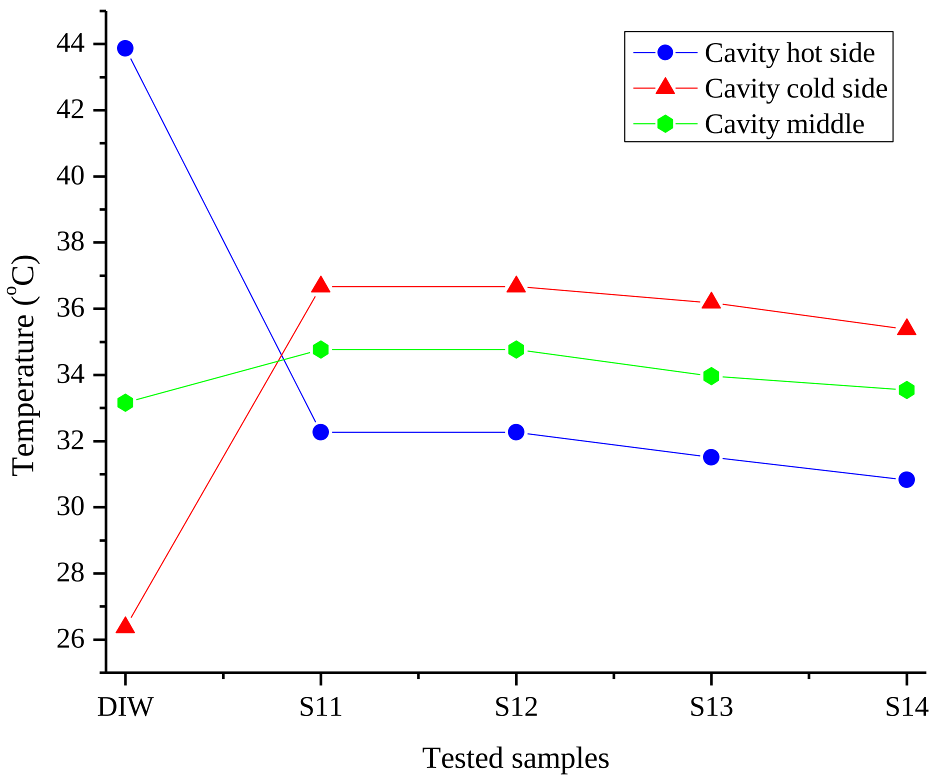

Figure 6.10: Cavity temperature profile for DIW and the tested BNF samples for 0.05 vol.%.

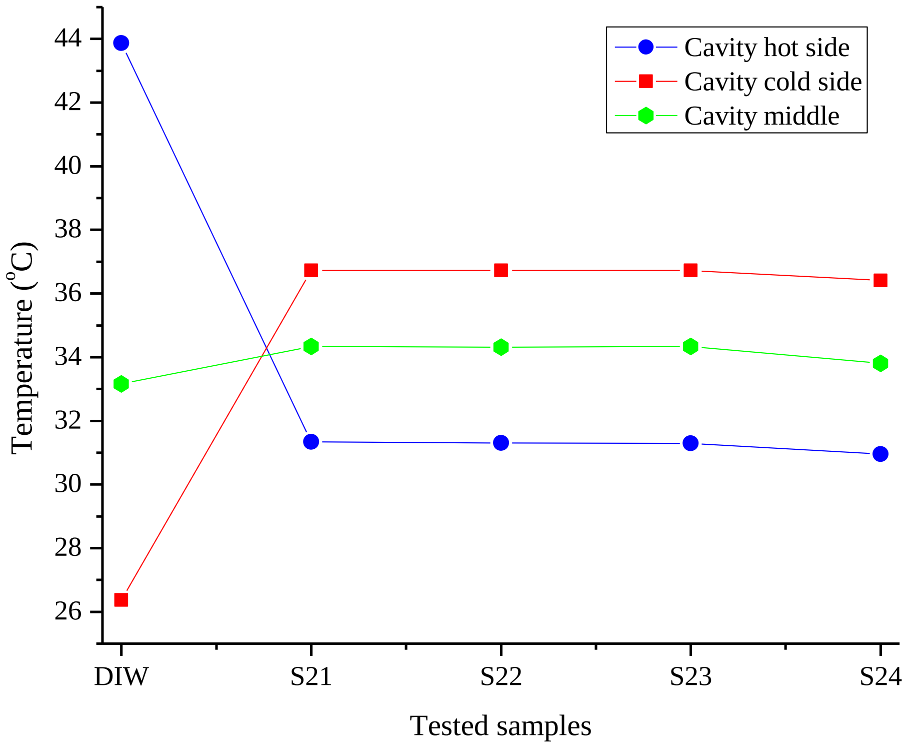

Figure 6.11: Cavity temperature profile for DIW and the tested BNF samples for 0.10 vol.%.

6.5 CONCLUSION

The natural convection behaviour of DIW and BNFs within a squared enclosure was conducted under various temperature change and estimated using four parameters: Nu_{av}, Ra, h_{av}, and Q_{av}. Stable binary nanofluids (0.05 vol.% and 0.10 vol%) were formulated and thermophysical properties (thermal conductivity and viscosity) were measured at temperature 20 - 50°C. The temperature distribution profile of the enclosure for the BNF samples employed in the investigation was discussed. Also, for all studied samples, a rise in temperature difference impacted an equivalent improvement for Ra, Nu_{av}, h_{av}, and Q_{av}. For this investigation, Nu_{av} was observed to have a close relation with φ, ΔT, Ra, and PWRs while h_{av} and Q_{av} were functions of φ, ΔT, and PWRs for all studied samples. Maximum Ra was achieved as related to open literature for natural convection of nanofluids in enclosures. Optimal Nu_{av} attained is 53.62 for $Ra = 4.32 \times 10^8$ at ΔT = 18.09 °C. Also, highest augmentation attained were 72.60% (Nu_{av}), 76.01% (h_{av}), and 72.20% (Q_{av}). This study present the hybridisation of ZnO and MgO nanoparticles into basefluid to prepare the binary nanofluid enhanced the thermal-fluid behaviour of basefluid, which helped the free convection behaviour of the binary nanofluid within a squared enclosure. The innovative results also support the benefit of using binary nanofluids over nanofluids. In conclusion, the application of suitably experimentally achieved models of experimental dataset for getting thermal properties is central to an experimental investigation of free convection heat transfer of BNF in enclosures.

CHAPTER 7

DEVELOPMENT OF ARTIFICIAL INTELLIGENCE MODELS TO PREDICT THERMAL CONDUCTIVITY OF BINARY NANOFLUIDS[1,2,3]

7.1 INTRODUCTION

Open literature confirms studies conducted related to experimental measurement of the thermal conductivity of different binary nanofluids with and without the development of empirical correlations to estimate the thermal conductivity, and modelling of the thermal conductivity using curve fitting via regression analysis and machine learning tools to develop empirical correlations to predict the same [72, 96, 141, 155, 368, 370-372, 596, 597]. The use of machine learning tools such as an Artificial neural network (ANN), Group method of data handling (GMDH), curve fitting, decision tree, dimensional analysis, random forest, generic algorithm, support vector machine, Adaptive Neuro-Fuzzy Inference System (ANFIS), Least squares support vector machine (LSSVM), etc. Their hybrids have been reported in the literature [66, 82, 96, 174, 248, 249, 368, 371, 596, 598]. This is due to the cost and complex nature of the experimental measurement of thermal properties of nanofluids. So, to limit the cost and time of experiments, researchers and scientists adopted the idea of developing models and correlations using the above-mentioned machine learning methods. Obtained artificial neural network (ANN) results were presented.

This chapter is reflected in parts in the following papers:

[1]Nwaokocha, C., Giwa S., Ghorbani B., Momin, M., Sharifpur, M., Gharzvini M., Chamkha, A.J., Meyer, J.P., *Experimental formulation and GMDH modelling of thermal conductivity of MgO–ZnO/deionised water hybrid nanofluids.* Ready for submission.
[2]Nwaokocha, C., Momin, M., Sharifpur, M. and Meyer, J., *Artificial neural network development to predict thermal conductivity of MgO–ZnO/Deionised Water binary nanofluids.* Ready for submission.
[3]Nwaokocha, C., Sharifpur, M. and Meyer, J., *Application of binary nanofluids – Emerging issues.* Ready for submission.

7.2 ARTIFICIAL NEURAL NETWORK MODEL TO PREDICT THERMAL CONDUCTIVITY OF BINARY NANOFLUIDS

Using the ANN method in MATLAB R2021a software, experimental data sets were classified as training, validation and testing on a random basis. The training data generates biases and masses for the testing, the validation data was used to modify the masses during training session, while the test data sets were used to determine the performance of the neural network. For this work, an optimized ANN to predict k_{bnf} was determined by comparing the performances of the varied neuron numbers within the inner layers, then finally using the best neuron number. This was done by modifying the ANN architecture to determine the optimized neuron number. The suggested learning algorithm is presented as Figure 7.1.

Using the proposed learning algorithm, eight hundred (800) experimental data set were obtained from the experimental thermal conductivity measurements of MgO-ZnO/DIW BNFs, which was classified as 560 (70%) data points for training, 120 (15%) data sets for validation and 120 (15%) data points for testing purpose. The performance values for the training, validation and testing were sorted in neuron number order and presented in Table 7.1. The loop worked using 6 to 23 neurons, simulating for 27 iterations, with the optimized network was finally selected based on performance. The best network was at neuron 19 due to having the best performance, as depicted in Figure 7.2. Table 7.2 presents the correlation existing amidst data inputs and output results for varying neuron numbers. As the values approach 1, a perfect positive correlation is established, meaning the target data and predicted values are related. The train, validating and testing figures of ANN are presented in Figures 7.3 to 7.6, which depicts that they are finely predicted by the ANN. Figure 7.6 shows that the neural network will predict the κ_{bnf} for various temperatures, nanosizes, PWR and volume concentration.

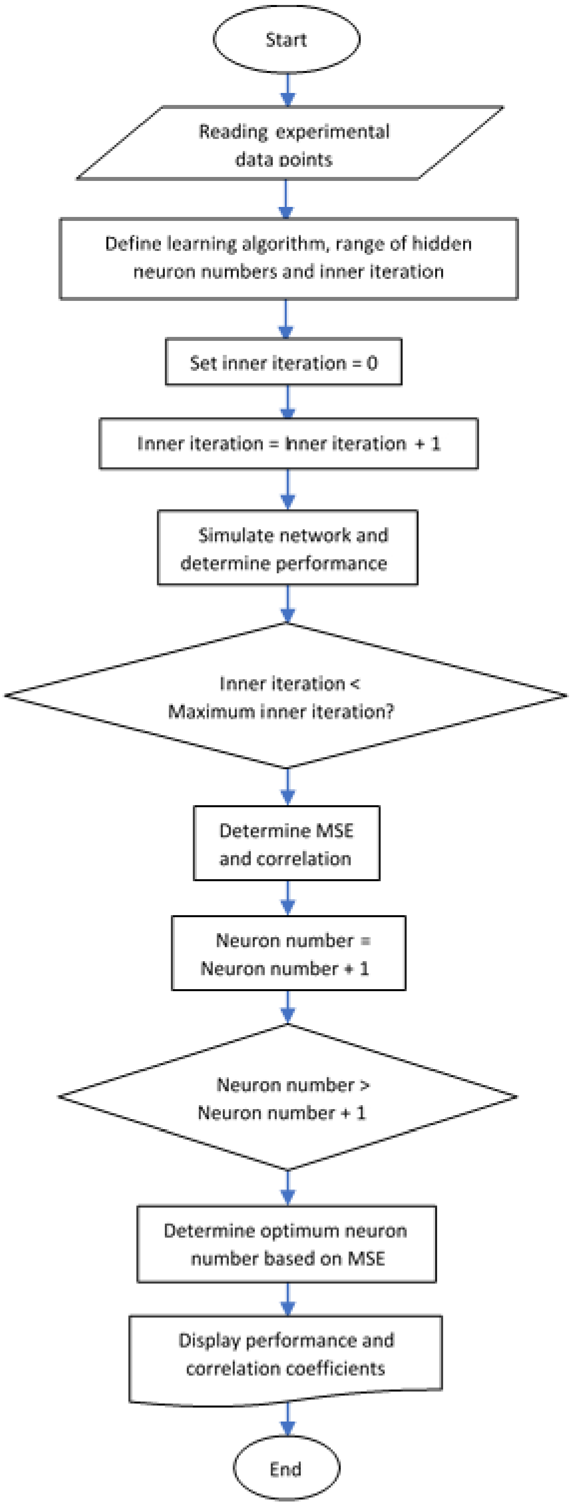

Figure 7.1. Proposed learning algorithm to determine optimized ANN.

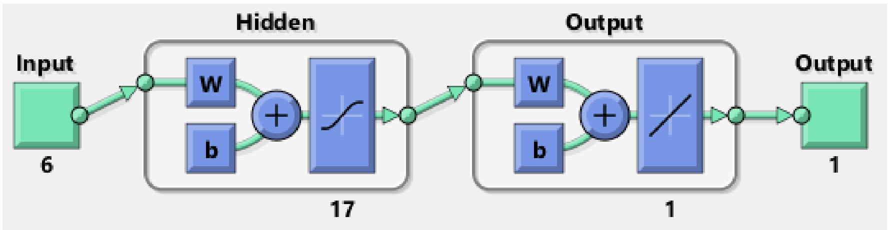

Figure 7.2. The optimized ANN.

Table 7.1. ANN performances.

Neuron number	Overall performance	Train performance	Validation performance	Test performance
19	2.18000E-07	2.40267E-07	1.40680E-06	1.89317E-06
20	3.96000E-07	4.45651E-07	1.49020E-06	1.78486E-06
21	4.32000E-07	4.57133E-07	4.28085E-06	1.89977E-06
23	5.59000E-07	7.55047E-07	1.71477E-06	1.52975E-06
15	6.05000E-07	6.12132E-07	1.07121E-06	6.82498E-06
22	7.25000E-07	8.09382E-07	1.00912E-06	1.71285E-06
14	7.45000E-07	7.95710E-07	3.56513E-06	3.73645E-06
9	7.53000E-07	8.57089E-07	9.88912E-07	1.88241E-06
17	7.65000E-07	8.35581E-07	7.92507E-07	1.68368E-06
12	7.91000E-07	7.98940E-07	2.51440E-06	1.29637E-06
18	8.60000E-07	1.27263E-06	2.56084E-06	2.46100E-06
16	9.47000E-07	9.82306E-07	2.28093E-06	1.21286E-06
13	9.83000E-07	1.00320E-06	1.05626E-06	1.48523E-06
11	1.30000E-06	1.61032E-06	3.29324E-06	2.82686E-06
8	1.31000E-06	1.33776E-06	4.20892E-06	1.08940E-06
10	1.54000E-06	1.66113E-06	3.35907E-07	1.91464E-06
7	1.63000E-06	2.17039E-06	3.17441E-06	4.51185E-06
6	2.36000E-06	2.42394E-06	2.56614E-06	3.60712E-06

Table 7.2. Correlation coefficients of data sets for varying neuron numbers.

Neuron numbers	All	Training	Validation	Testing
19	0.99974	0.99991	0.99942	0.99930
20	0.99968	0.99983	0.99931	0.99933
21	0.99974	0.99981	0.99983	0.99937
23	0.99961	0.99969	0.99935	0.99956
15	0.99973	0.99976	0.99948	0.99977
22	0.99962	0.99968	0.99962	0.99935
14	0.99935	0.99969	0.99859	0.99857
9	0.99960	0.99966	0.99958	0.99933
17	0.99962	0.99967	0.99969	0.99936
12	0.99955	0.99966	0.99926	0.99946
18	0.99935	0.99949	0.99902	0.99918
16	0.99952	0.99963	0.99913	0.99943
13	0.99957	0.99960	0.99956	0.99947
11	0.99921	0.99936	0.99889	0.99892
8	0.99932	0.99946	0.99850	0.99957
10	0.99923	0.99936	0.99896	0.99894
7	0.99895	0.99913	0.99887	0.99832
6	0.99897	0.99906	0.99888	0.99872

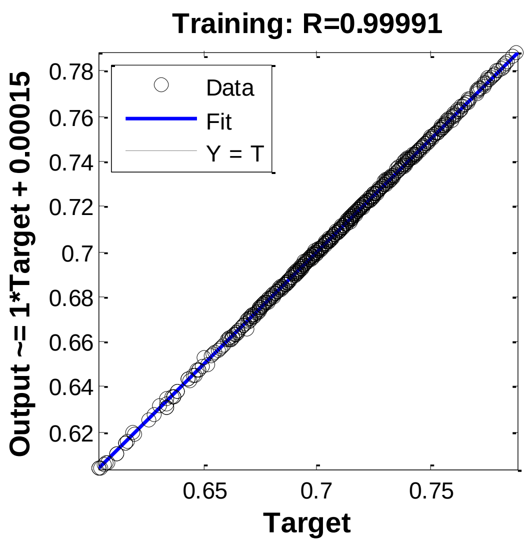

Figure 7.3. Training outputs.

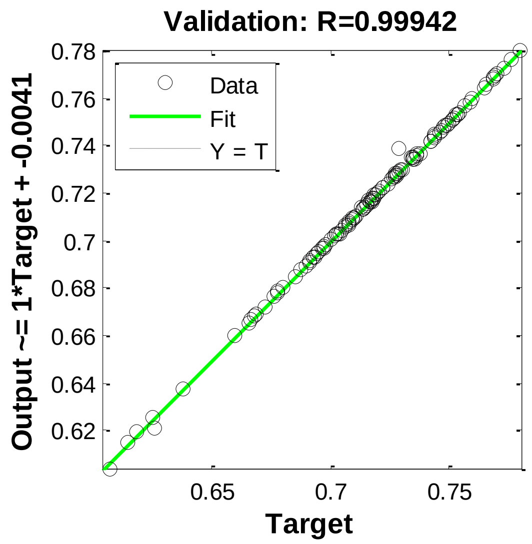

Figure 7.4. Validation outputs.

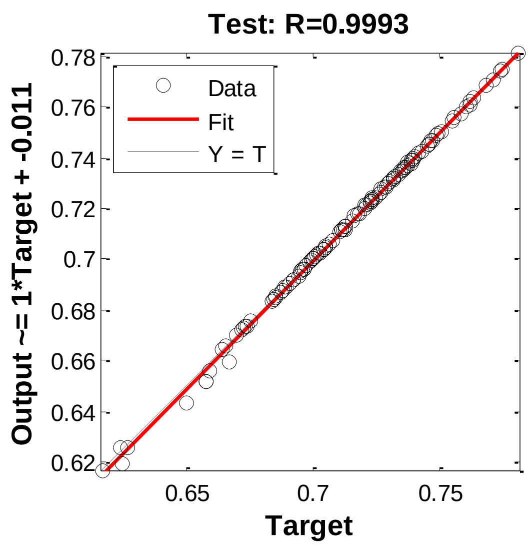

Figure 7.5. Testing outputs.

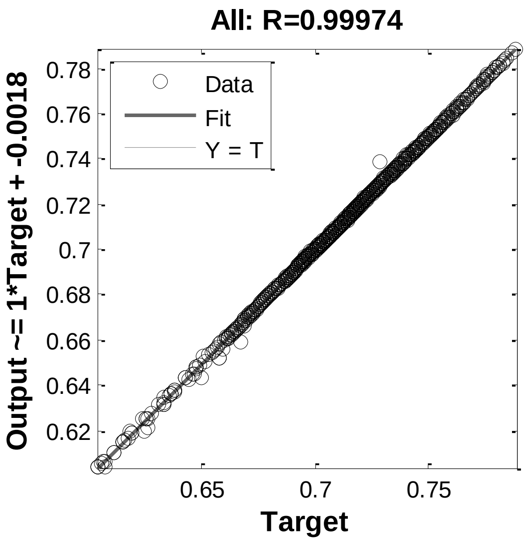

Figure 7.6. All outputs.

Figure 7.7 presents the error histogram, which projects the error rates for data received at the train, verification and testing stages of the ANN. This is used to estimate error values of the designed ANN and found to be low, as the error distribution was loaded around the zero-error line, which confirms that the developed ANN using MLP model will predict the thermal conductivity of MgO-ZnO/DIW BNFs with the required accuracy. Figure 7.8 presents the variation patterns amidst tentative results and ANN outcomes for experimental thermal conductivity outcomes of MgO-ZnO/DIW HNFs in terms of Epochs (presented on the horizontal axis) versus MSE (indicated on the vertical axis). The MSE values were high ab initio and thereafter decreased gradually with increasing epochs until an optimized MSE value of 1.4068e-6 just after 21 iterations was reached, as shown in the small green circle in the Figure. The graph's pattern signified a well-designed training phase for the ANN model.

7.3 SURFACE FITTING METHOD TO PREDICT THERMAL CONDUCTIVITY OF BINARY NANOFLUIDS

Here, the fitting method is used to predict the behaviour of BNFs so that *x* represents φ (vol.%) and *y* presents temperature. Using polynomials for the input data points (*x*,*y*), a fitted surface was produced for k_{bnf} as presented in Equation 7.1 and Figure 7.9. Table 7.3 depicts the surface coefficients.

$$k_{bnf}(x,y) = P00 + (P10 \times x) + (P01 \times y) + (P20 \times x^2) + (P11 \times xy) + (P02 \times y^2) \quad 7.1$$

Figure 7.9 revealed a variation in BNFs' behaviour for various temperatures and φ. It depicts an increase for k_{bnf} as temperatures and φ increase. It shows that temperature and φ has a direct relationship with k_{bnf}.

Table 7.3. Surface coefficients

P00	P10	P01	P20	P11	P02
0.8809	1.301	0.001203	1.868	0.04198	3.378e-05

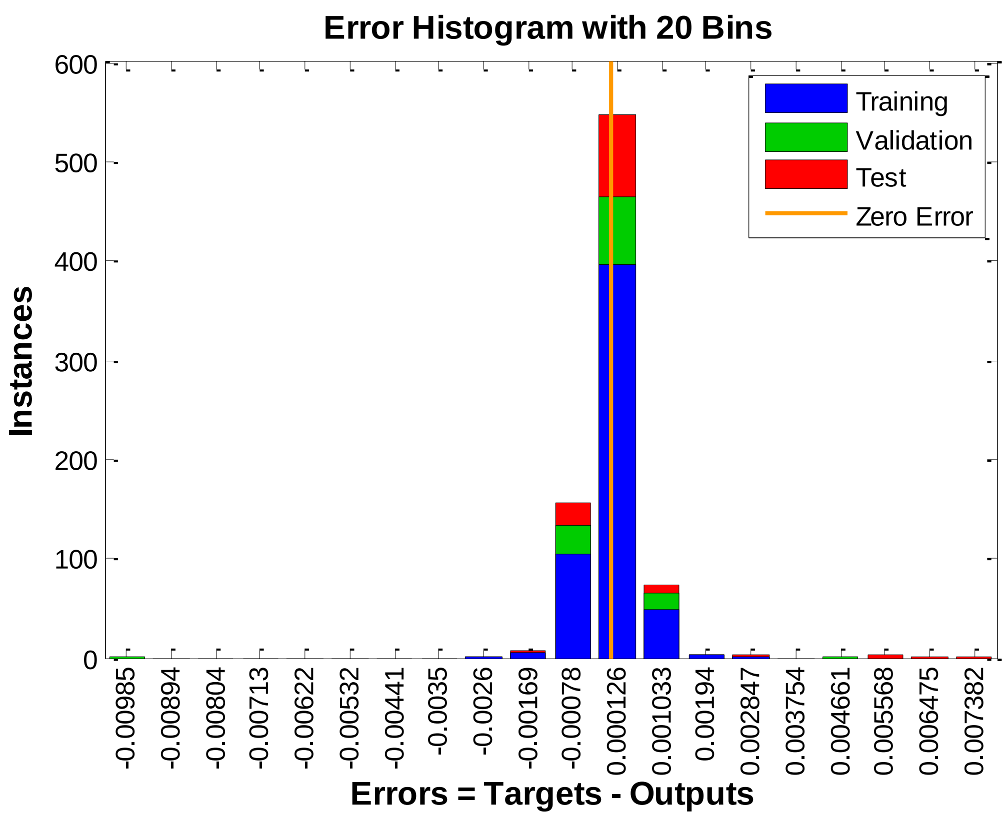

Figure 7.7. Error histogram.

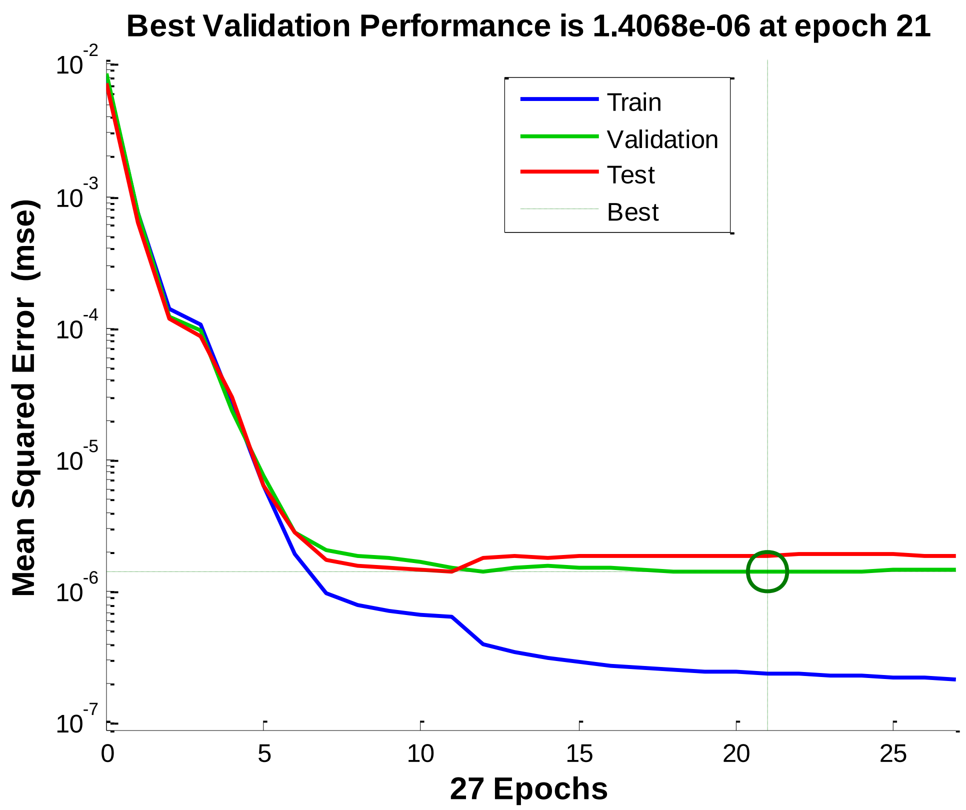

Figure 7.8. Variations of epoch against MSE.

7.4 COMPARING THE RESULTS OF ANN MODEL AND FITTING METHOD

Table 7.4 presents results for the MSE, the maximum absolute value of error, and correlation coefficients of ANN and Surface fitting methods. Correlation coefficients explain the relationship between output and targets for values 1 to -1, where 1 is positive and -1 is negative and zero is nil association among two types of data. The equation to estimate the coefficient of correlation is described as Equation 7.2.

Table 7.4. Statistical parameter.

	ANN	Fitting
Maximum absolute value of error	0.0018	0.2374
Mean Square Error	1.4068e-6	0.01731
Correlation Coefficients	0.99930	0.7662

$$r = \frac{n\sum xy - (\sum x)(\sum y)}{\sqrt{[\sum x^2 - (\sum x)^2][n\sum y^2 - (\sum y)^2]}} \quad (7.2)$$

where, r is the correlation coefficient, x is target, y is ANN outputs, and n is the number of data points. It is obvious that the ANN method has good performance over the fitting methods [174, 599, 600].

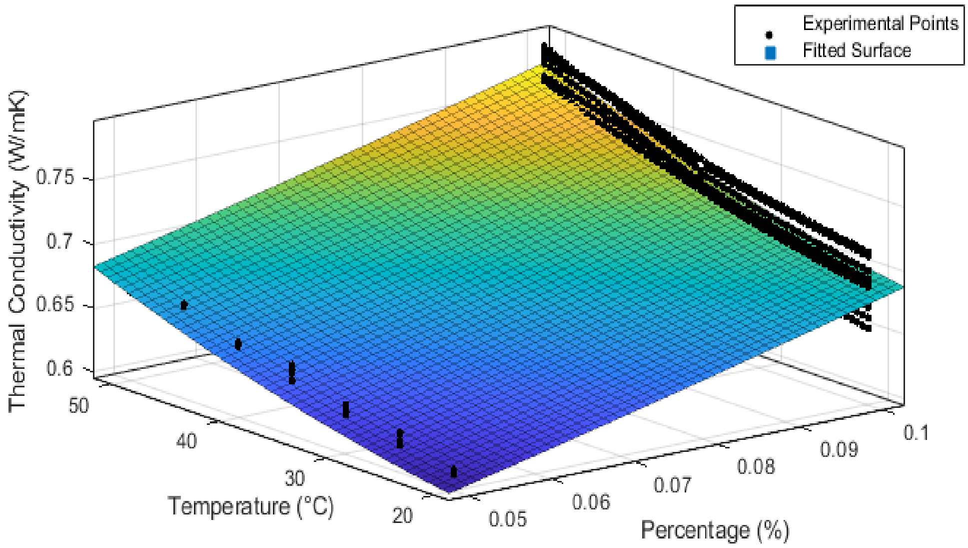

Figure 7.9. κ_{bnf} versus temperature and φ.

7.5 CONCLUSION

An artificial neural network (ANN) and surface fitting method was employed to predict the k of MgO-ZnO/DIW BNFs, using the experimental data sets of k for 0.1 vol.% MgO-ZnO/DIW BNFs. In both models, percentage weight ratio (PWR - 20:80, 40:60, 60:40, 80:20 (MgO-ZnO)), nanoparticles sizes (20 nm, 40 nm and 100 nm for MgO NPs and 20 nm for ZnO NPs), temperature (T - 20 to 50 °C) and volume concentration (0.05% and 0.1%) were used as input parameters, and TC obtained as output parameter. A learning algorithm was developed for the ANN model to determine the optimum neuron number. The ANN having 19 neurons in the inner layer got the optimized performance. A surface fitting method was also used on the experimental data, and the generated surface shows the behaviour of the binary nanofluids. The outcome affirmed that the designed ANN model is best for predicting the thermal conductivity of MgO-ZnO/DIW binary nanofluids for various temperatures, nanoparticle sizes, percent weight ratios and volume concentration over the surface fitting method.

CHAPTER 8

SUMMARY, CONCLUSIONS AND RECOMMENDATIONS

8.1 SUMMARY

The shortcomings in thermal management of energy applications led to the concept of nanosuspension, leading to the formulation of the new class of thermal fluids named nanofluids. The shortcomings range from surface modification, use of conventional fluids, area/volume ratio reduction, miniaturisation, etc. It is established that nanofluids possess enhanced thermal properties when compared to traditional working fluids, thus beneficial for thermo-convention application. The further improvement led to the formulation of binary nanofluids and ternary nanofluids to handle the limitations observed with mono-particle nanofluids. Mono-particle nanofluids and binary nanofluids were formulated using the two-step method. Optimization of parameters (amplitude, dispersion fraction and sonication time) was employed during formulation to allow for repeatability.

Thermo-convection heat transfer has found vast application in engineering applications, thus spurring continuous investigations of free convection heat transfer performance of nanofluids in different enclosure. Numerical methods have gain numbers than experimental studies for thermo-convection heat transfer behaviour using nanofluids in enclosures. To boost the thermo-convection performance of nanofluids in cavities, enhancing methods are cavity inclination, aspect ratio, magnetic stimulus, porous cavity, green base fluids, binary basefluids, green nanofluids, binary nanofluids, and ternary nanofluids.

The use of artificial intelligence models to predict the thermophysical properties of nanofluids is just gaining increase in the public domain, hence the focus of the current study in that direction. Also, the experimental investigation of thermo-convection heat transfer augmentation using binary nanofluids is scarce in the public domain, so the current study also focused on it with brilliant contributions.

8.2 CONCLUSIONS

Chapter 1 of this thesis presented the general introduction of the investigation, thus outlining the study's objectives and scope.

Chapter 2 presented a literature search on nanofluid as an innovative working fluid for thermal management in heat transfer applications. The search entails the formulation and measurement of thermal properties of nanohybrids. The parameters that influence nanohybrids' thermal properties, like basefluid, temperature, nano-shapes, nano-size, volume concentration, were reviewed based on available datasets in the open literature. The morphology and thermo-convection performance of nanohybrids were also reviewed. The use of artificial intelligence models to predict thermal properties were reviewed as well. The Chapter also presented a wide range of recent and future applications of nanofluids with focus on related issues that allow for suitability for industrial applications.

Chapter 3 detailed the experimental methodology needed for the formulation and measurement of thermal properties of nanohybrids (MgO-ZnO/DIW) for percentage weight ratio (PWR - 20:80, 40:60, 60:40, 80:20 (MgO-ZnO)), nanoparticles sizes (20 nm, 40 nm and 100 nm for MgO NPs and 20 nm for ZnO NPs), temperature (T - 20 to 50 °C) and volume concentration (0.05% and 0.1%). It entails the process for formulating binary nanofluids, the measurements of thermal properties of binary nanofluids, and the thermo-convection performance of binary nanofluids in a square cavity. The experimental setup for thermo-convection behaviour of nanohybrids in a squared cavity was conducted. The chapter also presented the validation of the cavity and data reduction. Also, model development for thermophysical properties and *Nu*, and the estimation of uncertainty for thermophysical properties and thermo-convection experiments were detailed in this chapter. Artificial intelligence method like ANN was introduced in predicting the thermal properties of MgO-ZnO/DIW binary nanofluids.

Chapter 4 presented the optimum parameters (amplitude, dispersion fraction, pulse used, and sonication time) for formulating mono-particle nanofluids and binary nanofluids. This enables the repeatability of such experiments. This investigation formulated mono-particle nanofluids of MgO and ZnO, for comparison with binary nanofluids of MgO-ZnO/DIW for φ of 0.05 vol.% and 0.1 vol.% via optimized operating parameters leading to a stable BNFs. TEM images detected nanoparticle sizes close to the manufacturers and a good degree of nanosuspension stability. In addition, the stability of BNFs as observed by the absorbance was found stable. Thus stability and morphology are confirmed satisfactory. Hence, further investigation on thermal properties and thermo-convection were done, and results were presented and discussed in subsequent chapters.

Chapter 5 presented the experimental measurement of thermal conductivity (κ), electrical conductivity (σ), pH, and viscosity (μ) of MgO-ZnO/DIW BNFs (0.05 and 0.10 vol%) were successfully studied for PWR of 20:80, 40:60, 60:40, 80:20 (MgO:ZnO) at temperatures gradients of 20 to 50°C. The κ of the BNFs for all PWR was augmented under the influence of increasing temperature as compared to DIW. The highest κ enhancement of 5.60% and 22.07% relative to the basefluid was obtained at 0.05 and 0.10 vol.%, respectively, which shows that the dispersion of MgO-ZnO NPs enhances κ greatly, especially at higher temperatures. Also, the pH of MgO-ZnO/DIW BNFs (0.05 and 0.10 vol%) for all mixing ratios reflects a steady decline as temperature increases. The BNFs possessed pH values more than 7, thus formulating an alkaline fluid. It was observed that temperature greatly influenced the pH of the BNFs, then volume concentration, and finally PWR. pH enhancements of 27.04% to 40.74% and 30.20% to 39.59% were achieved for BNFs (at φ of 0.05 and 0.1 vol%

respectively) at different PWRs for temperature ranges of 20–50 °C. Then, the BNFs' electrical conductivity (σ) for all the PWR was slightly enhanced under the influence of increasing temperature. Dispersing hybrid NPs into DIW significantly improved the σ of DIW. Maximum enhancement of 21.82% and 30.91% were observed for 0.05 and 0.1 vol%, respectively. In addition, the viscosity (μ) of MgO-ZnO/DIW BNFs (0.05 and 0.10 vol%) as temperature improves gradually exhibited a detracting trend for all nanohybrids and basefluid. Thus, it was deduced that using 0.05 vol% to formulate the BNFs led to reduced μ values, while an increase to 0.1 vol% produced enhanced μ values for its BNFs. The difference in MgO-ZnO NPs mixing ratio led to variation in μ for the BNFs for temperatures examined. The effective criteria in selecting BNFs for thermal applications is a function of the TEC value. It was observed that BNFs of 0.05 vol% were observed to have higher TEC values than that of 0.10 vol% BNFs. Also noticed is that an increment in temperature reduced the TEC values for both volume concentrations. The BNFs samples investigated in this work under the studied temperature range are suitable for thermal application. The PER revealed that at 0.10 vol% and temperature 20 – 50 ^{0}C, all studied binary nanofluids were fine for thermal cooling purposes. The 40:60 binary nanofluids was the best sample with minimum viscosity and maximum thermal conductivity, which is beneficial to engineering application. Using experimental results, correlations were proposed to estimate the studied BNFs' thermophysical properties.

Chapter 6 presented the thermo-convection behaviour of binary nanofluid and basefluid within a squared enclosure was conducted under various temperature differences and estimated using four parameters: Nu_{av}, Ra, h_{av}, and Q_{av}. Stable binary nanofluids (0.05 vol.% and 0.10 vol.%) were formulated and thermophysical properties (thermal conductivity and viscosity) measured at temperature 20–50 °C. The temperature distribution profile of the enclosure for all BNF samples employed in this investigation was presented. In addition, for all the studied samples, a rise in temperature difference impacted an equivalent improvement for Ra, Nu_{av}, h_{av}, and Q_{av}.

For this investigation, Nu_{av} was observed to possess a close affinity with φ, ΔT, Ra, and PWRs while h_{av} and Q_{av} were dependent on φ, ΔT, and PWRs for tested samples. Maximum Ra was achieved in comparison to open literature for free convection of nanofluids in enclosures. Optimal Nu_{av} attained is 53.62 for $Ra = 4.32 \times 10^8$ at $\Delta T = 18.09$ °C. Also, highest improvement attained were 72.60% (Nu_{av}), 76.01% (h_{av}), and 72.20% (Q_{av}). This study showed the hybridisation of ZnO and MgO nanoparticles into basefluid to prepare the binary nanofluid enhanced the thermal-fluid behaviour of basefluid, which supported the free convection behaviour of the binary nanofluid within a squared enclosure. The innovative results also support the benefits of using binary nanofluids more than nanofluids. In conclusion, using appropriate experimentally achieved models of experimental dataset for estimating thermophysical properties is central to an experimental investigation on natural convection heat transfer of a BNF in an enclosure.

Chapter 7 presented the use of artificial intelligence (AI) models to predict thermal properties, based on results of the experimental study. AI methods, like artificial neural network (ANN) and surface fitting method were deployed to model some thermophysical properties of the formulated nanohybrids. For ANN model, a learning algorithm was developed to determine the optimum neuron number. The ANN having 19 neurons in the inner layer got the optimized performance. A surface fitting method was also used on the experimental data and the generated surface shows the behaviour of the binary nanofluids. The outcome affirmed that the designed ANN model is best for predicting the TC of MgO-ZnO/DIW binary nanofluids for different temperatures, nanoparticle sizes, PWRs and volume concentration over the surface fitting method.

8.3 RECOMMENDATIONS

For future works, the following points were recommended:

- The influence of sonication energy on the thermophysical properties of binary nanofluids.
- The use of machine learning-based approaches for modelling the thermophysical properties of binary nanofluids.
- The use of computational fluid dynamics (CFD) simulation in modelling the thermophysical properties and thermo-convection heat transfer performance of binary nanofluids.
- Experimental studies of thermo-convection heat transfer performance of binary nanofluids in different cavity shapes such as a rectangle and cylinder.
- Experimental studies using green binary nanofluids for measurement of thermophysical properties and thermo-convection heat transfer performance.

REFERENCES

1. Akdag, A. and S. Sahin, *Evaluation of the Progress of Sustainable Energy Management in World Economies*, in *Handbook of Research on Strategic Management for Current Energy Investments*. 2021, IGI Global. p. 246-261.
2. Nwaokocha, C.N., et al., *Microbial fuel cell: Bio-energy production from Nigerian corn starch wastewater using iron electrodes.* Materials Today: Proceedings, 2020.
3. Cecchin, A., et al., *Relating industrial symbiosis and circular economy to the sustainable development debate*, in *Industrial symbiosis for the circular economy*. 2020, Springer. p. 1-25.
4. Giwa, S.O., et al., *Gas flaring attendant impacts of criteria and particulate pollutants: A case of Niger Delta region of Nigeria.* Journal of King Saud University-Engineering Sciences, 2019. **31**(3): p. 209-217.
5. McDave, K.E. and A. Hackman-Aidoo, *Africa and SDG 9: Toward a Framework for Development Through Intellectual Property.* US-China L. Rev., 2021. **18**: p. 12.
6. Gerken, I., T. Wetzel, and J.J. Brandner, *Efficiency Improvement of Miniaturized Heat Exchangers.* Fluids, 2021. **6**(1): p. 25.
7. Gong, W., et al., *Research and applications of drag reduction in thermal equipment: A review.* International Journal of Heat and Mass Transfer, 2021. **172**: p. 121152.
8. Liang, G. and I. Mudawar, *Review of pool boiling enhancement by surface modification.* International Journal of Heat and Mass Transfer, 2019. **128**: p. 892-933.
9. Maxwell, J.C., *A Treatise on Electricity and Magnetism*. Cambridge Library Collection - Physical Sciences. Vol. 1. 2010, Cambridge: Cambridge University Press.
10. Maxwell, J.C., *A treatise on electricity and magnetism*. Vol. 1. 1873: Clarendon press.
11. Revathi, G., et al., *Numerical simulation for Arrhenius activation energy on the nanofluid dissipative flow by a curved stretching sheet.* The European Physical Journal Special Topics, 2021: p. 1-10.
12. Ahuja, A.S., *Augmentation of heat transport in laminar flow of polystyrene suspensions. I. Experiments and results.* Journal of Applied Physics, 1975. **46**(8): p. 3408-3416.
13. Ahuja, A.S., *Augmentation of heat transport in laminar flow of polystyrene suspensions. II. Analysis of the data.* Journal of Applied Physics, 1975. **46**(8): p. 3417-3425.
14. Liu, K., U. Choi, and K.E. Kasza, *Measurements of pressure drop and heat transfer in turbulent pipe flows of particulate slurries.* NASA STI/Recon Technical Report N, 1988. **89**: p. 11150.
15. Choi, U. and T. Tran, *Experimental studies of the effects of non-Newtonian surfactant solutions on the performance of a shell-and-tube heat exchanger.* Recent developments in non-Newtonian flows and industrial applications, 1991. **124**: p. 47-52.
16. Choi, U., D.M. France, and B.D. Knodel, *Impact of advanced fluids on costs of district cooling systems*. 1992, Argonne National Lab., IL (United States).
17. Choi, S.U., Y.I. Cho, and K.E. Kasza, *Degradation effects of dilute polymer solutions on turbulent friction and heat transfer behavior.* Journal of non-newtonian fluid mechanics, 1992. **41**(3): p. 289-307.
18. Ali, N., et al., *Carbon-Based Nanofluids and Their Advances towards Heat Transfer Applications—A Review.* Nanomaterials, 2021. **11**(6): p. 1628.
19. Masuda, H., A. Ebata, and K. Teramae, *Alteration of thermal conductivity and viscosity of liquid by dispersing ultra-fine particles. Dispersion of Al2O3, SiO2 and TiO2 ultra-fine particles.* Thermophysical characteristics, 1993. **7**(4): p. 227–233.

20. Choi, S.U. and J.A. Eastman, *Enhancing thermal conductivity of fluids with nanoparticles*. 1995, Argonne National Lab., IL (United States).
21. Giwa, S., et al., *Influence of nanoparticles size, per cent mass ratio, and temperature on the thermal properties of water-based MgO–ZnO nanofluid: an experimental approach.* Journal of Thermal Analysis and Calorimetry, 2021. **143**(2): p. 1063-1079.
22. Gupta, M., et al., *Experimental analysis of heat transfer behavior of silver, MWCNT and hybrid (silver+ MWCNT) nanofluids in a laminar tubular flow*. Journal of Thermal Analysis and Calorimetry, 2020: p. 1-15.
23. Ramadhan, A., et al. *Investigation on stability of tri-hybrid nanofluids in water-ethylene glycol mixture*. in *IOP Conference Series: Materials Science and Engineering*. 2019. IOP Publishing.
24. Mousavi, S., F. Esmaeilzadeh, and X. Wang, *Effects of temperature and particles volume concentration on the thermophysical properties and the rheological behavior of CuO/MgO/TiO 2 aqueous ternary hybrid nanofluid.* Journal of Thermal Analysis and Calorimetry, 2019. **137**(3): p. 879-901.
25. Ghodsinezhad, H., M. Sharifpur, and J.P. Meyer, *Experimental investigation on cavity flow natural convection of Al2O3–water nanofluids.* International Communications in Heat and Mass Transfer, 2016. **76**: p. 316-324.
26. Aghakhani, S., et al., *Natural convective heat transfer and entropy generation of alumina/water nanofluid in a tilted enclosure with an elliptic constant temperature: Applying magnetic field and radiation effects.* International Journal of Mechanical Sciences, 2020. **174**: p. 105470.
27. Garbadeen, I., et al., *Experimental study on natural convection of MWCNT-water nanofluids in a square enclosure.* International Communications in Heat and Mass Transfer, 2017. **88**: p. 1-8.
28. Giwa, S., M. Sharifpur, and J. Meyer, *Experimental investigation into heat transfer performance of water-based magnetic hybrid nanofluids in a rectangular cavity exposed to magnetic excitation.* International Communications in Heat and Mass Transfer, 2020. **116**: p. 104698.
29. Giwa, S., M. Sharifpur, and J. Meyer, *Effects of uniform magnetic induction on heat transfer performance of aqueous hybrid ferrofluid in a rectangular cavity.* Applied Thermal Engineering, 2020. **170**: p. 115004.
30. Murshed, S., et al., *Experimental Research and Development on the Natural Convection of Suspensions of Nanoparticles—A Comprehensive Review.* Nanomaterials, 2020. **10**(9): p. 1855.
31. Giwa, S.O., et al., *Experimental Investigation on Stability, Viscosity, and Electrical Conductivity of Water-Based Hybrid Nanofluid of MWCNT-Fe2O3.* Nanomaterials, 2021. **11**(1): p. 136.
32. Awua, J.T., et al., *Experimental investigations into viscosity, pH and electrical conductivity of nanofluid prepared from palm kernel fibre and a mixture of water and ethylene glycol.* Bulletin of Materials Science, 2018. **41**(6): p. 156.
33. Sathyamurthy, R., et al., *Experimental investigation on cooling the photovoltaic panel using hybrid nanofluids.* Applied Nanoscience, 2021. **11**(2): p. 363-374.
34. Jamei, M., et al., *On the specific heat capacity estimation of metal oxide-based nanofluid for energy perspective – A comprehensive assessment of data analysis techniques.* International Communications in Heat and Mass Transfer, 2021. **123**: p. 105217.
35. Jamei, M., et al., *On the Thermal Conductivity Assessment of Oil-Based Hybrid Nanofluids using Extended Kalman Filter integrated with feed-forward neural network.* International Journal of Heat and Mass Transfer, 2021. **172**: p. 121159.

36. Dezfulizadeh, A., et al., *An experimental study on dynamic viscosity and thermal conductivity of water-Cu-SiO2-MWCNT ternary hybrid nanofluid and the development of practical correlations.* Powder Technology, 2021.
37. Kashyap, S., J. Sarkar, and A. Kumar, *Performance enhancement of regenerative evaporative cooler by surface alterations and using ternary hybrid nanofluids.* Energy, 2021. **225**: p. 120199.
38. Zayan, M., et al., *Experimental Investigation on Rheological Properties of Water Based Novel Ternary Hybrid Nanofluids.* 2021.
39. Xuan, Z., et al., *Thermo-economic performance and sensitivity analysis of ternary hybrid nanofluids.* Journal of Molecular Liquids, 2021. **323**: p. 114889.
40. Li, X., H. Wang, and B. Luo, *The thermophysical properties and enhanced heat transfer performance of SiC-MWCNTs hybrid nanofluids for car radiator system.* Colloids and Surfaces A: Physicochemical and Engineering Aspects, 2021. **612**: p. 125968.
41. Vidhya, R., T. Balakrishnan, and B.S. Kumar, *Investigation on thermophysical properties and heat transfer performance of heat pipe charged with binary mixture based ZnO-MgO hybrid nanofluids.* Materials Today: Proceedings, 2021. **37**: p. 3423-3433.
42. Tlili, I., *Impact of thermal conductivity on the thermophysical properties and rheological behavior of nanofluid and hybrid nanofluid.* Mathematical Sciences, 2021: p. 1-9.
43. Jana, S., A. Salehi-Khojin, and W.-H. Zhong, *Enhancement of fluid thermal conductivity by the addition of single and hybrid nano-additives.* Thermochimica acta, 2007. **462**(1-2): p. 45-55.
44. Chopkar, M., et al., *Development and characterization of Al2Cu and Ag2Al nanoparticle dispersed water and ethylene glycol based nanofluid.* Materials Science and Engineering: B, 2007. **139**(2-3): p. 141-148.
45. Abbas, F., et al., *Towards convective heat transfer optimization in aluminum tube automotive radiators: Potential assessment of novel Fe2O3-TiO2/water hybrid nanofluid.* Journal of the Taiwan Institute of Chemical Engineers, 2021.
46. Adetunji, C.O., et al., *Nanofluids for Water Treatment.* Applied Water Science Volume 1: Fundamentals and Applications, 2021: p. 503-523.
47. Bargal, M.H., et al., *Experimental investigation of the thermal performance of a radiator using various nanofluids for automotive PEMFC applications.* International Journal of Energy Research, 2021. **45**(5): p. 6831-6849.
48. Bretado-de los Rios, M.S., C.I. Rivera-Solorio, and K. Nigam, *An overview of sustainability of heat exchangers and solar thermal applications with nanofluids: A review.* Renewable and Sustainable Energy Reviews, 2021. **142**: p. 110855.
49. Fogaça, M.B., et al., *Effectiveness of a shell and helically coiled tube heat exchanger operated with gold nanofluids at low concentration: A multi-level factorial analysis.* Journal of Thermal Science and Engineering Applications, 2021. **13**(2): p. 021029.
50. Kaur, B., S. Chand, and B. Saini, *Nanofluids: Current Applications and Future Challenges*, in *Nanotechnology*. 2021, Jenny Stanford Publishing. p. 461-495.
51. Sanches, M., et al., *Nanofluids Characterization for Spray Cooling Applications.* Symmetry, 2021. **13**(5): p. 788.
52. Murshed, S.M.S., et al. *Trend of experimental natural convection of nanofluids*. in *14th International Conference on Heat Transfer, Fluid Mechanics and Thermodynamics (HEFAT 2019)*. 2019. Wicklow, Ireland: HEFAT.

53. Babar, H. and H.M. Ali, *Towards hybrid nanofluids: Preparation, thermophysical properties, applications, and challenges.* Journal of Molecular Liquids, 2019. **281**: p. 598-633.
54. Khalid, S.U., et al., *Heat pipes: progress in thermal performance enhancement for microelectronics.* Journal of Thermal Analysis and Calorimetry, 2021. **143**: p. 2227-2243.
55. Shah, T.R., H. Babar, and H.M. Ali, *Energy harvesting: role of hybrid nanofluids*, in *Emerging Nanotechnologies for Renewable Energy*. 2021, Elsevier. p. 173-211.
56. Heyhat, M., M. Abbasi, and A. Rajabpour, *Molecular dynamic simulation on the density of titanium dioxide and silver water-based nanofluids using ternary mixture model.* Journal of Molecular Liquids, 2021. **333**: p. 115966.
57. Kumar, V. and R.R. Sahoo, *Experimental And Numerical Study On Cooling System Waste Heat Recovery For Engine Air Preheating By Ternary Hybrid Nanofluid.* Journal of Enhanced Heat Transfer, 2021. **28**(4).
58. Giwa, S.O., M. Sharifpur, and J.P. Meyer, *Experimental study of thermo-convection performance of hybrid nanofluids of Al2O3-MWCNT/water in a differentially heated square cavity.* International Journal of Heat and Mass Transfer, 2020. **148**: p. 119072.
59. Mousavi, S.M., F. Esmaeilzadeh, and X.P. Wang, *Effects of temperature and particles volume concentration on the thermophysical properties and the rheological behavior of CuO/MgO/TiO2 aqueous ternary hybrid nanofluid.* Journal of Thermal Analysis and Calorimetry, 2019. **137**(3): p. 879-901.
60. Alklaibi, A., L.S. Sundar, and A. Sousa, *Experimental analysis of exergy efficiency and entropy generation of diamond/water nanofluids flow in a thermosyphon flat plate solar collector.* International Communications in Heat and Mass Transfer, 2021. **120**: p. 105057.
61. Alnaqi, A.A., et al., *Thermal-hydraulic analysis and irreversibility of the MWCNTs-SiO2/EG-H2O non-Newtonian hybrid nanofluids inside a zigzag micro-channels heat sink.* International Communications in Heat and Mass Transfer, 2021. **122**: p. 105158.
62. Alotaibi, S., et al., *Modeling thermal conductivity of ethylene glycol-based nanofluids using multivariate adaptive regression splines and group method of data handling artificial neural network.* Engineering Applications of Computational Fluid Mechanics, 2020. **14**(1): p. 379-390.
63. Al-Yasiri, Q., M. Szabó, and M. Arıcı, *Single and hybrid nanofluids to enhance performance of flat plate solar collectors: application and obstacles.* Periodica Polytechnica Mechanical Engineering, 2021. **65**(1): p. 86-102.
64. Parashar, N., et al., *An artificial neural network approach for the prediction of dynamic viscosity of MXene-palm oil nanofluid using experimental data.* Journal of Thermal Analysis and Calorimetry, 2020.
65. Hemmat Esfe, M., et al., *Designing an artificial neural network to predict thermal conductivity and dynamic viscosity of ferromagnetic nanofluid.* International Communications in Heat and Mass Transfer, 2015. **68**: p. 50-57.
66. Adun, H., et al., *A neural network-based predictive model for the thermal conductivity of hybrid nanofluids.* International Communications in Heat and Mass Transfer, 2020. **119**: p. 104930.
67. Bahiraei, M., S. Nazari, and H. Safarzadeh, *Modeling of energy efficiency for a solar still fitted with thermoelectric modules by ANFIS and PSO-enhanced neural network: A nanofluid application.* Powder Technology, 2021. **385**: p. 185-198.
68. Garoosi, F., *Presenting two new empirical models for calculating the effective dynamic viscosity and thermal conductivity of nanofluids.* Powder Technology, 2020. **366**: p. 788-820.

69. Gonçalves, I., et al., *Thermal Conductivity of Nanofluids: A Review on Prediction Models, Controversies and Challenges.* Applied Sciences, 2021. **11**(6): p. 2525.
70. Yildiz, C., M. Arici, and H. Karabay, *Comparison of a theoretical and experimental thermal conductivity model on the heat transfer performance of Al2O3-SiO2/water hybrid-nanofluid.* International Journal of Heat and Mass Transfer, 2019: p. 598-605.
71. Nasr, M.S., et al., *Application of Artificial Intelligence to Predict Enhanced Oil Recovery Using Silica Nanofluids.* Natural Resources Research, 2021. **30**(3): p. 2529-2542.
72. Singh, D.V., et al., *Exergy approach in decision-based design of absorption refrigeration system using artificial intelligence and simulink.* Journal of Thermal Analysis and Calorimetry, 2021: p. 1-27.
73. Choi, S.U.S., *Nanofluids: From Vision to Reality Through Research.* Journal of Heat Transfer, 2009. **131**(3): p. 033106-033106-9.
74. Choi, S.U.S. and J.A. Eastman, *Enhancing thermal conductivity of fluids with nanoparticles*. 1995 ASME International Mechanical Engineering Congress and Exhibition, San Francisco, CA (United States), 12-17 Nov 1995; Other Information: PBD: Oct 1995. 1995: ; Argonne National Lab., IL (United States).
75. Abo-Elkhair, R., M. Bhatti, and K.S. Mekheimer, *Magnetic force effects on peristaltic transport of hybrid bio-nanofluid (AuCu nanoparticles) with moderate Reynolds number: An expanding horizon.* International Communications in Heat and Mass Transfer, 2021. **123**: p. 105228.
76. Marzougui, S., et al., *Entropy generation on magneto-convective flow of copper–water nanofluid in a cavity with chamfers.* Journal of Thermal Analysis and Calorimetry, 2021. **143**(3): p. 2203-2214.
77. Abu-Hamdeh, N.H., et al., *The thermal properties of water-copper nanofluid in the presence of surfactant molecules using molecular dynamics simulation.* Journal of Molecular Liquids, 2021. **325**: p. 115149.
78. Ali, H.M., *Experimental study on the thermal behavior of RT-35HC paraffin within copper and Iron-Nickel open cell foams: Energy storage for thermal management of electronics.* International Journal of Heat and Mass Transfer, 2020. **146**: p. 118852.
79. Cárdenas Contreras, E.M., G.A. Oliveira, and E.P. Bandarra Filho, *Experimental analysis of the thermohydraulic performance of graphene and silver nanofluids in automotive cooling systems.* International Journal of Heat and Mass Transfer, 2019. **132**: p. 375-387.
80. Mashayekhi, R., et al., *Application of a novel conical strip insert to improve the efficacy of water–Ag nanofluid for utilization in thermal systems: a two-phase simulation.* Energy Conversion and Management, 2017. **151**: p. 573-586.
81. Saadati, H., K. Hadad, and A. Rabiee, *Safety margin and fuel cycle period enhancements of VVER-1000 nuclear reactor using water/silver nanofluid.* Nuclear Engineering and Technology, 2018. **50**(5): p. 639-647.
82. Toghraie, D., et al., *Designing an Artificial Neural Network (ANN) to predict the viscosity of Silver/Ethylene glycol nanofluid at different temperatures and volume fraction of nanoparticles.* Physica A: Statistical Mechanics and its Applications, 2019. **534**: p. 122142.
83. Huminic, G., et al., *Experimental study on viscosity of water based Fe–Si hybrid nanofluids.* Journal of Molecular Liquids, 2021. **321**: p. 114938.
84. Zaaroura, I., et al., *Thermal performance of self-rewetting gold nanofluids: Application to two-phase heat transfer devices.* International Journal of Heat and Mass Transfer, 2021. **174**: p. 121322.

85. Hafeez, M., et al., *Numerical simulation for electrical conducting rotating flow of Au (Gold)-Zn (Zinc)/EG (Ethylene glycol) hybrid nanofluid.* International Communications in Heat and Mass Transfer, 2021. **124**: p. 105234.
86. Bhatti, M.M., *Biologically inspired intra-uterine nanofluid flow under the suspension of magnetized gold (Au) nanoparticles: applications in nanomedicine.* Inventions, 2021. **6**(2): p. 28.
87. Khan, M.I., et al., *Modeling and simulation of micro-rotation and spin gradient viscosity for ferromagnetic hybrid (Manganese Zinc Ferrite, Nickle Zinc Ferrite) nanofluids.* Mathematics and Computers in Simulation, 2021. **185**: p. 497-509.
88. Saleh, B. and L.S. Sundar, *Experimental study on heat transfer, friction factor, entropy and exergy efficiency analyses of a corrugated plate heat exchanger using Ni/water nanofluids.* International Journal of Thermal Sciences, 2021. **165**: p. 106935.
89. Qi, S., X. Li, and H. Dong, *Reduced friction and wear of electro-brush plated nickel composite coatings reinforced by graphene oxide.* Wear, 2019. **426-427**: p. 228-238.
90. Sundar, L.S., M.K. Singh, and A.C. Sousa, *Turbulent heat transfer and friction factor of nanodiamond-nickel hybrid nanofluids flow in a tube: an experimental study.* International Journal of Heat and Mass Transfer, 2018. **117**: p. 223-234.
91. Sundar, L.S., M.K. Singh, and A.C. Sousa, *Heat transfer and friction factor of nanodiamond-nickel hybrid nanofluids flow in a tube with longitudinal strip inserts.* International Journal of Heat and Mass Transfer, 2018. **121**: p. 390-401.
92. Plant, R.D. and M.Z. Saghir, *Numerical and experimental investigation of high concentration aqueous alumina nanofluids in a two and three channel heat exchanger.* International Journal of Thermofluids, 2021. **9**: p. 100055.
93. Miroshnichenko, I.V., et al., *Natural convection of alumina-water nanofluid in an open cavity having multiple porous layers.* International Journal of Heat and Mass Transfer, 2018. **125**: p. 648-657.
94. Pordanjani, A.H., et al., *Effect of alumina nano-powder on the convection and the entropy generation of water inside an inclined square cavity subjected to a magnetic field: uniform and non-uniform temperature boundary conditions.* International Journal of Mechanical Sciences, 2019. **152**: p. 99-117.
95. Yahya, S.I., A. Rezaei, and B. Aghel, *Forecasting of water thermal conductivity enhancement by adding nano-sized alumina particles.* Journal of Thermal Analysis and Calorimetry, 2021: p. 1-10.
96. Giwa, S.O., et al., *Influence of base fluid, temperature, and concentration on the thermophysical properties of hybrid nanofluids of alumina–ferrofluid: experimental data, modeling through enhanced ANN, ANFIS, and curve fitting.* Journal of Thermal Analysis and Calorimetry, 2020.
97. Li, X., et al., *Experimental study on the thermo-physical properties of diathermic oil based SiC nanofluids for high temperature applications.* International Journal of Heat and Mass Transfer, 2016. **97**: p. 631-637.
98. Akilu, S., et al., *Thermophysical profile of SiCCuO/C nanocomposite in base liquid ethylene glycol.* Powder Technology, 2019. **354**: p. 540-551.
99. Arafat, M.Y. and S. Chakraborty. *An Analytical Study to Compare the Heat Transfer Performances of Water-Based TiO2, SiO2, TiC and SiC Nanofluids*. in *Defect and Diffusion Forum*. 2021. Trans Tech Publ.
100. Bai, M., et al., *In-situ Ti-6Al-4V/TiC composites synthesized by reactive spark plasma sintering: processing, microstructure, and dry sliding wear behaviour.* Wear, 2019. **432-433**: p. 202944.

101. Abhilash, P., U. Raghupati, and R.N. Kumar, *Design and CFD analysis of hair pin heat exchanger using aluminium and titanium carbide nanofluids.* Materials Today: Proceedings, 2021. **39**: p. 764-770.
102. Cadena-de la Peña, N.L., et al., *Experimental analysis of natural convection in vertical annuli filled with AlN and TiO2/mineral oil-based nanofluids.* International Journal of Thermal Sciences, 2017. **111**: p. 138-145.
103. Żyła, G. and J. Fal, *Experimental studies on viscosity, thermal and electrical conductivity of aluminum nitride–ethylene glycol (AlN–EG) nanofluids.* Thermochimica Acta, 2016. **637**: p. 11-16.
104. Traciak, J., J. Fal, and G. Zyła, *3D printed measuring device for the determination the surface tension of nanofluids.* Applied Surface Science, 2021: p. 149878.
105. Yadav, D., et al., *Density variation in nanofluids as a function of concentration and temperature.* Materials Today: Proceedings, 2021.
106. Krishnam, M., S. Bose, and C. Das, *Boron nitride (BN) nanofluids as cooling agent in thermal management system (TMS).* Applied Thermal Engineering, 2016. **106**: p. 951-958.
107. Żyła, G., et al., *Huge thermal conductivity enhancement in boron nitride – ethylene glycol nanofluids.* Materials Chemistry and Physics, 2016. **180**: p. 250-255.
108. Shit, S.P., et al., *Thermophysical properties of graphene and hexagonal boron nitride nanofluids: A comparative study by molecular dynamics.* Journal of Molecular Structure, 2021. **1239**: p. 130525.
109. Tao, Q., et al., *EXPERIMENTAL INVESTIGATION ON HEAT TRANSFER ENHANCEMENT OF A RADIATOR IN A SIMULATED PEMFC COOLING SYSTEM USING HEXAGONAL BORON NITRIDE NANOFLUIDS.* Heat Transfer Research, 2021. **52**(8).
110. Erkan, A., et al., *Comparison of effects of nanofluid utilization (Al2O3, SiO2, TiO2) with reference water in automotive radiators on exergetic properties of diesel engines.* SN Applied Sciences, 2021. **3**(3): p. 365.
111. Choi, T.J., et al., *Experimental Study on the Effect of Nanoparticle Migration on the Convective Heat Transfer Coefficient of EG/Water-based Al2O3 Nanofluids.* International Journal of Heat and Mass Transfer, 2021. **169**: p. 120903.
112. Sawicka, D., et al., *Numerical simulation of natural convection of Glycol-Al2O3 nanofluids from a horizontal cylinder.* Heat Transfer Engineering, 2021. **42**(3-4): p. 328-336.
113. Haider, F., T. Hayat, and A. Alsaedi, *Flow of hybrid nanofluid through Darcy-Forchheimer porous space with variable characteristics.* Alexandria Engineering Journal, 2021. **60**(3): p. 3047-3056.
114. Kamel, M.S., O. Al-Oran, and F. Lezsovits, *Thermal conductivity of Al2O3 and CeO2 nanoparticles and their hybrid based water nanofluids: An experimental study.* Periodica Polytechnica Chemical Engineering, 2021. **65**(1): p. 50-60.
115. Sandhu, H., et al. *Experimentally observed thermal conductivities for Al2O3, CNT, and CuO nanoparticles with water-EG based fluids*. in *AIP Conference Proceedings*. 2021. AIP Publishing LLC.
116. Ali, V., et al., *Navigating the effect of tungsten oxide nano-powder on ethylene glycol surface tension by artificial neural network and response surface methodology*. Powder Technology, 2021. **386**: p. 483-490.
117. Al-Oran, O. and F. Lezsovits, *A Hybrid Nanofluid of Alumina and Tungsten Oxide for Performance Enhancement of a Parabolic Trough Collector under the Weather Conditions of Budapest.* Applied Sciences, 2021. **11**(11): p. 4946.

118. Tiwari, A.K., et al., *Experimental and numerical investigation on the thermal performance of triple tube heat exchanger equipped with different inserts with WO3/water nanofluid under turbulent condition.* International Journal of Thermal Sciences, 2021. **164**: p. 106861.
119. Zhu, Y., et al., *A comprehensive experimental investigation of dynamic viscosity of MWCNT-WO3/water-ethylene glycol antifreeze hybrid nanofluid.* Journal of Molecular Liquids, 2021. **333**: p. 115986.
120. Aghanajafi, A., D. Toghraie, and B. Mehmandoust, *Numerical simulation of laminar forced convection of water-CuO nanofluid inside a triangular duct.* Physica E-Low-Dimensional Systems & Nanostructures, 2017. **85**: p. 103-108.
121. Reddy, N.R., P. Abhilash, and M. Rahul, *Enhancement of heat transfer in radiator using copper oxide nano fluids.* Materials Today: Proceedings, 2021. **39**: p. 643-648.
122. Rostami, S., et al., *Modeling the thermal conductivity ratio of an antifreeze-based hybrid nanofluid containing graphene oxide and copper oxide for using in thermal systems.* Journal of Materials Research and Technology, 2021. **11**: p. 2294-2304.
123. Rostami, S., et al., *Measurement of the thermal conductivity of MWCNT-CuO/water hybrid nanofluid using artificial neural networks (ANNs).* Journal of Thermal Analysis and Calorimetry, 2020: p. 1-9.
124. Ledari, B.H., M. Sabzpooshani, and M. Khayat, *An experimental investigation on the thermo-hydraulic properties of CuO and Fe3O4 oil-based nanofluids in inclined U-tubes: A comparative study.* Powder Technology, 2021. **379**: p. 191-202.
125. Stalin, P.M.J., et al., *Investigations on thermal properties of CeO2/water nanofluids for heat transfer applications.* Materials Today: Proceedings, 2021.
126. Pan, S., et al., *Discussion on the combustion, performance and emissions of a dual fuel diesel engine fuelled with methanol-based CeO2 nanofluids.* Fuel, 2021. **302**: p. 121096.
127. Maniglia, R., K.J. Reed, and J. Texter, *Reactive CeO2 nanofluids for UV protective films.* Journal of colloid and interface science, 2017. **506**: p. 346-354.
128. Rostami, S., et al., *Improving the thermal conductivity of ethylene glycol by addition of hybrid nano-materials containing multi-walled carbon nanotubes and titanium dioxide: applicable for cooling and heating.* Journal of Thermal Analysis and Calorimetry, 2021. **143**(2): p. 1701-1712.
129. Indumathi, N., et al., *Marangoni Convection of Titanium Dioxide/Ethylene Glycol Dusty Nanoliquid MHD Flow Past a Flat Plate*, in *Advances in Fluid Dynamics*. 2021, Springer. p. 243-253.
130. Pourpasha, H., S.Z. Heris, and Y. Mohammadfam, *Comparison between multi-walled carbon nanotubes and titanium dioxide nanoparticles as additives on performance of turbine meter oil nano lubricant.* Scientific Reports, 2021. **11**(1): p. 1-19.
131. Zubair, M.M., et al., *Experimental study on heat transfer of an engine radiator with T i O 2/EG-water nano-coolant.* SN Applied Sciences, 2021. **3**(4): p. 1-9.
132. Giwa, S.O., M. Sharifpur, and J.P. Meyer, *Effects of uniform magnetic induction on heat transfer performance of aqueous hybrid ferrofluid in a rectangular cavity.* Applied Thermal Engineering, 2020. **170**: p. 115004.
133. Talebi, M., et al., *Experimental study of the effect of position and intensity of a constant magnetic field on the forced convection heat transfer of Fe2O3/water nanofluid in the developing thermal region.* Journal of Solid and Fluid Mechanics, 2021. **11**(1): p. 43-58.
134. Saleh, B. and L.S. Sundar, *Entropy generation and exergy efficiency analysis of ethylene glycol-water based nanodiamond+ Fe3O4 hybrid nanofluids in a circular tube.* Powder Technology, 2021. **380**: p. 430-442.

135. Saleh, B. and L.S. Sundar, *Thermal Efficiency, Heat Transfer, and Friction Factor Analyses of MWCNT+ Fe3O4/Water Hybrid Nanofluids in a Solar Flat Plate Collector under Thermosyphon Condition.* Processes, 2021. **9**(1): p. 180.
136. Peng, Y., et al., *Analysis of the effect of roughness and concentration of Fe3O4/water nanofluid on the boiling heat transfer using the artificial neural network: An experimental and numerical study.* International Journal of Thermal Sciences, 2021. **163**: p. 106863.
137. Guo, Y., et al., *Tribological behaviors of novel epoxy nanocomposites filled with solvent-free ionic SiO2 nanofluids.* Composites Part B: Engineering, 2021. **215**: p. 108751.
138. Fikri, M., et al. *Investigation on stability of TiO2-SiO2 nanofluids with ratio (70: 30) in W/EG mixture (60: 40)*. in *IOP Conference Series: Materials Science and Engineering*. 2021. IOP Publishing.
139. Nwidee, L.N., et al., *Nanofluids for Enhanced Oil Recovery Processes: Wettability Alteration Using Zirconium Oxide*, in *Offshore Technology Conference Asia*. 2016, Offshore Technology Conference: Kuala Lumpur, Malaysia. p. 7.
140. Çolak, A.B., *Experimental study for thermal conductivity of water-based zirconium oxide nanofluid: Developing optimal artificial neural network and proposing new correlation.* International Journal of Energy Research, 2021. **45**(2): p. 2912-2930.
141. Sun, C., et al., *Producing ZrO2/LP107160 NF and presenting a correlation for prediction of thermal conductivity via GMDH method: An empirical and numerical investigation.* Physica E: Low-dimensional Systems and Nanostructures, 2021. **127**: p. 114511.
142. Elcioglu, E.B. and S.S. Murshed, *Ultrasonically tuned surface tension and nano-film formation of aqueous ZnO nanofluids.* Ultrasonics Sonochemistry, 2021. **72**: p. 105424.
143. Çiftçi, E., *Distilled Water-Based AlN+ ZnO Binary Hybrid Nanofluid Utilization in a Heat Pipe and Investigation of Its Effects on Performance.* International Journal of Thermophysics, 2021. **42**(3): p. 1-21.
144. Ahmed, W., et al., *Experimental investigation of convective heat transfer growth on ZnO@ TiO 2/DW binary composites/hybrid nanofluids in a circular heat exchanger.* Journal of Thermal Analysis and Calorimetry, 2021. **143**(2): p. 879-898.
145. Hemmat Esfe, M., A. Alirezaie, and M. Rejvani, *An applicable study on the thermal conductivity of SWCNT-MgO hybrid nanofluid and price-performance analysis for energy management.* Applied Thermal Engineering, 2017. **111**: p. 1202-1210.
146. Esfe, M.H. and S. Esfandeh, *Comparative thermal analysis of an EG-based nanofluid containing DWCNTs.* The European Physical Journal Plus, 2021. **136**(4): p. 1-16.
147. Faisal Javed, M., et al., *Optimization of SWCNTs and MWCNTs (single and multi-wall carbon nanotubes) in peristaltic transport with thermal radiation in a non-uniform channel.* Journal of Molecular Liquids, 2019. **273**: p. 383-391.
148. Esfe, M.H. and M.H. Kamyab, *Optimization of Viscosity in MWCNT-MgO (35–65%)/5W50 Nanofluid and Comparison of Experimental Results with the Designed ANN.* Arabian Journal for Science and Engineering, 2021. **46**(1): p. 827-840.
149. Said, Z., et al., *Thermophysical properties using ND/water nanofluids: An experimental study, ANFIS-based model and optimization.* Journal of Molecular Liquids, 2021. **330**: p. 115659.
150. Yi, H., Y. Zhao, and S. Song, *Development of superior stable two-dimensional montmorillonite nanosheet based working nanofluids for direct solar energy harvesting and utilization.* Applied Clay Science, 2021. **200**: p. 105886.

151. Ba, T.L., et al., *Comparative Study of Carbon Nanosphere and Carbon Nanopowder on Viscosity and Thermal Conductivity of Nanofluids.* Nanomaterials, 2021. **11**(3): p. 608.
152. Yashawantha, K.M., G. Gurjar, and A.V. Vinod, *Stability and Thermal Conductivity of Ethylene Glycol and Water Nanofluid Containing Graphite Nanoparticles*, in *Innovations in Sustainable Energy and Technology*. 2021, Springer. p. 231-242.
153. Jeong, M.G., et al., *Synthesis of therminol-graphite nanofluids and photo-thermal conversion properties.* International Journal of Energy Research, 2021.
154. Giwa, S., et al., *Influence of nanoparticles size, per cent mass ratio, and temperature on the thermal properties of water-based MgO–ZnO nanofluid: an experimental approach.* Journal of Thermal Analysis and Calorimetry, 2020: p. 1-17.
155. Sharifpur, M., S. Yousefi, and J.P. Meyer, *A new model for density of nanofluids including nanolayer.* International Communications in Heat and Mass Transfer, 2016. **78**: p. 168-174.
156. Du, C., et al., *Thermal conductivity enhancement of nanofluid by adding multiwalled carbon nanotubes: Characterization and numerical modeling patterns.* Mathematical Methods in the Applied Sciences, 2020: p. 1-22.
157. Mehrabi, M., M. Sharifpur, and J.P. Meyer, *Electrical conductivity and pH modelling of magnesium oxide–ethylene glycol nanofluids.* Bulletin of Materials Science, 2019. **42**(3): p. 108.
158. Sharifpur, M., et al., *Thermal conductivity and viscosity of Mango bark/water nanofluids.* 2017.
159. Wole-Osho, I., et al., *An experimental investigation into the effect of particle mixture ratio on specific heat capacity and dynamic viscosity of Al2O3-ZnO hybrid nanofluids.* Powder Technology, 2020. **363**: p. 699-716.
160. Almanassra, I.W., et al., *Stability and thermophysical properties test of carbide-derived carbon thermal fluid; a comparison between functionalized and emulsified suspensions.* Powder Technology, 2021. **377**: p. 415-428.
161. Afzal, Q., et al., *Thermal and concentration convection in nanofluids for peristaltic flow of magneto couple stress fluid in a nonuniform channel.* Journal of Thermal Analysis and Calorimetry, 2021: p. 1-16.
162. Akram, N., et al., *Experimental investigations of the performance of a flat-plate solar collector using carbon and metal oxides based nanofluids.* Energy, 2021: p. 120452.
163. Alwawi, F.A., et al., *Heat Transmission Reinforcers Induced by MHD Hybrid Nanoparticles for Water/Water-EG Flowing over a Cylinder.* Coatings, 2021. **11**(6): p. 623.
164. Gündem, A., M. Hoşöz, and E. Keklik, *Performance Comparison of Propylene Glycol-Water and Ethylene Glycol-Water Mixtures as Engine Coolants in a Flat-Tube Automobile Radiator.* International Journal of Automotive Science And Technology, 2021. **5**(2): p. 147-156.
165. Pérez-Tavernier, J., et al., *Heat transfer performance of a nano-enhanced propylene glycol: water mixture.* International Journal of Thermal Sciences, 2019. **139**: p. 413-423.
166. Gu, X., et al., *Investigation on the heat transfer characteristics of propylene glycol–water mixture in the shell side of a spiral-wound heat exchanger.* Heat Transfer, 2021. **50**(1): p. 893-906.
167. Sundar, L.S., et al., *Second Law of Thermodynamic Analysis of 40: 60% Propylene Glycol and Water Mixture Based Nanodiamond Nanofluid under Transition Flow.* Diamond and Related Materials, 2021: p. 108480.

168. Markal, B. and R. Varol, *Investigation of the effects of miscible and immiscible binary fluids on thermal performance of pulsating heat pipes.* Heat and Mass Transfer, 2021: p. 1-16.
169. Battisti, R., et al., *Energy efficiency comparison between a conventional tray column and a novel heat-intensified thermosyphon-assisted falling film distillation unit: an assessment for mixtures with different relative volatilities.* Chemical Engineering Communications, 2021: p. 1-12.
170. Zhao, X., et al., *Optimal design and control of an energy-efficient triple-side-stream quaternary extractive distillation process.* Chemical Engineering and Processing-Process Intensification, 2021: p. 108510.
171. Tiwari, A.K., et al., *4S consideration (synthesis, sonication, surfactant, stability) for the thermal conductivity of CeO2 with MWCNT and water based hybrid nanofluid: An experimental assessment.* Colloids and Surfaces A: Physicochemical and Engineering Aspects, 2021. **610**: p. 125918.
172. Giwa, S., et al., *Experimental measurement of viscosity and electrical conductivity of water-based γ-Al 2 O 3/MWCNT hybrid nanofluids with various particle mass ratios.* Journal of Thermal Analysis and Calorimetry, 2020: p. 1-14.
173. Sharifpur, M., et al., *Experimental Investigation into Natural Convection of Zinc Oxide/Water Nanofluids in a Square Cavity.* Heat Transfer Engineering, 2020: p. 1-13.
174. Yang, X., et al., *Applying Artificial Neural Networks (ANNs) for prediction of the thermal characteristics of water/ethylene glycol-based mono, binary and ternary nanofluids containing MWCNTs, titania, and zinc oxide.* Powder Technology, 2021.
175. Chen, L., W. Yu, and H. Xie, *Enhanced thermal conductivity of nanofluids containing Ag/MWNT composites.* Powder technology, 2012. **231**: p. 18-20.
176. Sajid, M.U. and H.M. Ali, *Thermal conductivity of hybrid nanofluids: A critical review.* International Journal of Heat and Mass Transfer, 2018. **126**: p. 211-234.
177. Eastman, J.A., et al., *Anomalously increased effective thermal conductivities of ethylene glycol-based nanofluids containing copper nanoparticles.* Applied physics letters, 2001. **78**(6): p. 718-720.
178. Asadi, A., et al., *Heat transfer efficiency of Al2O3-MWCNT/thermal oil hybrid nanofluid as a cooling fluid in thermal and energy management applications: An experimental and theoretical investigation.* International Journal of Heat and Mass Transfer, 2018. **117**: p. 474-486.
179. Wole-Osho, I., et al., *An intelligent approach to predicting the effect of nanoparticle mixture ratio, concentration and temperature on thermal conductivity of hybrid nanofluids.* Journal of Thermal Analysis and Calorimetry, 2021: p. 1-18.
180. Gupta, M., D. Singh, and S.P. Singh, *Ultrasonic and Thermophysical Studies of Ethylene Glycol Nanofluids Containing Titania Nanoparticles and Their Heat Transfer Enhancements.* 2021.
181. Pare, A. and S.K. Ghosh, *A unique thermal conductivity model (ANN) for nanofluid based on experimental study.* Powder Technology, 2021. **377**: p. 429-438.
182. Carrillo-Berdugo, I., et al., *Interfacial molecular layering enhances specific heat of nanofluids: evidence from molecular dynamics.* Journal of Molecular Liquids, 2021. **325**: p. 115217.
183. Vicki, W., M. Abdullah, and P. Gunnasegaran. *Effect of volume concentration and nanofluid temperature on the thermal conductivity of mono and hybrid Al2O3-TiO2 nanofluid*. in *AIP Conference Proceedings*. 2021. AIP Publishing LLC.
184. Pare, A. and S.K. Ghosh, *Surface qualitative analysis and ANN modelling for pool boiling heat transfer using Al2O3-water based nanofluids.* Colloids and Surfaces A: Physicochemical and Engineering Aspects, 2021. **610**: p. 125926.

185. Rizvi, S.M.M., B. El Far, and D. Shin, *Heat capacity and viscosity of ternary carbonate nanofluids.* International Journal of Energy Research, 2021. **45**(4): p. 6350-6359.
186. Sundar, L.S., et al., *Heat Transfer and Second Law Analysis of Ethylene Glycol-Based Ternary Hybrid Nanofluid Under Laminar Flow.* Journal of Thermal Science and Engineering Applications, 2021. **13**(5): p. 051021.
187. Zayan, M., et al., *Synthesis and Characterization of Novel Ternary Hybrid Nanoparticles as Thermal Additives in H2O.* 2021.
188. Dezfulizadeh, A., et al., *An experimental study on dynamic viscosity and thermal conductivity of water-Cu-SiO2-MWCNT ternary hybrid nanofluid and the development of practical correlations.* Powder Technology, 2021. **389**: p. 215-234.
189. Ahmed, W., et al., *Heat transfer growth of sonochemically synthesized novel mixed metal oxide ZnO+ Al2O3+ TiO2/DW based ternary hybrid nanofluids in a square flow conduit.* Renewable and Sustainable Energy Reviews, 2021. **145**: p. 111025.
190. Jeong, S. and B. Jo, *Understanding mechanism of enhanced specific heat of single molten salt-based nanofluids: Comparison with acid-modified salt.* Journal of Molecular Liquids, 2021: p. 116561.
191. Sayed, E.T., et al., *Augmenting Performance of Fuel Cells Using Nanofluids.* Thermal Science and Engineering Progress, 2021: p. 101012.
192. Rubbi, F., et al., *A comprehensive review on advances of oil-based nanofluids for concentrating solar thermal collector application.* Journal of Molecular Liquids, 2021: p. 116771.
193. Rubbi, F., et al., *State-of-the-art review on water-based nanofluids for low temperature solar thermal collector application.* Solar Energy Materials and Solar Cells, 2021. **230**: p. 111220.
194. Cuce, E., et al., *On the Use of Nanofluids in Solar Energy Applications.* Journal of Thermal Science, 2020.
195. Said, Z., et al., *Recent advances on the fundamental physical phenomena behind stability, dynamic motion, thermophysical properties, heat transport, applications, and challenges of nanofluids.* Physics Reports, 2021.
196. Wang, H., et al., *The MXene/water nanofluids with high stability and photo-thermal conversion for direct absorption solar collectors: A comparative study.* Energy, 2021. **227**: p. 120483.
197. Mukherjee, S., et al., *Experimental investigation on thermo-physical properties and subcooled flow boiling performance of Al2O3/water nanofluids in a horizontal tube.* International Journal of Thermal Sciences, 2021. **159**: p. 106581.
198. Ebrahimi, S. and S.F. Saghravani, *Experimental study of the thermal conductivity features of the water based Fe 3 O 4/CuO nanofluid.* Heat and Mass Transfer, 2018. **54**(4): p. 999-1008.
199. Morsi, R.E. and R.A. El-Salamony, *Effect of cationic, anionic and non-ionic polymeric surfactants on the stability, photo-catalytic and antimicrobial activities of yttrium oxide nanofluids.* Journal of Molecular Liquids, 2020. **297**: p. 111848.
200. Kumar, R.S., T.A.-A. Ganat, and T. Sharma, *Performance evaluation of silica nanofluid for sand column transport with simultaneous wettability alteration: An approach to environmental issue.* Journal of Cleaner Production, 2021. **303**: p. 127047.
201. Jha, N.K., et al., *Interaction of low salinity surfactant nanofluids with carbonate surfaces and molecular level dynamics at fluid-fluid interface at ScCO2 loading.* Journal of Colloid and Interface Science, 2021. **586**: p. 315-325.
202. Abd Aziz, R. and W.S. Yin, *Stability studies of hybrid TiO2 based nanofluids.* Journal of Modern Manufacturing Systems and Technology, 2021. **5**(1): p. 37-45.

203. Sundar, L.S., *Energy, economic, environmental and heat transfer analysis of a flat plate solar collector with pH treated Fe3O4/water nanofluid.* International Journal of Energy for a Clean Environment, 2021.

204. Urmi, W.T., et al., *An overview on synthesis, stability, opportunities and challenges of nanofluids.* Materials Today: Proceedings, 2021.

205. Adio, S.A., M. Sharifpur, and J.P. Meyer, *Influence of ultrasonication energy on the dispersion consistency of Al2O3–glycerol nanofluid based on viscosity data, and model development for the required ultrasonication energy density.* Journal of experimental nanoscience, 2016. **11**(8): p. 630-649.

206. Ma, M., et al., *Effect of surfactant on the rheological behavior and thermophysical properties of hybrid nanofluids.* Powder Technology, 2021. **379**: p. 373-383.

207. Sandhya, M., et al., *A systematic review on graphene-based nanofluids application in renewable energy systems: Preparation, characterization, and thermophysical properties.* Sustainable Energy Technologies and Assessments, 2021. **44**: p. 101058.

208. Manasrah, A.D., et al., *Surface modification of carbon nanotubes with copper oxide nanoparticles for heat transfer enhancement of nanofluids.* RSC advances, 2018. **8**(4): p. 1791-1802.

209. Choudhary, R., et al., *Stability analysis of Al2O3/water nanofluids.* Journal of Experimental Nanoscience, 2017. **12**(1): p. 140-151.

210. Chen, D., et al., *Experimental investigation of viscosity, enhanced thermal conductivity and zeta potential of a TiO2 electrolyte – based nanofluid.* International Communications in Heat and Mass Transfer, 2020. **118**: p. 104840.

211. Kanti, P., et al., *Experimental determination of thermophysical properties of Indonesian fly-ash nanofluid for heat transfer applications.* Particulate Science and Technology, 2021. **39**(5): p. 597-606.

212. Elias, M., et al., *Experimental investigation on the thermo-physical properties of Al2O3 nanoparticles suspended in car radiator coolant.* International Communications in Heat and Mass Transfer, 2014. **54**: p. 48-53.

213. Nikkam, N., et al., *Experimental investigation on thermo-physical properties of copper/diethylene glycol nanofluids fabricated via microwave-assisted route.* Applied Thermal Engineering, 2014. **65**(1-2): p. 158-165.

214. Senthilraja, S., K. Vijayakumar, and R. Gangadevi, *A comparative study on thermal conductivity of Al2O3/water, CuO/water and Al2O3–CuO/water nanofluids.* Digest Journal of Nanomaterials and Biostructures, 2015. **10**(4): p. 1449-1458.

215. Sundar, L.S., et al., *Experimental thermal conductivity of ethylene glycol and water mixture based low volume concentration of Al2O3 and CuO nanofluids.* International Communications in Heat and Mass Transfer, 2013. **41**: p. 41-46.

216. Amiri, M., S. Movahedirad, and F. Manteghi, *Thermal conductivity of water and ethylene glycol nanofluids containing new modified surface SiO2-Cu nanoparticles: Experimental and modeling.* Applied Thermal Engineering, 2016. **108**: p. 48-53.

217. Sundar, L.S., et al., *Thermal conductivity and viscosity of water based nanodiamond (ND) nanofluids: An experimental study.* International Communications in Heat and Mass Transfer, 2016. **76**: p. 245-255.

218. Kakati, H., A. Mandal, and S. Laik, *Promoting effect of Al2O3/ZnO-based nanofluids stabilized by SDS surfactant on CH4+ C2H6+ C3H8 hydrate formation.* Journal of industrial and engineering chemistry, 2016. **35**: p. 357-368.

219. Sundar, L.S., M.K. Singh, and A.C. Sousa, *Investigation of thermal conductivity and viscosity of Fe3O4 nanofluid for heat transfer applications.* International communications in heat and mass transfer, 2013. **44**: p. 7-14.

220. Dagdevir, T. and V. Ozceyhan, *Optimization of process parameters in terms of stabilization and thermal conductivity on water based TiO2 nanofluid preparation by using Taguchi method and Grey relation analysis.* International Communications in Heat and Mass Transfer, 2021. **120**: p. 105047.
221. Zulkafli, R.W. and V.V. Wanatasanappan. *Experimental investigation on the dispersion stability of Al2O3-CuO hybrid nanofluid using ultraviolet (UV)-visible spectroscopy and Zeta potential analyzer*. in *AIP Conference Proceedings*. 2021. AIP Publishing LLC.
222. Ouikhalfan, M., et al., *Stability and thermal conductivity enhancement of aqueous nanofluid based on surfactant-modified TiO2.* Journal of Dispersion Science and Technology, 2020. **41**(3): p. 374-382.
223. Giwa, S.O., et al., *Experimental investigation on stability, viscosity, and electrical conductivity of water-based hybrid nanofluid of MWCNT-Fe2O3.* Nanomaterials, 2021. **11**(1): p. 136.
224. Joubert, J., et al., *Enhancement in heat transfer of a ferrofluid in a differentially heated square cavity through the use of permanent magnets.* Journal of Magnetism and Magnetic Materials, 2017. **443**: p. 149-158.
225. Hamid, K.A., et al., *Experimental investigation of nanoparticle mixture ratios on TiO2–SiO2 nanofluids heat transfer performance under turbulent flow.* International Journal of Heat and Mass Transfer, 2018. **118**: p. 617-627.
226. Nabil, M.F., et al., *Experimental investigation of heat transfer and friction factor of TiO2-SiO2 nanofluids in water:ethylene glycol mixture.* International Journal of Heat and Mass Transfer, 2018. **124**: p. 1361-1369.
227. Aparna, Z., et al., *Thermal conductivity of aqueous Al2O3/Ag hybrid nanofluid at different temperatures and volume concentrations: an experimental investigation and development of new correlation function.* Powder Technology, 2019. **343**: p. 714-722.
228. Asokan, N., P. Gunnasegaran, and V. Vicki Wanatasanappan, *Experimental investigation on the thermal performance of compact heat exchanger and the rheological properties of low concentration mono and hybrid nanofluids containing Al2O3 and CuO nanoparticles.* Thermal Science and Engineering Progress, 2020. **20**: p. 100727.
229. Hamid, K.A., et al., *Improved thermal conductivity of TiO2–SiO2 hybrid nanofluid in ethylene glycol and water mixture.* IOP Conference Series: Materials Science and Engineering, 2017. **257**: p. 012067.
230. Kakavandi, A. and M. Akbari, *Experimental investigation of thermal conductivity of nanofluids containing of hybrid nanoparticles suspended in binary base fluids and propose a new correlation.* International Journal of Heat and Mass Transfer, 2018. **124**: p. 742-751.
231. Keklikcioglu Cakmak, N., *The impact of surfactants on the stability and thermal conductivity of graphene oxide de-ionized water nanofluids.* Journal of Thermal Analysis and Calorimetry, 2019.
232. Parsian, A. and M. Akbari, *New experimental correlation for the thermal conductivity of ethylene glycol containing Al2O3–Cu hybrid nanoparticles.* Journal of Thermal Analysis and Calorimetry, 2018. **131**(2): p. 1605-1613.
233. Aybar, H.Ş., et al., *A review of thermal conductivity models for nanofluids.* Heat Transfer Engineering, 2015. **36**(13): p. 1085-1110.
234. Choi, T.Y., et al., *Measurement of the thermal conductivity of a water-based single-wall carbon nanotube colloidal suspension with a modified 3-ω method.* Nanotechnology, 2009. **20**(31): p. 315706.

235. Wang, X.-j. and D.-s. Zhu, *Investigation of pH and SDBS on enhancement of thermal conductivity in nanofluids.* Chemical Physics Letters, 2009. **470**(1-3): p. 107-111.
236. Toghraie, D., V.A. Chaharsoghi, and M. Afrand, *Measurement of thermal conductivity of ZnO–TiO 2/EG hybrid nanofluid.* Journal of Thermal Analysis and Calorimetry, 2016. **125**(1): p. 527-535.
237. Chen, L.F., et al. *Enhanced thermal conductivity of nanofluid by synergistic effect of multi-walled carbon nanotubes and Fe2O3 nanoparticles*. in *Applied Mechanics and Materials*. 2014. Trans Tech Publ.
238. Askari, S., et al., *Investigation of Fe3O4/Graphene nanohybrid heat transfer properties: Experimental approach.* International Communications in Heat and Mass Transfer, 2017. **87**: p. 30-39.
239. Esfahani, N.N., D. Toghraie, and M. Afrand, *A new correlation for predicting the thermal conductivity of ZnO–Ag (50%–50%)/water hybrid nanofluid: An experimental study.* Powder Technology, 2018. **323**: p. 367-373.
240. Rostami, S., A.A. Nadooshan, and A. Raisi, *An experimental study on the thermal conductivity of new antifreeze containing copper oxide and graphene oxide nano-additives.* Powder Technology, 2019. **345**: p. 658-667.
241. Harandi, S.S., et al., *An experimental study on thermal conductivity of F-MWCNTs–Fe3O4/EG hybrid nanofluid: effects of temperature and concentration.* International Communications in Heat and Mass Transfer, 2016. **76**: p. 171-177.
242. Soltani, F., D. Toghraie, and A. Karimipour, *Experimental measurements of thermal conductivity of engine oil-based hybrid and mono nanofluids with tungsten oxide (WO3) and MWCNTs inclusions.* Powder Technology, 2020.
243. Gangadevi, R. and B. Vinayagam, *Experimental determination of thermal conductivity and viscosity of different nanofluids and its effect on a hybrid solar collector.* Journal of Thermal Analysis and Calorimetry, 2019. **136**(1): p. 199-209.
244. Mechiri, S., V. Vasu, and A. Venu Gopal, *Investigation of thermal conductivity and rheological properties of vegetable oil based hybrid nanofluids containing Cu–Zn hybrid nanoparticles.* Experimental Heat Transfer, 2017. **30**(3): p. 205-217.
245. Cakmak, N.K., et al., *Preparation, characterization, stability, and thermal conductivity of rGO-Fe3O4-TiO2 hybrid nanofluid: An experimental study.* Powder Technology, 2020. **372**: p. 235-245.
246. Meyer, J.P., et al., *The viscosity of nanofluids: a review of the theoretical, empirical, and numerical models.* Heat Transfer Engineering, 2016. **37**(5): p. 387-421.
247. Adewumi, G.A., et al., *Investigation of the viscosity and stability of green nanofluids from coconut fibre carbon nanoparticles: effect of temperature and mass fraction.* 2018.
248. Adio, S.A., et al., *Experimental investigation and model development for effective viscosity of MgO–ethylene glycol nanofluids by using dimensional analysis, FCM-ANFIS and GA-PNN techniques.* International Communications in Heat and Mass Transfer, 2016. **72**: p. 71-83.
249. Afrand, M., et al., *Predicting the viscosity of multi-walled carbon nanotubes/water nanofluid by developing an optimal artificial neural network based on experimental data.* International Communications in Heat and Mass Transfer, 2016. **77**: p. 49-53.
250. Afrand, M., et al., *Prediction of dynamic viscosity of a hybrid nano-lubricant by an optimal artificial neural network.* International Communications in Heat and Mass Transfer, 2016. **76**: p. 209-214.
251. Arthur, O. and M.A. Karim, *An investigation into the thermophysical and rheological properties of nanofluids for solar thermal applications.* Renewable and Sustainable Energy Reviews, 2016. **55**: p. 739-755.

252. Asadi, M. and A. Asadi, *Dynamic viscosity of MWCNT/ZnO–engine oil hybrid nanofluid: an experimental investigation and new correlation in different temperatures and solid concentrations.* International Communications in Heat and Mass Transfer, 2016. **76**: p. 41-45.
253. Garbadeen, I., et al. *Numerical study on natural convection of MWCNT nanofluids in a enclosure based on experimental conductivity and viscosity*. in *11th International Conference on Heat Transfer, Fluid Mechanics and Thermodynamics*. 2015. International Conference on Heat Transfer, Fluid Mechanics and Thermodynamics.
254. Kallamu, U.M., et al. *Experimental investigation on viscosity of nanofluids prepared from banana fibre-nanoparticles*. in *11th International Conference on Heat Transfer, Fluid Mechanics and Thermodynamics (HEFAT 2016)*. 2016.
255. Singh, S. and K.S. Kumar. *Influence of nanomaterials on nanofluid application–a review*. in *AIP Conference Proceedings*. 2021. AIP Publishing LLC.
256. Soltani, O. and M. Akbari, *Effects of temperature and particles concentration on the dynamic viscosity of MgO-MWCNT/ethylene glycol hybrid nanofluid: experimental study.* Physica E: Low-dimensional Systems and Nanostructures, 2016. **84**: p. 564-570.
257. Hemmat Esfe, M., et al., *Experimental determination of thermal conductivity and dynamic viscosity of Ag–MgO/water hybrid nanofluid.* International Communications in Heat and Mass Transfer, 2015. **66**: p. 189-195.
258. Suresh, S., et al., *Synthesis of Al2O3–Cu/water hybrid nanofluids using two step method and its thermo physical properties.* Colloids and Surfaces A: Physicochemical and Engineering Aspects, 2011. **388**(1): p. 41-48.
259. Alirezaie, A., et al., *Investigation of rheological behavior of MWCNT (COOH-functionalized)/MgO-engine oil hybrid nanofluids and modelling the results with artificial neural networks.* Journal of Molecular Liquids, 2017. **241**: p. 173-181.
260. Motahari, K., M.A. Moghaddam, and M. Moradian, *Experimental investigation and development of new correlation for influences of temperature and concentration on dynamic viscosity of MWCNT-SiO2 (20-80)/20W50 hybrid nano-lubricant.* Chinese Journal of Chemical Engineering, 2018. **26**(1): p. 152-158.
261. Hamid, K.A., et al., *Experimental investigation of thermal conductivity and dynamic viscosity on nanoparticle mixture ratios of TiO2-SiO2 nanofluids.* International Journal of Heat and Mass Transfer, 2018. **116**: p. 1143-1152.
262. Wanatasanapan, V.V., M.Z. Abdullah, and P. Gunnasegaran, *Effect of TiO2-Al2O3 nanoparticle mixing ratio on the thermal conductivity, rheological properties, and dynamic viscosity of water-based hybrid nanofluid.* Journal of Materials Research and Technology, 2020. **9**(6): p. 13781-13792.
263. Yarmand, H., et al., *Nanofluid based on activated hybrid of biomass carbon/graphene oxide: synthesis, thermo-physical and electrical properties.* International Communications in Heat and Mass Transfer, 2016. **72**: p. 10-15.
264. Zawrah, M., et al., *Stability and electrical conductivity of water-base Al2O3 nanofluids for different applications.* HBRC journal, 2016. **12**(3): p. 227-234.
265. Nithyanandam, T., et al., *Review on the Effect of Various Nanofluids, Concentration and Its Thermophysical Properties in Pool Boiling Performance.* Annals of the Romanian Society for Cell Biology, 2021: p. 1899-1912.
266. Chereches, E.I. and A.A. Minea, *Electrical conductivity of new nanoparticle enhanced fluids: An experimental study.* Nanomaterials, 2019. **9**(9): p. 1228.
267. Ganesh Kumar, P., et al., *Experimental study on thermal properties and electrical conductivity of stabilized H2O-solar glycol mixture based multi-walled carbon nanotube nanofluids: developing a new correlation.* Heliyon, 2019. **5**(8): p. e02385.

268. Jamilpanah, P., H. Pahlavanzadeh, and A. Kheradmand, *Thermal conductivity, viscosity, and electrical conductivity of iron oxide with a cloud fractal structure.* Heat and Mass Transfer, 2017. **53**(4): p. 1343-1354.
269. Adio, S.A., M. Sharifpur, and J.P. Meyer, *Investigation into effective viscosity, electrical conductivity, and pH of γ-Al2O3-glycerol nanofluids in Einstein concentration regime.* Heat Transfer Engineering, 2015. **36**(14-15): p. 1241-1251.
270. Sundar, L.S., et al., *Electrical conductivity enhancement of nanodiamond–nickel (ND–Ni) nanocomposite based magnetic nanofluids.* International Communications in Heat and Mass Transfer, 2014. **57**: p. 1-7.
271. Adio, S.A., M. Sharifpur, and J.P. Meyer, *Factors affecting the pH and electrical conductivity of MgO–ethylene glycol nanofluids.* Bulletin of Materials Science, 2015. **38**(5): p. 1345-1357.
272. Ijam, A., et al., *Stability, thermo-physical properties, and electrical conductivity of graphene oxide-deionized water/ethylene glycol based nanofluid.* International Journal of Heat and Mass Transfer, 2015. **87**: p. 92-103.
273. Ganguly, S., S. Sikdar, and S. Basu, *Experimental investigation of the effective electrical conductivity of aluminum oxide nanofluids.* Powder Technology, 2009. **196**(3): p. 326-330.
274. Abdolbaqi, M.K., et al., *Experimental investigation of thermal conductivity and electrical conductivity of BioGlycol–water mixture based Al2O3 nanofluid.* Applied Thermal Engineering, 2016. **102**: p. 932-941.
275. Qing, S.H., et al., *Thermal conductivity and electrical properties of hybrid SiO2-graphene naphthenic mineral oil nanofluid as potential transformer oil.* Materials Research Express, 2017. **4**(1): p. 015504.
276. Guo, Y., et al., *Experimental investigation of thermal and electrical conductivity of silicon oxide nanofluids in ethylene glycol/water mixture.* International Journal of Heat and Mass Transfer, 2018. **117**: p. 280-286.
277. Shoghl, S.N., J. Jamali, and M.K. Moraveji, *Electrical conductivity, viscosity, and density of different nanofluids: An experimental study.* Experimental Thermal and Fluid Science, 2016. **74**: p. 339-346.
278. Heyhat, M.M. and A. Irannezhad, *Experimental investigation on the competition between enhancement of electrical and thermal conductivities in water-based nanofluids.* Journal of Molecular Liquids, 2018. **268**: p. 169-175.
279. Naddaf, A. and S.Z. Heris, *Experimental study on thermal conductivity and electrical conductivity of diesel oil-based nanofluids of graphene nanoplatelets and carbon nanotubes.* International Communications in Heat and Mass Transfer, 2018. **95**: p. 116-122.
280. Manjunatha, S., et al., *Theoretical Study of Convective Heat Transfer in Ternary Nanofluid Flowing past a Stretching Sheet.* Journal of Applied and Computational Mechanics, 2021.
281. Alade, I.O., et al., *Application of support vector regression and artificial neural network for prediction of specific heat capacity of aqueous nanofluids of copper oxide.* Solar Energy, 2020. **197**: p. 485-490.
282. Adun, H., et al., *A critical review of specific heat capacity of hybrid nanofluids for thermal energy applications.* Journal of Molecular Liquids, 2021: p. 116890.
283. Shahrul, I., et al., *A comparative review on the specific heat of nanofluids for energy perspective.* Renewable and sustainable energy reviews, 2014. **38**: p. 88-98.
284. Heris, S.Z., S.G. Etemad, and M.N. Esfahany, *Experimental investigation of oxide nanofluids laminar flow convective heat transfer.* International communications in heat and mass transfer, 2006. **33**(4): p. 529-535.

285. Veilleux, J. and S. Coulombe, *A total internal reflection fluorescence microscopy study of mass diffusion enhancement in water-based alumina nanofluids.* Journal of Applied Physics, 2010. **108**(10): p. 104316.
286. Murshed, S., K. Leong, and C. Yang, *Determination of the effective thermal diffusivity of nanofluids by the double hot-wire technique.* Journal of Physics D: Applied Physics, 2006. **39**(24): p. 5316.
287. Chen, H., et al., *Rheological behaviour of ethylene glycol based titania nanofluids.* Chemical physics letters, 2007. **444**(4-6): p. 333-337.
288. Zhou, S.-Q. and R. Ni, *Measurement of the specific heat capacity of water-based Al 2 O 3 nanofluid.* Applied Physics Letters, 2008. **92**(9): p. 093123.
289. De Robertis, E., et al., *Application of the modulated temperature differential scanning calorimetry technique for the determination of the specific heat of copper nanofluids.* Applied Thermal Engineering, 2012. **41**: p. 10-17.
290. Vajjha, R.S. and D.K. Das, *Specific heat measurement of three nanofluids and development of new correlations.* Journal of heat transfer, 2009. **131**(7).
291. Oster, K., et al., *Ionic liquid-based nanofluids (ionanofluids) for thermal applications: an experimental thermophysical characterization.* Pure and Applied Chemistry, 2019. **91**(8): p. 1309-1340.
292. Amiri, A., et al., *Transformer oil based multi-walled carbon nanotube–hexylamine coolant with optimized electrical, thermal and rheological enhancements.* Rsc Advances, 2015. **5**(130): p. 107222-107236.
293. Bandarra Filho, E. and L.R. de Oliveira. *Experimental study of thermal conductivity, viscosity and breakdown voltage of mineral oil-based TiO2 nanofluids*. in *Frontiers of Science and Technology: Reports on Technologies for Sustainability–Selected extended papers from the Brazilian-German Conference on Frontiers of Science and Technology Symposium (BRAGFOST), Potsdam 5-10 October 2017*. 2021. Walter de Gruyter GmbH & Co KG.
294. Oparanti, S.O., A.A. Khaleed, and A.A. Abdelmalik, *AC breakdown analysis of synthesized nanofluids for oil-filled transformer insulation.* The International Journal of Advanced Manufacturing Technology, 2021: p. 1-9.
295. Hernaiz, M., et al., *The contact angle of nanofluids as thermophysical property.* Journal of colloid and interface science, 2019. **547**: p. 393-406.
296. Estellé, P., et al., *Current trends in surface tension and wetting behavior of nanofluids.* Renewable and Sustainable Energy Reviews, 2018. **94**: p. 931-944.
297. Kujawska, A., et al., *The effect of boiling in a thermosyphon on surface tension and contact angle of silica and graphene oxide nanofluids.* Colloids and Surfaces A: Physicochemical and Engineering Aspects, 2021. **627**: p. 127082.
298. Lee, S.-H. and S.P. Jang, *Extinction coefficient of aqueous nanofluids containing multi-walled carbon nanotubes.* International Journal of Heat and Mass Transfer, 2013. **67**: p. 930-935.
299. Kashefi, M.H., S. Saedodin, and S.H. Rostamian, *Effect of silica nano-additive on flash point, pour point, rheological and tribological properties of lubricating engine oil: an experimental study.* Journal of Thermal Analysis and Calorimetry, 2021: p. 1-14.
300. Oparanti, S., A. Khaleed, and A. Abdelmalik, *Nanofluid from Palm Kernel Oil for High Voltage Insulation.* Materials Chemistry and Physics, 2021. **259**: p. 123961.
301. Afzal, A., et al., *Back propagation modeling of shear stress and viscosity of aqueous Ionic-MXene nanofluids.* Journal of Thermal Analysis and Calorimetry, 2021: p. 1-21.
302. Sica, L.U., et al., *Cold start analysis of an engine coolant-MWCNT nanofluid: Synthesis and viscosity behavior under shear stress.* Proceedings of the Institution of Mechanical Engineers, Part D: Journal of Automobile Engineering, 2021: p. 09544070211019217.

303. He, Q., et al., *Experimental investigation on photothermal properties of nanofluids for direct absorption solar thermal energy systems.* Energy Conversion and Management, 2013. **73**: p. 150-157.
304. Minea, A.A. and S.S. Murshed, *A review on development of ionic liquid based nanofluids and their heat transfer behavior.* Renewable and Sustainable Energy Reviews, 2018. **91**: p. 584-599.
305. Walvekar, R., et al., *Stability, thermo-physical and electrical properties of naphthenic/POME blended transformer oil nanofluids.* Thermal Science and Engineering Progress, 2021. **23**: p. 100878.
306. Saman, N.M., et al., *Effects of Plasma Treated Alumina Nanoparticles on Breakdown Strength, Partial Discharge Resistance, and Thermophysical Properties of Mineral Oil-Based Nanofluids.* Materials, 2021. **14**(13): p. 3610.
307. Ganesh Kumar, P., et al., *Effect of shot blasting on droplet contact angle of carbon aided phase change nanocomposites.* Surface Engineering, 2021: p. 1-10.
308. Mashhadian, A., M.M. Heyhat, and O. Mahian, *Improving environmental performance of a direct absorption parabolic trough collector by using hybrid nanofluids.* Energy Conversion and Management, 2021. **244**: p. 114450.
309. Hazra, S., M. Michael, and T. Nandi, *Investigations on optical and photo-thermal conversion characteristics of BN-EG and BN/CB-EG hybrid nanofluids for applications in direct absorption solar collectors.* Solar Energy Materials and Solar Cells, 2021. **230**: p. 111245.
310. Beheshti, A., M. Shanbedi, and S.Z. Heris, *Heat transfer and rheological properties of transformer oil-oxidized MWCNT nanofluid.* Journal of Thermal Analysis and Calorimetry, 2014. **118**(3): p. 1451-1460.
311. Amiri, A., et al., *Highly dispersed multiwalled carbon nanotubes decorated with Ag nanoparticles in water and experimental investigation of the thermophysical properties.* The Journal of Physical Chemistry C, 2012. **116**(5): p. 3369-3375.
312. Agrawal, P., et al., *Radiative MHD hybrid-nanofluids flow over a permeable stretching surface with heat source/sink embedded in porous medium.* International Journal of Numerical Methods for Heat & Fluid Flow, 2021.
313. Grosu, Y., et al., *Nanofluids based on molten carbonate salts for high-temperature thermal energy storage: Thermophysical properties, stability, compatibility and life cycle analysis.* Solar Energy Materials and Solar Cells, 2021. **220**: p. 110838.
314. Motamedi, M., et al., *Mitigating the losses in nanofluid-based direct solar absorption receivers.* Renewable Energy, 2021. **178**: p. 1174-1186.
315. Du, S., et al., *Conceptual design of porous volumetric solar receiver using molten salt as heat transfer fluid.* Applied Energy, 2021. **301**: p. 117400.
316. Sahoo, R.R., *Effect of various shape and nanoparticle concentration based ternary hybrid nanofluid coolant on the thermal performance for automotive radiator.* Heat and Mass Transfer, 2021. **57**(5): p. 873-887.
317. Giwa, S., M. Sharifpur, and J. Meyer, *Experimental study of thermo-convection performance of hybrid nanofluids of Al2O3-MWCNT/water in a differentially heated square cavity.* International Journal of Heat and Mass Transfer, 2020. **148**: p. 119072.
318. Hassan, A., et al., *Thermal management and uniform temperature regulation of photovoltaic modules using hybrid phase change materials-nanofluids system.* Renewable Energy, 2020. **145**: p. 282-293.
319. Dehghan, M., M.S. Valipour, and S. Saedodin, *Microchannels enhanced by porous materials: Heat transfer enhancement or pressure drop increment?* Energy Conversion and Management, 2016. **110**: p. 22-32.

320. Gasia, J., et al., *Experimental evaluation of the use of fins and metal wool as heat transfer enhancement techniques in a latent heat thermal energy storage system.* Energy Conversion and Management, 2019. **184**: p. 530-538.
321. Joybari, M.M., et al., *Heat transfer enhancement of phase change materials by fins under simultaneous charging and discharging.* Energy Conversion and Management, 2017. **152**: p. 136-156.
322. Munyalo, J.M. and X. Zhang, *Particle size effect on thermophysical properties of nanofluid and nanofluid based phase change materials: A review.* Journal of Molecular Liquids, 2018. **265**: p. 77-87.
323. Zou, D., et al., *Preparation of a novel composite phase change material (PCM) and its locally enhanced heat transfer for power battery module.* Energy Conversion and Management, 2019. **180**: p. 1196-1202.
324. Akilu, S., et al., *Properties of glycerol and ethylene glycol mixture based SiO2-CuO/C hybrid nanofluid for enhanced solar energy transport.* Solar Energy Materials and Solar Cells, 2018. **179**: p. 118-128.
325. Shehzad, S., et al., *Influence of fin orientation on the natural convection of aqueous-based nano-encapsulated PCMs in a heat exchanger equipped with wing-like fins.* Chemical Engineering and Processing-Process Intensification, 2021. **160**: p. 108287.
326. Khanafer, K., K. Vafai, and M. Lightstone, *Buoyancy-driven heat transfer enhancement in a two-dimensional enclosure utilizing nanofluids.* International journal of heat and mass transfer, 2003. **46**(19): p. 3639-3653.
327. Shirzad, M., et al., *Improve the thermal performance of the pillow plate heat exchanger by using nanofluid: Numerical simulation.* Advanced Powder Technology, 2019. **30**(7): p. 1356-1365.
328. Sahu, M. and J. Sarkar, *Steady-State Energetic and Exergetic Performances of Single-Phase Natural Circulation Loop with Hybrid Nanofluids.* Journal of Heat Transfer, 2019. **141**(8).
329. Giwa, S.O., M. Sharifpur, and J.P. Meyer. *HEAT TRANSFER ENHANCEMENT OF DILUTE AL 2 O 3-MWCNT WATER BASED HYBRID NANOFLUIDS IN A SQUARE CAVITY*. in *International Heat Transfer Conference Digital Library*. 2018. Begel House Inc.
330. Sharifpur, M., et al., *Optimum concentration of nanofluids for heat transfer enhancement under cavity flow natural convection with TiO2–Water.* International Communications in Heat and Mass Transfer, 2018. **98**: p. 297-303.
331. Solomon, A.B., et al. *Convection heat transfer with water based mango bark nanofluids*. in *Int. Conf. Heat Transf. Fluid Mech. Thermodyn.,* . 2017. Portorož, Slovenia, 2017.
332. Ajarostaghi, S.S.M., M. Zaboli, and M. Nourbakhsh, *Numerical evaluation of turbulence heat transfer and fluid flow of hybrid nanofluids in a pipe with innovative vortex generator.* Journal of Thermal Analysis and Calorimetry, 2021. **143**(2): p. 1583-1597.
333. Putra, N., W. Roetzel, and S.K. Das, *Natural convection of nano-fluids.* Heat and mass transfer, 2003. **39**(8-9): p. 775-784.
334. Hu, Y., et al., *Experimental and numerical investigation on natural convection heat transfer of TiO2–water nanofluids in a square enclosure.* Journal of Heat Transfer, 2014. **136**(2).
335. Li, H., et al., *Thermophysical and natural convection characteristics of ethylene glycol and water mixture based ZnO nanofluids.* International Journal of Heat and Mass Transfer, 2015. **91**: p. 385-389.

336. Ho, C., et al., *Natural convection heat transfer of alumina-water nanofluid in vertical square enclosures: an experimental study.* International Journal of Thermal Sciences, 2010. **49**(8): p. 1345-1353.
337. Joshi, P.S. and A. Pattamatta, *Enhancement of natural convection heat transfer in a square cavity using MWCNT/Water nanofluid: an experimental study.* Heat and Mass Transfer, 2018. **54**(8): p. 2295-2303.
338. Solomon, A.B., et al., *Experimental study on the influence of the aspect ratio of square cavity on natural convection heat transfer with Al2O3/Water nanofluids.* International Communications in Heat and Mass Transfer, 2017. **88**: p. 254-261.
339. Umar, E., K. Kamajaya, and N.P. Tandian, *Experimental Study of Natural Convective Heat Transfer of Water-ZrO2 Nanofluids in Vertical Sub Channel.* Contemporary Engineering Sciences, 2015. **8**(33): p. 1593-1605.
340. Mahian, O., et al., *Natural convection of silica nanofluids in square and triangular enclosures: theoretical and experimental study.* International Journal of Heat and Mass Transfer, 2016. **99**: p. 792-804.
341. Ilyas, S.U., R. Pendyala, and M. Narahari, *Experimental investigation of natural convection heat transfer characteristics in MWCNT-thermal oil nanofluid.* Journal of Thermal Analysis and Calorimetry, 2019. **135**(2): p. 1197-1209.
342. Choudhary, R. and S. Subudhi, *Aspect ratio dependence of turbulent natural convection in Al2O3/water nanofluids.* Applied Thermal Engineering, 2016. **108**: p. 1095-1104.
343. Ali, M., et al., *The effect of alumina–water nanofluid on natural convection heat transfer inside vertical circular enclosures heated from above.* Heat transfer engineering, 2013. **34**(15): p. 1289-1299.
344. Mahrood, M.R.K., S.G. Etemad, and R. Bagheri, *Free convection heat transfer of non Newtonian nanofluids under constant heat flux condition.* International Communications in Heat and Mass Transfer, 2011. **38**(10): p. 1449-1454.
345. Solomon, A.B., et al., *Natural convection enhancement in a porous cavity with Al2O3-Ethylene glycol/water nanofluids.* International Journal of Heat and Mass Transfer, 2017. **108**: p. 1324-1334.
346. Sajid, M.U. and H.M. Ali, *Recent advances in application of nanofluids in heat transfer devices: A critical review.* Renewable and Sustainable Energy Reviews, 2019. **103**: p. 556-592.
347. Vanaki, S.M., P. Ganesan, and H. Mohammed, *Numerical study of convective heat transfer of nanofluids: a review.* Renewable and Sustainable Energy Reviews, 2016. **54**: p. 1212-1239.
348. He, W., et al., *Using of Artificial Neural Networks (ANNs) to predict the thermal conductivity of Zinc Oxide–Silver (50%–50%)/Water hybrid Newtonian nanofluid.* International Communications in Heat and Mass Transfer, 2020. **116**: p. 104645.
349. Zadkhast, M., D. Toghraie, and A. Karimipour, *Developing a new correlation to estimate the thermal conductivity of MWCNT-CuO/water hybrid nanofluid via an experimental investigation.* Journal of Thermal Analysis and Calorimetry, 2017. **129**(2): p. 859-867.
350. Akhgar, A., et al., *Developing dissimilar artificial neural networks (ANNs) to prediction the thermal conductivity of MWCNT-TiO2/Water-ethylene glycol hybrid nanofluid.* Powder Technology, 2019. **355**: p. 602-610.
351. Komeili Birjandi, A., et al., *Thermal conductivity estimation of nanofluids with TiO2 nanoparticles by employing artificial neural networks.* International Journal of Low-Carbon Technologies, 2021.
352. Esfe, M.H., et al., *Applicability of artificial neural network and nonlinear regression to predict thermal conductivity modeling of Al2O3–water nanofluids using*

experimental data. International Communications in Heat and Mass Transfer, 2015. **66**: p. 246-249.

353. Kalogirou, S.A., *Applications of artificial neural-networks for energy systems.* Applied energy, 2000. **67**(1-2): p. 17-35.

354. Kurt, H. and M. Kayfeci, *Prediction of thermal conductivity of ethylene glycol–water solutions by using artificial neural networks.* Applied energy, 2009. **86**(10): p. 2244-2248.

355. Mohanraj, M., S. Jayaraj, and C. Muraleedharan, *Applications of artificial neural networks for refrigeration, air-conditioning and heat pump systems—A review.* Renewable and Sustainable Energy Reviews, 2012. **16**(2): p. 1340-1358.

356. Papari, M.M., et al., *Modeling thermal conductivity augmentation of nanofluids using diffusion neural networks.* International journal of thermal sciences, 2011. **50**(1): p. 44-52.

357. Longo, G.A., et al., *Application of artificial neural network (ANN) for the prediction of thermal conductivity of oxide–water nanofluids.* Nano Energy, 2012. **1**(2): p. 290-296.

358. Tahani, M., M. Vakili, and S. Khosrojerdi, *Experimental evaluation and ANN modeling of thermal conductivity of graphene oxide nanoplatelets/deionized water nanofluid.* International Communications in Heat and Mass Transfer, 2016. **76**: p. 358-365.

359. Aghayari, R., et al., *Comparison of the Experimental and Predicted Data for Thermal Conductivity of Fe3O4/water Nanofluid Using Artificial Neural Networks.* Nanomedicine Research Journal, 2016. **1**(1): p. 15-22.

360. Hosseinian Naeini, A., et al., *Nanofluid thermal conductivity prediction model based on artificial neural network.* Transp Phenom Nano Micro Scales, 2016. **4**(2): p. 41-46.

361. Verma, K., et al., *Measurement and prediction of thermal conductivity of nanofluids containing TiO2 nanoparticles.* Journal of nanoscience and nanotechnology, 2017. **17**(2): p. 1068-1075.

362. Esfe, M.H., et al., *Thermal conductivity of Cu/TiO2–water/EG hybrid nanofluid: Experimental data and modeling using artificial neural network and correlation.* International communications in heat and mass transfer, 2015. **66**: p. 100-104.

363. Amani, M., et al., *Modeling and optimization of thermal conductivity and viscosity of MnFe 2 O 4 nanofluid under magnetic field using an ANN.* Scientific reports, 2017. **7**(1): p. 1-13.

364. Esfe, M.H., et al., *Estimation of thermal conductivity of ethylene glycol-based nanofluid with hybrid suspensions of SWCNT–Al 2 O 3 nanoparticles by correlation and ANN methods using experimental data.* Journal of Thermal Analysis and Calorimetry, 2017. **128**(3): p. 1359-1371.

365. Esfe, M.H., et al., *Experimental evaluation, new correlation proposing and ANN modeling of thermal properties of EG based hybrid nanofluid containing ZnO-DWCNT nanoparticles for internal combustion engines applications.* Applied Thermal Engineering, 2018. **133**: p. 452-463.

366. Rostamian, S.H., et al., *An inspection of thermal conductivity of CuO-SWCNTs hybrid nanofluid versus temperature and concentration using experimental data, ANN modeling and new correlation.* Journal of Molecular Liquids, 2017. **231**: p. 364-369.

367. Moghaddari, M., et al., *Thermal conductivity and structuring of multiwalled carbon nanotubes based nanofluids.* Journal of Molecular Liquids, 2020. **307**: p. 112977.

368. Sharifpur, M., S.A. Adio, and J.P. Meyer, *Experimental investigation and model development for effective viscosity of Al2O3–glycerol nanofluids by using dimensional analysis and GMDH-NN methods.* International Communications in Heat and Mass Transfer, 2015. **68**: p. 208-219.

369. Maleki, A., et al., *Applying different types of artificial neural network for modeling thermal conductivity of nanofluids containing silica particles.* Journal of Thermal Analysis and Calorimetry, 2021. **144**(4): p. 1613-1622.
370. Mohamadian, F., L. Eftekhar, and Y. Haghighi Bardineh, *Applying GMDH artificial neural network to predict dynamic viscosity of an antimicrobial nanofluid.* Nanomedicine Journal, 2018. **5**(4): p. 217-221.
371. Ahmadi, M.H., et al., *Application GMDH artificial neural network for modeling of Al2O3/water and Al2O3/ethylene glycol thermal conductivity.* Int J Heat Technol, 2018. **36**(3): p. 773-782.
372. Loni, R., et al., *GMDH modeling and experimental investigation of thermal performance enhancement of hemispherical cavity receiver using MWCNT/oil nanofluid.* Solar Energy, 2018. **171**: p. 790-803.
373. Kumar, V. and J. Sarkar, *Research and development on composite nanofluids as next-generation heat transfer medium.* Journal of Thermal Analysis and Calorimetry, 2019.
374. Sujith, S.V., A.K. Solanki, and R.S. Mulik, *Experimental evaluation on rheological behavior of Al2O3-pure coconut oil nanofluids.* Journal of Molecular Liquids, 2019. **286**: p. 110905.
375. Škulcová, A., et al., *Physical properties and thermal behavior of novel ternary green solvents.* Journal of Molecular Liquids, 2019. **287**: p. 110991.
376. Hayat, T., S. Nadeem, and A.U. Khan, *Numerical analysis of Ag-CuO/water rotating hybrid nanofluid with heat generation and absorption.* Canadian Journal of Physics, 2019. **97**(6): p. 644-650.
377. Hayat, T., et al., *Peristaltic transport of nanofluid in a compliant wall channel with convective conditions and thermal radiation.* Journal of Molecular Liquids, 2016. **220**: p. 448-453.
378. Tshivhi, K.S. and O.D. Makinde, *Magneto-nanofluid coolants past heated shrinking/stretching surfaces: Dual solutions and stability analysis.* Results in Engineering, 2021: p. 100229.
379. Rahnama, Z. and G. Ansarifar, *Predicting and optimizing the thermal-hydraulic, natural circulation, and neutronics parameters in the NuScale nuclear reactor using nanofluid as a coolant via machine learning methods through GA, PSO and HPSOGA algorithms.* Annals of Nuclear Energy, 2021. **161**: p. 108375.
380. Siricharoenpanich, A., S. Wiriyasart, and P. Naphon, *Study on the thermal dissipation performance of GPU cooling system with nanofluid as coolant.* Case Studies in Thermal Engineering, 2021. **25**: p. 100904.
381. Elsaid, E.M. and M.S. Abdel-wahed, *Impact of hybrid nanofluid coolant on the boundary layer behavior over a moving cylinder: Numerical case study.* Case Studies in Thermal Engineering, 2021. **25**: p. 100951.
382. Mukherjee, S., et al., *Effects of SiO2 nanoparticles addition on performance of commercial engine coolant: experimental investigation and empirical correlation.* Energy, 2021: p. 120913.
383. Vasu, V. and K.M. Kumar, *Analysis of Nanofluids as Cutting Fluid in Grinding EN-31 Steel.* Nano-Micro Letters, 2011. **3**(4): p. 209-214.
384. Sarma, D., J. Borah, and M. Chandrasekaran, *Multi optimization of nano fluid based machining of titanium alloy: A green manufacturing approach.* Materials Today: Proceedings, 2021.
385. Ravi, S. and P. Gurusamy, *Review of nanofluids as coolant in metal cutting operations.* Materials Today: Proceedings, 2021. **37**: p. 2387-2390.

386. Hegab, H., et al., *Analysis, modeling, and multi-objective optimization of machining Inconel 718 with nano-additives based minimum quantity coolant.* Applied Soft Computing, 2021. **108**: p. 107416.
387. Barewar, S.D., et al., *Investigating a novel Ag/ZnO based hybrid nanofluid for sustainable machining of inconel 718 under nanofluid based minimum quantity lubrication.* Journal of Manufacturing Processes, 2021. **66**: p. 313-324.
388. Khan, A.M., et al., *Holistic sustainability assessment of hybrid Al–GnP-enriched nanofluids and textured tool in machining of Ti–6Al–4V alloy*. The International Journal of Advanced Manufacturing Technology, 2021. **112**(3): p. 731-743.
389. Kao, M.J., et al., *Copper-oxide brake nanofluid manufactured using arc-submerged nanoparticle synthesis system.* Journal of Alloys and Compounds, 2007. **434-435**: p. 672-674.
390. Mahale, V., J. Bijwe, and S. Sinha, *Influence of nano-potassium titanate particles on the performance of NAO brake-pads.* Wear, 2017. **376-377**: p. 727-737.
391. Venkatesh, A., et al., *Investigation on the effect of nanofluid on performance behaviour of a waste cooking oil on a small diesel engine.* International Journal of Ambient Energy, 2021. **42**(5): p. 540-545.
392. Nag, P. and M.M. Molla. *Non-Newtonian effect on double diffusive natural convection of nanofluid within a square cavity*. in *AIP Conference Proceedings*. 2021. AIP Publishing LLC.
393. Peña-Parás, L., et al., *Thermal transport and tribological properties of nanogreases for metal-mechanic applications.* Wear, 2015. **332-333**: p. 1322-1326.
394. Siddiqui, M.A., et al., *Numerical study of energy transmission through copper-based nanofluid contained in a partially heated isosceles triangular cavity in the presence of heat source/sink.* Physica Scripta, 2021. **96**(5): p. 055222.
395. Heidarian, A., R. Rafee, and M.S. Valipour, *Hydrodynamic analysis of the nanofluids flow in a microchannel with hydrophobic and superhydrophobic surfaces.* Journal of the Taiwan Institute of Chemical Engineers, 2021.
396. Tao, Q., et al., *Numerical investigation on the temperature distribution inside the engine compartment of a fuel cell vehicle with nanofluids as coolant.* International Journal of Energy Research, 2021. **45**(6): p. 9613-9626.
397. Jia, B.-q., et al., *Spray characteristics of Al-nanoparticle-containing nanofluid fuel in a self-excited oscillation injector.* Fuel, 2021. **290**: p. 120057.
398. Chang, H., et al., *Tribological property of TiO2 nanolubricant on piston and cylinder surfaces.* Journal of Alloys and Compounds, 2010. **495**(2): p. 481-484.
399. Ali, M.K.A., et al., *Reducing frictional power losses and improving the scuffing resistance in automotive engines using hybrid nanomaterials as nano-lubricant additives.* Wear, 2016. **364-365**: p. 270-281.
400. Xia, W., et al., *Study on growth behaviour of oxide scale and its effects on tribological property of nano-TiO2 additive oil-in-water lubricant.* Wear, 2017. **376-377**: p. 792-802.
401. Xu, Y., et al., *Synergistic effects of electroless piston ring coatings and nano-additives in oil on the friction and wear of a piston ring/cylinder liner pair.* Wear, 2019. **422-423**: p. 201-211.
402. Adelekan, D.S., et al., *Performance of a domestic refrigerator in varying ambient temperatures, concentrations of TiO2 nanolubricants and R600a refrigerant charges.* Heliyon, 2021. **7**(2): p. e06156.
403. Gao, T., et al., *Mechanics analysis and predictive force models for the single-diamond grain grinding of carbon fiber reinforced polymers using CNT nano-lubricant.* Journal of Materials Processing Technology, 2021. **290**: p. 116976.

404. Kharabati, S., S. Saedodin, and S.H. Rostamian, *Experimental investigation of thermal and rheological behavior of silica/soybean oil nano lubricant in low-temperature performance of internal combustion engine.* Energy Sources, Part A: Recovery, Utilization, and Environmental Effects, 2021: p. 1-15.
405. Habib, S., et al., *Improved self-healing performance of polymeric SSTSS nanocomposites reinforced with talc nanoparticles (TNPs) and urea-formaldehyde microcapsules (UFMCs).* Arabian Journal of Chemistry, 2021. **14**: p. 102926.
406. Sowmyashree, A., et al., *Novel nano corrosion inhibitor, integrated zinc titanate nano particles: Synthesis, characterization, thermodynamic and electrochemical studies.* Surfaces and Interfaces, 2021. **22**: p. 100812.
407. Yuan, Q., et al., *Influence of Al2O3 nanoparticles on the corrosion behavior of brass in simulated cooling water.* Journal of Alloys and Compounds, 2018. **764**: p. 512-522.
408. Ying, L.X., et al., *TiO2 Sol strengthened Cu-Sn-PTFE composite coatings with high homogeneity and superior resistance to wear.* Wear, 2019. **426-427**: p. 258-264.
409. Rashidi, A.M., et al., *Erosion-corrosion synergism in an alumina/sea water nanofluid.* Microfluidics and Nanofluidics, 2014. **17**(1): p. 225-232.
410. ADAH, C.A., et al., *Comparative studies of inhibitive properties of Ficus polita and Ficus platyphylla on corrosion inhibition of mild steel in acidic medium.* 2021.
411. Alhuyi Nazari, M., et al., *A review on pulsating heat pipes: From solar to cryogenic applications.* Applied Energy, 2018. **222**: p. 475-484.
412. Alhuyi Nazari, M., et al., *How to improve the thermal performance of pulsating heat pipes: A review on working fluid.* Renewable and Sustainable Energy Reviews, 2018. **91**: p. 630-638.
413. Kumaresan, G., et al., *Experimental study on effect of wick structures on thermal performance enhancement of cylindrical heat pipes.* Journal of Thermal Analysis and Calorimetry, 2019. **136**(1): p. 389-400.
414. Sözen, A., et al., *Upgrading of the performance of an air-to-air heat exchanger using graphene/water nanofluid.* International Journal of Thermophysics, 2021. **42**(3): p. 1-15.
415. Sankar, P.J., S. Venkatachalapathy, and L.G. Asirvatham, *Combined effects of filling ratio and wick surface coating on thermal performance of cylindrical heat pipes.* Heat and Mass Transfer, 2021: p. 1-12.
416. Yılmaz Aydın, D., et al., *The impacts of nanoparticle concentration and surfactant type on thermal performance of a thermosyphon heat pipe working with bauxite nanofluid.* Energy Sources, Part A: Recovery, Utilization, and Environmental Effects, 2021. **43**(12): p. 1524-1548.
417. Sarbolookzadeh Harandi, S., et al., *An experimental study on thermal conductivity of F-MWCNTs–Fe3O4/EG hybrid nanofluid: Effects of temperature and concentration.* International Communications in Heat and Mass Transfer, 2016. **76**: p. 171-177.
418. Diglio, G., et al., *Borehole heat exchanger with nanofluids as heat carrier.* Geothermics, 2018. **72**: p. 112-123.
419. Bhattad, A., J. Sarkar, and P. Ghosh, *Discrete phase numerical model and experimental study of hybrid nanofluid heat transfer and pressure drop in plate heat exchanger.* International Communications in Heat and Mass Transfer, 2018. **91**: p. 262-273.
420. Huang, D., Z. Wu, and B. Sunden, *Effects of hybrid nanofluid mixture in plate heat exchangers.* Experimental Thermal and Fluid Science, 2016. **72**: p. 190-196.
421. Hung, Y.-H., et al., *Performance evaluation of an air-cooled heat exchange system for hybrid nanofluids.* Experimental Thermal and Fluid Science, 2017. **81**: p. 43-55.
422. Maghrabie, H.M., et al., *Intensification of heat exchanger performance utilizing nanofluids.* International Journal of Thermofluids, 2021. **10**: p. 100071.

423. Maghrabie, H.M., M. Attalla, and A.A. Mohsen, *Performance assessment of a shell and helically coiled tube heat exchanger with variable orientations utilizing different nanofluids.* Applied Thermal Engineering, 2021. **182**: p. 116013.
424. Noorbakhsh, M., et al., *Thermal analysis of nanofluids flow in a double pipe heat exchanger with twisted tapes insert in both sides.* Journal of Thermal Analysis and Calorimetry, 2021: p. 1-12.
425. Ponangi, B.R., V. Krishna, and K. Seetharamu, *Performance of compact heat exchanger in the presence of novel hybrid graphene nanofluids.* International Journal of Thermal Sciences, 2021. **165**: p. 106925.
426. Singh, S.K. and J. Sarkar, *Thermohydraulic behavior of concentric tube heat exchanger inserted with conical wire coil using mono/hybrid nanofluids.* International Communications in Heat and Mass Transfer, 2021. **122**: p. 105134.
427. Dalkılıç, A.S., et al., *Optimization of the finned double-pipe heat exchanger using nanofluids as working fluids.* Journal of Thermal Analysis and Calorimetry, 2021. **143**(2): p. 859-878.
428. Ahmed, W., et al., *Characteristics investigation on heat transfer growth of sonochemically synthesized ZnO-DW based nanofluids inside square heat exchanger.* Journal of Thermal Analysis and Calorimetry, 2021. **144**(4): p. 1517-1534.
429. Anitha, S., K. Loganathan, and M. Pichumani, *Approaches for modelling of industrial energy systems: correlation of heat transfer characteristics between magnetohydrodynamics hybrid nanofluids and performance analysis of industrial length-scale heat exchanger.* Journal of Thermal Analysis and Calorimetry, 2021. **144**(5): p. 1783-1798.
430. Sharma, D., et al., *Numerical Investigation of heat transfer enhancement of SiO2-water based nanofluids in Light water nuclear reactor.* Materials Today: Proceedings, 2017. **4**(9): p. 10118-10122.
431. Rahnama, Z. and G. Ansarifar, *Nanofluid application for heat transfer, safety, and natural circulation enhancement in the NuScale nuclear reactor as a small modular reactor using computational fluid dynamic (CFD) modeling via neutronic and thermal-hydraulics coupling.* Progress in Nuclear Energy, 2021. **138**: p. 103796.
432. Moraru, V., et al., *Emergency cooling of superheated surfaces by nanofluids additives in the event of a water boiling crisis.* International Journal of Heat and Mass Transfer, 2021. **169**: p. 120932.
433. Ahmed, F., et al., *Computational assessment of thermo-hydraulic performance of Al2O3-water nanofluid in hexagonal rod-bundles subchannel.* Progress in Nuclear Energy, 2021. **135**: p. 103700.
434. Sharma, D., *Numerical Investigation of Heat Transfer Characteristics of Al 2 O 3–H 2 O Based Nanofluid Flow in Light Water Nuclear Reactor*, in *Recent Advances in Mechanical Engineering*. 2021, Springer. p. 63-72.
435. Narei, H., R. Ghasempour, and Y. Noorollahi, *The effect of employing nanofluid on reducing the bore length of a vertical ground-source heat pump.* Energy Conversion and Management, 2016. **123**: p. 581-591.
436. Jakhar, S., M.K. Paliwal, and N. Purohit, *Assessment of alumina/water nanofluid in a glazed tube and sheet photovoltaic/thermal system with geothermal cooling.* Journal of Thermal Analysis and Calorimetry, 2021: p. 1-18.
437. Kotadia, H.T.H.S.D. and S.D.M. Shah, *Developments and Future Insights of Using Nanofluids for Heat Transfer Enhancements in Geothermal Systems.*
438. Assad, M.E.H. and M.A. Nazari, *Heat exchangers and nanofluids*, in *Design and performance optimization of renewable energy systems*. 2021, Elsevier. p. 33-42.

439. Shafiq, A., et al., *Thermally Enhanced Darcy-Forchheimer Casson-Water/Glycerine Rotating Nanofluid Flow with Uniform Magnetic Field.* Micromachines, 2021. **12**(6): p. 605.
440. Javadi, H., et al., *Impact of Employing Hybrid Nanofluids as Heat Carrier Fluid on the Thermal Performance of a Borehole Heat Exchanger.* Energies, 2021. **14**(10): p. 2892.
441. Liu, J., P.F. Martin, and B.P. McGrail, *Rare-earth element extraction from geothermal brine using magnetic core-shell nanoparticles-techno-economic analysis.* Geothermics, 2021. **89**: p. 101938.
442. Yao, S., et al., *Effects of nanoparticle types and size on boiling feat transfer performance under different pressures.* AIP Advances, 2018. **8**(2): p. 025005.
443. Jun, S., et al., *Enhancement of Pool Boiling Heat Transfer in Water Using Sintered Copper Microporous Coatings.* Nuclear Engineering and Technology, 2016. **48**(4): p. 932-940.
444. Kamel, M.S., et al., *Amelioration of pool boiling thermal performance in case of using a new hybrid nanofluid.* Case Studies in Thermal Engineering, 2021. **24**: p. 100872.
445. Huang, M., et al., *Effect of concentration and sedimentation on boiling heat transfer coefficient of GNPs-SiO2/deionized water hybrid Nanofluid: An experimental investigation.* International Communications in Heat and Mass Transfer, 2021. **122**: p. 105141.
446. Thakur, P., N. Kumar, and S.S. Sonawane, *Enhancement of pool boiling performance using MWCNT based nanofluids: A sustainable method for the wastewater and incinerator heat recovery.* Sustainable Energy Technologies and Assessments, 2021. **45**: p. 101115.
447. Shabarish, M. and V.A. Ra, *Investigation of Pool Boiling Heat Transfer Characteristics of Graphene-Water Nanofluids.* International Journal of Research in Engineering, Science and Management, 2021. **4**(6): p. 18-23.
448. Ali, H.M., M.U. Sajid, and A. Arshad, *Heat transfer applications of TiO2 nanofluids.* Application of Titanium Dioxide, 2017.
449. Cui, Y., et al., *Comprehensive review of the recent advances in PV/T system with loop-pipe configuration and nanofluid.* Renewable and Sustainable Energy Reviews, 2021. **135**: p. 110254.
450. Lau, G., J. Mohammadpour, and A. Lee, *Cooling performance of an impinging synthetic jet in a microchannel with nanofluids: an Eulerian approach.* Applied Thermal Engineering, 2021. **188**: p. 116624.
451. Chen, T., et al., *Numerical and experimental study on optimization of CPU system cooled by nanofluids.* Case Studies in Thermal Engineering, 2021. **24**: p. 100848.
452. Kashyap, S., J. Sarkar, and A. Kumar, *Effect of surface modifications and using hybrid nanofluids on energy-exergy performance of regenerative evaporative cooler.* Building and Environment, 2021. **189**: p. 107507.
453. Saez, V., et al., *Graphene quantum dots nanoparticles changed the rheological properties of hydrophilic gels (carbopol).* Journal of Molecular Liquids, 2019. **287**: p. 110949.
454. Gan, C., et al., *Glucose-based novel gemini surfactants: Surface activities, aggregation properties and a preliminary study as nanocarrier for resveratrol.* Journal of Molecular Liquids, 2019. **283**: p. 781-787.
455. Chen, F., et al., *Graphene quantum dots in biomedical applications: Recent advances and future challenges.* Frontiers in Laboratory Medicine, 2017. **1**(4): p. 192-199.
456. Tripathi, D. and O.A. Bég, *A study on peristaltic flow of nanofluids: Application in drug delivery systems.* International Journal of Heat and Mass Transfer, 2014. **70**: p. 61-70.

457. Kleinstreuer, C., J. Li, and J. Koo, *Microfluidics of nano-drug delivery.* International Journal of Heat and Mass Transfer, 2008. **51**(23): p. 5590-5597.
458. Joseph, R.R. and S.S. Venkatraman, *Drug delivery to the eye: what benefits do nanocarriers offer?* Nanomedicine, 2017. **12**(6): p. 683-702.
459. Shalaby, T., A. Gawish, and H. Hamad, *A Promising Platform of Magnetic Nanofluid and Ultrasonic Treatment for Cancer Hyperthermia Therapy: In Vitro and in Vivo Study.* Ultrasound in Medicine & Biology, 2021. **47**(3): p. 651-665.
460. Kumaran, G. and R. Sivaraj, *Nonlinear thermal radiation effect on MHD Williamson nanofluid past a wedge/flat plate/stagnation point of the plate with activation energy.* Computational Thermal Sciences: An International Journal.
461. Basha, H.T. and R. Sivaraj, *Numerical simulation of blood nanofluid flow over three different geometries by means of gyrotactic microorganisms: applications to the flow in a circulatory system.* Proceedings of the Institution of Mechanical Engineers, Part C: Journal of Mechanical Engineering Science, 2021. **235**(2): p. 441-460.
462. Tang, Y., et al., *Effect of nanofluid distribution on therapeutic effect considering transient bio-tissue temperature during magnetic hyperthermia.* Journal of Magnetism and Magnetic Materials, 2021. **517**: p. 167391.
463. Gupta, U., J. Sharma, and M. Devi, *Double-diffusive instability of Casson nanofluids with numerical investigations for blood-based fluid.* The European Physical Journal Special Topics, 2021: p. 1-11.
464. Patade, S.R., et al., *Preparation and characterisations of magnetic nanofluid of zinc ferrite for hyperthermia.* Nanomaterials and Energy, 2020. **9**(1): p. 8-13.
465. Yan, J.-F. and J. Liu, *Nanocryosurgery and its mechanisms for enhancing freezing efficiency of tumor tissues.* Nanomedicine: Nanotechnology, Biology and Medicine, 2008. **4**(1): p. 79-87.
466. Yu, Z., et al., *Nanoparticles: A New Approach to Upgrade Cancer Diagnosis and Treatment.* Nanoscale Research Letters, 2021. **16**(1): p. 1-17.
467. Henda, M.B., et al., *Applications of activation energy along with thermal and exponential space-based heat source in bioconvection assessment of magnetized third grade nanofluid over stretched cylinder/sheet.* Case Studies in Thermal Engineering, 2021: p. 101043.
468. Henda, M.B., et al., *Case Studies in Thermal Engineering.*
469. Alshomrani, A.S., *Numerical investigation for bio-convection flow of viscoelastic nanofluid with magnetic dipole and motile microorganisms.* Arabian Journal for Science and Engineering, 2021. **46**(6): p. 5945-5956.
470. Sukumar, S. and S.P. Kar, *NUMERICAL ANALYSIS OF NON-FOURIER PHASE-CHANGE HEAT TRANSFER IN BIOLOGICAL TISSUES WITH THE ADDITION OF NANOPARTICLES.* Computational Thermal Sciences: An International Journal, 2021. **13**(3).
471. Sukumar, S. and S.P. Kar, *Enhancement of Cooling Rate Using Biodegradable MgO Nanoparticles During a Cryopreservation Process*, in *Advances in Air Conditioning and Refrigeration*. 2021, Springer. p. 23-32.
472. Ur Rasheed, H., et al., *Effects of joule heating and viscous dissipation on magnetohydrodynamic boundary layer flow of Jeffrey nanofluid over a vertically stretching cylinder.* Coatings, 2021. **11**(3): p. 353.
473. Bilal, M., H. Arshad, and M. Ramzan, *Unsteady Hybrid-Nanofluid Flow Comprising Ferrousoxide and CNTs Through Porous Horizontal Channel With Dilating/Squeezing Walls.* 2021.
474. Namgung, B., et al., *Engineered cell-laden alginate microparticles for 3D culture.* Biochemical Society Transactions, 2021. **49**(2): p. 761-773.

475. Nguyen, L.H., et al., *The Role of Anisotropy in Distinguishing Domination of Néel or Brownian Relaxation Contribution to Magnetic Inductive Heating: Orientations for Biomedical Applications.* Materials, 2021. **14**(8): p. 1875.
476. Schneider, S., et al., *Facile Patterning of Thermoplastic Elastomers and Robust Bonding to Glass and Thermoplastics for Microfluidic Cell Culture and Organ-on-Chip.* Micromachines, 2021. **12**(5): p. 575.
477. Nguyen, C.T., et al., *Heat transfer enhancement using Al2O3–water nanofluid for an electronic liquid cooling system.* Applied Thermal Engineering, 2007. **27**(8): p. 1501-1506.
478. Lin, Y.-H., S.-W. Kang, and H.-L. Chen, *Effect of silver nano-fluid on pulsating heat pipe thermal performance.* Applied Thermal Engineering, 2008. **28**(11): p. 1312-1317.
479. Teng, T.-P., et al., *Thermal efficiency of heat pipe with alumina nanofluid.* Journal of Alloys and Compounds, 2010. **504**: p. S380-S384.
480. Mohsen Elkhouly, M., M.A. ElBouz, and G.E. Sultan, *Theoretical Study of Mixed Convection Cooling of Microprocessor Using CuO Nanofluid.(Dept. M).* MEJ. Mansoura Engineering Journal, 2021. **46**(2): p. 12-19.
481. Zunaid, M., P. Singh, and A. Husain, *Numerical Analysis of Inclined Jet Micro-channel Heat Sink Using Nanofluids*, in *Recent Advances in Mechanical Engineering*. 2021, Springer. p. 851-860.
482. Bahiraei, M., N. Mazaheri, and M.R. Daneshyar, *Employing elliptical pin-fins and nanofluid within a heat sink for cooling of electronic chips regarding energy efficiency perspective.* Applied Thermal Engineering, 2021. **183**: p. 116159.
483. El-Khouly, M., M. El Bouz, and G. Sultan, *Experimental and computational study of using nanofluid for thermal management of electronic chips.* Journal of Energy Storage, 2021. **39**: p. 102630.
484. Sarvar-Ardeh, S., R. Rafee, and S. Rashidi, *Hybrid nanofluids with temperature-dependent properties for use in double-layered microchannel heat sink; hydrothermal investigation.* Journal of the Taiwan Institute of Chemical Engineers, 2021.
485. Gonzalez-Gallardo, C.L., A. Díaz Díaz, and J.R. Casanova-Moreno, *Improving plasma bonding of PDMS to gold-patterned glass for electrochemical microfluidic applications.* Microfluidics and Nanofluidics, 2021. **25**(2): p. 20.
486. Hassanpour-Tamrin, S., A. Sanati-Nezhad, and A. Sen, *A simple and low-cost approach for irreversible bonding of polymethylmethacrylate and polydimethylsiloxane at room temperature for high-pressure hybrid microfluidics.* Scientific Reports, 2021. **11**(1): p. 4821.
487. Noreen, S., et al., *Entropy generation in electromagnetohydrodynamic water based three Nano fluids via porous asymmetric microchannel.* European Journal of Mechanics - B/Fluids, 2021. **85**: p. 458-466.
488. Li, Y.-X., et al., *Bio-convective Darcy-Forchheimer periodically accelerated flow of non-Newtonian nanofluid with Cattaneo–Christov and Prandtl effective approach.* Case Studies in Thermal Engineering, 2021: p. 101069.
489. Shahsavar, A., et al., *Experimental investigation of the usability of the rifled serpentine tube to improve energy and exergy performances of a nanofluid-based photovoltaic/thermal system.* Renewable Energy, 2021. **170**: p. 410-425.
490. Sohani, A., et al., *Selecting the best nanofluid type for A photovoltaic thermal (PV/T) system based on reliability, efficiency, energy, economic, and environmental criteria.* Journal of the Taiwan Institute of Chemical Engineers, 2021.
491. Kazemian, A., et al., *Performance optimization of a nanofluid-based photovoltaic thermal system integrated with nano-enhanced phase change material.* Applied Energy, 2021. **295**: p. 116859.

492. Yazdanifard, F., M. Ameri, and R. Taylor, *Parametric investigation of a nanofluid-NEPCM based spectral splitting photovoltaic/thermal system.* Energy Conversion and Management, 2021. **240**: p. 114232.
493. Shahsavar, A., *Experimental evaluation of energy and exergy performance of a nanofluid-based photovoltaic/thermal system equipped with a sheet-and-sinusoidal serpentine tube collector.* Journal of Cleaner Production, 2021. **287**: p. 125064.
494. Shahsavar, A., et al., *A comparative experimental investigation of energetic and exergetic performances of water/magnetite nanofluid-based photovoltaic/thermal system equipped with finned and unfinned collectors.* Energy, 2021. **220**: p. 119714.
495. Lee, M., Y. Shin, and H. Cho, *Theoretical study on performance comparison of various solar collectors using binary nanofluids.* Journal of Mechanical Science and Technology, 2021. **35**(3): p. 1267-1278.
496. Zeng, J. and Y. Xuan, *Analysis on interaction between solar light and suspended nanoparticles in nanofluids.* Journal of Quantitative Spectroscopy and Radiative Transfer, 2021. **269**: p. 107692.
497. Zuo, X., et al., *Experimental investigation on photothermal conversion properties of lampblack ink nanofluids.* Solar Energy, 2021. **218**: p. 1-10.
498. Wang, K., et al., *Experimental optimization of nanofluids based direct absorption solar collector by optical boundary conditions.* Applied Thermal Engineering, 2021. **182**: p. 116076.
499. He, Y., S. Vasiraju, and L. Que, *Hybrid nanomaterial-based nanofluids for micropower generation.* RSC Advances, 2014. **4**(5): p. 2433-2439.
500. Attia, S.Y., et al., *Supercapacitor electrode materials: addressing challenges in mechanism and charge storage.* Reviews in Inorganic Chemistry, 2021(000010151520200022).
501. Liu, R., et al., *Fundamentals, Advances and Challenges of Transition Metal Compounds-based.*
502. Hosseini, S.E. and B. Butler, *Design and analysis of a hybrid concentrated photovoltaic thermal system integrated with an organic Rankine cycle for hydrogen production.* Journal of Thermal Analysis and Calorimetry, 2021. **144**(3): p. 763-778.
503. Sun, C., et al., *Liquid paraffin thermal conductivity with additives tungsten trioxide nanoparticles: synthesis and propose a new composed approach of fuzzy logic/artificial neural network.* Arabian Journal for Science and Engineering, 2021. **46**(3): p. 2543-2552.
504. Puneeth, V., et al., *Bioconvection of a radiating hybrid nanofluid past a thin needle in the presence of heterogeneous–homogeneous chemical reaction.* Journal of Heat Transfer, 2021. **143**(4): p. 042502.
505. Pawar, P., et al., *Pool Boiling Heat Transfer Augmentation in a Novel Aqueous Binary Mixture of Surfactants.* Journal of Heat Transfer, 2021. **143**(4): p. 044501.
506. Lei, J., R. Ding, and J. Zhang, *Study on seepage and adsorption characteristics of porous media containing adsorbent based on lattice Boltzmann.* AIP Advances, 2021. **11**(4): p. 045126.
507. da Silva, W.L. and J.H.Z. dos Santos, *Applications of ionic liquids in environmental remediation*, in *Green Sustainable Process for Chemical and Environmental Engineering and Science*. 2021, Elsevier. p. 15-21.
508. Leclerc, C.A., et al., *Rapid design and prototyping of microfluidic chips via computer numerical control micromilling and anisotropic shrinking of stressed polystyrene sheets.* Microfluidics and Nanofluidics, 2021. **25**(2): p. 1-12.
509. Teran-Cuadrado, G. and E. Polo-Cuadrado, *Effectiveness of a bio-catalytic agent used in the bioremediation of crude oil-polluted seawater.* Heliyon, 2021. **7**(4): p. e06926.

510. Eid, M.R. and A.F. Al-Hossainy, *High-performance nanofluid synthesis and DFT-TDDFT study of graphene nanosheets along bent surface for enhanced oil-recovery implementations.* Case Studies in Thermal Engineering, 2021. **25**: p. 100983.
511. Mahmoudpour, M. and P. Pourafshary, *Investigation of the effect of engineered water/nanofluid hybrid injection on enhanced oil recovery mechanisms in carbonate reservoirs.* Journal of Petroleum Science and Engineering, 2021. **196**: p. 107662.
512. Hu, Y., et al., *Hybrid application of nanoparticles and polymer in enhanced oil recovery processes.* Polymers, 2021. **13**(9): p. 1414.
513. Al-Anssari, S., et al., *Synergistic Effect of Nanoparticles and Polymers on the Rheological Properties of Injection Fluids: Implications for Enhanced Oil Recovery.* Energy & Fuels, 2021. **35**(7): p. 6125-6135.
514. Negi, G., S. Anirbid, and P. Sivakumar, *Applications of silica and titanium dioxide nanoparticles in enhanced oil recovery: Promises and challenges.* Petroleum Research, 2021.
515. Tulu, A. and W. Ibrahim, *Effects of Second-Order Slip Flow and Variable Viscosity on Natural Convection Flow of CNTs− Fe3O4/Water Hybrid Nanofluids due to Stretching Surface.* Mathematical Problems in Engineering, 2021. **2021**.
516. Khan, M.R., et al., *Comparative study on heat transfer and friction drag in the flow of various hybrid nanofluids effected by aligned magnetic field and nonlinear radiation.* Scientific Reports, 2021. **11**(1): p. 1-14.
517. Waqas, H., et al., *Bioconvection transport of magnetized Walter's B nanofluid across a cylindrical disk with nonlinear radiative heat transfer.* Case Studies in Thermal Engineering, 2021: p. 101097.
518. Ragui, K., R. Bennacer, and M. El Ganaoui, *Oscillatory flow of Koo–Kleinstreuer and aggregate nanofluids in cylindrical annuli: Toward an innovative solution to deal with nanofluids instability.* Physics of Fluids, 2021. **33**(4): p. 042013.
519. Awasthi, M.K. and G. Hoshoudy, *Study of heat and mass transport on the instability of a swirling viscoelastic liquid film.* The European Physical Journal E, 2021. **44**(3): p. 1-9.
520. Kapen, P.T., et al., *Linear stability analysis of (Cu-Al2O3)/water hybrid nanofluid flow in porous media in presence of hydromagnetic, small suction and injection effects.* Alexandria Engineering Journal, 2021. **60**(1): p. 1525-1536.
521. Ahuja, J. and P. Girotra, *RAYLEIGH-TAYLOR INSTABILITY IN NANOFLUIDS THROUGH POROUS MEDIUM.* Journal of Porous Media, 2021. **24**(8).
522. Yadav, D., Y.-M. Chu, and Z. Li, *Examination of the nanofluid convective instability of vertical constant throughflow in a porous medium layer with variable gravity.* Applied Nanoscience, 2021: p. 1-14.
523. Awasthi, M.K., Z. Uddin, and R. Asthana, *Temporal instability of a power-law viscoelastic nanofluid layer.* The European Physical Journal Special Topics, 2021: p. 1-8.
524. Sundar, L.S., M.K. Singh, and A.C.M. Sousa, *Enhanced heat transfer and friction factor of MWCNT–Fe3O4/water hybrid nanofluids.* International Communications in Heat and Mass Transfer, 2014. **52**: p. 73-83.
525. Hussein, A.M., *Thermal performance and thermal properties of hybrid nanofluid laminar flow in a double pipe heat exchanger.* Experimental Thermal and Fluid Science, 2017. **88**: p. 37-45.
526. Yarmand, H., et al., *Graphene nanoplatelets–silver hybrid nanofluids for enhanced heat transfer.* Energy Conversion and Management, 2015. **100**: p. 419-428.
527. Farbod, M., A. Ahangarpour, and S.G. Etemad, *Stability and thermal conductivity of water-based carbon nanotube nanofluids.* Particuology, 2015. **22**: p. 59-65.

528. Tiwari, A.K., et al., *3S (Sonication, surfactant, stability) impact on the viscosity of hybrid nanofluid with different base fluids: An experimental study*. Journal of Molecular Liquids, 2021. **329**: p. 115455.
529. Bakhtiari, R., et al., *Preparation of stable TiO2-Graphene/Water hybrid nanofluids and development of a new correlation for thermal conductivity*. Powder Technology, 2021. **385**: p. 466-477.
530. Han, Z.H., et al., *Application of hybrid sphere/carbon nanotube particles in nanofluids.* Nanotechnology, 2007. **18**(10): p. 105701.
531. Turcu, R., et al., *Polypyrrole coated magnetite nanoparticles from water based nanofluids.* Journal of Physics D: Applied Physics, 2008. **41**(24): p. 245002.
532. Jha, N. and S. Ramaprabhu, *Synthesis and thermal conductivity of copper nanoparticle decorated multiwalled carbon nanotubes based nanofluids.* The Journal of Physical Chemistry C, 2008. **112**(25): p. 9315-9319.
533. Baghbanzadeh, M., et al., *Synthesis of spherical silica/multiwall carbon nanotubes hybrid nanostructures and investigation of thermal conductivity of related nanofluids.* Thermochimica acta, 2012. **549**: p. 87-94.
534. Lee, J. and I. Mudawar, *Assessment of the effectiveness of nanofluids for single-phase and two-phase heat transfer in micro-channels.* International Journal of Heat and Mass Transfer, 2007. **50**(3-4): p. 452-463.
535. Junankar, A.A., et al., *A Review: Enhancement of turning process performance by effective utilization of hybrid nanofluid and MQL.* Materials Today: Proceedings, 2021. **38**: p. 44-47.
536. Shah, T.R. and H.M. Ali, *Applications of hybrid nanofluids in solar energy, practical limitations and challenges: a critical review.* Solar Energy, 2019. **183**: p. 173-203.
537. Chougule, S.S. and S.K. Sahu. *Model of Heat Conduction in hybrid nanofluid*. in *2013 IEEE International Conference ON Emerging Trends in Computing, Communication and Nanotechnology (ICECCN)*. 2013. IEEE.
538. Nadooshan, A.A., H. Eshgarf, and M. Afrand, *Measuring the viscosity of Fe3O4-MWCNTs/EG hybrid nanofluid for evaluation of thermal efficiency: Newtonian and non-Newtonian behavior.* Journal of Molecular Liquids, 2018. **253**: p. 169-177.
539. Popiel, C. and J. Wojtkowiak, *Simple formulas for thermophysical properties of liquid water for heat transfer calculations (from 0 C to 150 C).* Heat transfer engineering, 1998. **19**(3): p. 87-101.
540. Prasher, R., et al., *Measurements of nanofluid viscosity and its implications for thermal applications.* Applied physics letters, 2006. **89**(13): p. 133108.
541. Ijam, A., et al., *A glycerol–water-based nanofluid containing graphene oxide nanosheets.* Journal of Materials Science, 2014. **49**(17): p. 5934-5944.
542. Tayebi, T. and A.J. Chamkha, *Free convection enhancement in an annulus between horizontal confocal elliptical cylinders using hybrid nanofluids.* Numerical Heat Transfer, Part A: Applications, 2016. **70**(10): p. 1141-1156.
543. Berkovsky, B. and V. Polevikov, *Numerical study of problems on high-intensive free convection.* 1977.
544. Cioni, S., S. Ciliberto, and J. Sommeria, *Experimental study of high-Rayleigh-number convection in mercury and water.* Dynamics of Atmospheres and Oceans, 1996. **24**(1): p. 117-127.
545. Leong, W., K. Hollands, and A. Brunger, *Experimental Nusselt numbers for a cubical-cavity benchmark problem in natural convection.* International Journal of Heat and Mass Transfer, 1999. **42**(11): p. 1979-1989.

546. Esfe, M.H., S.M. Motallebi, and M. Bahiraei, *Employing response surface methodology and neural network to accurately model thermal conductivity of TiO2–water nanofluid using experimental data.* Chinese Journal of Physics, 2021. **70**: p. 14-25.
547. Tariq, R., et al., *Regression-based empirical modeling of thermal conductivity of CuO-water nanofluid using data-driven techniques.* International Journal of Thermophysics, 2020. **41**(4): p. 1-28.
548. Rostami, S., et al., *Predict the thermal conductivity of SiO 2/water–ethylene glycol (50: 50) hybrid nanofluid using artificial neural network.* Journal of Thermal Analysis and Calorimetry, 2020: p. 1-10.
549. Sharker, K.K., M.N. Islam, and S. Das, *Counterion effect on Krafft temperature and related properties of octadecyltrimethylammonium bromide.* Journal of Surfactants and Detergents, 2017. **20**(4): p. 923-932.
550. Topallar, H. and B. Karadag, *Mechanism of micelle formation in sodium dodecyl sulfate and cetyltrimethylammonium bromide.* Journal of Surfactants and Detergents, 1998. **1**(1): p. 49-51.
551. Syam Sundar, L., A.C. Sousa, and M.K. Singh, *Heat transfer enhancement of low volume concentration of carbon nanotube-Fe3O4/water hybrid nanofluids in a tube with twisted tape inserts under turbulent flow.* Journal of Thermal Science and Engineering Applications, 2015. **7**(2): p. 021015.
552. Ghadimi, A., R. Saidur, and H. Metselaar, *A review of nanofluid stability properties and characterization in stationary conditions.* International journal of heat and mass transfer, 2011. **54**(17-18): p. 4051-4068.
553. Kumar, D.D. and A.V. Arasu, *A comprehensive review of preparation, characterization, properties and stability of hybrid nanofluids.* Renewable and Sustainable Energy Reviews, 2018. **81**: p. 1669-1689.
554. Giwa, S.O., et al., *Influence of nanoparticles size, per cent mass ratio, and temperature on the thermal properties of water-based MgO–ZnO nanofluid: an experimental approach.* Journal of Thermal Analysis and Calorimetry, 2021. **143**(2): p. 1063-1079.
555. Moldoveanu, G.M., et al., *Al 2 O 3/TiO 2 hybrid nanofluids thermal conductivity.* Journal of Thermal Analysis and Calorimetry, 2019. **137**(2): p. 583-592.
556. Asadi, A. and F. Pourfattah, *Heat transfer performance of two oil-based nanofluids containing ZnO and MgO nanoparticles; a comparative experimental investigation.* Powder Technology, 2019. **343**: p. 296-308.
557. Siddiqui, F.R., et al., *On trade-off for dispersion stability and thermal transport of Cu-Al2O3 hybrid nanofluid for various mixing ratios.* International Journal of Heat and Mass Transfer, 2019. **132**: p. 1200-1216.
558. Taherialekouhi, R., S. Rasouli, and A. Khosravi, *An experimental study on stability and thermal conductivity of water-graphene oxide/aluminum oxide nanoparticles as a cooling hybrid nanofluid.* International Journal of Heat and Mass Transfer, 2019. **145**: p. 118751.
559. Mamand, S.M., *Thermal Conductivity Calculations for Nanoparticles Embedded in a Base Fluid.* Applied Sciences, 2021. **11**(4): p. 1459.
560. Kumar, A. and S. Subudhi, *Nanofluids: Definition & Classification*, in *Thermal Characteristics and Convection in Nanofluids*. 2021, Springer. p. 11-24.
561. Safaei, M.R., et al., *Thermal analysis of a binary base fluid in pool boiling system of glycol–water alumina nano-suspension.* Journal of Thermal Analysis and Calorimetry, 2021. **143**(3): p. 2453-2462.
562. Ebrahimi, D., et al., *Mixed convection heat transfer of a nanofluid in a closed elbow-shaped cavity (CESC).* Journal of Thermal Analysis and Calorimetry, 2021: p. 1-22.

563. Singh, S.P., et al., *Enhancement of thermal conductivity and ultrasonic properties by incorporating CdS nanoparticles to PVA nanofluids.* Zeitschrift für Naturforschung A, 2021.
564. Olabi, A., et al., *Application of nanofluids for enhanced waste heat recovery: a review.* Nano Energy, 2021: p. 105871.
565. Cao, Y., et al., *Intensification of CO 2 absorption using MDEA-based nanofluid in a hollow fibre membrane contactor.* Scientific Reports, 2021. **11**(1): p. 1-12.
566. Sundar, L.S., et al., *Nanodiamond-Fe3O4 nanofluids: preparation and measurement of viscosity, electrical and thermal conductivities.* International Communications in Heat and Mass Transfer, 2016. **73**: p. 62-74.
567. Abdullah, A.M., et al., *Tailoring the viscosity of water and ethylene glycol based TiO2 nanofluids.* Journal of Molecular Liquids, 2020. **297**: p. 111982.
568. Isaza-Ruiz, M., et al., *Viscosity and stability analysis of hitec salt-based alumina nanofluids.* Solar Energy Materials and Solar Cells, 2021. **222**: p. 110923.
569. Zahmatkesh, I. and M.R.H. Shandiz, *MHD double-diffusive mixed convection of binary nanofluids through a vertical porous annulus considering Buongiorno's two-phase model.* Journal of Thermal Analysis and Calorimetry, 2021: p. 1-15.
570. Jin, C., et al., *Investigation on hybrid nanofluids based on carbon nanotubes filled with metal nanoparticles: Stability, thermal conductivity, and viscosity.* Powder Technology, 2021.
571. Afzal, A., S.A. Khan, and C.A. Saleel, *Role of ultrasonication duration and surfactant on characteristics of ZnO and CuO nanofluids.* Materials Research Express, 2019. **6**(11): p. 1150d8.
572. Konakanchi, H., et al., *Measurements of pH of Three Nanofluids and Development of New Correlations.* Heat Transfer Engineering, 2015. **36**(1): p. 81-90.
573. Mehrali, M., et al., *Experimental and numerical investigation of the effective electrical conductivity of nitrogen-doped graphene nanofluids.* Journal of nanoparticle research, 2015. **17**(6): p. 1-17.
574. Ma, X., et al., *Heat and mass transfer enhancement of the bubble absorption for a binary nanofluid.* Journal of Mechanical Science and Technology, 2007. **21**(11): p. 1813.
575. Bashir, S., et al., *Analyzing the impact of induced magnetic flux and Fourier's and Fick's theories on the Carreau-Yasuda nanofluid flow.* Scientific Reports, 2021. **11**(1): p. 1-18.
576. Shukla, S., U. Gupta, and M. Devi, *LTNE effects on binary nanofluid convection: A modified model.* Materials Today: Proceedings, 2021.
577. Peng, Y., et al., *Potential application of Response Surface Methodology (RSM) for the prediction and optimization of thermal conductivity of aqueous CuO (II) nanofluid: A statistical approach and experimental validation.* Physica A: Statistical Mechanics and its Applications, 2020: p. 124353.
578. Said, Z., et al., *Thermophysical properties using ND/water nanofluids: An experimental study, ANFIS-based model and optimization.* Journal of Molecular Liquids, 2021: p. 115659.
579. Wole-Osho, I., et al., *An intelligent approach to predicting the effect of nanoparticle mixture ratio, concentration and temperature on thermal conductivity of hybrid nanofluids.* Journal of Thermal Analysis and Calorimetry, 2021. **144**(3): p. 671-688.
580. Sundar, L.S., et al., *Thermal conductivity and viscosity of hybrid nanfluids prepared with magnetic nanodiamond-cobalt oxide (ND-Co3O4) nanocomposite.* Case studies in thermal engineering, 2016. **7**: p. 66-77.

581. Esfe, M.H., et al., *A novel applicable experimental study on the thermal behavior of SWCNTs (60%)-MgO (40%)/EG hybrid nanofluid by focusing on the thermal conductivity.* Powder technology, 2019. **342**: p. 998-1007.
582. Sadeghzadeh, M., et al., *Prediction of thermo-physical properties of TiO2-Al2O3/water nanoparticles by using artificial neural network.* Nanomaterials, 2020. **10**(4): p. 697.
583. Arani, A.A.A. and F. Pourmoghadam, *Experimental investigation of thermal conductivity behavior of MWCNTS-Al 2 O 3/ethylene glycol hybrid Nanofluid: Providing new thermal conductivity correlation.* Heat and Mass Transfer, 2019. **55**(8): p. 2329-2339.
584. Khalid, S., et al., *Thermal–electrical–hydraulic properties of Al 2 O 3–SiO 2 hybrid nanofluids for advanced PEM fuel cell thermal management.* Journal of Thermal Analysis and Calorimetry, 2021. **143**(2): p. 1555-1567.
585. Sajjadi, H., et al., *Natural Convection Heat Transfer in a Porous Cavity with Sinusoidal Temperature Distribution Using Cu/Water Nanofluid: Double MRT Lattice Boltzmann Method.* Communications in Computational Physics, 2021. **29**(1): p. 292-318.
586. Joshi, P.S. and A. Pattamatta, *Buoyancy induced convective heat transfer in particle, tubular and flake type of nanoparticle suspensions.* International Journal of Thermal Sciences, 2017. **122**: p. 1-11.
587. Dixit, D.D. and A. Pattamatta, *Natural convection heat transfer in a cavity filled with electrically conducting nano-particle suspension in the presence of magnetic field.* Physics of Fluids, 2019. **31**(2): p. 023302.
588. Takabi, B. and S. Salehi, *Augmentation of the heat transfer performance of a sinusoidal corrugated enclosure by employing hybrid nanofluid.* Advances in Mechanical Engineering, 2014. **6**: p. 147059.
589. Ilyas, S.U., R. Pendyala, and M. Narahari, *An experimental study on the natural convection heat transfer in rectangular enclosure using functionalized alumina-thermal oil-based nanofluids.* Applied Thermal Engineering, 2017. **127**: p. 765-775.
590. Sheremet, M. and M. Rashidi, *Thermal convection of nano-liquid in an electronic cabinet with finned heat sink and heat generating element.* Alexandria Engineering Journal, 2021. **60**(3): p. 2769-2778.
591. Minea, A.A. and S.M. Sohel Murshed, *Ionic Liquids-Based Nanocolloids—A Review of Progress and Prospects in Convective Heat Transfer Applications.* Nanomaterials, 2021. **11**(4): p. 1039.
592. Lee, K.L., et al., *The influence of wall temperature distribution on the mixed convective losses from a heated cavity.* Applied Thermal Engineering, 2019. **155**: p. 157-165.
593. Feng, S., et al., *Thermal management of 3D chip with non-uniform hotspots by integrated gradient distribution annular-cavity micro-pin fins.* Applied Thermal Engineering, 2021. **182**: p. 116132.
594. Suganthi, K. and K. Rajan, *Improved transient heat transfer performance of ZnO–propylene glycol nanofluids for energy management.* Energy conversion and management, 2015. **96**: p. 115-123.
595. Aljabair, S., et al., *Mixed convection in sinusoidal lid driven cavity with non-uniform temperature distribution on the wall utilizing nanofluid.* Heliyon, 2021. **7**(5): p. e06907.
596. Wang, J., et al., *Established prediction models of thermal conductivity of hybrid nanofluids based on artificial neural network (ANN) models in waste heat system.* International Communications in Heat and Mass Transfer, 2020. **110**: p. 104444.
597. Sharifpur, M., et al., *Experimental investigation and model development for thermal conductivity of α-Al2O3-glycerol nanofluids.* International Communications in Heat and Mass Transfer, 2017. **85**: p. 12-22.

598. Ahmadi, M.H., et al., *Applicability of connectionist methods to predict dynamic viscosity of silver/water nanofluid by using ANN-MLP, MARS and MPR algorithms.* Engineering Applications of Computational Fluid Mechanics, 2019. **13**(1): p. 220-228.
599. Orooji, Y., et al., *Gd2ZnMnO6/ZnO nanocomposites: green sol-gel auto-combustion synthesis, characterization and photocatalytic degradation of different dye pollutants in water*. Journal of Alloys and Compounds, 2020. **835**: p. 155240.
600. Mehdizadeh, P., et al., *Green synthesis using cherry and orange juice and characterization of TbFeO3 ceramic nanostructures and their application as photocatalysts under UV light for removal of organic dyes in water.* Journal of Cleaner Production, 2020. **252**: p. 119765.
601. Everts, M., *Single-phase mixed convection of developing and fully developed flow in smooth horizontal tubes in the laminar, transitional, quasi-turbulent and turbulent flow regimes*, in *Mechanical and Aeronautical Engineering*. 2018, University of Pretoria.
602. Giwa, S.O., *Investigation into thermal-fluid properties of hybrid ferrofluids as heat transfer fluids*, in *Mechanical and Aeronautical Engineering*. 2020, University of Pretoria.
603. Moffat, R.J., *Describing the uncertainties in experimental results.* Experimental thermal and fluid science, 1988. **1**(1): p. 3-17.
604. ASHRAE, *ASHRAE handbook fundamentals, 2021, chapter psychrometrics*. 2021: American Society of Heating, Refrigerating and Air-Conditioning Engineers, Inc.

APPENDICES

A. Weights of NPs and Surfactants

A.1 Introduction

This section of the appendix presents the estimation of the amounts of nanoparticles and surfactants used to form binary nanofluids (BNFs) samples. The optimum dispersion fractions obtained for the formulation of BNFs were used to estimate the weights of nanoparticles and surfactants. The amounts of nanoparticles employed in the formulation of BNFs depended on φ, nanoparticles percent weight, and types of nanoparticles hybridised.

A.2 Calculation for Weights of Nanoparticles and Surfactants for BNFs

Nanoparticles of MgO (20 nm and 100 nm) and ZnO (20 nm) at percent weight ratio of 20:80, 40:60, 60:40, and 80:20 (MgO/ZnO) were suspended in DIW (1400 mL) to formulate 0.1 vol.% BNFs using a two-step method. The dispersion fraction of the surfactant (SDS) was 1.0.

Equation 3.1 was used to estimate the weights of MgO and ZnO nanoparticles as a function of φ (0.05 and 0.10) as given in Table A1. Also, the weights of SDS were calculated using Equation 3.2 and as a dependent of φ.

Table A.1: Weights (g) of NPs and surfactant (SDS) engaged in BNF formulation.

S/N	MgO-ZnO (wt%)	MgO (g)	ZnO (g)	SDS (g)	BF (l)
		0.05 vol.%			
1	20-80	1.0408	4.1633	5.2041	1400
2	40-60	2.3650	3.5475	5.3212	1400
3	60-40	2.9494	1.9662	4.9156	1400
4	80-20	2.7114	0.6779	3.3893	1400
		0.1 vol.%			
1	20-80	2.0827	8.3308	10.4135	1400
2	40-60	4.7323	7.0985	11.8308	1400
3	60-40	5.9017	3.9345	9.8361	1400
4	80-20	5.4255	1.3564	6.7819	1400

A.3 Conclusion

The weights of nanoparticles and surfactants used in the formulation of BNFs in this present investigation were estimated and presented. These weights were observed to be dependent primarily on ρ and percent weight of individual NPs, and φ, as related to the type of BNFs to be formulated. Additionally, the total amounts of materials (BNPs and surfactants) depended on the type of BNFs to be formulated, which was related to φ, type of surfactants, dispersion fraction of surfactants, NPs percent weight, and the types of NPs combined as BNPs.

B. Calibration of Thermocouples

B.1 Introduction

The calibration of the thermocouples employed in the square cavity for the thermo-convection investigation of BNFs was discussed in this appendix. In addition, the calibration factors of individual thermocouples were also shown.

B.2 Calibration of Thermocouples

A Programmable water baths (PolyScience, USA: PR 20R-30-A12E, −30°C and 200°C, precision 0.0050 °C), was employed for the in-situ calibration of the thermocouples at temperatures of 5 – 60 °C at 2.5 °C intervals. Temperature measurements of 400 points were measured at the predetermined temperature using a frequency of 2 Hz, and the average was determined. The calibration procedure was conducted in triplicates (to minimize error), and the means of the measured temperature dataset for the thermocouples were estimated. For each thermocouple, the average measured temperature was plotted against the reference temperature as measured using PT-100 (thermal bath internal thermocouple) as provided in Figure B.1. Fitting of the reference and average measured temperature for each thermocouple was done to estimate the calibration factors using Equation B.1.

$$T_{cal} = mT_{uncali} + c \qquad \textbf{B.1}$$

For the thermocouples, the m and c were used as the calibration parameters. A linear relationship with $R^2 \approx 1$ was noticed amidst the mean measured temperature and the reference temperature for all the thermocouples. This revealed a good correlation between both variables showing excellent performance of the thermocouples in valuing the reference temperatures.

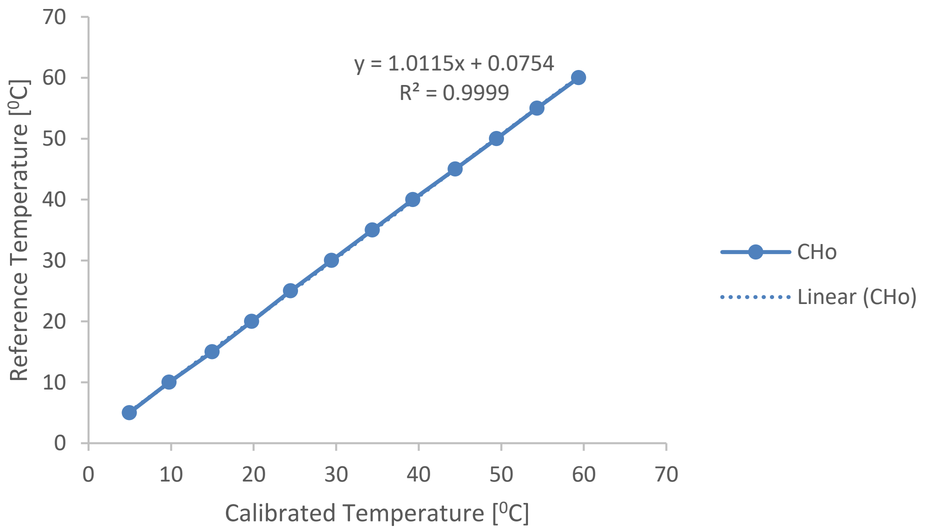
y = 1.0115x + 0.0754
R² = 0.9999
Reference Temperature [⁰C]
Calibrated Temperature [⁰C]
CHo
Linear (CHo)

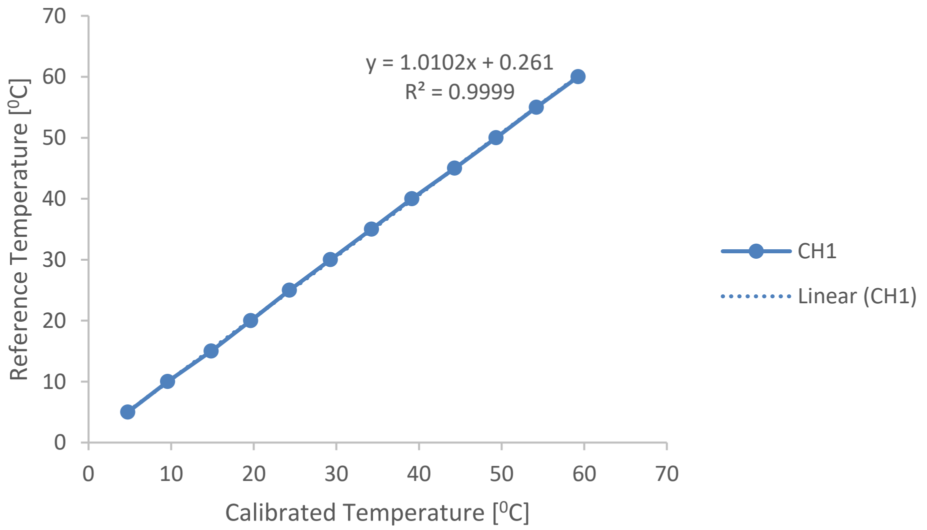
y = 1.0102x + 0.261
R² = 0.9999
Reference Temperature [⁰C]
Calibrated Temperature [⁰C]
CH1
Linear (CH1)

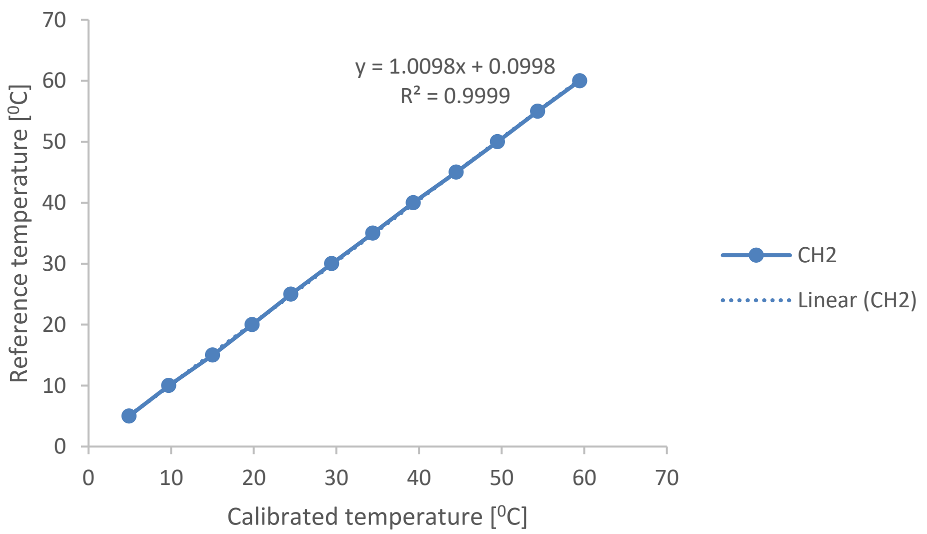
y = 1.0098x + 0.0998
R² = 0.9999
Reference temperature [⁰C]
Calibrated temperature [⁰C]
CH2
Linear (CH2)

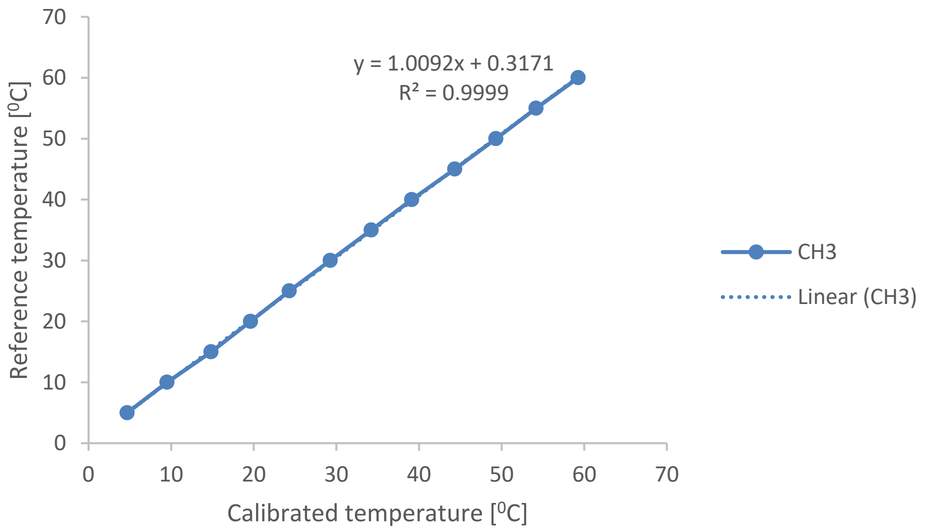
y = 1.0092x + 0.3171
R² = 0.9999
Reference temperature [0C]
Calibrated temperature [0C]
CH3
Linear (CH3)

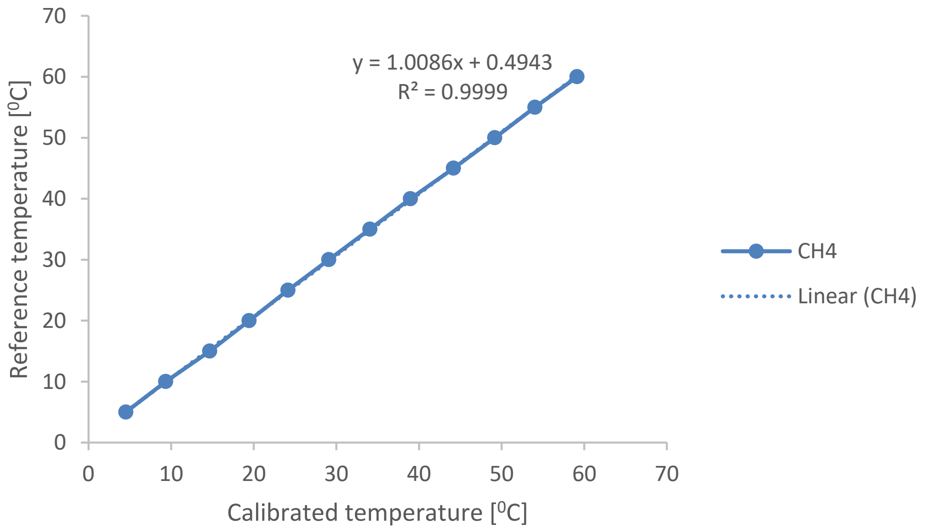
y = 1.0086x + 0.4943
R² = 0.9999
Reference temperature [0C]
Calibrated temperature [0C]
CH4
Linear (CH4)

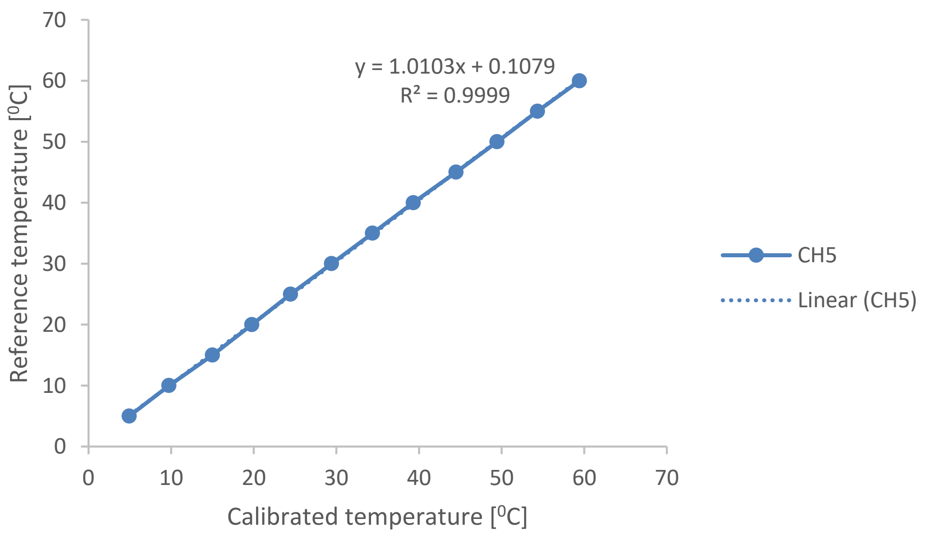
y = 1.0103x + 0.1079
R² = 0.9999
Reference temperature [0C]
Calibrated temperature [0C]
CH5
Linear (CH5)

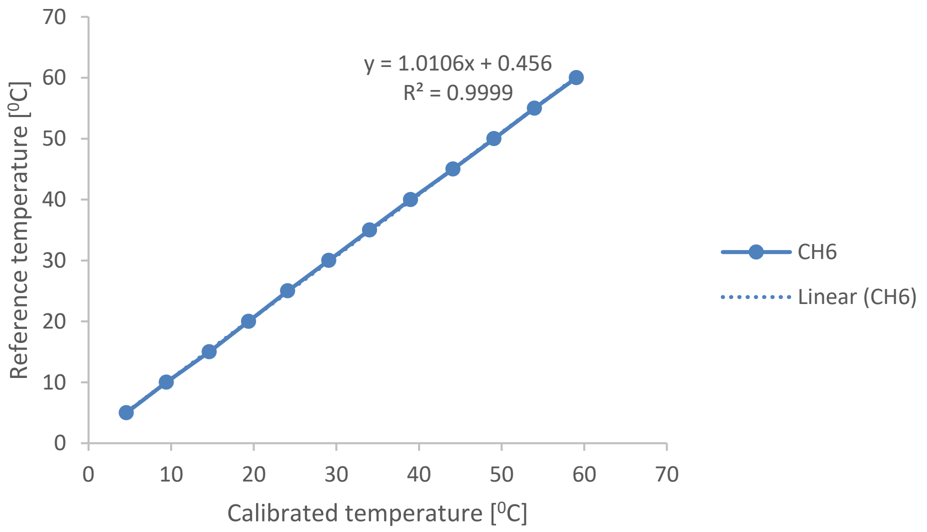
y = 1.0106x + 0.456
R² = 0.9999
Reference temperature [⁰C]
Calibrated temperature [⁰C]
0
10
20
30
40
50
60
70
CH6
Linear (CH6)

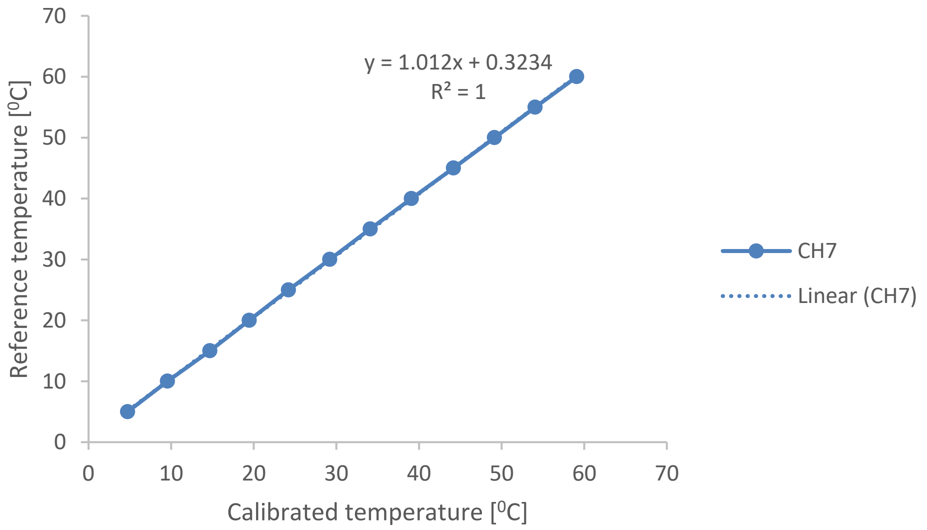
y = 1.012x + 0.3234
R² = 1
Reference temperature [⁰C]
Calibrated temperature [⁰C]
0
10
20
30
40
50
60
70
CH7
Linear (CH7)

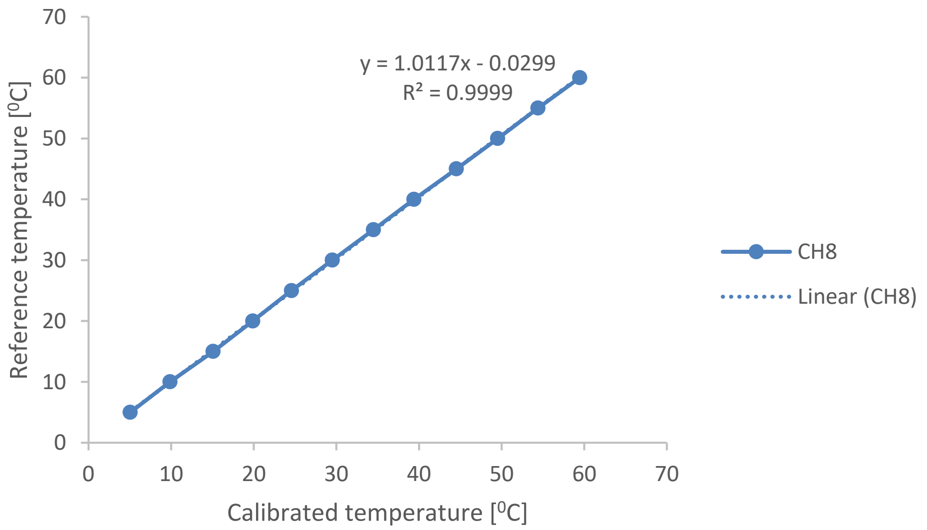
y = 1.0117x - 0.0299
R² = 0.9999
Reference temperature [⁰C]
Calibrated temperature [⁰C]
0
10
20
30
40
50
60
70
CH8
Linear (CH8)

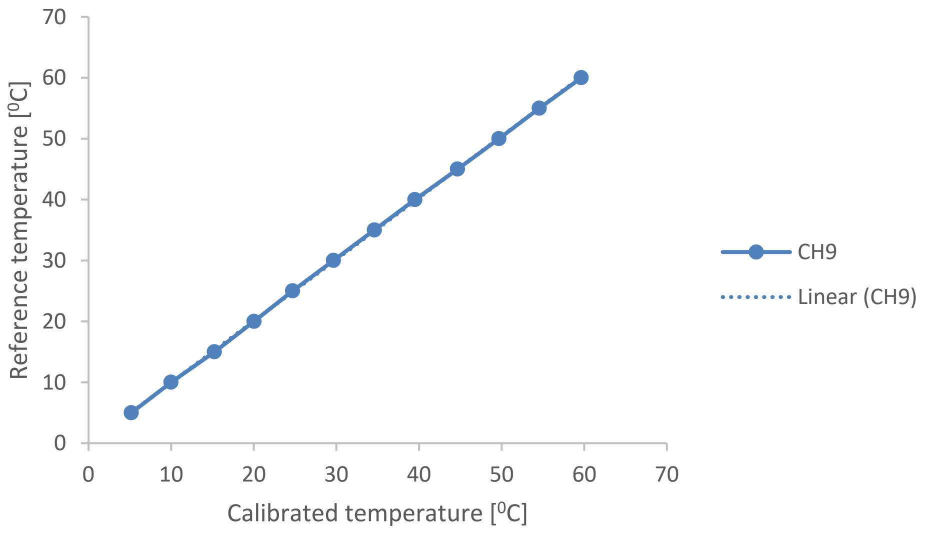
Reference temperature [⁰C]
Calibrated temperature [⁰C]
CH9
Linear (CH9)

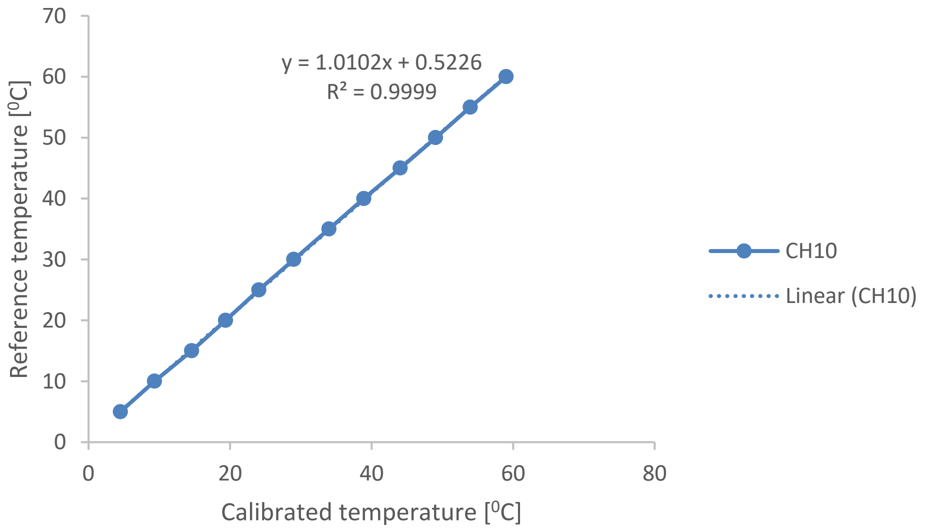
y = 1.0102x + 0.5226
R² = 0.9999
Reference temperature [⁰C]
Calibrated temperature [⁰C]
CH10
Linear (CH10)

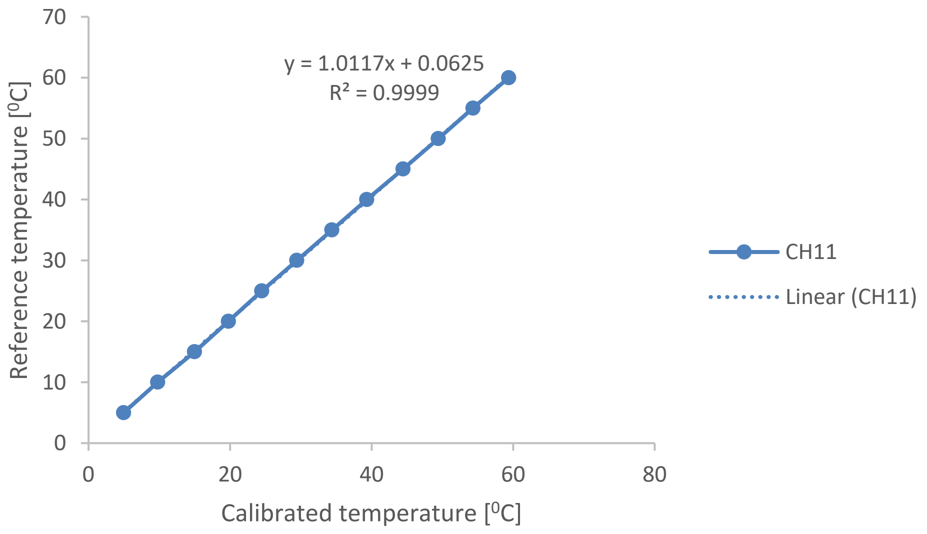
y = 1.0117x + 0.0625
R² = 0.9999
Reference temperature [⁰C]
Calibrated temperature [⁰C]
CH11
Linear (CH11)

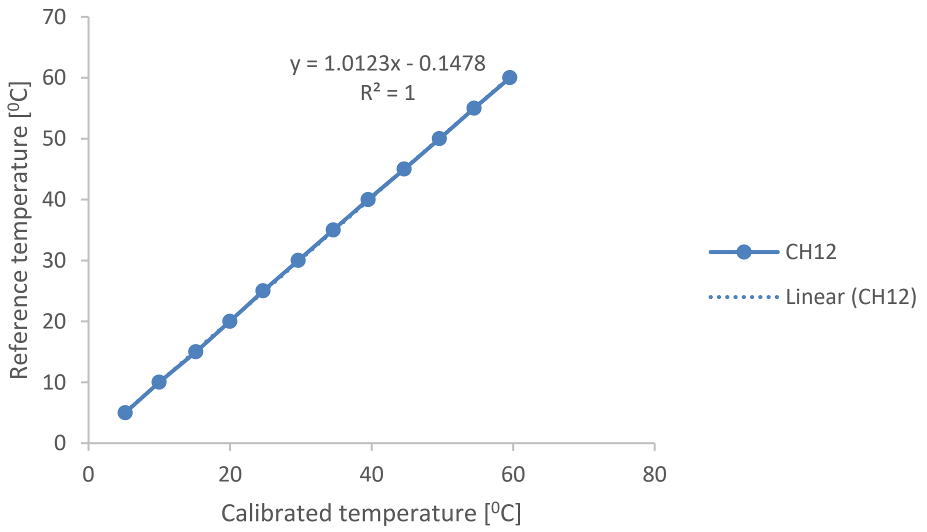
y = 1.0123x - 0.1478
R² = 1
CH12
Linear (CH12)
Reference temperature [⁰C]
Calibrated temperature [⁰C]
0
10
20
30
40
50
60
70
0
20
40
60
80

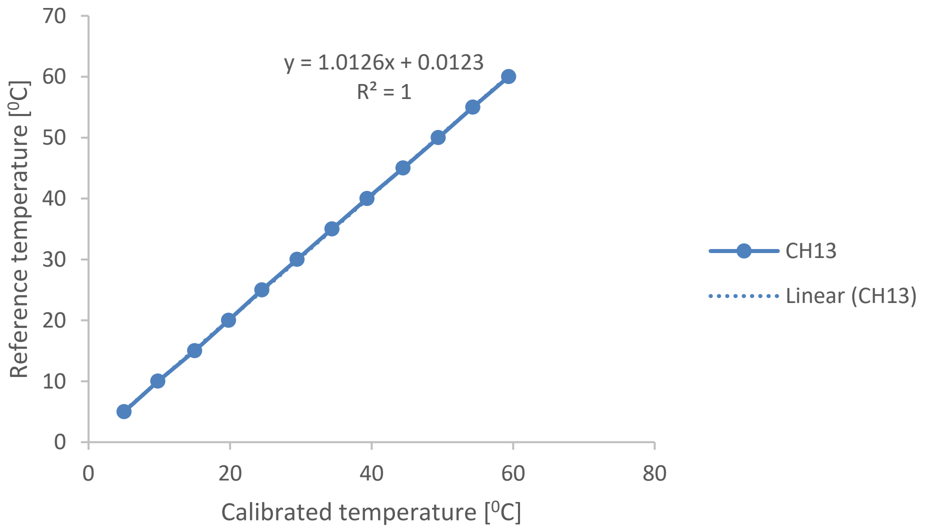
y = 1.0126x + 0.0123
R² = 1
CH13
Linear (CH13)
Reference temperature [⁰C]
Calibrated temperature [⁰C]
0
10
20
30
40
50
60
70
0
20
40
60
80

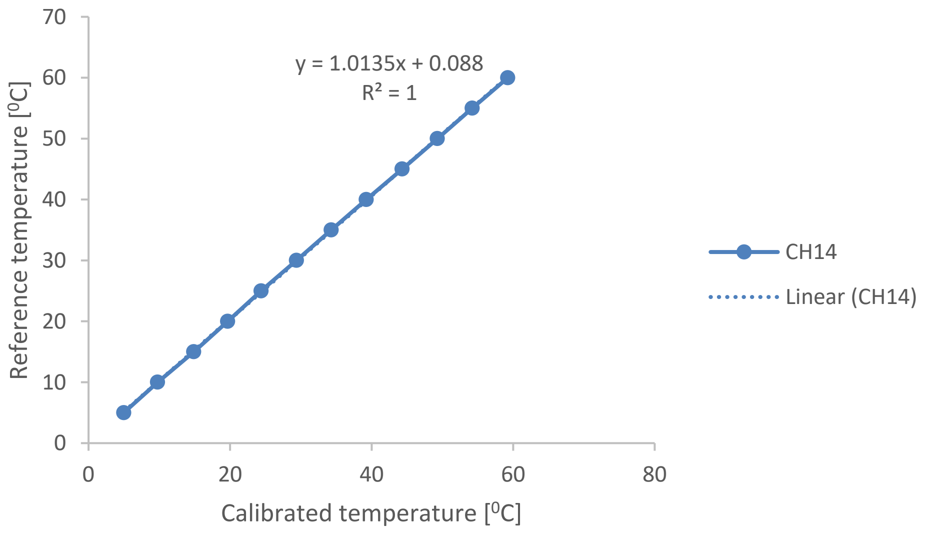
y = 1.0135x + 0.088
R² = 1
CH14
Linear (CH14)
Reference temperature [⁰C]
Calibrated temperature [⁰C]
0
10
20
30
40
50
60
70
0
20
40
60
80

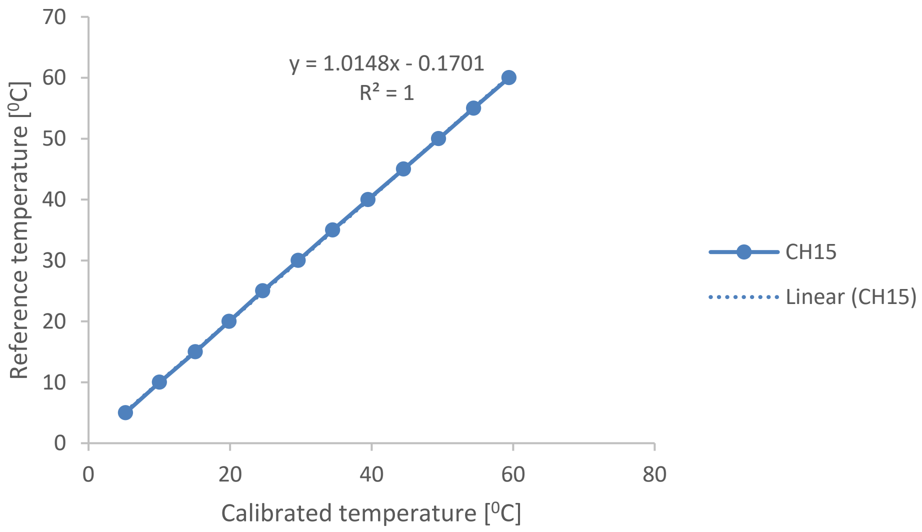

y = 1.0148x - 0.1701
R² = 1
Reference temperature [⁰C]
Calibrated temperature [⁰C]
CH15
Linear (CH15)

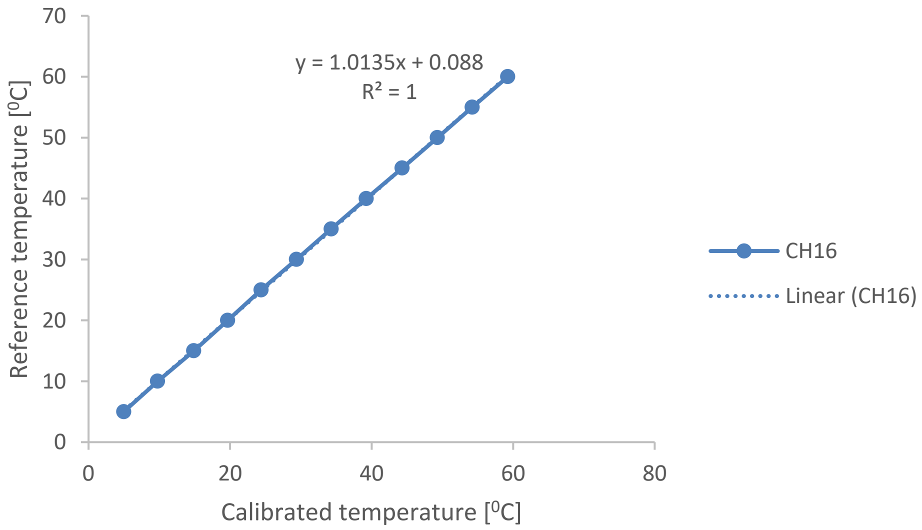

y = 1.0135x + 0.088
R² = 1
Reference temperature [⁰C]
Calibrated temperature [⁰C]
CH16
Linear (CH16)

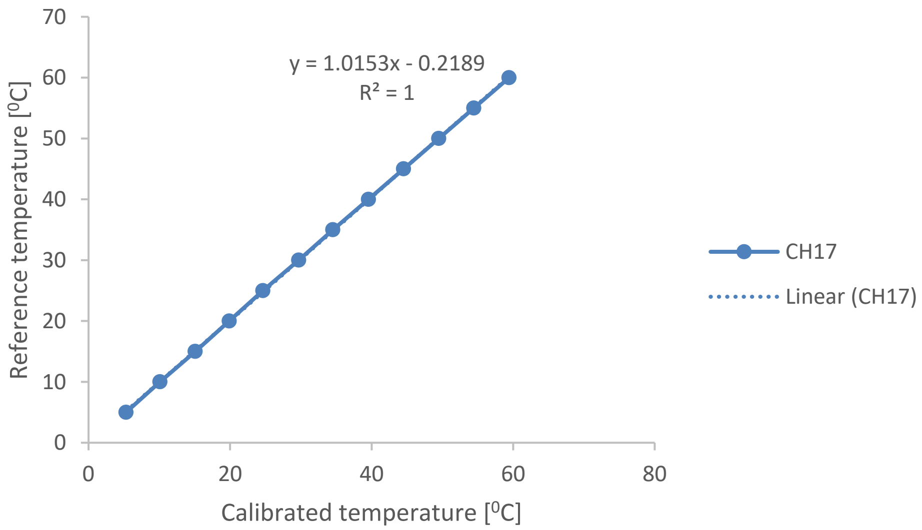

y = 1.0153x - 0.2189
R² = 1
Reference temperature [⁰C]
Calibrated temperature [⁰C]
CH17
Linear (CH17)

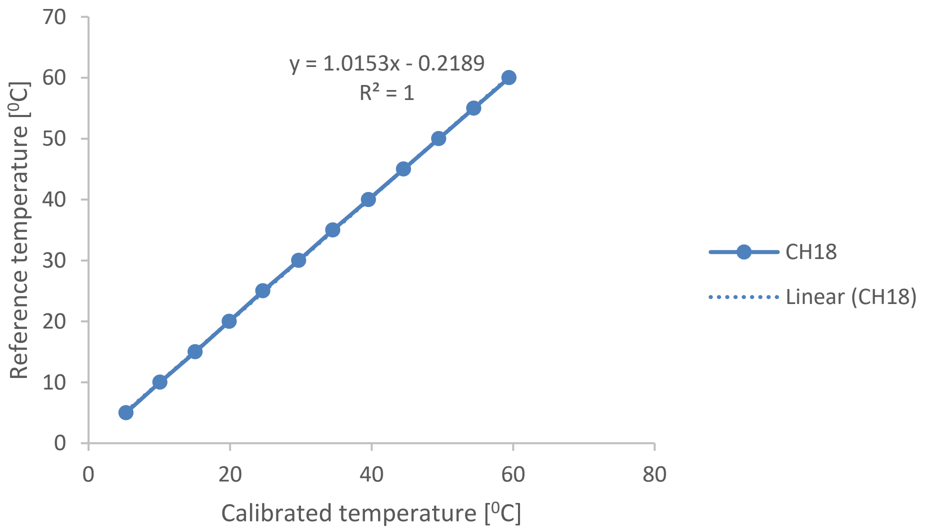

y = 1.0153x - 0.2189
R² = 1
Reference temperature [⁰C]
Calibrated temperature [⁰C]
CH18
Linear (CH18)

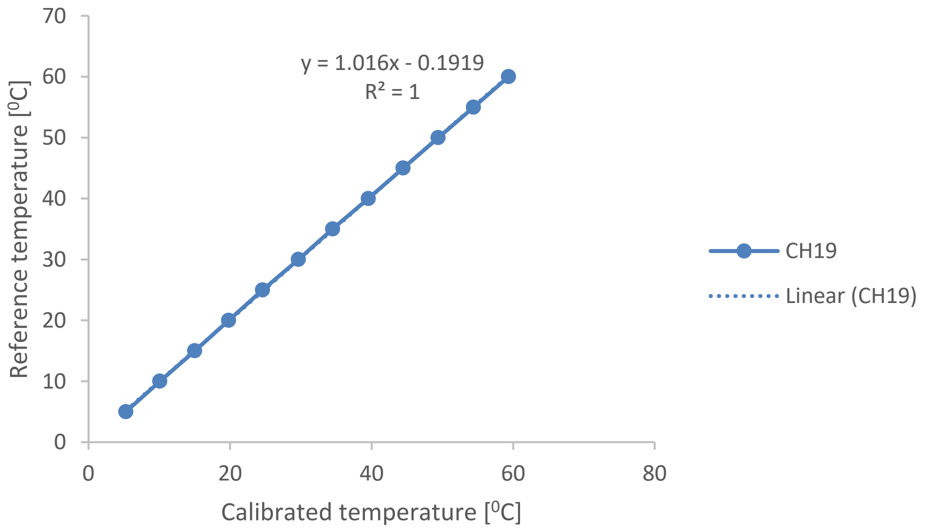

y = 1.016x - 0.1919
R² = 1
Reference temperature [⁰C]
Calibrated temperature [⁰C]
CH19
Linear (CH19)

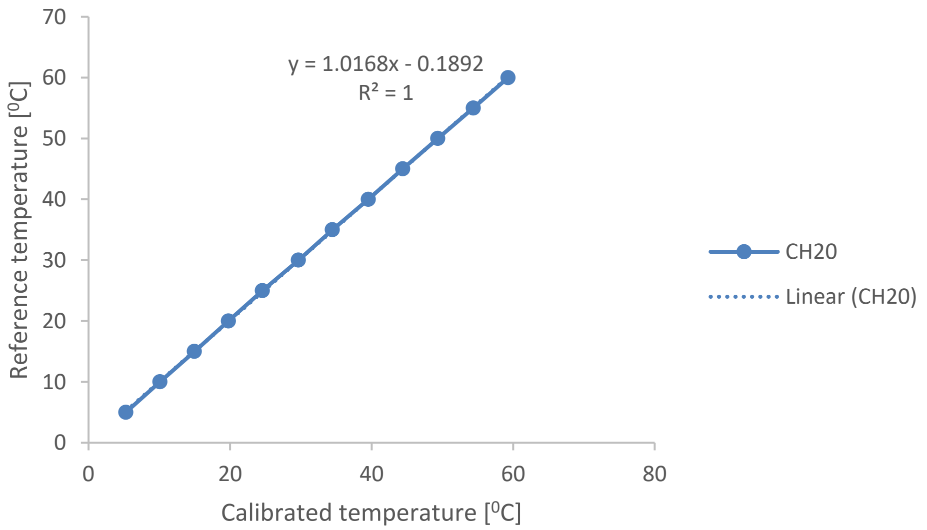

y = 1.0168x - 0.1892
R² = 1
Reference temperature [⁰C]
Calibrated temperature [⁰C]
CH20
Linear (CH20)

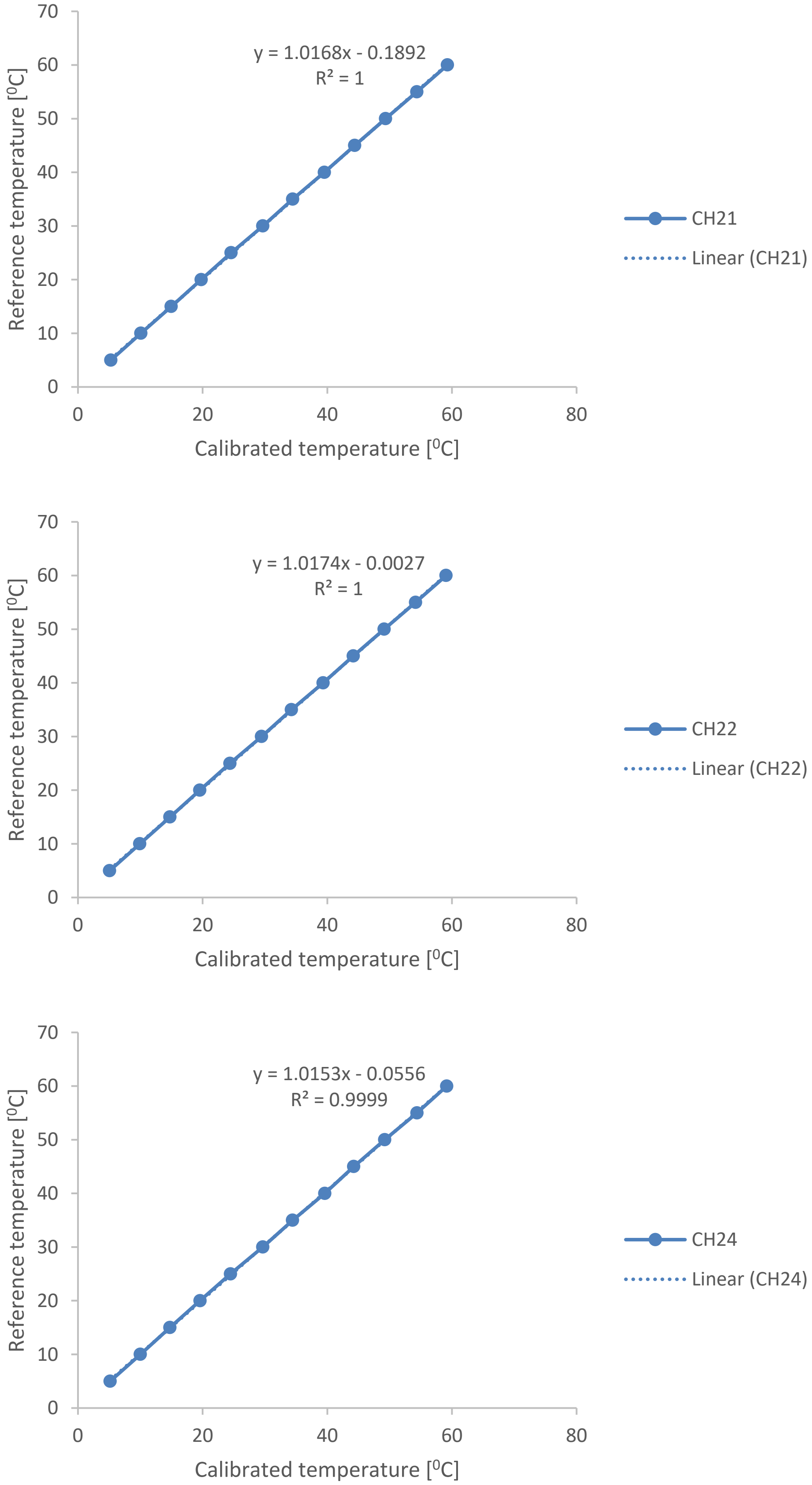

Figure B.1: Average measured temperatures of thermocouples against reference temperatures (CH 0 – 22, 24).

The use of various channels of the data logger could be ascribed to the variations in the calibration parameters achieved for the thermocouples. Also, the changes in the characteristics of the junction of the thermocouples after soldering them to the various positions can be responsible for the variation in the calibration factors of the thermocouples. After calibration, the average deviation between the average measured temperature of the thermocouples and reference temperatures was 0.169 °C.

B.3 Conclusion

The calibration of the thermocouples was performed and presented. The thermocouples were calibrated for temperature 10 – 50 °C using a thermal bath of the accuracy of ±0.005 °C. Linear relationships were observed between the average measured temperature of the thermocouples and the reference temperature. The average deviation of the thermocouples was 0.169 °C.

C. Uncertainty Analysis

C.1 Introduction

Uncertainty analysis was employed to analyse the uncertainty associated with the variables relevant to this investigation. This appendix entails the content of the uncertainty analysis approach, precision of the instrument used for the investigation (thermophysical properties and thermo-convection) and the associated results for the uncertainties [601, 602].

C.2 Theory

In measurement processes, two types of errors happen – bias and precision. The bias error estimates the precision of measurement, as specified by the instrument's manufacturer. These errors arise from calibration, imperfection of measuring tools and equipment, etc. Precision errors relate to data spread, which defines the precision of dataset. These errors emanate from differences in the measurement process, electrical noise, etc [601, 602].

The magnitude of the bias and precision errors relates to a 95% probability in which the actual error is more than the estimated error. For a single measurement, uncertainty is related to both precision and bias [601, 602]. Uncertainty is presented in Equation C.1 [205]:

$$\delta x_i = \sqrt{\left({b_i}^2 + {p_i}^2\right)} \qquad \textbf{C.1}$$

Where:

x_i is a single measurement and δx_i relates to standard deviation multiplied by Student's t-variable [603]. The reading R of measurement is related to various parameters and can be calculated using a series of equations.

$$R = R(x_1, x_2, x_3, \dots\dots., x_n) \qquad \textbf{C.2}$$

With the uncertainties of x_i known, the uncertainty in R can be estimated as expressed in Equation C.3.

$$\delta R = \frac{\partial R}{\partial X_i}\delta x_i \quad \textbf{C.3}$$

Where δR is the sensitivity coefficient employed to determine the influence of x_i on the general uncertainty. The root sum square method is used to estimate the uncertainty of various independent variables.

$$\delta R = \left(\sum_{i=1}^{n}\left(\frac{\partial R}{\partial X_i}\delta x_i\right)^2\right)^{\frac{1}{2}} \quad \textbf{C.4}$$

The accuracy of the thermocouples was determined by applying regression analysis, which is a statistical tool used to establish a mathematical relationship between two or more variables. The *x* value is the known parameter while the *y* value is determined via measurements. Hence, the uncertainty was propagated from the *y* parameter [603]. Equation C.5 was applied to evaluate the uncertainty of the *y* factor."

$$\delta y = \pm t S_{yx}\sqrt{\frac{1}{N}+\frac{1}{M}+\frac{(x_i-\bar{x})^2}{S_{xx}}} \quad \textbf{C.5}$$

Where S_{xx} is defined as:

$$S_{xx} = \sum_{i=1}^{N}(x_i-\bar{x})^2 \quad \textbf{C.6}$$

S_{yx} is determined by first estimating S_{xy}, a, and b.

$$S_{xy} = \sum_{i=1}^{N}(x_i-\bar{x})(y_i-\bar{y}) \quad \textbf{C.7}$$

$$b = \frac{S_{xy}}{S_{xx}} \quad \textbf{C.8}$$

$$a = \bar{y} - b\bar{x} \quad \textbf{C.9}$$

$$y_{ci} = a + bx_i \quad \textbf{C.10}$$

$$S_{yx} = \sqrt{\frac{\sum_{i=1}^{N}(y_i-y_{ci})^2}{N-2}} \quad \textbf{C.11}$$

The uncertainty in the x variable was evaluated by dividing the uncertainty in y by the slope of the regression line.

$$\delta x = \frac{\delta y}{m} \qquad \text{C.12}$$

C.3 Equipment

The accuracy specified by the manufacturer was considered as the bias for the instruments while the precision was evaluated using the standard deviation of the 1000 measurement points acquired via the data logger for temperature and flow rate measurements. For the viscometer and thermal conductivity meter, the accuracy (bias) specified by the manufacturer was used. The determined precision was multiplied by Student's *t*-value with a confidence limit of 95% [601, 602]. The accuracy of the instruments used in this study is given in Table C.1.

Table C.1: Accuracy of equipment used in this investigation.

Instrument	Range	Accuracy
Electrical conductivity meter	0 µS - 200 mS	± 1%
Flow meter	0.0666 – 0.3333 l/s	±0.01% of full-scale flow rate + 2% (measured value)
Graduated cylinder	250 ml	± 2.0 ml
Thermal bath	-200 – 150 °C	± 0.005 °C
Thermal conductivity meter	0.2 – 2.0 W/m K	±10%
Thermocouple	< 150 °C	±0.1 °C
Vernier calipers	0.02 mm	0.02 mm
Viscometer	0.3 – 10,000 mPa.s	±3%
Weighing balance	10 mg – 220 g	0.02

C.3.1 Thermocouples

The calibration of thermocouples was discussed earlier in B.3, where the accuracy of the thermal bath and thermocouples were ±0.005 °C and 0.1 °C, respectively. The precision was evaluated using Equation C.2.5 to C.2.12 with the uncertainty evaluated using Equation C.1. The average uncertainty of the thermocouples was ±0.159%.

C.3.2 Flow Meters

Each of the flow meters has an accuracy of ±0.01% of full-scale flow rate + 2% (measured value) used as the bias. The precision was calculated by multiplying the standard deviation of the flow rate acquired by the data logger by the Student's *t*-value. The uncertainty was then estimated using Equation C.1.

C.3.3 Digital Weighing Balance

The accuracy of the digital weighing balance was 0.001 g, and this was used as the bias. The standard deviation of the BNPs and surfactants (total) weights for each BNFs as presented in Table A.1 was obtained and used as the precision. This was multiplied by the Student's *t*-value, and Equation C.1 was used to estimate uncertainty.

C.3.4 Thermal Conductivity Meter

Similarly, the accuracy of the thermal conductivity meter was engaged as the bias. The standard deviation of the measurements taken for each BNFs and basefluid was multiplied by the Student's *t*-value and used as the precision. Using Equation 3.26, an extension of Equation C.1, the uncertainty of κ for BNFs and basefluids was estimated. As mentioned in Appendix A, the volume of the basefluids (DIW) used in this study was 1400 mL, and the graduated cylinder had an accuracy of ±2.0 ml.

C.3.5 Viscometer

With the accuracy of the viscometer used as the bias and the precision calculated from the multiplication of the standard deviation of the measured μ (for BNFs and basefluids) by Student's *t*-value, the uncertainty of μ (for BNFs and basefluids) was estimated using Equation 3.25 (an extension of Equation C.1). It is important to note that the viscometer has an accuracy specified for the temperature sensor related with μ measurement.

C.4 Parameters

C.4.1 Temperatures

From the known uncertainty of the thermocouples, the uncertainty related with the measurement of temperatures inside and outside the cavity was obtained. The uncertainty of the temperature of water flowing from and to the thermal baths was assumed to be equal under adiabatic conduction of close to perfect insulation. This is expressed by Equation C.13.

$$\delta T_{in} = \delta T_o \qquad \textbf{C.13}$$

The uncertainties of the bulk temperature, temperature gradient, temperature hot and cold side of the cavity were estimated using Equations C.14 – C.17, respectively. It is of note that T is the absolute temperature used in the correlations for estimating the uncertainty of other properties.

$$\delta T_{Bulk,H} = \frac{1}{3}\sqrt{\left(\delta T_{o,1}\right)^2 + \left(\delta T_{o,2}\right)^2 + (\delta T_i)^2} \qquad \textbf{C.14}$$

$$\delta \Delta T = \sqrt{\left(\frac{1}{2}\delta T_{o,1}\right)^2 + \left(\frac{1}{2}\delta T_{o,2}\right)^2 + (\delta T_i)^2} \qquad \textbf{C.15}$$

$$\delta T_H = \frac{1}{3}\sqrt{\left(\delta T_{H,1}\right)^2 + \left(\delta T_{H,2}\right)^2 + \left(\delta T_{H,3}\right)^2} \qquad \textbf{C.16}$$

$$\delta T_C = \frac{1}{3}\sqrt{\left(\delta T_{C,1}\right)^2 + \left(\delta T_{C,2}\right)^2 + \left(\delta T_{C,3}\right)^2} \qquad \textbf{C.17}$$

C.4.2 Cavity Area

The uncertainty of the cavity area was determined using Equation C.18.

$$\delta A = \sqrt{\left(\frac{\partial A}{\partial W}\delta W\right)^2 + \left(\frac{\partial A}{\partial H}\delta H\right)^2} \qquad \textbf{C.18}$$

Where: $\partial W = \partial H = \partial L$

C.4.3 Thermophysical Properties

To estimate the uncertainty of μ and κ of the basefluids, Equations C.19 – C.20 representing the correlations developed from the experimental data obtained in this work for μ and κ of the basefluids were used.

$$\kappa_{DIW} = 0.5741 + 1.393 \times 10^{-3}T \quad \text{C.19}$$

$$\mu_{DIW} = 1.18357 - 0.1271T \quad \text{C.20}$$

The empirical formula [539, 604] employed for the evaluation of the uncertainty of other thermal properties for the BFs are presented as Equations C.21 – C.23.

$$\rho_{DIW} = (999.842594 + 0.067939952T - 0.00909529T^2 + 1.00168 \times 10^{-4}T^3 - 1.120083 \times 10^{-6}T^4 + 6.536332 \times 10^{-9}T^5 \quad \text{C.21}$$

$$\beta_{DIW} = 8.41 \times 10^{-7}T^3 - 1.55704 \times 10^{-4}T^2 + 0.015892349T - 0.055807193 \quad \text{C.22}$$

$$C_{p-DIW} = 4.214 - 2.286 \times 10^{-3}T + 4.991 \times 10^{-5}T^2 - 4.519 \times 10^{-7}T^3 + 1.857 \times 10^{-9}T^4 \quad \text{C.23}$$

The uncertainty of κ, ρ, β, and C_p of the basefluids (DIW) was estimated using Equations C.24 – C.27, respectively.

$$\delta\kappa_{bf} = \sqrt{\left(\frac{\partial\kappa_{bf}}{\partial T}\delta T\right)^2} \quad \text{C.24}$$

$$\delta\rho_{bf} = \sqrt{\left(\frac{\partial\rho_{bf}}{\partial T}\delta T\right)^2} \quad \text{C.25}$$

$$\delta\beta_{bf} = \sqrt{\left(\frac{\partial\beta_{bf}}{\partial T}\delta T\right)^2} \quad \text{C.26}$$

$$\delta C_{p-bf} = \sqrt{\left(\frac{\partial C_{p-bf}}{\partial T}\delta T\right)^2} \quad \text{C.27}$$

With the use of Equation C.28 for φ which is a simple version of Equation 3.1, the uncertainty of φ was estimated using Equation C.29.

$$\varphi = \frac{v_{hnp}}{v_{hnp}+v_{bf}} = \frac{\frac{m_{hnp}}{\rho_{hnp}}}{\frac{m_{hnp}}{\rho_{hnp}}+v_{bf}} \quad \textbf{C.28}$$

$$\delta\varphi = \sqrt{\left(\frac{\partial\varphi}{\partial m_{hnp}}\delta m_{hnp}\right)^2 + \left(\frac{\partial\varphi}{\partial v_{bf}}\delta v_{bf}\right)^2} \quad \textbf{C.29}$$

Where:

$$\frac{\partial\varphi}{\partial m_{hnp}} = \frac{\rho_{hnp}v_{bf}}{(m_{hnp}+\rho_{hnp}v_{bf})^2} \quad \text{and} \quad \frac{\partial\varphi}{\partial v_{bf}} = \frac{-m_{hnp}\rho_{hnp}}{(m_{hnp}+\rho_{hnp}v_{bf})^2}$$

Empirical models for ρ_{hnf}, $C_{p\text{-}hnf}$, and β_{hnf} as expressed using Equations C.30 – C.32 were used to determine their uncertainty as expressed in Equations C.33 – C.35, respectively.

$$\rho_{hnf} = (1-\varphi)\rho_{bf} + \varphi\rho_{hnp} \quad \textbf{C.30}$$

$$C_{p-hnf} = \frac{(1-\varphi)(\rho C_p)_{bf}+(\rho C_p)_{hnp}}{\rho_{hnf}} \quad \textbf{C.31}$$

$$\beta_{hnf} = \frac{(1-\varphi)(\rho\beta)_{bf}+(\rho\beta)_{hnp}}{\rho_{hnf}} \quad \textbf{C.32}$$

$$\delta\rho_{hnf} = \sqrt{\left(\frac{\partial\rho_{hnf}}{\partial\varphi}\delta\varphi\right)^2 + \left(\frac{\partial\rho_{hnf}}{\partial\rho_{bf}}\delta\rho_{bf}\right)^2} \quad \textbf{C.33}$$

Where:

$$\frac{\partial\rho_{hnf}}{\partial\varphi} = \rho_{hnp} - \rho_{bf} \quad \text{and} \quad \frac{\partial\rho_{hnf}}{\partial\rho_{bf}} = 1-\varphi$$

$$\delta C_{p-hnf} = \sqrt{\left(\frac{\partial C_{p-hnf}}{\partial\varphi}\delta\varphi\right)^2 + \left(\frac{\partial C_{p-hnf}}{\partial\rho_{bf}}\delta\rho_{bf}\right)^2 + \left(\frac{\partial C_{p-hnf}}{\partial C_{p-bf}}\delta C_{p-bf}\right)^2 + \left(\frac{\partial C_{p-hnf}}{\partial\rho_{hnf}}\delta\rho_{hnf}\right)^2} \quad \textbf{C.34}$$

Where:
$\frac{\partial C_{p-hnf}}{\partial \varphi} = \frac{-(\rho C_p)_{bf}}{\rho_{hnf}}$, $\frac{\partial C_{p-hnf}}{\partial \rho_{bf}} = \frac{C_{p-bf}(1-\varphi)}{\rho_{hnf}}$, $\frac{\partial C_{p-hnf}}{\partial C_{p-bf}} = \frac{\rho_{bf}(1-\varphi)}{\rho_{hnf}}$, and $\frac{\partial C_{p-hnf}}{\partial \rho_{hnf}} =$

$\frac{-\left((1-\varphi)(\rho C_p)_{bf}+(\rho C_p)_{hnp}\right)}{(\rho_{hnf})^2}$

$$\delta\beta_{hnf} = \sqrt{\left(\frac{\partial \beta_{hnf}}{\partial \varphi}\delta\varphi\right)^2 + \left(\frac{\partial \beta_{hnf}}{\partial \rho_{bf}}\delta\rho_{bf}\right)^2 + \left(\frac{\partial \beta_{hnf}}{\partial \beta_{bf}}\delta\beta_{bf}\right)^2 + \left(\frac{\partial \beta_{hnf}}{\partial \rho_{hnf}}\delta\rho_{hnf}\right)^2} \qquad \textbf{C.35}$$

Where:

$\frac{\partial \beta_{hnf}}{\partial \varphi} = \frac{-(\rho\beta)_{bf}}{\rho_{hnf}}$, $\frac{\partial \beta_{hnf}}{\partial \rho_{bf}} = \frac{\beta_{bf}(1-\varphi)}{\rho_{hnf}}$, $\frac{\partial \beta_{hnf}}{\partial \beta_{bf}} = \frac{\rho_{bf}(1-\varphi)}{\rho_{hnf}}$, and $\frac{\partial \beta_{hnf}}{\partial \rho_{hnf}} =$

$\frac{-\left((1-\varphi)(\rho\beta)_{bf}+(\rho\beta)_{hnp}\right)}{(\rho_{hnf})^2}$

To estimate the uncertainty of κ_{hnf}, Equation C.36 was employed.

$$\delta\kappa_{hnf} = \sqrt{\left(\frac{\partial \kappa_{hnf}}{\partial \varphi}\delta\varphi\right)^2 + \left(\frac{\partial \kappa_{hnf}}{\partial \kappa_{bf}}\delta\kappa_{bf}\right)^2} \qquad \textbf{C.36}$$

C.4.4 Heat Transfer Rate

The estimation of the uncertainty of the heat transferred (Q) involved the substitution of Equations C.37 – C.39 into Equation 3.28.

$$\frac{\partial Q}{\partial \dot{m}} = C_{p-bf}\Delta T \qquad \textbf{C.37}$$

$$\frac{\partial Q}{\partial C_{p-bf}} = \dot{m}\Delta T \qquad \textbf{C.38}$$

$$\frac{\partial Q}{\partial \Delta T} = \dot{m}C_{p-bf} \qquad \textbf{C.39}$$

C.4.5 Convective Heat Transfer Coefficient

Equations C.40 – C.43 were substituted into Equation 3.28 to estimate the uncertainty of *h*.

$$\frac{\partial h}{\partial Q} = \frac{1}{(T_h - T_c)A} \quad \text{C.40}$$

$$\frac{\partial h}{\partial A} = \frac{-Q}{(T_h - T_c)A^2} \quad \text{C.41}$$

$$\frac{\partial h}{\partial T_h} = \frac{-Q}{(T_h - T_c)^2 A} \quad \text{C.42}$$

$$\frac{\partial h}{\partial T_c} = \frac{Q}{(T_h - T_c)^2 A} \quad \text{C.43}$$

C.4.6 Nusselt Number

Similarly, the uncertainty of *Nu* was estimated by substituting Equations C.44 – C.46 into Equation 3.27.

$$\frac{\partial Nu}{\partial h} = \frac{L_c}{\kappa} \quad \text{C.44}$$

$$\frac{\partial Nu}{\partial L_c} = \frac{h}{\kappa} \quad \text{C.45}$$

$$\frac{\partial Nu}{\partial h} = \frac{-hL_c}{\kappa} \quad \text{C.46}$$

C.5 Conclusion

The theory and method of uncertainty were highlighted. The accuracy of instruments engaged as the bias and the precision were used to estimate the uncertainty associated with the relevant parameters involved in this present study.